

# THE ASTROPHYSICAL JOURNAL

An International Review of Spectroscopy and  
Astronomical Physics

FOUNDED IN 1895 BY GEORGE E. HALE AND JAMES E. KEELER

## EDITORS

PAUL W. MERRILL

*Mount Wilson Observatory of the  
Carnegie Institution of Washington*

J. H. MOORE

*Lick Observatory  
University of California*

HARLOW SHAPLEY

*Harvard College Observatory  
Cambridge, Massachusetts*

OTTO STRUVE

*Yerkes Observatory of the  
University of Chicago*

## COLLABORATORS

S. B. NICHOLSON, *Mount Wilson Observatory*; D. B. McLAUGHLIN, *University of Michigan*; J. A. PEARCE,  
*Dominion Astrophysical Observatory, Victoria*; S. A. MITCHELL, *Leander McCormick Observatory*;  
LYMAN SPITZER, JR., *Yale University*; W. W. MORGAN, *Yerkes Observatory*; CECILIA H.  
PAYNE-GAPOSCHKIN, *Harvard College Observatory*; H. N. RUSSELL,  
*Princeton University*; F. H. SEARES, *Mount  
Wilson Observatory*

VOLUME 98

JULY-NOVEMBER 1943



THE UNIVERSITY OF CHICAGO PRESS  
CHICAGO, ILLINOIS

THE CAMBRIDGE UNIVERSITY PRESS, LONDON

PUBLISHED JULY, SEPTEMBER, NOVEMBER, 1943

COMPOSED AND PRINTED BY THE UNIVERSITY OF CHICAGO PRESS  
CHICAGO, ILLINOIS, U.S.A.



Astron. Obs.  
Wahner

## CONTENTS

### NUMBER 1

ROTATIONAL DISTRIBUTION OF <i>CH</i> MOLECULES IN THE NUCLEUS OF COMET CUNNINGHAM (1940c). Andrew McKellar . . . . .	1
THE PROPERTIES OF SOLAR PROMINENCES AS RELATED TO TYPE. Edison Pettit . . . . .	6
SIX-COLOR PHOTOMETRY OF STARS. I. THE LAW OF SPACE REDDENING FROM THE COLORS OF O AND B STARS. Joel Stebbins and A. E. Whitford . . . . .	20
THE STRONGER LINES OF SINGLY IONIZED DYSPROSIUM AND IDENTIFICATIONS IN THE SOLAR SPECTRUM. Arthur S. King and Charlotte E. Moore . . . . .	33
SOME USES OF THE DIRECT-INTENSITY MICROPHOTOMETER. Robley C. Williams and W. Albert Hiltner . . . . .	43
NGC 5053 AND NGC 6838. James Cuffey . . . . .	49
DYNAMICAL FRICTION. III. A MORE EXACT THEORY OF THE RATE OF ESCAPE OF STARS FROM CLUSTERS. S. Chandrasekhar . . . . .	54
A SPECTROSCOPIC STUDY OF THE REGION OF THE DOUBLE CLUSTER IN PERSEUS. William P. Bidelman . . . . .	61
A STUDY OF THE RADIAL VELOCITY OF $\beta$ CEPHEI. Burke Smith . . . . .	82
SPECTROGRAPHIC OBSERVATIONS OF PECULIAR STARS. VI. P. Swings and O. Struve . . . . .	91
THE SPECTRUM OF 48 LIBRAE (HD 142983). Otto Struve . . . . .	98
RECENT PROGRESS IN ASTROPHYSICS	
EDLÉN'S IDENTIFICATION OF THE CORONAL LINES WITH FORBIDDEN LINES OF <i>Fe</i> x, xi, xiii, xiv, xv; <i>Ni</i> xii, xiii, xv, xvi; <i>Ca</i> xii, xiii, xv; <i>A</i> x, xiv. P. Swings . . . . .	116
V. G. FESSENKOFF'S DYNAMICAL THEORY OF THE ZODIACAL LIGHT. Otto Struve . . . . .	129
NOTES	
CALCIUM II EMISSION IN $\nu$ SAGITTARII. Harold F. Weaver . . . . .	131
REVIEWS . . . . .	132
ERRATA . . . . .	136

### NUMBER 2

JOHN STANLEY PLASKETT, 1865-1941. R. F. Sanford . . . . .	137
COMETARY EMISSION SPECTRA IN THE VISUAL REGION. P. Swings, A. McKellar, and R. Minkowski . . . . .	142
SUPPLEMENT TO THE MOUNT WILSON CATALOGUE AND BIBLIOGRAPHY OF STARS OF CLASSES B AND A WHOSE SPECTRA HAVE BRIGHT HYDROGEN LINES. Paul W. Merrill and Cora G. Burwell . . . . .	153

MCCORMICK SPECTRAL STATISTICS. A. N. Vyssotsky and Emma T. R. Williams . . .	185
GALACTIC STRUCTURE AND KINETIC THEORY. A. N. Vyssotsky and Emma T. R. Williams	187
POINT-SOURCE STELLAR MODELS WITH OPACITY DUE TO ELECTRON SCATTERING. Louis R. Henrich . . . . .	192
ON THE NEGATIVE HYDROGEN ION AND ITS ABSORPTION COEFFICIENT. S. Chandrasekhar and Margaret Kiess Kroghdahl . . . . .	205
RADIAL VELOCITIES OF PROPER-MOTION STARS. II. Daniel M. Popper . . . . .	209
THE SPECTRUM OF AX MONOCEROTIS (HD 45910). Otto Struve . . . . .	212
CHANGES IN THE LINE CONTOURS OF $\epsilon$ URSAE MAJORIS. O. Struve and W. A. Hiltner . .	225
A NEW ORBIT FOR THE SPECTROSCOPIC BINARY $\theta^2$ ORIONIS A. Guido Münch . . . .	228
RECENT PROGRESS IN ASTROPHYSICS	
MEASURES OF TOTAL INTENSITIES OF THE LINES OF <i>H</i> AND <i>Ca</i> II IN STELLAR SPECTRA BY D. BARBIER, D. CHALONGE, and N. MORGULEFF. Otto Struve . . . . .	231
GALACTIC RESEARCH IN HOLLAND DURING 1942. Bart J. Bok . . . . .	235
REVIEWS . . . . .	240

---

 NUMBER 3

FRANK SCHLESINGER, 1871-1943. Frederick Slocum . . . . .	241
SOME COMPARISONS OF SPECTRAL CLASSIFICATIONS. Frederick H. Seares and Mary C. Joyner . . . . .	244
DISCUSSIONS OF COLOR INDEX AND SPECTRAL TYPE. Frederick H. Seares and Mary C. Joyner . . . . .	261
EFFECTIVE WAVE LENGTHS OF STANDARD MAGNITUDES; COLOR TEMPERATURE AND SP: C-TRAL TYPE. Frederick H. Seares and Mary C. Joyner . . . . .	302
SPECTROSCOPIC OBSERVATIONS OF T ARIETIS. Alfred H. Joy and Paul W. Merrill . . .	331
THE SPECTRUM OF BF CYGNI. Paul W. Merrill . . . . .	334
PARABOLIZING MIRRORS WITHOUT A FLAT. Frank E. Ross . . . . .	341
A SPECTROGRAPHIC STUDY OF THE TRIPLE SYSTEM IN 59 d SERPENTIS. Elizabeth Cornwall Tilley . . . . .	347
THE SPECTRUM OF $\alpha^2$ CANUM VENATICORUM. O. Struve and P. Swings . . . . .	361
NOTES	
CONTRACTIVE EVOLUTION OF MASSIVE STARS. G. Gamow . . . . .	498
ON WC AND WN STARS. G. Gamow . . . . .	500
ON THE LIFETIME OF CLUSTERS OF EXTRAGALACTIC NEBULAE. Merle Tuberg . . . .	501
THE SPECTRUM VARIABLE 73 DRACONIS. Geneva E. Durham . . . . .	504
INDEX . . . . .	507

AUG 13 1943

VOLUME 98

NUMBER 1

# THE ASTROPHYSICAL JOURNAL

AN INTERNATIONAL REVIEW OF SPECTROSCOPY  
AND ASTRONOMICAL PHYSICS

Founded in 1895 by GEORGE E. HALE and JAMES E. KEELER

Edited by

PAUL W. MERRILL  
Mount Wilson Observatory of the  
Carnegie Institution of Washington

HARLOW SHAPLEY  
Harvard College Observatory  
Cambridge, Massachusetts

J. H. MOORE  
Lick Observatory  
University of California

OTTO STRUVE  
Yerkes Observatory of the  
University of Chicago

JULY 1943

• ROTATIONAL DISTRIBUTION OF CH MOLECULES IN THE NUCLEUS OF COMET CUNNINGHAM (1940c) - - - - -	Andrew McKellar	1
THE PROPERTIES OF SOLAR PROMINENCES AS RELATED TO TYPE - - - - -	Edison Pettit	6
SIX-COLOR PHOTOMETRY OF STARS. I. THE LAW OF SPACE REDDENING FROM THE COLORS OF O AND B STARS - - - - -	Joel Stebbins and A. E. Whitford	20
THE STRONGER LINES OF SINGLY IONIZED DYSPROSIUM AND IDENTIFICATIONS IN THE SOLAR SPECTRUM - - - - -	Arthur S. King and Charlotte E. Moore	33
SOME USES OF THE DIRECT-INTENSITY MICROPHOTOMETER - - - - -	Robley C. Williams and W. Albert Hiltner	43
NGC 5053 AND NGC 6838 - - - - -	James Cuffey	49
DYNAMICAL FRICTION. III. A MORE EXACT THEORY OF THE RATE OF ESCAPE OF STARS FROM CLUSTERS - - - - -	S. Chandrasekhar	54
A SPECTROSCOPIC STUDY OF THE REGION OF THE DOUBLE CLUSTER IN PERSEUS - - - - -	William P. Bidelman	61
A STUDY OF THE RADIAL VELOCITY OF $\beta$ CEPHEI - - - - -	Burke Smith	82
SPECTROGRAPHIC OBSERVATIONS OF PECULIAR STARS. VI - - - - -	P. Swings and O. Struve	91
THE SPECTRUM OF 48 LIBRAE (HD 142983) - - - - -	Otto Struve	98
RECENT PROGRESS IN ASTROPHYSICS		
EDLÉN'S IDENTIFICATION OF THE CORONAL LINES WITH FORBIDDEN LINES OF Fe x, xi, xiii, xiv, xv; Ni xii, xiii, xv, xvi; Ca xii, xiii, xv; A x, xiv - - - - -	P. Swings	116
V. G. FESSEKOFF'S DYNAMICAL THEORY OF THE ZODIACAL LIGHT - - - - -	Otto Struve	129
NOTES		
CALCIUM II EMISSION IN $\nu$ SAGITTARI - - - - -	Harold F. Weaver	131
REVIEWS - - - - -		132
ERRATA - - - - -		136

THE UNIVERSITY OF CHICAGO PRESS  
CHICAGO, ILLINOIS, U.S.A.

# THE ASTROPHYSICAL JOURNAL

AN INTERNATIONAL REVIEW OF SPECTROSCOPY  
AND ASTRONOMICAL PHYSICS

Edited by

PAUL W. MERRILL

Mount Wilson Observatory of the  
Carnegie Institution of Washington

J. H. MOORE

Lick Observatory  
University of California

HARLOW SHAPLEY

Harvard College Observatory  
Cambridge, Massachusetts

OTTO STRUVE

Yerkes Observatory of the  
University of Chicago

With the Collaboration of the American Astronomical Society

Collaborating Editors:

1942-43

S. A. MITCHELL  
Leander McCormick Observatory

LYMAN SPITZER, Jr.  
Yale University

W. W. MORGAN  
Yerkes Observatory

1942-44

CECILIA H. PAYNE-GAPOSCHKIN  
Harvard College Observatory

H. N. RUSSELL  
Princeton University

F. H. SEARES  
Mount Wilson Observatory

1943-45

S. B. NICHOLSON  
Mount Wilson Observatory

D. B. McLAUGHLIN  
University of Michigan

J. A. PEARCE  
Dominion Astrophysical Observa-  
tory, Victoria

The *Astrophysical Journal* is published bimonthly by the University of Chicago at the University of Chicago Press, 5750 Ellis Avenue, Chicago, Illinois, during July, September, November, January, March, and May. The subscription price is \$10.00 a year; the price of single copies is \$2.00. Orders for service of less than a full year will be charged at the single-copy rate. Postage is prepaid by the publishers on all orders from the United States and its possessions, Argentina, Bolivia, Brazil, Chile, Colombia, Costa Rica, Cuba, Dominican Republic, Ecuador, Guatemala, Haiti, Republic of Honduras, Mexico, Morocco (Spanish Zone), Nicaragua, Panama, Paraguay, Peru, Rio de Oro, El Salvador, Spain (including Balearic Islands, Canary Islands, and the Spanish Offices in Northern Africa; Andorra), Spanish Guinea, Uruguay, and Venezuela. Postage is charged extra as follows: for Canada and Newfoundland, 42 cents on annual subscriptions (total \$10.42); on single copies, 7 cents (total \$2.07); for all other countries in the Postal Union, 96 cents on annual subscriptions (total \$10.96), on single copies 16 cents (total \$2.16). Patrons are requested to make all remittances payable to The University of Chicago Press, in United States currency or its equivalent by postal or express money orders or bank drafts.

The following are authorized agents:

For the British Empire, except North America, India, and Australasia: The Cambridge University Press, Bentley House, 200 Euston Road, London, N.W. 1, England. Prices of yearly subscriptions and of single copies may be had on application.

Claims for missing numbers should be made within the month following the regular month of publication. The publishers expect to supply missing numbers free only when losses have been sustained in transit, and when the reserve stock will permit.

Business correspondence should be addressed to The University of Chicago Press, Chicago, Illinois.

Communications for the editors and manuscripts should be addressed to: Otto Struve, Editor of THE ASTROPHYSICAL JOURNAL, Yerkes Observatory, Williams Bay, Wisconsin.

Line drawings and photographs should be made by the author, and all marginal notes such as co-ordinates, wave lengths, etc., should be included in the cuts. It will not be possible to set up such material in type.

One copy of the corrected galley proof should be returned as soon as possible to the editor, Yerkes Observatory, Williams Bay, Wisconsin. Authors should take notice that the manuscript will not be sent to them with the proof.

The cable address is "Observatory, Williamsbay, Wisconsin."

The articles in this journal are indexed in the *International Index to Periodicals*, New York, N.Y.

Applications for permission to quote from this journal should be addressed to The University of Chicago Press, and will be freely granted.

Entered as second-class matter, July 31, 1940, at the Post-Office at Chicago, Ill., under the act of March 3, 1879. Acceptance for mailing at special rate of postage provided for in United States Postal Act of October 3, 1917, Section 1103, amended February 28, 1925.

[PRINTED  
IN U.S.A.]

# THE ASTROPHYSICAL JOURNAL

AN INTERNATIONAL REVIEW OF SPECTROSCOPY AND  
ASTRONOMICAL PHYSICS

VOLUME 98

JULY 1943

NUMBER 1

## ROTATIONAL DISTRIBUTION OF $CH$ MOLECULES IN THE NUCLEUS OF COMET CUNNINGHAM (1940c)

ANDREW McKELLAR

Dominion Astrophysical Observatory, Victoria, B.C.

*Received March 20, 1943*

### ABSTRACT

From the observed profile of the  $\lambda 4315$   $^2\Delta$ ,  $^2\Pi$   $CH$  band in the spectrum of Comet Cunningham at heliocentric distance  $r = 0.54$  astronomical unit, the distribution of molecules on the rotational levels of the upper  $^2\Delta$  state is found. From this, assuming the resonance mechanism for the production of the band, the distribution among the rotational levels of the normal  $^2\Pi$  state is derived. The results indicate that nearly all the molecules exist in the two lowest rotational levels,  $K'' = 1$  and  $K'' = 2$ .

The problem of explaining the unusual rotational structure of certain molecular emission bands in the spectra of cometary nuclei, particularly the  $\lambda 3883$  and  $\lambda 4216$  band sequences of  $CN$  and also the  $\lambda 4315$  band of  $CH$ , has received considerable attention during the past several years. This problem was solved in a most satisfactory manner by Swings.<sup>1</sup> He pointed out that if it be assumed that the bands are produced by pure resonance, the exciting radiation being sunlight, consideration must be given to the fact that the wave-length distribution of this exciting radiation would be far from smooth because of the irregular contour of the solar spectrum, resulting from the presence of many strong absorption lines. Thus, even assuming a regular distribution of molecules to obtain among the rotational levels of the normal electronic state, for a given type of molecule in the head of a comet, the resonance mechanism would lead to an irregular distribution among the rotational levels of the upper electronic state and therefore to a correspondingly irregular intensity distribution for the emission band or bands produced.

In a paper<sup>2</sup> dealing with intensity measurements on emission bands in the spectra of Comets 1939d and 1940c, given at the University of Chicago Conference on Spectroscopy in June, 1942, the present writer described spectrophotometric results on  $CN$  and  $CH$  which not only qualitatively but also quantitatively gave strong support to the extension of the resonance mechanism proposed by Swings. We can therefore adopt with considerable confidence the conclusion that resonance plays the main role in the production of cometary emission bands. It would now seem that the logical extension of the above work should be to obtain directly from the observed intensity profile of a given cometary band the distribution of molecules among the rotational levels of the upper electronic state involved in its production and therefrom, assuming the resonance mechanism, to derive the relative numbers of molecules in the rotational levels of the normal electronic

<sup>1</sup> *Lick Obs. Bull.*, **19**, 131, 1941.

<sup>2</sup> *Rev. Mod. Phys.*, **14**, 179, 1942.

state. Such data as the latter will likely prove of importance in advancing our knowledge of the formation of diatomic molecules by the photodissociation of "parent" polyatomic molecules in the heads of comets and other physical processes taking place in cometary gases. The present note describes the results of such a calculation for  $CH$  using the profile of the  $\lambda$  4315 band as observed in the spectrum of Comet Cunningham (1940c) at a heliocentric distance  $r = 0.54$  astronomical unit.

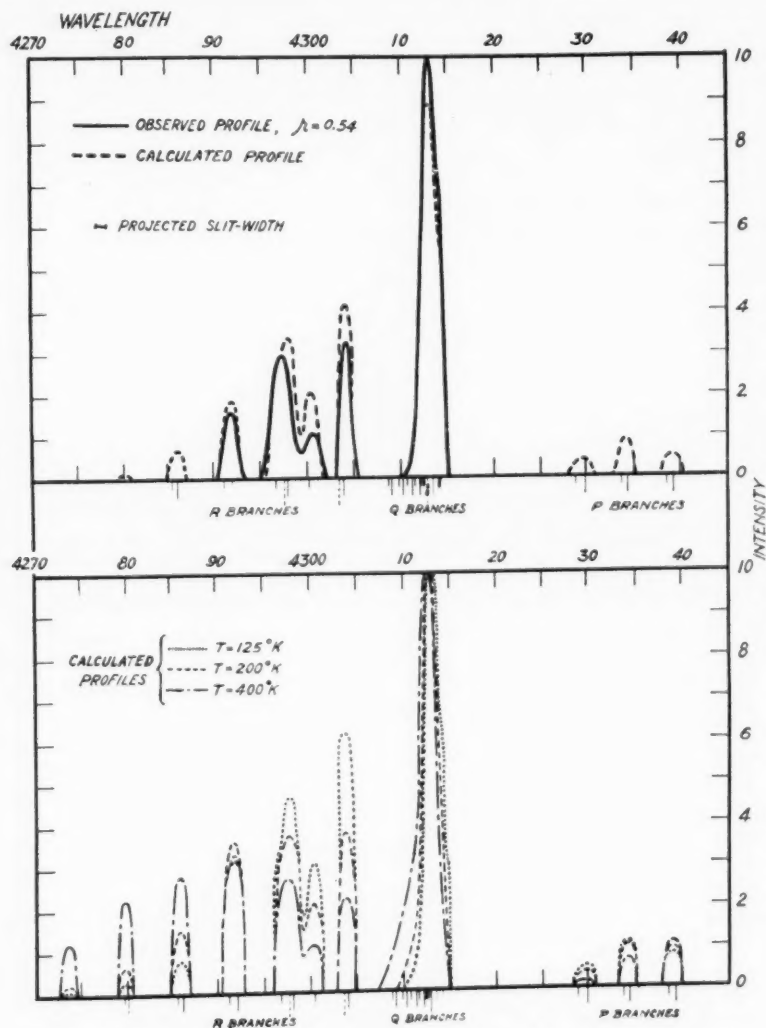


FIG. 1.—Observed and calculated profiles,  $CH$  band, Comet 1940c,  $r = 0.54$

#### METHOD AND PROCEDURE

Since details concerning the observational material and the photometry of spectrograms of Comet Cunningham (1940c) have been given in the reference in footnote 2, they need not be repeated here. It is sufficient to state that the intensity profile of the

$\lambda$  4315 band used for the present work is the mean derived from three spectrograms of the comet obtained January 1, 2, and 3, 1941, when its distance from the sun was 0.54 astronomical unit and its radial velocity with respect to the sun was  $-30.8$  km/sec. The observed profile, in which only the R and Q branches were strong enough to measure, is shown by the solid lines in the upper part of Figure 1.

The band corresponds to a  ${}^2\Delta$ ,  ${}^2\Pi$  electronic transition and is made up of four R, four Q, and four P branches as well as some weaker satellite branches. When dealing with fairly low-dispersion spectra of this band, as at present, it is convenient and justifiable to consider the two  $R_1$  branches together as one, the two  $R_2$  branches as one, and similarly for the Q and P branches. Thus, disregarding all but a few lines of the satellite branches, we have essentially only double R, Q, and P branches. The laboratory wave lengths of the lines of the branches considered in this way are indicated at the bottom of the upper and of the lower parts of Figure 1. This is equivalent to neglecting the spin doubling of the rotational levels of the  ${}^2\Delta$  and  ${}^2\Pi$  states. We shall also, in dealing with the populations of the rotational levels, neglect the  $\Lambda$ -doubling and consider the sum of all the substates with, say,  $K'' = 2$  as the  $K'' = 2$  state.

The relative populations of the rotational levels of the upper,  ${}^2\Delta$ , state were found empirically as those which best reproduced the observed band profile. This could be done directly, but, in the present case, the theoretical profile expected on the basis of a Maxwell-Boltzmann distribution of molecules among the states for a temperature of  $250^\circ$  K was calculated. By comparing this with the observed profile the modifications in the distribution necessary to obtain the best fit were readily made. In carrying out these modifications more weight was given to the R branches and less to the Q branches, since the former were quite well resolved. It might be noted that the empirically determined and the calculated profiles of the band shown with the observed profile in Figure 1 are made up of lines which are plotted as rectangles of height equal to the intensity, width equal to the projected spectrographic slit-width, and having their corners suitably rounded. The results of the empirical method outlined are shown both in the upper part of Table 1 and in the upper part of Figure 1. In the table, the relative numbers of CH molecules in the rotational states  $K' = 2, 3, 4$ , etc., are listed. For comparison, there are shown the relative populations of the upper states calculated on the assumptions that thermal equilibrium at the temperatures  $T = 125^\circ$  K,  $200^\circ$  K, and  $400^\circ$  K exists among the rotational levels of the normal  ${}^2\Pi$  state and that the rotational levels of the upper  ${}^2\Delta$  state are populated from them by Swings's resonance mechanism. Figure 1 shows, in the upper part, a comparison between the observed CH band profile and that empirically obtained as outlined. Again, as a comparison, the profiles derived, assuming thermal equilibrium at the above three temperatures for the normal-state levels, are given in the lower section of the figure.

The second and final step is, with the aid of the resonance mechanism, taking into consideration both the intensity contour of the solar spectrum in the  $\lambda$  4300 region as effectively shifted by the comet's radial velocity and the  $i$ -factors of the molecular transitions involved, to derive the distribution of molecules among the rotational levels of the normal  ${}^2\Pi$  state which would yield the already determined relative populations in the upper states. This was done by solving for the  $n''$ 's a number of linear simultaneous equations (in the present case five) of the form:

$$\begin{aligned} n'_K = & (I_{R_1} \cdot i_{R_1} + I_{R_2} \cdot i_{R_2} + I_{R_{Q_{21}}} \cdot i_{R_{Q_{21}}}) n''_{K-1} \\ & + (I_{Q_1} \cdot i_{Q_1} + I_{Q_2} \cdot i_{Q_2} + I_{Q_{R_{12}}} \cdot i_{Q_{R_{12}}} + I_{Q_{P_{21}}} \cdot i_{Q_{P_{21}}}) n''_K \\ & + (I_{P_1} \cdot i_{P_1} + I_{P_2} \cdot i_{P_2}) n''_{K+1}. \end{aligned}$$

The first term on the right-hand side takes account of the various ways in which the upper state designated by the rotational quantum number  $K$  can be populated by the R

branches and the second and third terms by the Q and P branches, respectively;  $n_K'$  is the relative number of molecules in the rotational state  $K$  of the upper,  ${}^2\Delta$ , electronic state, while  $n_{K-1}'$ ,  $n_K'$ , and  $n_{K+1}'$  are the relative populations of the rotational levels  $K-1$ ,  $K$ , and  $K+1$  of the normal,  ${}^2\Pi$ , electronic state.  $I_{R_1}$  is the intensity of the solar spectrum<sup>3</sup> at the wave length of the band line  $R_1$  ( $K-1$ ), considering the effect of the comet's radial velocity, and the other  $I$ 's are the intensities of the solar spectrum at the effective wave lengths of the appropriate band lines of the branches designated by the subscripts. Here  $i_{R_1}$  is the intensity factor of the R branch transition  $R_1$  ( $K-1$ ), and the other  $i$ 's are corresponding intensity factors for the indicated rotational transitions. These factors are functions of the rotational quantum numbers.<sup>4</sup> Hence the numerical values of all the terms in brackets are directly determinable and the equations readily solved.

#### RESULTS AND DISCUSSION

The results of the first part of the above procedure, as already mentioned, are shown in Figure 1 and the upper part of Table 1. The lower section of the table gives the relative populations derived for the normal  ${}^2\Pi$  state. The relative populations in the upper  ${}^2\Delta$  state, assuming the resonance mechanism to be the only one operative, simply reflect the molecular distribution among the rotational levels of the ground electronic state in which, it would be expected, exist the great bulk of the  $CH$  molecules in the head of the comet. If the rotational levels of the upper electronic state are being appreciably populated by any means other than resonance, as, for example, the possible formation of  $CH$  in the  ${}^2\Delta$  state as a product of the dissociation of a polyatomic molecule, the distribution of molecules we have found for the rotational levels of the  ${}^2\Pi$  state will be in error. In amount this error will vary in a direct way as the effectiveness of these other mechanisms. In the light of our present knowledge it would seem, however, that the effect of mechanisms other than resonance should be small.

For purposes of comparison, the distributions of  $CH$  molecules assuming temperature equilibrium at  $T = 125^\circ \text{K}$ ,  $200^\circ \text{K}$ , and  $400^\circ \text{K}$  are shown also for the  ${}^2\Pi$  state in the lower part of the table. It is seen that the distribution of molecules derived from the band profile does not correspond to a Maxwell-Boltzmann distribution at any temperature, although fairly good agreement is apparent with that at  $T = 125^\circ \text{K}$  except for the  $K'' = 2$  level. For this level the population is about twice the value calculated on the basis of thermal equilibrium. That no such agreement holds is not surprising. Indeed, since the pressure is so low in the heads and even nuclei of comets that atomic and molecular collisions must be relatively rare, it would be surprising to find an energy distribution among the molecules corresponding to temperature equilibrium.

According to the present results, nearly all the  $CH$  molecules exist in the two lowest rotational states of the normal electronic state. Two inferences may be drawn from this: Either the molecules are largely formed, possessing very little rotational energy, by the dissociation of polyatomic "parent" molecules, or, if upon formation they do possess several quanta of rotational energy, the frequency of their release of such energy by pure rotational transitions involving the emission of far infrared radiation must be much greater than the frequency with which they acquire rotational energy by absorption of radiation or by collisions. Whether or not the first of these holds, pure rotational transitions must be taking place in the  $CH$  molecules with emission in the far infrared. It therefore seems odd that such a definite discontinuity in population should occur between  $K'' = 3$  and  $K'' = 2$  or, to put it differently, that the  $K'' = 2$  state should be so highly populated. Unless  $CH$  molecules are constantly being formed in the  ${}^2\Pi$  state possessing one quantum of energy above the lowest possible, no very obvious reason for

<sup>3</sup> This is obtainable from the *Photometric Atlas of the Solar Spectrum* by Minnaert, Mulders, and Houtgast, Utrecht, 1940.

<sup>4</sup> See, e.g., Jevons, *Report on Band Spectra of Diatomic Molecules* (London: Physical Society, 1932), pp. 133 ff.

the relatively high population of the  $K'' = 2$  level is apparent. Perhaps further spectrophotometric work on CH bands for other comets and at other heliocentric distances may clarify this point.

It would be very interesting to observe simultaneously, if it should be possible in the case of some future bright comet, the (0, 0) bands of either or both the  $^2\Sigma$ ,  $^2\Pi$  transitions of CH ( $\lambda$  3870 and  $\lambda$  3143) as well as the  $\lambda$  4300  $^2\Delta$ ,  $^2\Pi$  band discussed here. This would

TABLE 1  
RELATIVE POPULATIONS OF ROTATIONAL LEVELS IN THE EXCITED  
( $^2\Delta$ ) AND NORMAL ( $^2\Pi$ ) ELECTRONIC STATES OF CH FOR COMET  
CUNNINGHAM (1940c) AT  $r=0.54$  A.U.

$K'$	UPPER $^2\Delta$ STATE			
	Relative Populations from Observed Band Profile	Relative Populations for Temperature Equilibrium in Normal State		
		$T = 125^\circ \text{ K}$	$T = 200^\circ \text{ K}$	$T = 400^\circ \text{ K}$
2.....	1.00	1.00	1.00	1.00
3.....	0.96	0.70	0.88	1.11
4.....	0.35	0.36	0.67	1.18
5.....	$\leq 0.11$	0.07	0.23	0.63
6.....	$\leq 0.02$	0.02	0.11	0.46
7.....	0.00	0.00	0.04	0.26

$K''$	NORMAL $^2\Pi$ STATE			
	Relative Populations from Observed Band Profile	Relative Populations for Temperature Equilibrium in Normal State		
		$T = 125^\circ \text{ K}$	$T = 200^\circ \text{ K}$	$T = 400^\circ \text{ K}$
1.....	1.00	1.00	1.00	1.00
2.....	1.01	0.52	0.67	0.82
3.....	0.20	0.20	0.36	0.60
4.....	$\leq 0.12$	0.05	0.16	0.40
5.....	$\leq 0.02$	0.01	0.06	0.24
6.....	0.00	0.00	0.02	0.15
7.....	0.00	0.00	0.00	0.06

not be easy, because both these bands are somewhat less intense than the  $\lambda$  4300 band, the region around the origin of the  $\lambda$  3870 band is overlapped by the strong  $\lambda$  3883 band of CN, and the  $\lambda$  3143 band is in the astronomical far ultraviolet. However, if this could be done, and if the resonance mechanism is greatly predominant in producing all the bands, those from all three transitions should, by the treatment used here, yield populations for the rotational levels of the normal electronic state which are in agreement with one another.

It is planned to carry out the present type of study on the CN bands in the spectra of Comets 1939d and 1940c and probably Comet Whipple II of which spectrograms are currently being obtained.

## THE PROPERTIES OF SOLAR PROMINENCES AS RELATED TO TYPE\*

EDISON PETTIT

Mount Wilson Observatory

Received February 2, 1943

### ABSTRACT

*Comparative properties of prominences.*—After a brief historical introduction, types of prominences are discussed according to (1) association with sunspots, (2) origin, (3) motion, (4) structure. A description of individual types and their subdivisions follows.

*Arrangement of classes.*—The original classes, active (I), eruptive (II), sunspot (III), tornado (IV), quiescent (V), are retained, but (V) is placed first in the diagram (Fig. 1). Class VI, coronals, has been added. These classes are subdivided and arranged diagrammatically to show connected characteristics.

*Quiescent prominences (class V)* lack external streamers and have a palisaded structure not found in other types.

*Coronal prominences (class VI)* form in space above the solar surface and rain down upon it to definite centers of attraction. Prominences like these often occur in groups over sunspots; they are then classified IIIa and IIIb. Coronal prominences may appear in the last stages of development of the active type, Ic.

*Active prominences (class I)* include the interactive, type Ia, in which two prominences interchange matter along streamers or by the exchange of knots; the common active type, Ib, in which streamers and knots are drawn into a center of attraction on the sun; and the coronal active type, Ic, in which the activity of the center of attraction becomes so great that it also draws coronals from space.

*Eruptive prominences (class II)* are divided into three subdivisions. Quasi-eruptives, type IIa, are active or active sunspot prominences which are pulled bodily into the center of attraction or spot area. Common eruptives, type IIb<sub>1</sub>, and eruptive arches, type IIb<sub>2</sub>, are active or active sunspot prominences which rise from the sun and disappear at great distances above the solar surface. The catalogue of eruptive prominences, types IIb<sub>1</sub> and IIb<sub>2</sub>, now contains 65 entries. Maximum heights are distributed about uniformly between 100,000 and 500,000 km; only about 23 per cent are outside these limits. The average duration is 2<sup>h</sup> 31<sup>m</sup>. It is estimated that about 400 eruptive prominences per year occur at sunspot maximum and 25–50 near minimum. Although the angle of ejection is usually small, one of 63° has been observed.

*Sunspot prominences (class III)* have nine subdivisions. Cap prominences, type IIIa, form above the spot area like a low cloud cap. The common coronal sunspot type, class IIIa, consists of a number of coronals converging to the spot area in a fanlike pattern. The looped coronal sunspot type, class IIIb, is like IIIa, except that the coronals form strongly curved arcs or complete loops. The active sunspot type, class IIIc, consists of a prominence like one of class Ib pouring into a sunspot area. The common surges, type IIId<sub>1</sub>, rise from and sink back into a spot area without losing continuity, like an elastic band. Expanding surges, type IIIc<sub>2</sub>, break into a spray and begin to fade before returning to the spot area. The ejections, type IIIe, are small lumps of chromospheric matter which are ejected by the spot areas and which do not return. Secondary eruptions, type IIIf, arise from other prominences associated with sunspots. Coronal clouds, type IIIg, form in space above a spot area and rain streamers upon it. An illustration is given (Pl. III).

*Tornado prominences (class IV)* include the columnar (type IVa) and skeleton (type IVb). They disappear when the rotational velocity becomes too great, or they may develop the properties of active or eruptive prominences.

*Typical prominences of uncertain properties.*—Some very faint prominences of large size and swirls in which a prominence rotates like a whirlpool and has a motion of translation are described. Plumes which seem to be quite stable have been studied. Their stems show no rotation when tested for Doppler displacement in the spectrum.

*Streamer characteristics.*—The formation of streamers is described. Their lengths vary from a few thousand to several hundred thousand km; their widths vary from 500 to 5000 km, averaging about 1000 km. Broad streamers rapidly deplete a prominence.

A discussion of the classification of prominences necessarily requires a general knowledge of all the phenomena involved. This knowledge, acquired over a long period, can best be summarized in a brief comparative description.

To make the ideas clear and to give a visual conception, at the beginning of the dis-

\* Contributions from the Mount Wilson Observatory, Carnegie Institution of Washington, No. 679.

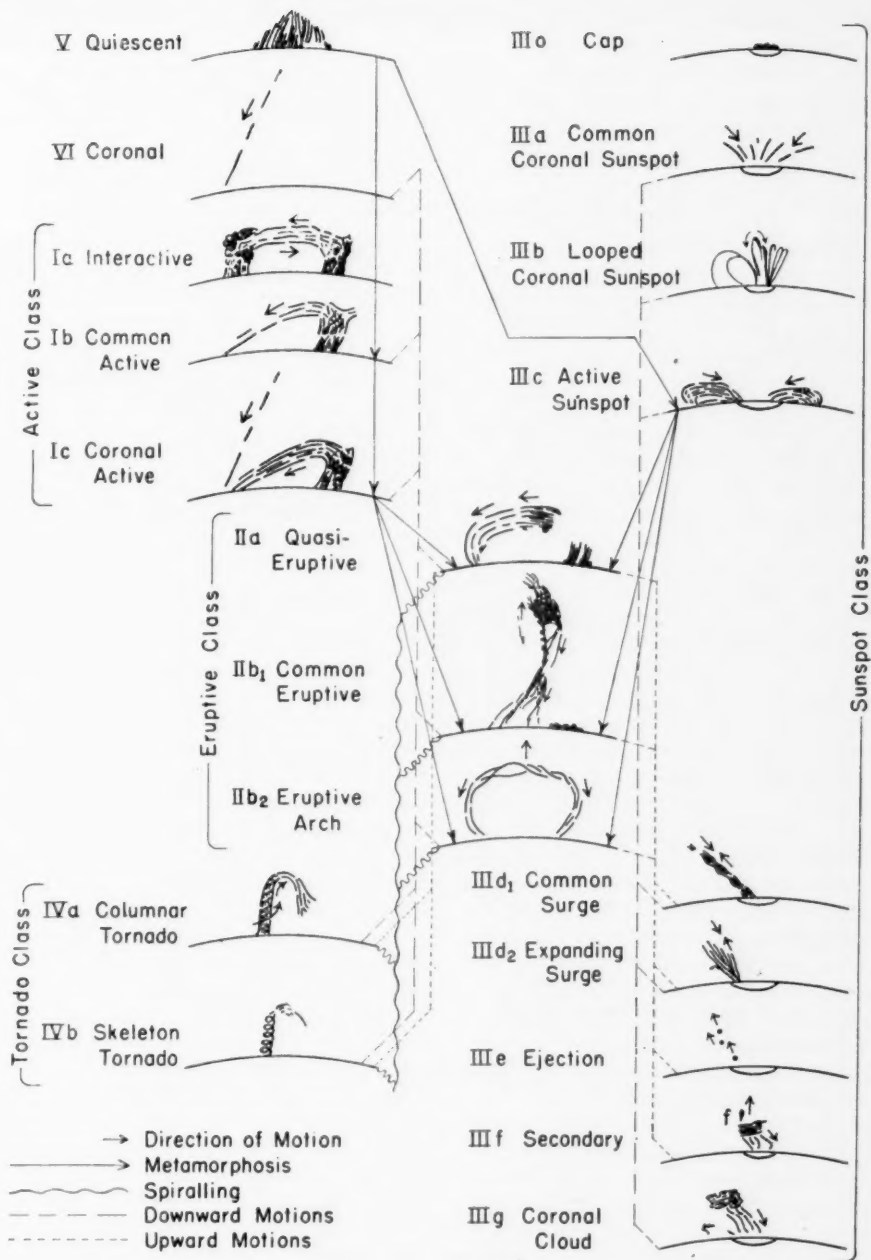


FIG. 1.—Types of prominences illustrated by drawings from photographs. While most types are found isolated as shown, several of the sunspot class are frequently found together. In class III<sub>f</sub> the part of the prominence classified is indicated by the letter *f*.

cussion we introduce Figure 1, which shows the various types and their relationships. The actual forms of prominences are quite varied, but those believed to be the most common are indicated. Most types are usually found isolated, as shown in the figure, although subdivisions *o*, *d*<sub>1</sub>, *d*<sub>2</sub>, *e*, *f*, and *g* of the sunspot type (III) are generally combined with subdivisions *a*, *b*, and *c*. The secondary eruption III*f*, which always emerges from another sunspot prominence, is indicated by *f* in the figure.

#### THE COMPARATIVE PROPERTIES OF PROMINENCES

Soon after the invention of the wide-slit method of examining prominences spectroscopically two distinct divisions were recognized, the one called "quiescent" or "hydrogenous," and the other "eruptive" or "metallic." In each division the first alternative designation refers to motion, the second to the spectrum.

The term "quiescent" seems to have been applied to any prominence in which casual observation revealed no bodily motion; otherwise the term "eruptive" was applied. Indications of great activity during which sheaves of streamers connected a prominence with the sun were not regarded as a differentiating factor.

The chief characteristics of the visual spectrum of a quiescent prominence thus defined are the Balmer series of hydrogen and D3 of helium. The importance of the H and K lines in the prominence spectrum was not known for many years, and the *He* I lines  $\lambda$  6678 and  $\lambda$  7065 are difficult to see, hence the designation "hydrogenous" was applied to quiescent prominences.

We now distinguish between "eruptive" and "metallic" prominences. Among the earliest observations a few instances are recorded in which a quiescent prominence which we should now call "active" or "active sunspot" would suddenly and for no apparent reason begin to rise and then, after a short time, fade out at an elevation which amounted sometimes to several hundred thousand kilometers. For these prominences we have retained the designation "eruptive,"<sup>1</sup> although after the motion begins their spectra are the same as before and would therefore previously have identified them as hydrogenous.

Metallic prominences appear only over sunspots. A sunspot prominence is more complicated than any other, as indicated by Figure 1. As was first pointed out by the author,<sup>2</sup> the prevalent motions are downward into the spot area. The principal exception is the subdivision of the sunspot class which we now call "surges," which rise from the spot area with high velocity but, unlike the eruptives, disappear by retraction into the sun. Surge prominences, which rise through the chromosphere, may have a higher temperature than other types, for they are often very bright, and the chromospheric lines ordinarily just below the threshold of visibility appear in the spectrum. In the visual spectrum these lines are principally the *b*-group of magnesium and iron; the iron lines  $\lambda\lambda$  4923, 5018, 5234, 5276, 5316, 5362, 6678; the D lines of sodium; and  $\lambda\lambda$  5015, 6678, and 7065 of helium. Hence the term "metallic" was applied to these prominences, which, because of their upward motion, were also identified with the eruptives. Thus the spectrum may tell us that a prominence is associated with a sunspot, but it is of little service in the problem of classification.

Aside from the quiescent and eruptive prominences, the only other type recognized by the early visual observers was the twisted column. C. A. Young called such objects cyclones,<sup>3</sup> or "whirling waterspouts, capped with a great cloud," and seemed to put them into the category of eruptive prominences without separate classification. Since the forms of the members of this group commonly simulate tornadoes, we have adopted this designation.<sup>4</sup>

The available differentiating factors which make possible a classification of promi-

<sup>1</sup> *Pub. Yerkes Obs.*, 3, 206, 1925.

<sup>2</sup> *The Sun*, pp. 223, 224, 1910.

<sup>2</sup> *Pub. Yerkes Obs.*, 3, 227 and 232, 1925.

<sup>4</sup> *Pub. Yerkes Obs.*, 3, 205, 1925.

nences in groups with distinguishing and related characteristics may be listed as follows: (1) association with sunspots; (2) origin—whether a prominence arises from the chromosphere or is formed in coronal space; (3) motion; (4) structure.

Association with sunspots is the first characteristic used to separate all prominences into two groups. Prominences associated with sunspots are so characteristic that one can frequently predict that a spot is about to appear on the eastern limb by the prominence above it which appears first.

While origin has been of great service in subdividing the sunspot class, it is of little value in classifying the other prominences, which include the great majority. In a sense the eruptives have their origin in the active and active sunspot prominences, but their development is regarded as a transformation. We must therefore look for the origin of the material of the two types from which the eruptives are formed.

Although formerly it was thought that all prominences arise from the chromosphere, we now know that many do not, and we are in doubt about the origin of others. Of the many subdivisions of the sunspot type only the surges and ejections are known to be formed in the spot area. They definitely rise from the chromosphere and can therefore be called chromospheric. Secondaries arise from prominences connected with sunspots. The origin of cap prominences and of the wings of the active sunspot prominences is still in doubt. All the other sunspot prominences are formed in coronal space, from which streamers of chromospheric gases, which we shall call coronals, are drawn into the spot area.

The known chromospheric and coronal prominences form and develop very rapidly, and their entire life-history can be observed in a short space of time, often only a few minutes. All other prominences, except the eruptives and secondaries, have a period of development measured in days and, because of the intermittent character of the observations and the disconcerting effect of solar rotation, their origin is still a matter of doubt.

Motion and structure are intimately related; hence, in discussing their relation to the problem of classification, they are conveniently treated together. The motions of prominences are: (1) motion of the prominence as a whole; (2) motions in streamers torn from a prominence which enter the chromosphere at a center of attraction or sunspot area, or move directly into another prominence; also motions of coronals; (3) motions of knots (small lumps) which behave like the streamers in (2), moving sometimes along a streamer, sometimes along a path where no streamer exists; (4) internal turbulence; (5) spiralling.

Prominences showing the least motion are characterized by the term "quiescent." They have no external streamers, and, in the best examples, their internal structure has a palisaded appearance.

Prominences of the active and eruptive types are characterized by filamentary detail within which are found numerous condensations in motion. If the external streamers and moving knots become more active, the internal structure becomes coarser, and the whole prominence begins to move. If its motion carries it over into a center of attraction, we call it "quasi-eruptive," and if it rises directly into space and fades away it is called "eruptive."

The only other bodily movements on a large scale are the slow displacements due to growth or attraction to the chromosphere which may culminate in a quasi-eruption. No bodily movement of one prominence completely into another has ever been observed.

Helical structure occasionally appears in prominences in a highly active or eruptive state. The most perfect specimens, however, are found in the tornadoes, which look like sections of a screw or of a twisted rope. No horizontal bodily movement has so far been observed in tornadoes.

The foregoing considerations lead to the classification of prominences into six groups: I, active; II, eruptive; III, sunspot; IV, tornado; V, quiescent; and VI, coronal. These

major groups and several subdivisions have been discussed in earlier papers.<sup>5</sup> The application of the motion-picture method to observations with the interference polarizing monochromator<sup>6</sup> has recently led to a better understanding of the known subdivisions and has indicated others.

#### AN ARRANGEMENT OF TYPES

The arrangement of types shown in Figure 1 is based upon the following considerations. All prominences are first divided broadly into those connected and those not connected with spots. Those not associated with spots are found to be, for the most part, associated with centers of attraction located anywhere on the solar surface. We can, therefore, arrange most prominences in order of the increasing activity of the spot area or of the center of attraction associated with them.

Metamorphosis offers a more logical sequence. Thus, quiescent prominences may develop into the active type, active into coronal active, and coronal active into quasi-eruptive or eruptive. Quiescent prominences may also develop into sunspot active, followed by the same development as for the active type. These sequences are shown by arrows (Fig. 1).

Prominences can also be arranged according to certain common characteristics: (1) spiralling, very infrequently seen in active or active sunspot types, first becoming conspicuous in the eruptives and most pronounced in the tornadoes; (2) downward motion (Fig. 1), beginning in the coronals or coronal sunspot prominences and found in all other types except the ejections and secondaries; (3) predominantly upward motion, beginning in the quasi-eruptives and passing down to the coronal cloud type, on the one hand, and through the tornadoes, on the other. These common characteristics of type are indicated in the diagram by a wavy line for spiralling, dashed line for downward motions, and dotted line for upward motions. We shall now discuss the characteristics of the various types in more detail.

#### QUIESCENT PROMINENCES (CLASS V)

Class V, originally placed last, is now placed first, for this seems to be its logical place in the sequence of development of a prominence. Since all the other classes still appear in the order originally given, the designation V is retained.

The term "quiescent" is a relative one, indicating a minimum of activity. Experience shows that activity indicates impending destruction and that an active prominence cannot long endure; hence duration may be considered as a criterion of quiescence. A long-lived prominence, such as one of the extended ribbon-like structures<sup>7</sup> sometimes seen on the disk, may, however, at times be active in certain sections; and the interval of quiescence may be short. A better criterion for class V is the absence of external streamers entering centers of attraction on the chromosphere. This absence of external streamers indicates that no centers of attraction are disturbing the prominence and, with a few exceptions, is an indication of quiescence. The surges, secondaries, ejections, and cap prominences of the sunspot class are without external streamers, but their proper classification is seldom in doubt. Tornadoes also are often found without external streamers, but with good definition they will not be mistaken for quiescent prominences. Streamers in line with a prominence are difficult to see, and prominences with such streamers must be identified by other means.

The external outline of a quiescent prominence (class V) will remain practically un-

<sup>5</sup> Pettit, *Mt. W. Contr.*, Nos. 451 and 552; *Ap. J.*, **76**, 9, 1932; *ibid.*, **84**, 319, 1936; McMath and Pettit, *Mt. W. Contr.*, Nos. 568 and 597; *Ap. J.*, **85**, 279, 1937; *ibid.*, **88**, 244, 1938.

<sup>6</sup> Pettit, *Pub. A.S.P.*, **53**, 171, 1941.

<sup>7</sup> The Meudon observers have described the gross properties of these "alignments" which may endure for several solar rotations; see M. et Mme L. d'Azambuja, *L'Astronomie*, October, November, and December, 1941.

changed for hours at a time. Turbulence, as indicated by the structure, is almost absent. The best examples of prominences of class V have a palisaded appearance which resembles a forest of withes. In the degenerate form these withes may be widely separated and faint, but in the more brilliant prominences they are closely packed. At times as many as 20 or 30 of these withes appear, their individual dimensions changing little over a period of an hour. Their widths vary, but 2000 km is a representative value. As the figure shows, the withes are not necessarily connected with the chromosphere. Whether there is any upward movement of gases in the withes is still unknown. Active prominences, although frequently mistaken for quiescent, never show this withe structure.

The "haystack" is probably the most common form of quiescent prominence. The drawing in Figure 1 represents such a prominence which appeared in position angle  $153^\circ$  on August 21–23, 1942. Because of the prevalence of centers of attraction, quiescent prominences are not often found in the contemporary sunspot zones. It is difficult to identify quiescent prominences on the disk by means of their structure or streamers, since little structure is visible, only the most prominent streamers appearing as absorption markings.

#### INTERACTIVE PROMINENCES (CLASS Ia)

Interactive prominences are much less frequently seen than the common active type, Ib. Streamers and knots moving from one prominence to another indicate that electric charges of either sign can exist within a prominence if we assume that electric fields are the motive forces. This type is, therefore, of considerable theoretical interest. Sometimes several prominences are connected by streamers. Occasionally a tornado participates as a component of an interactive prominence.

An examination of the eight best series of spectroheliograms of interactive prominences taken at the Yerkes and Mount Wilson observatories was made with the blink comparator. The streamers revealed only unidirectional motion; i.e., there was no interchange of streamers. This result was, however, inconclusive, since in each prominence only one or two streamers showed knots, streamer ends, or sections from which motion could be recognized.

Finally, a film obtained with the monochromator of the interactive prominence which appeared in position angle  $83^\circ$  on August 7–8, 1942 (Pl. Ia), showed two prominences with two connecting streamers along which the material was moving in opposite directions, thus demonstrating clearly an interchange of prominence gases. Like the ordinary active prominences, the interactive type may also pass into the eruptive class, as was recently observed.<sup>8</sup>

#### COMMON ACTIVE PROMINENCES (CLASS Ib)

An active prominence is a mass of crossed and interlacing filaments in which brighter fragments can be seen. If the external streamers are few and unimportant, the structure of the prominence will be closely woven or indistinct; there may be a suggestion of palisading. If there are several strong streamers, the internal structure is coarse and may be entirely rent apart.

Active prominences are by far the most prevalent on the sun. Streamers connecting them with the chromosphere provide the principal means of classification. Quasi-eruptives and eruptives, even though retaining forms similar to the active prominences from which they are derived, can readily be distinguished by their motions. The active sunspot type, which is similar to the common active type, may appear when the spot cannot be seen on the limb but is usually found with other subdivisions of the sunspot class, which makes identification easy. The fact that active prominences are found from pole to pole often differentiates them from the active sunspot type. If several streamers leave an active prominence they enter the chromosphere in one or two small areas comparable

<sup>8</sup> Pettit, *Pub. A.S.P.*, 54, 253, 1942.

in size to that of a large sunspot or small spot group; the diameter of these centers of attraction seldom exceeds  $3^\circ$ . Observations on the disk have as yet revealed no marking in the chromosphere which can be identified with a center of attraction.

We cannot tell observationally whether the formation of a center of attraction precedes the formation of charges of the opposite sign in active prominences. Nevertheless, material is nearly always torn from the top of a prominence before it is from lower regions much nearer the center of attraction. This suggests that normally an electric field exists at the top of a prominence but is revealed only when the center of attraction develops.

*Streamer characteristics.*—The formation of knots and streamers usually follows this pattern: A portion of the prominence becomes frayed and torn, several shreds pointing in one direction. An end of a shred, some 2000 km wide, breaks away, forming a knot which moves along an arc, lengthening as it proceeds downward into the chromosphere. Sometimes the frayed end lengthens for a while, forming a streamer instead of a knot. This streamer section then breaks away and moves endwise into the chromosphere. If no break occurs, the streamer grows like a tendril and extends downward into the chromosphere. It then either fades out or breaks away from the prominence and is sucked into the chromosphere like a retracting rubber band, fading as it proceeds. Knots may also form upon a streamer and move with it into the center of attraction. Other streamers, knots, and streamer sections may form and follow trajectories a little above or below the first one, but all enter the chromosphere at nearly the same point.

The length of a streamer varies enormously—from a few thousand kilometers in small active prominences to several hundred thousand in the eruptives. The width seems to average about 1000 km, measures of 500 km being common, those of 4000 or 5000 km rare.

Broad streamers rapidly deplete a prominence, as was illustrated by the active prominence in position angle  $298^\circ$  on July 20, 1941, which came over the east limb as an interactive on July 6. Plate Ib shows the interactive phase on July 13. Two days later, two centers of attraction developed between the components, making two independent active prominences, and the forward member reached the west limb on July 20. Suddenly another center of attraction of great intensity formed near this component. Plate Ib (2, 3, 4) shows exposures taken with intervals of 6 minutes and 1 hour. The two streamers leaving the top are each 5000 km wide and about 85,000 km long. The prominence, 70,000 km high when the action started, declined to a height of 46,000 km within an hour and became fainter.

Spiralling is seen occasionally in streamers of active prominences but is an infrequent phenomenon. Although the most obvious explanation is the presence of a magnetic field, this does not account for the fact that what appear to be neighboring streamers do not spiral.

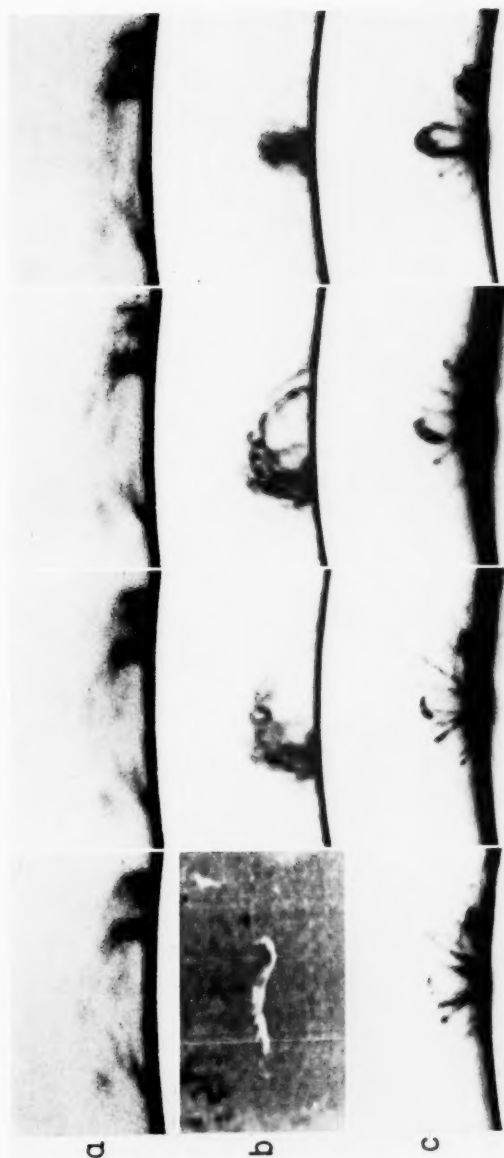
#### CORONAL ACTIVE PROMINENCES (CLASS Ic) AND CORONALS (CLASS VI)

As the streamers from a class Ib prominence become more numerous, indicating an increase of intensity of the center of attraction, occasionally long streamers of slight curvature moving with speeds of 100–200 km/sec come into the center of attraction from the coronal region. They may appear at elevations of about 150,000 km and usually move the entire distance to the center of attraction with constant velocity. If a change in velocity does occur, the two laws of motion are fulfilled.<sup>9</sup> These streamers of chromospheric gases we shall call "coronals."

While coronals are a distinct class of prominences, they are seldom found singly but more frequently occur in groups forming prominences of either the sunspot or advanced active type. Naturally we could assign all prominences made principally of coronals to subdivisions of class VI, but usage and the fact that these subdivisions are the most

<sup>9</sup> McMath and Pettit, *Mt. W. Contr.*, No. 597; *Ap. J.*, 88, 244, 1938.

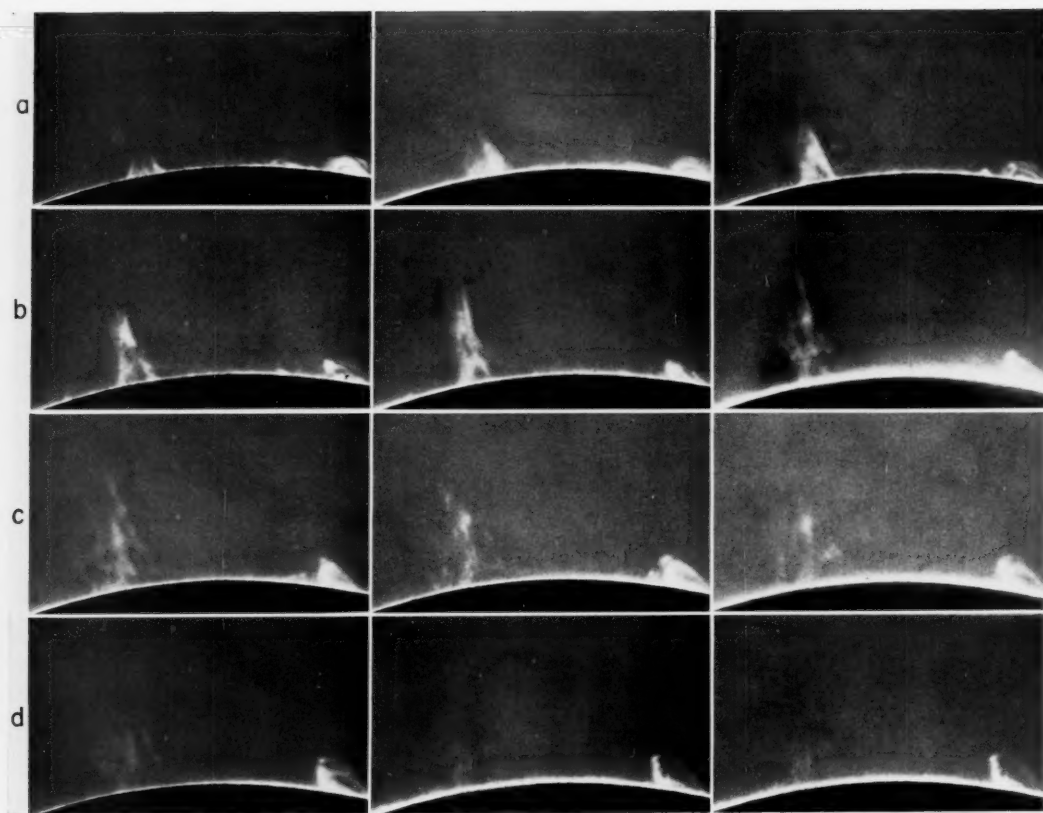
# PLATE I



## DEVELOPMENT OF PROMINENCES

(a) Interactive prominence (class Ia) of August 7, 1942; exposure intervals, 5 minutes. Upper streamer moved to right, lower streamers to left. (b) Development of an active prominence: (1) July 13, 1941; on disk as interactive (class Ia). (2, 3) July 20; interval, 6 minutes; western component, shredded by center of attraction, becomes active (class Ib). (4) Exposure 1 hour later shows depletion of prominence due to shredding by center of attraction. (c) May 8, 1941; development of double loop in class III/6 sunspot prominence; 5-minute intervals. Two dots grow into two overlapping loops, together forming a brilliant arch.

## PLATE II



EXPANDING SURGE (CLASS III d<sub>2</sub>) PHOTOGRAPHED ON AUGUST 12, 1941

The initial protuberance on the chromosphere had a ragged surface. The prominence expanded as it rose, and faded as it sank back into the chromosphere. An active sunspot prominence (class III c) shows on the right. Exposures at intervals of 7 minutes.

common of the sunspot class, on the one hand, and are found at a critical stage of development in the active type, on the other, make such an assignment an irrational one. When found with active prominences, coronals differ from the other streamers in that they brighten as they approach the center of attraction.

The term "coronal" was chosen for the following reasons. Like the ordinary features of prominences, coronals can be photographed in the hydrogen and calcium lines. Their origin in coronal space probably means that chromospheric gases exist there in the unexcited state, invisible until a center of attraction develops sufficiently to excite them. Though invisible, these gases are as much a real part of the corona as those emitting the coronal line spectrum; indeed, these chromospheric gases of the corona must bring with them the other coronal gases when they are excited by a center of attraction and are pulled into it.<sup>10</sup> Coronals are also found entering the sun even though no other prominence is present, indicating that centers of attraction may develop anywhere on the solar surface independently of the prominences.

Coronals fall into the chromosphere in an irregular and haphazard manner. None, however, have been observed to enter another prominence directly. Several of them may follow one another along the same path, or they may take different paths, or come in sheaves, so to speak. Some centers of attraction, although strong enough to convert an active prominence into a quasi-eruptive, do not receive coronals. If observations were continued after a center of attraction had destroyed an active prominence in this manner, it is possible that coronals would be found coming into it. This result has not been reported as yet.

These circumstances all point to a localized distribution of chromospheric gases in the corona. The appearance of coronals over spot areas (as slightly curved streamers or arches) is more persistent than over centers of attraction. Even over spots, however, there are periods of quiescence when no coronals form.

#### QUASI-ERUPTIVE PROMINENCES (CLASS IIa)

If the center of attraction which is shredding an active prominence becomes still more active, great ribbons are torn off. The streamers become more sharply curved and may enter the chromosphere, making an angle with it exceeding  $100^\circ$ , although ordinarily this angle is about  $60^\circ$ . In this stage of development the streamers commonly rise somewhat before entering the chromosphere. At this time the whole body of the prominence may tear away from the trunk which connects it with the chromosphere, rise some distance in a sharply curved arc higher than any of the streamers, then, moving downward, enter the center of attraction. The effect is like the cracking of a whip. Active sunspot prominences also become quasi-eruptive and exhibit the same phenomena.

The quasi-eruptive stage was first observed in the "sigma" prominence<sup>11</sup> of class Ib, September 23, 1919, and again in the class IIIc prominence<sup>12</sup> of August 27, 1935. The fact that this phenomenon has been observed in a number of other prominences, some of which rose to considerable heights,<sup>13</sup> suggests that this type is a "missing link" between the class Ib or IIIc and the true eruptives. It has therefore been styled quasi-eruptive.<sup>13</sup>

The argument for a close connection between the quasi-eruptive and the eruptive type is further strengthened by the fact that part of a prominence can become eruptive while the remainder becomes quasi-eruptive. Usually the eruptive phenomenon precedes the quasi-eruptive, but the two may be simultaneous. The eruptive prominence

<sup>10</sup> At an eclipse, prominences of class III show the coronal lines in their spectra, and an entire prominence of this class has been photographed by S. A. Mitchell as a hazy image in the green line (*Ap. J.*, **75**, 1, 1932. See Pl. IV).

<sup>11</sup> *Pub. Yerkes Obs.*, **3**, Pl. XXVIII, 1925.

<sup>12</sup> Pettit, *Mt. W. Contr.*, No. 552; *Ap. J.*, **84**, 319, 1936.

<sup>13</sup> McMath and Pettit, *Mt. W. Contr.*, No. 568; *Ap. J.*, **85**, 279, 1937.

of August 12, 1938, is an example in which about half the rising mass separated from the remainder with which it was intermingled and returned to the chromosphere at the original center of attraction.<sup>14</sup>

There are no very sure indications by which to predict when a prominence will become quasi-eruptive or eruptive. If the motion is largely upward we cannot at first be sure to which class it belongs; if a prominence which has been followed for some time shows a rapid increase in coarseness of structure and a violent leaning toward the center of attraction, a quasi-eruption is likely to occur. As ordinarily a quasi-eruption lasts only 50–100 minutes, the observer is not long in doubt. As yet we have only a very little evidence of a substantial brightening of the photosphere or chromosphere near a prominence before or during its eruptive phase.

In a quasi-eruptive prominence the body moves more slowly than the streamers. Thus, in the prominence of September 23, 1919, the velocity of the body was 76 km/sec, while that of the streamers was 100 km/sec. In the prominence of July 24, 1936, the maximum velocities (at the chromosphere) were 70 and 118 km/sec. The disparity in velocity was even greater when the eruption began.

Spiralling is sometimes seen in quasi-eruptives. Another of their characteristics is the rapid fading of the whole object as it moves into the center of attraction. The latter quality is much like the fading of an eruptive prominence or of streamers in active prominences.

#### ERUPTIVE PROMINENCES (CLASSES $11b_1$ , $11b_2$ )

Eruptive prominences, as they have been called for seventy-two years, are those which rise to great heights and fade away. They always start as active or active sunspot prominences which may have been in existence for many days. No eruptive prominence has been known to rise directly out of the chromosphere, although, if the prominence were considerably in front of or beyond the limb, it might appear to do so. M. Waldmeier<sup>15</sup> has observed eruptives which began on the disk and passed beyond the limb, but these prominences were already in existence before the eruption began.

Eruptive prominences are among the rarer types. The catalogue<sup>16</sup> of all the eruptives for which 4 or more measures of height are available now contains 65 entries, dating from E. L. Trouvelot's early measurements.<sup>17</sup> One-half of these prominences were measured in the  $H\alpha$  line (one-third visually and one-sixth photographically). The others were measured photographically in the calcium lines, H or K.

The actual frequency of eruptive prominences is hard to estimate. If all other eruptive prominences for which less than 4 observations were reported are added to the catalogue, the total number would probably not exceed 75. The earliest of these was observed on September 4, 1868, by J. Janssen,<sup>18</sup> while still at the Guntoor (India) eclipse station. This makes an observational average of one each year. The number which occurred is actually much greater, for the early observations were casual. The first 24 entries of the catalogue cover 30 years, while the last 24 cover only 5 years.

Because of the difficulties of solar observing during the winter months in northern latitudes, we will arrive at a better value of the frequency of eruptives by confining our attention to the spring and summer seasons. During the past sunspot maximum a close watch was kept on prominences during the months from March to October, and series of measures on eruptives were reported by a number of observatories. In 1937, 16 eruptives were observed, and 7 in 1938. During the past year, which was near sunspot minimum, the writer observed only 2, and no others have been reported. From these data we can derive an approximate frequency figure for eruptives at sunspot maximum and minimum.

<sup>14</sup> McMath and Pettit, *Pub. A.S.P.*, **51**, 154, 1939.

<sup>15</sup> *Zs. f. Ap.*, **15**, 299, 1938.

<sup>16</sup> Pettit, *Pub. A.S.P.*, **52**, 172, 1940.

<sup>17</sup> *Comptes rendus*, **101**, 475, 1885.

<sup>18</sup> *Oeuvres scientifiques*, **1**, 180, 1929.

Few eruptives begin their motions at heights less than 65,000 km; hence the tops of such prominences in the pre-eruptive state will always be visible when their angular distances from the limb do not exceed  $23^{\circ}.8$ , i.e., within a zone which includes 40 per cent of the whole solar surface. Further, since observational hours for all observers would not exceed 20 per cent of the total time for half the year, i.e., March to October, a reasonable estimate seems to indicate that the observed numbers ought to be multiplied by at least 25, which would give 400 per year at sunspot maximum and about 25 to 50 per year near sunspot minimum.

The heights attained by eruptive prominences have varied widely; while 8 have exceeded a solar radius, only 1 has exceeded a solar diameter. Table 1 shows the frequency with which eruptives have reached certain elevations. The number given as attaining less than 100,000 km is too small, since those failing to reach this elevation may not be recognized. Apparently the frequency between 100,000 and 500,000 km is about constant, this range including 75 per cent of the catalogue entries. The chance that an erup-

TABLE 1  
NUMBER OF ERUPTIVE PROMINENCES FOUND  
WITHIN VARIOUS HEIGHT LIMITS

Heights (Unit = $10^5$ km)	No.	Heights (Unit = $10^5$ km)	No.
0-100.....	3	600- 700.....	2
100-200.....	10	700- 800.....	3
200-300.....	14	800-1000.....	4
300-400.....	12	1000-1500.....	0
400-500.....	13	1500-1600.....	1
500-600.....	3		

tive will rise above 500,000 km is about 0.2. This result has a practical application, for, when an eruption is recognized, the photographic apparatus should be arranged to permit a rise of 500,000 km.

The highest observed eruptive, No. 49 (and 49b), rose to an elevation of 1,550,000 km above the chromosphere. The fastest moving was No. 47, which reached a velocity of 728 km/sec. The duration varied from a few minutes to  $10^h 38^m$  for No. 49. The average recorded duration,  $2^h 31^m$ , is a little less than the actual duration, because observations began on some of the prominences after the eruption started.

Although most eruptives move hundreds of thousands of kilometers in straight-line paths, deviations are sometimes observed. Usually the trajectory is inclined to the vertical only a few degrees, but the inclination of two trajectories has exceeded  $50^{\circ}$ . The bearing of this inclination on velocity determinations will be discussed in a *Contribution* on prominence velocities.

The prominence expands as it rises<sup>19</sup> and disappears by fading away while in motion. During the whole eruption it sends streamers back to the original center of attraction and to other centers which form near-by. In the early stages of an eruption a considerable number of streamers are pulled from the prominence, but in the later and final stages only 2 or 3 are visible. Thus in the prominence catalogued as No. 1 there were 14 streamers in the early stages of the eruption and only 2 in the final stage. An exception was No. 45, in which 10 streamers could be counted throughout the eruption.

This return of streamers to centers of attraction on the sun while an eruption is in

<sup>19</sup> Pettit, *Mt. W. Contr.*, No. 451; *Ap. J.*, 76, 9, 1932.

progress and the occasional division of a prominence into two parts, one of which is eruptive, while the other is quasi-eruptive, are scarcely explainable on any but an electrical hypothesis in which charged particles of opposite sign are separated by the action of the center of attraction.

It has become increasingly evident that eruptive prominences are of two types, though the character of the upward movement is the same in both. In class IIb<sub>1</sub> an isolated cloud rises while streamers move back into the chromosphere. In class IIb<sub>2</sub> the prominence has the form of an arch whose crest rises while the entire object expands like an elastic band, each side pouring into a center of attraction (or spot area). While we have to depend on verbal descriptions for the forms of some of these prominences, it is reasonably sure that Nos. 2, 5, 7, 9, 13, 24, 46, 48, 56, 57, and 61 are members of class IIb<sub>2</sub>. Another<sup>20</sup> is No. 62, reported since publication of the catalogue.

#### PROMINENCES OF THE SUNSPOT TYPE (CLASS III)

While prominences over sunspots vary somewhat in appearance, the general type is unmistakable. Thus the coming of a sunspot may often be predicted with confidence from the appearance of a prominence of class III above the sun's eastern limb. Prominences of class III are never found without spots, although spots are frequently without prominences, at least for short intervals. Sunspot groups in the early or later stages of development seem to exhibit prominences to a greater extent than at other times. Over small spot groups or individual spots the prominences are usually weak and relatively simple in structure. Over the largest groups, however, the prominences are much brighter and more complicated.

#### CAP PROMINENCES (CLASS IIIo)

Spot groups are occasionally surmounted by a bright chromospheric cap, a few thousand kilometers high and 20,000–40,000 km in diameter, which resembles a desert mesa of the southwestern United States. Its lifetime is comparatively long, possibly several hours, sometimes a day or more. Surges frequently come from the chromosphere at the edge of a cap prominence; those which seem to rise out of the cap may appear to do so simply because of their orientation. M. A. Ellison<sup>21</sup> has observed that surges seen on the disk "occur at a distance of about 50,000 km from the umbra of an active sunspot," and since the cap prominence usually appears over the umbral region, Ellison's observation verifies our conclusion.

Prominences of class IIIo may be found in combination with any of the other subdivisions of class III but become more prevalent as we proceed downward in the diagram (Fig. 1). As in the quiescent prominences, no considerable motions are found in class IIIo, and no transformations are known to take place; hence it is placed first in the diagram of class III in Figure 1.

#### COMMON CORONAL SUNSPOT PROMINENCES (CLASS IIIa)

Over a relatively weak sunspot group converging streamers or broken sections of streamers may appear, moving into the spot area in a fanlike pattern. These are formed in the coronal space above the spot area and, when first seen, are already faint streamers rapidly brightening as they approach. In this respect they are identical with the streamers of class V. However, they usually form at heights less than 75,000 km and have velocities much smaller than those of the coronals of class Ic. Class IIIa may also occur over the stronger spot groups and is the most common spot type.

<sup>20</sup> Pettit, *Pub. A.S.P.*, 52, 414, 1940.

<sup>21</sup> *M.N.*, 102, 11, 1942.

## LOOPEd CORONAL SUNSPOT PROMINENCES (CLASS IIIb)

The more active sunspot groups are sometimes accompanied by a cluster of streamers in the form of converging arches or complete loops in a fountain-like pattern which stands above the spot area. One of these arches first appears as a stationary dot in coronal space over the spot area. This dot brightens, then lengthens in a curved arch toward the spot group. Sometimes, however, it lengthens in two directions and forms a complete loop, one branch of which is usually much the fainter. If two dots form simultaneously near together, the bright and faint branches of the two resulting loops may overlap, apparently forming a single bright loop. Plate 1c shows this formation over the dying spot group, Mt. W. No. 8084, in position angle  $43^\circ$ , on May 8, 1941.

Loops may, on rare occasions, arise from the chromosphere. An example will be described under class III $d_2$ .

## ACTIVE SUNSPOT PROMINENCES (CLASS IIIc)

Sometimes a prominence of class IIIa is accompanied on one or both sides by a prominence like those of class Ib, pouring streamers into the spot area; these lateral prominences are known as class IIIc. Curiously, examples of a IIIb prominence similarly associated with a IIIc prominence seem to be very rare. In the entire record of daily photographs at Mount Wilson, only two mediocre examples were found. Active sunspot prominences have many of the characteristics of class Ib and may develop into prominences of class II. There is a distinct difference, however. The curved streamers of a sunspot prominence are not plane figures, probably a consequence of the magnetic field of the spot area.

SURGES (CLASS III $d$ )

In the earlier work with the 13-foot spectroheliograph,<sup>12</sup> "small eruptions of short life" were discussed, in which mean velocities exceeding 500 km/sec were indicated. Later work with the motion-picture method<sup>13</sup> showed that these eruptions are not ordinary class IIb prominences but that they rise from and return to the chromosphere, always preserving their continuity. They have, therefore, been called surges.

By far the greater number of surges are extruded from sunspot groups. Even the small surges occasionally seen without visible sunspot areas are all in the sunspot zone.

Surges may be small bumps which rise a few thousand kilometers and subside, or they may develop into giant arms which reach into space more than 100,000 km and are then retracted without apparent loss of material<sup>9</sup> except where occasionally a small portion is thrown off the end. These we shall call common surges class III $d_1$ .

Class III $d_2$  surges begin much like III $d_1$ , but the initial bump is ragged, and eventually the prominence breaks into a spray as it reaches out. Often its outer portions fade nearly away before entirely returning to the chromosphere. Plate II shows a III $d_2$  prominence which appeared over the spot group Mt. W. No. 7244 on the west limb August 12, 1941.

In a variation of class III $d_2$  linear components form elongated loops which, momentarily, suggest IIIb. One such prominence (classified by the authors as IIIb) was recorded by R. R. McMath and H. E. Sawyer.<sup>22</sup> This surge was one of the few prominences in motion which have been known to intermingle partially with another at the point of contact. A deformation of the stationary prominence was also observed.

The life of a surge is short, ranging from 10 to 20 minutes for the small ones to a little more than 1 hour for the largest. Surges are projected at all angles between the vertical and horizontal. Over an active spot group surges are sometimes recurrent, rising again and again from practically the same point. On November 23, 1941, 8 surges in position angle  $97^\circ$  were photographed in  $4\frac{1}{2}$  hours, rising from the nascent spot group, Mt. W. No. 7332. There is a tendency for a group to extrude surges of type either III $d_1$  or III $d_2$  exclusively.

<sup>22</sup> *Pub. U. Mich. Obs.*, 7, 191, Pl. I, 1939.

## EJECTIONS (CLASS IIIe)

Sunspot groups sufficiently active to produce frequent surges sometimes eject small lumps of chromospheric material, often at a high angle to the vertical, which rise, leave the sun, and fade away without returning. They are a faint and uncommon phenomenon. Some of these ejections are circular in outline and a few thousand kilometers in diameter; others are elongated into short lines. All seem to move in straight lines with uniform motion, which from time to time<sup>9</sup> suddenly decreases somewhat.

## SECONDARIES (CLASS IIIf)

A very small part of a stationary prominence is sometimes ejected without disturbing the remainder. Such a secondary ejection which involved only a very minor part of the prominence rose<sup>23</sup> from the IIIg prominence over the great spot group of March 20, 1920. Another secondary was ejected from the eruptive prominence<sup>24</sup> of September 17, 1937. When associated with moving prominences, secondaries may proceed in almost any direction quite independently of the parent-prominences. As yet they have been observed only in class III or in eruptions connected with sunspots.

## CORONAL CLOUDS (CLASS IIIg)

Occasionally dots form in space above a sunspot group. Other dots then appear, and all coalesce into a suspended cloud from which streamers pour into the spot area. Young<sup>25</sup> and Secchi called attention to this phenomenon, although they did not describe it in detail. The writer secured a motion picture of one of these coronal clouds (class IIIg) on September 23, 1941, shown in Plate III in a series of photographs at 5-minute intervals covering most of the life of the prominence. Such a prominence, after formation, has a tendency to remain at about the same height above the sun but moves along parallel to the surface in the direction of the principal streamers. Its dissolution seems to be by shredding.

The appearance of the prominence in Plate III strongly suggests that the lateral prominences of class IIIc, particularly those of the butterfly type, may also be of coronal origin, although proof is still wanting.

## COLUMNAR TORNADOES (CLASS IVa)

These are twisted columns so dense that only the side toward the observer is visible. Occasionally they have only one or two turns, yet again they look like closely wound springs or fine-threaded screws. Most prominences of this type are from 5000 to 22,000 km in diameter and 25,000 to 100,000 km in height. Dimensions greater than these are rare. From the top of the trunk, or vortex, a faint smokelike column rises and, in many cases, bends over, nearly touching the chromosphere. In some tornadoes a sheath surrounds the base and rises about one-third the height of the vortex, disappearing and forming now and again. In one measurable prominence<sup>26</sup> the peripheral velocity of the vortex was 54 km/sec, and a knot in the smokelike column was ejected from the vortex at 64 km/sec.

The destruction of these objects seems to take place in several ways: (1) The peripheral velocity may become so high that the prominence explodes like the desert dust whirl.<sup>19</sup> (2) The vortex may rise bodily and fade away<sup>27</sup> with the characteristics of eruptive prominences. (3) A prominence of class IVa may also assume the characteristics of

<sup>23</sup> *Pub. Yerkes Obs.*, 3, 228, Pl. XXXV, 1925.

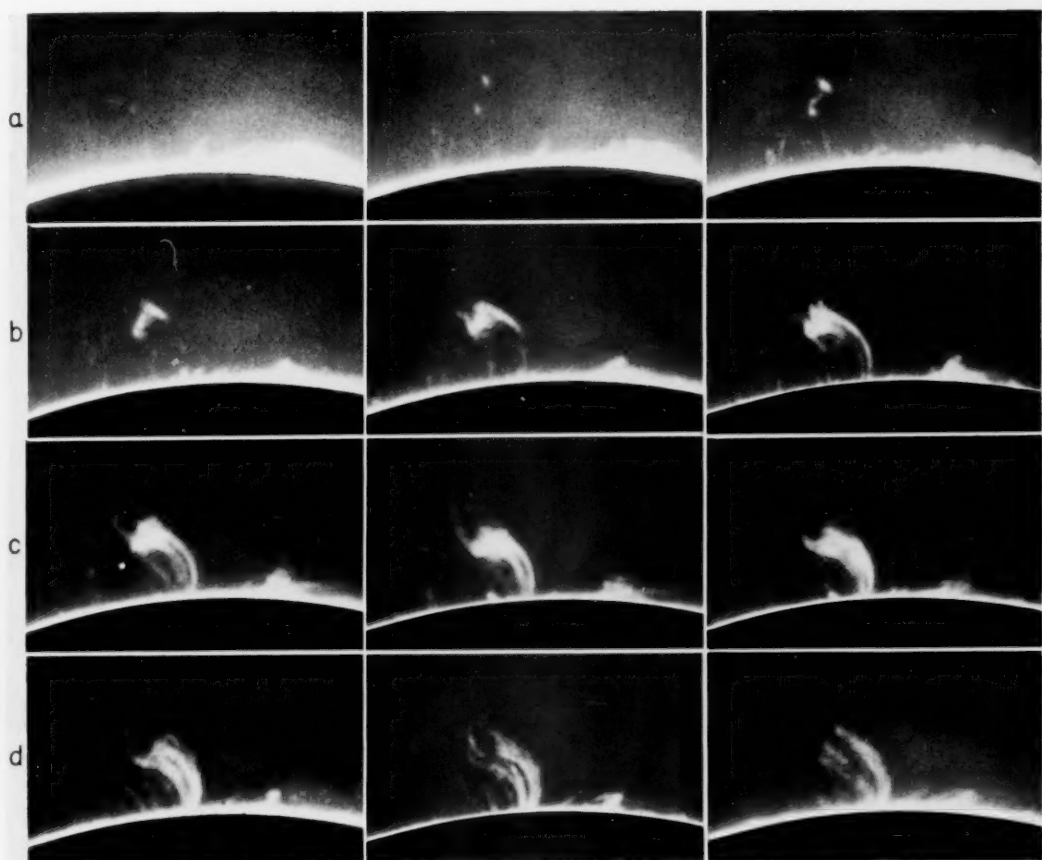
<sup>24</sup> *Mt. W. Contr.*, No. 597, p. 7; *A. J.*, 88, 231, 1938.

<sup>25</sup> *The Sun*, p. 221, 1910.

<sup>26</sup> *Pub. A.S.P.*, 53, 289, 1941.

<sup>27</sup> *Ibid.*, see caption of Pl. XXVIII.

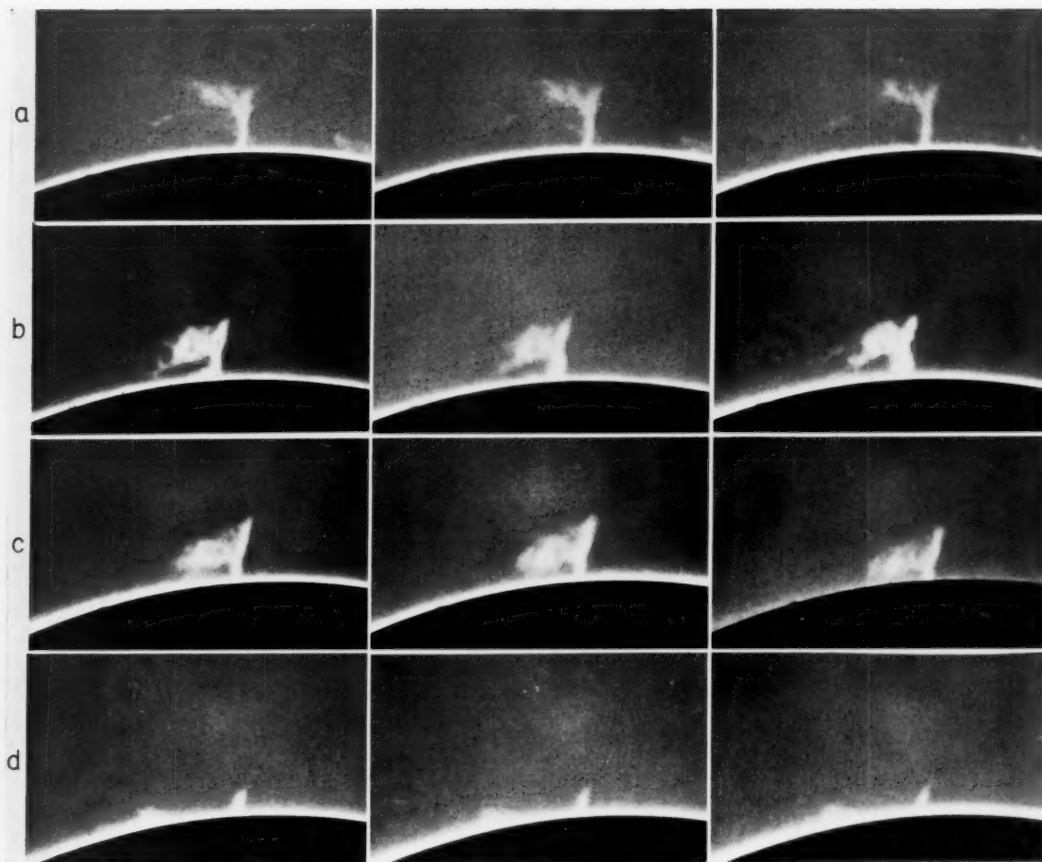
### PLATE III



FORMATION OF A CORONAL CLOUD (CLASS IIIg), SEPTEMBER 23, 1941

A large sunspot group is near the middle of the arc of the solar limb in each exposure. Note the formation of two dots in coronal space above the spot. Other dots formed, and the group grew into a cloud from which streamers poured into the spot-area. A surge appeared on the right. Exposures at intervals of 5 minutes.

# PLATE IV



TORNADO PROMINENCE (CLASS IVa), with ACTIVE CHARACTERISTICS

(a) September 19, 1941; first exposure 22<sup>h</sup>36<sup>m</sup> G.C.T. (b) September 20; first exposure 17<sup>h</sup>45<sup>m</sup>. (c) September 20; first exposure 23<sup>h</sup>15<sup>m</sup>. (d) September 21; first exposure 19<sup>h</sup>34<sup>m</sup>. Exposures at intervals of 15 minutes. A center of attraction on the solar limb was about 11 mm from the left edge of each photograph.

an active prominence and have a lifetime of several days. Plate IV shows a tornado which appeared at position angle  $120^\circ$  on September 19, 1941. Throughout the day it was a highly active prominence and was badly shredded by a center of attraction. On September 19 and 20, a sheaf of streamers, which itself at times showed a helical structure, was torn from the vortex. The vortex could still be seen on September 21, carried far over the limb by solar rotation (Pl. IV).

#### SKELETON TORNADOES (CLASS IVb)

Skeleton tornadoes are built up of individual twisting streamers, which give them the appearance of a crossed latticework. They are usually without the smokelike column issuing from the top. A class IVb prominence, observed by F. Slocum, has already been mentioned.<sup>4</sup> Two bifurcated class IVb tornadoes were photographed at the Yerkes Observatory, one on September 22, 1911, on the southeast limb by F. Slocum, and the other on August 11, 1915, on the east limb by the author. In each prominence the vortex was split into the form of a Y, and the two branches seemingly spiraled in opposite directions.

#### TYPICAL PROMINENCES OF UNCERTAIN PROPERTIES

We have now accounted for all the prominence types for which the observations are sufficient to establish the properties outlined in the beginning of this discussion. A number of types, however, have not been sufficiently studied to establish their observable properties.

In observations with the spectrohelioscope with the first slit very narrow and the second slit just wide enough to include the  $H\alpha$  line, the surface intensities of most prominences are found to be between 0.05 and 0.1 of the chromospheric intensity at the limb. The surface intensities of the surges often approach the chromospheric intensity and on rare occasions may even exceed it. On the other hand, some very faint prominences, often of large size, scarcely visible with the spectrohelioscope, are seen easily with the monochromator; the surface brightness is only a few per cent that of the ordinary prominences. It was thought that they might prove to be ordinary prominences in the earliest stages of development, but they seem to be quite stable.

A type we have called the "swirl" seems to have two forms. In the first, the entire object rotates, sometimes in a horizontal plane and sometimes in some other; its appearance is something like the vortex of a whirlpool. It also has a motion of translation not observed in tornadoes. In the other form, the swirl has the outward shape of a mushroom and is very bright. Suddenly it begins to emit spiral arms which grow in any plane and tend toward a center of attraction. The velocities of the arms are very high, 200 km/sec in some cases.

Prominences in the form of plumes are also known. They seem to be quite stable in form and in structural detail. No rotation of the stem could be detected in several of these tested with the 75-foot spectrograph in the second order at the 150-foot tower. They are, therefore, not of the tornado type.

## SIX-COLOR PHOTOMETRY OF STARS

### I. THE LAW OF SPACE REDDENING FROM THE COLORS OF O AND B STARS\*

JOEL STEBBINS<sup>1</sup> AND A. E. WHITFORD<sup>2</sup>

Mount Wilson Observatory and Washburn Observatory

Received May 7, 1943

#### ABSTRACT

The new photoelectric photometer described makes possible measures of stars and nebulae in six spectral regions from  $\lambda$  3530 to  $\lambda$  10,300 Å. With the 60-inch reflector useful results can be obtained for stars as faint as the ninth magnitude.

Measures (Table 3) have been obtained of the colors of 69 stars of spectrum O and B of various degrees of reddening. The scale for the difference, ultraviolet *minus* infrared, is about five times the international scale for color index.

The deviations from the  $1/\lambda$  law of selective absorption (Table 6) are in the sense that the intermediate regions are fainter than they would be if the  $1/\lambda$  law held from  $\lambda$  3530 to  $\lambda$  10,300 Å. There is no reason to change the previous determination of a high ratio of total to selective absorption,  $A_{pg}/E_{int} = 6$ , but the numerical value of this ratio must remain uncertain in the absence of observations in the far infrared.

The law of selective absorption is found to be the same for all directions in the Galaxy, indicating that interstellar material is essentially uniform in quality everywhere.

The present series of papers is the result of an attempt to utilize the advantages of a photoelectric cell with a large range of spectral sensitivity for color measures of stars and nebulae. Much of our previous work was with a combination of a Kunz potassium-hydride cell and two filters which gave equivalent effective wave lengths at  $\lambda$  4260 and  $\lambda$  4770 Å, a range of only 500 Å; but a new cesium-oxide cell from the Western Electric Company has yielded usable data from  $\lambda$  3300 to  $\lambda$  12,500 Å, more than eighteen times the previous range. These extreme measures were obtained with a focal-plane spectro-photometer in which the converging beam from the mirror of the 60-inch or 100-inch reflector is made parallel by a negative lens and then, after passing through a prism, is brought by another lens to a focus on the slit (of the photometer) which isolates the desired spectral region. Many measures with this instrument are on hand, but the final reductions will be delayed. In the meantime a combination of the same photocell with a series of filters has been developed which gives good measures in six spectral regions from  $\lambda$  3530 to  $\lambda$  10,300 Å. The advantage of this arrangement is that it can be applied to extended surfaces like the nebulae, and the nebulae can be compared with stars of different types.

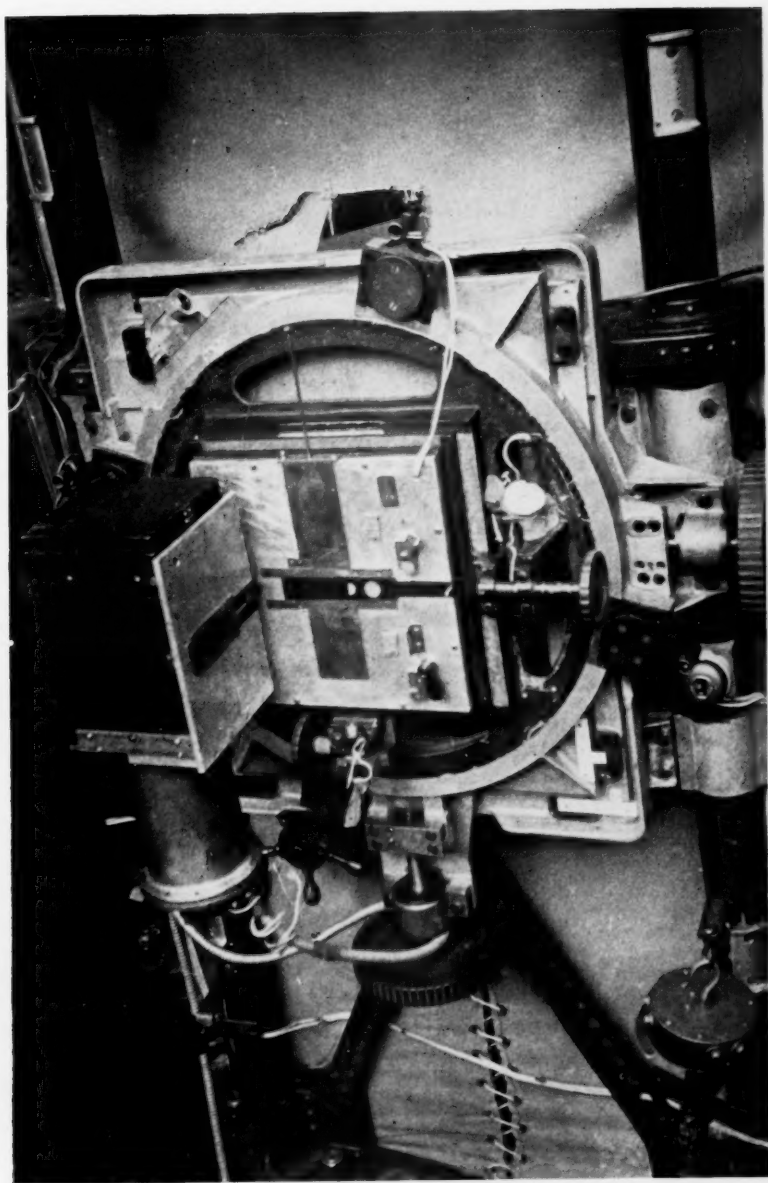
Plate V gives a general view of the instrument at the Newtonian focus of the 60-inch reflector. The photometer is attached by a square aluminum plate to the ring which fits to the double-slide base and is interchangeable with other attachments of the 60-inch or the 100-inch telescope. In the illustration the cell box and tank attached to a hinged plate have been swung back to the finding position. Four diaphragms, of which three are visible in the picture, are in a slide in the focal plane. Their diameters range from 1.5 mm to 19.0 mm, or from 0.7 to 8.6, on the 60-inch. The filter box is just inside the focal plane. A safety catch prevents opening the shutter to the cell unless the cell box is in the observing position. The window of the cell box is a positive lens, practically in

\* Contributions from the Mount Wilson Observatory, Carnegie Institution of Washington, No. 680.

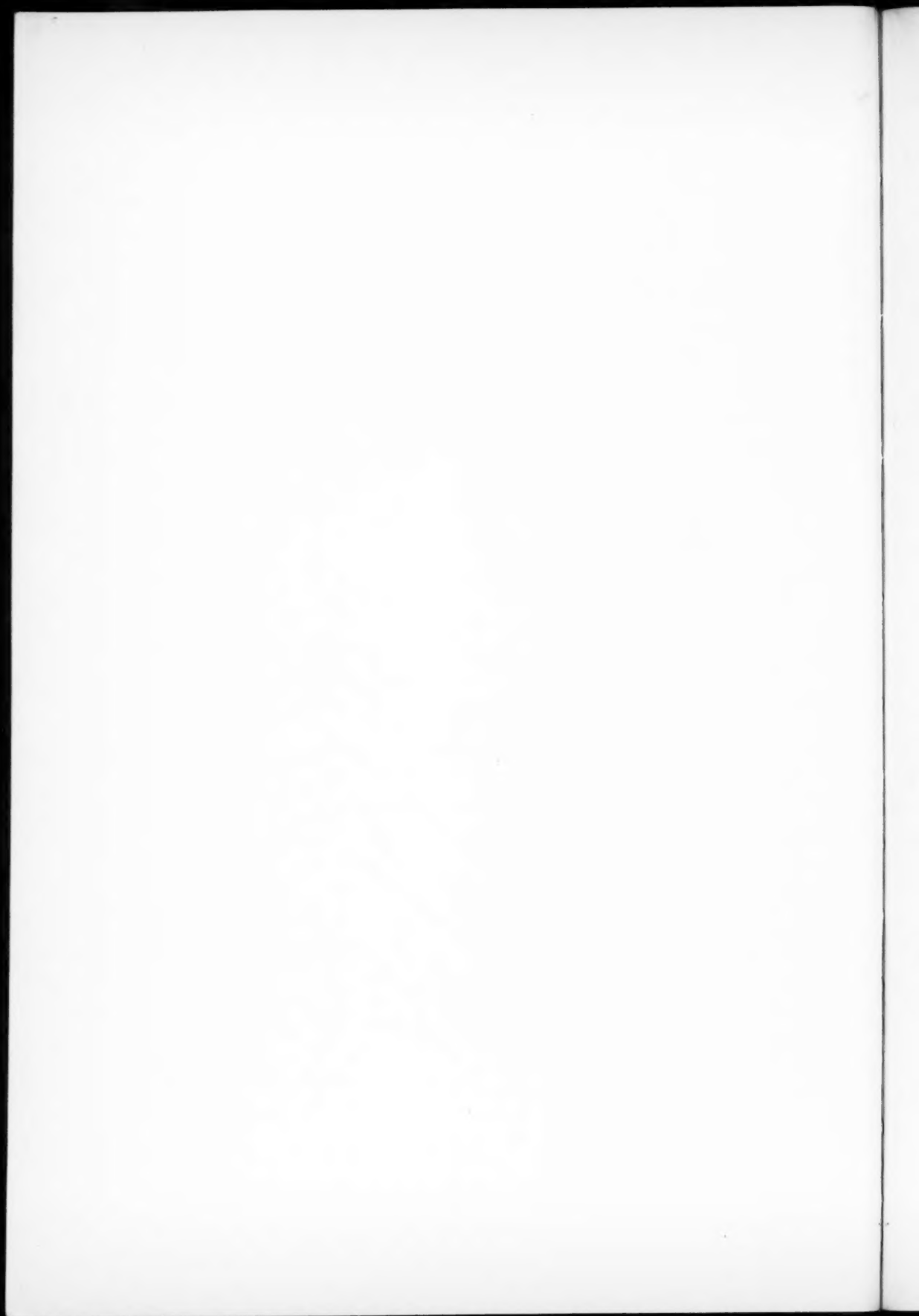
<sup>1</sup> Research Associate of the Mount Wilson Observatory, Carnegie Institution of Washington.

<sup>2</sup> On leave at Massachusetts Institute of Technology.

PLATE V



PHOTOMETER FOR STARS AND NEBULAE



the focal plane, which forms an image of the large mirror on the cell and hence gives the same uniform extrafocal image whether the source be a star, a nebula, or the sky background.

The arrangement of the photocell and amplifier is much like that described by Whitford.<sup>3</sup> The cesium-oxide cell is inclosed in a metal-covered glass tube which is sealed to a brass tank containing the amplifying tube. The combination permits the refrigeration of the cell and evacuation of the whole space containing the cell and amplifier. The refrigeration with dry ice reduces the dark current of the cell to less than 1/1000 its amount at room temperature. During an observing run the cell box is packed with dry ice about the middle of each afternoon, again half an hour before dark, and once more at midnight. A total of perhaps 2 or 3 pounds of dry ice are actually used, but during a run we aim to have available about 5–10 pounds per night. A metal-covered cable leads to the control box and galvanometer at the recorder's station in the clockroom of the 60-inch or at the foot of the north column of the 100-inch. When a large focal diaphragm is used, all the lights in the dome must be extinguished, especially red lights, to which the cell is very sensitive. We have not been troubled by diffuse sky radiation.

A summary of typical conditions of the circuit and installation on the 60-inch telescope follows:

AUGUST 13, 1942

Cell, Western Electric, Type D97087, No. X62042	
Amplifying tube, Western Electric, Type 96475	
Voltage on cell.....	96 volts
Galvanometer sensitivity.....	$4 \times 10^{-10}$ amp/mm at 1.8 m
Resistance in circuit.....	$3.06 \times 10^{10}$ ohms
Voltage sensitivity.....	63,000 mm/volt
Current sensitivity.....	$5.2 \times 10^{-16}$ amp/mm
Current amplification.....	$1.3 \times 10^6$
Dark current.....	$4 \times 10^{-15}$ amp.
Mean fluctuation in 5 seconds....	$\pm 0.6$ mm = $\pm 10$ microvolts
Star, type cG0, 1 mm deflection....	13.5 visual magnitude = $1.3 \times 10^{-11}$ lumen
Sensitivity of cell.....	$3.4 \times 10^{-12}$ amp/mag 4.0 = 40 micro-amp/lumen

The sensitivity of the cell is referred to a cG0 star with a color temperature of about 5600° K, measured through the atmosphere. The intensity of the star at the focus of the 60-inch, in lumens of the same color, follows from the visual magnitude 0.8 for a standard candle at a distance of 1 km. We compare different cells by adopting as a standard the current from an A0 star of magnitude 1.0 with a 15-inch telescope, magnitude 4.0 with the 60-inch, or 5.0 with the 100-inch. With the present cell the over-all sensitivity is 0.3 mag. less for A0 than for cG0, and the sensitivity is considerably greater for K and M stars.

The over-all sensitivity of  $3.4 \times 10^{-12}$  amp/mag 4.0 for an A0 star and a dark current of  $4 \times 10^{-15}$  amp. are not particularly good for the photometry of faint stars, but the great range of spectral sensitivity makes this cell valuable. The Kunz potassium-hydride cell, described in the original paper by Whitford,<sup>4</sup> gave a response equivalent to  $23 \times 10^{-12}$  amp/mag 4.0 on the 60-inch, with a dark current of  $10^{-16}$  amp. or less. We have yet to find anything superior to the Kunz cell for freedom from dark current and for great sensitivity to stars of color temperature of 10,000° K or higher. The Kunz cell has most of its sensitivity between  $\lambda$  4000 and  $\lambda$  5000 Å, with a maximum near  $\lambda$  4500 Å.

The time for a full galvanometer deflection is 15 seconds. For faint stars a higher resistance of  $15 \times 10^{10}$  ohms increases the deflections fivefold, with times of 30 seconds. The range of intensity for linear response of the cell is something like 10 mag.; and, with

<sup>3</sup> John Strong and Others, *Procedures in Experimental Physics*, p. 424, New York, 1938.

<sup>4</sup> *Ap. J.*, 76, 220, 1932.

TABLE 1

## FILTERS

Color	Glass	mm	Glass	mm	Remarks
Ultra.....	UG1	2			Cemented
X.....	UG1	2	RG1	2	
Violet.....	BG12	3	GG13	2	
Blue.....	C038	2	C430	5	
Green.....	C338	2	BG18	2	
Red.....	RG1	2	C396	3	
Infra.....	C254	2			

TABLE 2

## SENSITIVITY OF CELL AND FILTERS

$\lambda$	Cell	Ultra	Violet	Blue	$\lambda$	Cell	Green	Red	Infra
3200.....		8			5000.....	64	18.6		
3300.....	500	40			5200.....	62	36.3		
3400.....	450	50.4			5400.....	63	39.1		
3500.....	385	49.0			5600.....	65	35.4		
3600.....	280	35.2			5800.....	70	29.6		
3700.....	178	22.4	10.7		6000.....	76	23.3		
3800.....	150	18.0	26.4		6200.....	84	17.1	26.9	
3900.....	130	12.4	38.0		6400.....	95	11.6	38.5	
4000.....	112	4.4	44.8		6600.....	102	7.4	40.5	
4100.....	98		47.7		6800.....	109	4.4	40.4	
4200.....	90		45.0	16.2	7000.....	116	2.7	38.1	
4300.....	83		40.8		7200.....	122	1.5	33.8	
4400.....	77		35.1	30.5	7400.....	129	0.4	29.2	
4500.....	74		31.0		7600.....	135		24.4	
4600.....	72		25.2	37.2	7800.....	139		20.3	
4700.....	69		18.3		8000.....	141		16.2	0.3
4800.....	67		10.4	36.7	8200.....	141		12.8	
4900.....	65		4.4		8400.....	138		9.7	
5000.....	64		1.0	34.0	8500.....	137			3.0
5200.....	62			25.2	8600.....	135		6.8	
5400.....	63			17.9	8800.....	130		4.9	
5600.....	65			12.0	9000.....	125		3.0	11.4
5800.....	70			7.8	9200.....	118		1.9	
6000.....	76			2.7	9400.....	111		1.3	
					9500.....	106			34.6
					10,000.....	80			41.2
					10,500.....	54			34.7
					11,000.....	32			22.1
					11,500.....	15			11.3
					12,000.....	7			5.6
					12,500.....	2.8			2.3
					13,000.....	1.9			1.6
					13,500.....	0.6			0.5
Mean $\lambda$ .....		3530	4220	4880	Mean $\lambda$ .....		5700	7190	10,300
1/ $\lambda$ .....		2.83	2.37	2.05	1/ $\lambda$ .....		1.75	1.39	0.97

the 60-inch, measures with filters can be made of stars of any type down to visual magnitude 9.0, though 7.5 is the ordinary convenient limit. For stars brighter than magnitude 4.0 a wire-gauze screen absorbing 3.0 mag., or even one absorbing 6.0 mag., is placed over the large mirror.

The filters for use with the present cell were selected, after repeated trials, to give nearly the same response in each of the six spectral regions for a solar-type star. They are Jena or Corning glasses in 1-inch squares, usually cut from 2-inch squares giving duplicate pieces of the same glass. The numbers and thicknesses are in Table 1. There are two glasses to each filter except the first and last. With so many recurring references to the individual filters we have shortened the names of these two to "Ultra" and "Infra."

Because of the strong infrared leak of ultraviolet glasses we used two filters, UG1 and the cemented combination,  $X = \text{UG1} + \text{RG1}$ . Since the RG1 cuts out all the ultraviolet, the difference between Ultra and  $X$  is the net transmission of the ultraviolet, except for a small correction for the infrared absorption of the RG1 component of  $X$ . The transmissions of the filters at different wave lengths were determined with the cell and

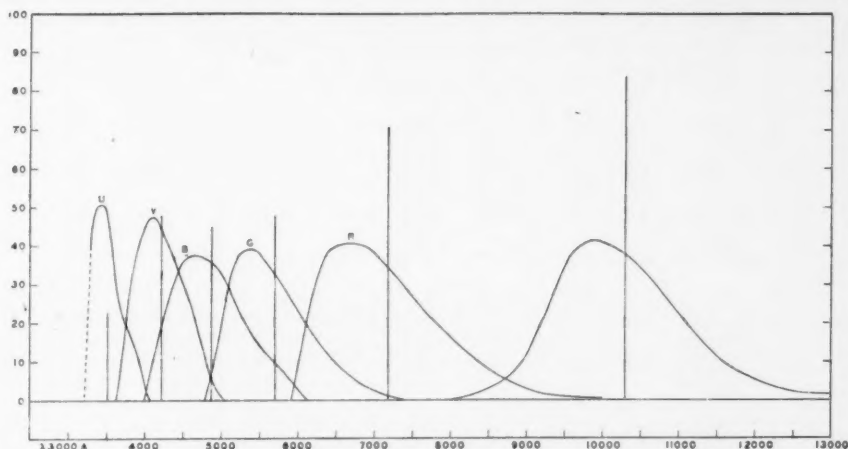


FIG. 1—Color-curves of filters

a monochromator. The color sensitivity of the cell itself was also determined in the laboratory with a monochromator, the results being reduced to constant energy for the source by simultaneous measures with a thermocouple. The values for the combination of the cell with each filter are in Table 2. Because of the high peak in the ultraviolet curve of the cell, the values for the Ultra filter have been divided by 5; otherwise the figures give the relative responses for a source of equal energy at all wave lengths.

At the bottom of Table 2 are the mean effective wave lengths for the combination of the cell with each filter. Then  $1/\lambda$  is taken as the effective reciprocal wave length. The sensitivity-curves could have been plotted on a  $1/\lambda$  basis and the means determined directly—there is little difference.

The data of Table 2 are shown in Figure 1. The curves overlap considerably, but that defect is inherent in the nature of filters which transmit a reasonable proportion of the original radiation. While it is true that the selected spectral regions are far from pure, the same criticism applies with even greater weight to photographic and visual receivers, on which most determinations of stellar colors have been based.

As mentioned previously, the primary object in the design of this photometer was the measurement of colors of extended faint surfaces like the nebulae. We already have satisfactory observations of about 10 extragalactic nebulae, together with a hundred or

TABLE 3  
COLORS OF O AND B STARS

No.	HD	<i>m</i>	Spec.	C <sub>1</sub>	U	V	B	G	R	I	U-I	Obs.
1.....	14633	7.3	O8	-0.30	-2.25	-1.15	-0.52	-0.03	+0.54	+1.45	-3.70	3
2.....	214680	4.91	O9s	-0.23	-2.26	-1.16	-0.53	-0.05	+0.58	+1.33	-3.59	5
3.....	1337	6.12	O8n	-0.20	-2.11	-1.07	-0.46	-0.05	+0.51	+1.14	-3.25	1
4.....	188209	5.51	O8s	-0.17	-2.02	-0.99	-0.44	-0.05	+0.48	+1.09	-3.11	2
5.....	198846*	7.1	O9nn	-0.13	-1.99	-0.97	-0.43	-0.14	.....	+0.93	-2.92	1
6.....	203064	5.06	O8nn	-0.16	-1.95	-0.94	-0.39	-0.02	+0.41	+0.92	-2.87	1
7.....	24912	4.05	O7n	-0.14	-1.85	-0.89	-0.36	-0.03	+0.40	+0.91	-2.76	1
8.....	199579	6.01	O6	-0.12	-1.77	-0.84	-0.35	-0.03	+0.38	+0.86	-2.63	1
9.....	209975	5.17	O9	-0.12	-1.73	-0.81	-0.34	-0.04	+0.37	+0.81	-2.54	2
10.....	193322	5.82	O8	-0.07	-1.64	-0.75	-0.31	-0.04	+0.35	+0.82	-2.46	1
11.....	210839	5.19	O6nf	-0.04	-1.48	-0.61	-0.23	-0.01	+0.24	+0.56	-2.04	1
12.....	207198	5.97	O9s	+0.03	-1.31	-0.55	-0.18	-0.02	+0.20	+0.48	-1.79	1
13.....	207538	7.03	O9ss	+0.03	-1.22	-0.47	-0.15	-0.03	+0.18	+0.50	-1.72	2
14.....	192639	7.02	O7f	+0.02	-1.23	-0.49	-0.16	-0.02	+0.18	+0.38	-1.61	1
15.....	192281	7.47	O5	+0.07	-1.16	-0.43	-0.10	-0.01	+0.12	+0.37	-1.53	2
16.....	193514	7.29	O8	+0.10	-1.08	-0.35	-0.07	+0.01	+0.05	+0.13	-1.21	2
1.....	5394*	2.25	B0ne	-0.11	-2.21	-1.17	-0.55	-0.05	+0.61	+1.32	-3.53	2
2.....	204172	5.84	B0	-0.19	-2.04	-1.02	-0.45	-0.05	+0.49	+1.16	-3.20	3
3.....	186994	7.32	B0	-0.22	-1.99	-1.04	-0.44	-0.05	+0.48	+1.16	-3.15	3
4.....	10516	4.19	B0ne	-0.14	-1.88	-0.91	-0.36	-0.00	+0.36	+0.80	-2.68	2
5.....	209339	6.48	B0	-0.12	-1.73	-0.85	-0.35	-0.03	+0.40	+0.87	-2.60	1
6.....	184915	5.04	B0n	-0.14	-1.61	-0.83	-0.33	-0.05	+0.38	+0.92	-2.53	1
7.....	2905	4.24	cB0ea	-0.09	-1.64	-0.77	-0.30	-0.04	+0.35	+0.73	-2.37	2
8.....	191201	7.12	B0	-0.07	-1.53	-0.71	-0.25	-0.03	+0.28	+0.76	-2.29	1
9.....	206773	6.98	B0ne	-0.05	-1.51	-0.61	-0.18	-0.03	+0.21	+0.48	-1.99	1
10.....	+35°3955	7.3	B0	-0.04	-1.39	-0.63	-0.23	-0.07	+0.30	+0.55	-1.94	1
11.....	203374	6.64	B0ne	+0.01	-1.33	-0.53	-0.17	-0.01	+0.18	+0.43	-1.76	1
12.....	213087	5.66	cB0	+0.01	-1.19	-0.55	-0.15	-0.03	+0.18	+0.52	-1.71	1
13.....	192422	7.10	cB0	+0.05	-0.99	-0.37	-0.06	-0.01	+0.07	+0.10	-1.09	2
14.....	205196	7.36	cB0	+0.15	-0.77	-0.11	+0.02	+0.02	-0.04	-0.10	-0.67	1
15.....	195592	7.15	cB0ea	+0.30	-0.14	+0.13	+0.18	+0.04	-0.21	-0.62	+0.48	3
16.....	194839	7.45	cB0ea	+0.34	+0.09	+0.34	+0.30	+0.01	-0.31	-0.80	+0.89	3
17.....	166734*	8.8	B0ea	+0.39	+0.09	+0.40	+0.38	+0.05	-0.43	-1.06	+1.15	3
18.....	169034*	8.6	cB0	+0.45	+0.66	+0.63	+0.50	+0.05	-0.55	-1.38	+2.04	2
1.....	205021	3.32	B1	-0.25	-2.13	-1.17	-0.54	-0.07	+0.61	+1.36	-3.49	2
2.....	201819	6.40	B1n	-0.18	-2.04	-1.07	-0.47	-0.05	+0.53	+1.24	-3.28	2
3.....	214993*	5.18	B1s	-0.20	-1.97	-1.08	-0.48	-0.04	+0.52	+1.21	-3.18	4
4.....	218376	4.93	cB1	-0.18	-1.88	-0.97	-0.42	-0.05	+0.47	+1.06	-2.94	2
5.....	198781	6.38	B1n	-0.15	-1.67	-0.87	-0.35	-0.04	+0.38	+0.85	-2.52	1
6.....	24398	2.91	cB1	-0.04	-1.59	-0.79	-0.33	-0.04	+0.37	+0.78	-2.37	1
7.....	205139	5.52	B1s	-0.08	-1.57	-0.73	-0.29	-0.01	+0.31	+0.75	-2.32	1
7a.....	173219*	7.9	B1e	-0.07	-1.70	-0.76	-0.26	-0.00	+0.27	+0.44	-2.14	1
8.....	190919	7.30	cB1	-0.00	-1.30	-0.61	-0.17	-0.02	+0.20	+0.60	-1.90	1
9.....	218342	7.46	cB1	+0.10	-1.11	-0.42	-0.12	+0.03	+0.08	+0.22	-1.33	1
10.....	199216	7.13	cB1	+0.11	-0.87	-0.35	-0.03	-0.03	+0.06	+0.25	-1.12	1
11.....	203938	7.10	cB1	+0.13	-0.78	-0.33	-0.07	-0.01	+0.08	+0.15	-0.93	1
12.....	216411	7.16	cB1ea	+0.15	-0.71	-0.16	-0.05	+0.05	-0.01	-0.07	-0.64	2
13.....	169454	6.84	cB1e	+0.29	+0.03	+0.28	+0.30	+0.02	-0.31	-0.76	+0.79	2

TABLE 3—Continued

No.	HD	<i>m</i>	Spec.	<i>C</i> <sub>1</sub>	U	V	B	G	R	I	U-I	Obs.
1.....	24760	2.96	B2	-0.20	-2.12	-1.14	-0.53	-0.07	+0.60	+1.33	-3.45	1
2.....	188252	5.70	B2s	-.18	-1.96	-1.08	-.49	-.05	+.54	+1.24	-3.20	1
3.....	157056	3.37	B2	-.28	-1.92	-1.11	-.54	-.05	+.60	+1.21	-3.13	1
4.....	217101	6.07	B2	-.17	-1.90	-1.05	-.50	-.05	+.55	+1.21	-3.11	1
5.....	188439	6.15	B2nn	-.19	-1.92	-0.99	-.43	-.06	+.49	+1.12	-3.04	1
6.....	166182	4.32	B2s	-.20	-1.77	-1.02	-.47	-.04	+.51	+1.24	-3.01	2
7.....	224572	4.93	B2n	-.19	-1.87	-1.01	-.45	-.05	+.50	+1.11	-2.98	1
8.....	193536	6.28	B2	-.17	-1.75	-1.03	-.49	-.06	+.54	+1.17	-2.92	1
9.....	171871	7.39	B2s	-.14	-1.79	-1.07	-.44	-.02	+.46	+1.08	-2.87	1
10.....	184279	6.78	B2se	-.19	-1.62	-0.85	-.37	-.05	+.42	+0.84	-2.46	1
11.....	206165	4.87	cB2	+.02	-1.19	-0.59	-.20	-.04	+.25	+0.47	-1.66	1
12.....	197770	6.36	cB2	+.03	-1.08	-0.53	-.18	-.03	+.22	+0.44	-1.52	1
13.....	198478	4.89	cB2ca	+.05	-0.98	-0.43	-.12	-.01	+.12	+0.23	-1.21	2
14.....	193183	7.12	cB2	+.08	-0.85	-0.35	-.07	-.02	+.09	+0.25	-1.10	1
15.....	200857	7.16	cB2	+.16	-0.52	-0.25	+.01	-.03	+.02	-0.02	-0.50	1
16.....	194279	7.05	cB2	+.33	+0.20	+0.36	+.34	+.03	-.37	-0.92	+1.12	2
1.....	194335	5.68	B3ne	-.18	-2.30	-1.21	-.54	-.04	+.58	+1.24	-3.54	1
2.....	214168	5.83	B3ne	-.14	-1.94	-1.06	-.45	-.04	+.49	+1.16	-3.10	1
3.....	200120	4.86	B3ne	-.22	-2.00	-1.00	-.41	-.02	+.43	+1.06	-3.06	2
4.....	199081	4.68	B3	-.16	-1.66	-1.06	-.50	-.03	+.54	+1.21	-2.87	2
5.....	212455	8.0	cB3	+0.09	-0.87	-0.47	-0.11	-0.03	+0.14	+0.24	-1.11	1

## NOTES TO TABLE 3

- HD 5394  $\gamma$  Cassiopeiae. *C*<sub>1</sub> is discordant; color may be variable.  
 166734 From color presumably a c star.  
 169034 O'Keefe calls spectrum B2, *M* = -5.2. This is reddest of 1332 B stars.  
 173219 Spectrum peculiar; star omitted in Table 6.  
 198846 Red measure is obviously defective. Others retained, but all might be rejected.  
 214993 12 Lacertae, short-period variable. No change of color in three observations same night.

more stars of all spectral types for comparison. The present paper, however, deals with the colors of O and B stars which were observed more or less incidentally to the main program. It is now generally agreed that the reddened colors of early-type stars near the galactic plane are due to selective space absorption and that the interstellar material that produces this reddening is the same that produces the dark spots in the Milky Way and also obscures the extragalactic nebulae over the whole zone of low latitude. One of the current problems of astronomy is the determination of the nature of this absorbing cosmic dust. It is known that the absorption or scattering does not follow the Rayleigh law of variation,  $1/\lambda^4$ , but varies more nearly as  $1/\lambda$ . The colors of a number of O and B stars of different degrees of reddening in different parts of the sky should determine this law of space reddening and its uniformity in quality throughout the Galaxy.

In Table 3 are the colors of some 69 stars of spectrum O and B, selected from our previous list of 1332 stars.<sup>5</sup> The first column gives the running number for each spectral class. The second column gives the number in the *Henry Draper Catalogue*; an asterisk (\*) refers to a note at the end of the table. The magnitude *m* in the third column is always visual. If given to two decimals, it is from the Harvard photometry; if to one decimal, it is a visual magnitude derived from photoelectric measures but still referred to the Harvard system.

<sup>5</sup> *Mt. W. Contr.*, No. 621; *Ap. J.*, 91, 20, 1940.

The spectra in the fourth column are largely from Plaskett and Pearce,<sup>6</sup> but many of the cB stars and all the Be stars are from the classification of P. W. Merrill<sup>7</sup> and others at Mount Wilson. The spectra of many of these reddened B stars have been studied by J. A. O'Keefe;<sup>8</sup> where he gives an absolute magnitude of  $-4.0$  or brighter, the star is noted as a c supergiant.

The fifth column contains the photoelectric color index  $C_1$  taken from the list of 1332 B stars.

The sixth to eleventh columns contain the six colors of the present work, with the appropriate heading in each column. The corresponding wave lengths and reciprocal wave lengths are in Tables 2 and 4. The plus sign (+) stands for a lesser intensity. The colors of each star were reduced to outside the atmosphere and then referred on the magnitude scale to the mean of the blue, green, and red of that star. The tabular figure for each color is the difference in magnitude between that star and the mean of ten stars of the main sequence with an average spectrum of dG6. For instance, for the first star, HD 14633, the Ultra is 2.25 mag. brighter than standard, the violet is 1.15 mag. brighter, and so on. The three  $\Delta$  mags. of blue, green, and red should add up to zero or to  $\pm 0.01$  mag.

TABLE 4  
EXTINCTION AND PROBABLE ERRORS

Quantity	U	V	B	G	R	I	U-I
$\lambda$ .....	3530	4220	4880	5700	7190	10,300	.....
$1/\lambda$ .....	2.83	2.37	2.05	1.75	1.39	0.97	.....
$a$ .....	0 <sup>m</sup> 530	0 <sup>m</sup> 292	0 <sup>m</sup> 180	0 <sup>m</sup> 136	0 <sup>m</sup> 058	0 <sup>m</sup> 030	.....
P.E. $\{m < 7.0$ .....	$\pm 0.016$	$\pm 0.008$	$\pm 0.009$	$\pm 0.008$	$\pm 0.008$	$\pm 0.017$	$\pm 0.027$
1 obs. $\{m > 7.0$ .....	$\pm 0.053$	$\pm 0.025$	$\pm 0.020$	$\pm 0.015$	$\pm 0.018$	$\pm 0.039$	$\pm 0.073$

The difference  $U - I$  in the next to last column is the color index with the extreme base line  $\lambda\lambda$  3530-10,300 Å, the stars of each spectral class being arranged in the order of this difference.

The last column gives the number of observations, usually one observation per night. More than half the stars were measured on one night only, as it seemed better to increase the number of stars than to repeat all of them.

The usual approximate formula for the atmospheric extinction,

$$\text{Extinction} = a \sec z,$$

was considered to be sufficient. In Table 4 are the mean values of  $a$  for the different wave lengths, taken from C. G. Abbot's<sup>9</sup> determinations for Mount Wilson. The excellent agreement of the measures of the same stars on different nights justifies the use of a mean extinction.

In Table 4 are also the probable errors for each color for those stars in Table 3 with more than one observation each. The larger errors for the fainter stars are not due entirely to the smaller deflections; some of these stars had to be observed at larger zenith distances than average. From the way the  $\Delta$  mags. are formed, the errors increase in both directions from the green; and any variation in the color gradient with the extinction will become most evident in the Ultra and Infra values. Even the maximum accidental error of  $\pm 0.073$  mag. in the difference  $U - I$  is practically negligible in comparison

<sup>6</sup> *Pub. Dom. Ap. Obs.*, 5, No. 2, 1931; No. 3, 1933.

<sup>7</sup> *Mt. W. Contr.*, Nos. 471 and 576; *Ap. J.*, 78, 87, 1933; 86, 274, 1937.

<sup>8</sup> *Ap. J.*, 94, 353, 1941.

<sup>9</sup> *The Sun*, p. 297, New York, 1929.

with the range of several magnitudes between normal and reddened B stars. We usually obtained two or more observations of the reddest stars.

Any pair of the colors gives a good color index of a star, but we have selected  $V-B$  and  $U-I$  for comparison with our previous  $C_1$ . The comparison is made graphically in Figure 2. Since there is naturally a close correlation between  $V-B$  and  $U-I$ , the graphs are a good check on  $C_1$ . Because of its discordance, one star, the variable  $\gamma$  Cassiopeiae, has been omitted from the diagram. There are four or five points which indicate errors up to 0.10 mag. in  $C_1$ ; otherwise the agreements are satisfactory. There-

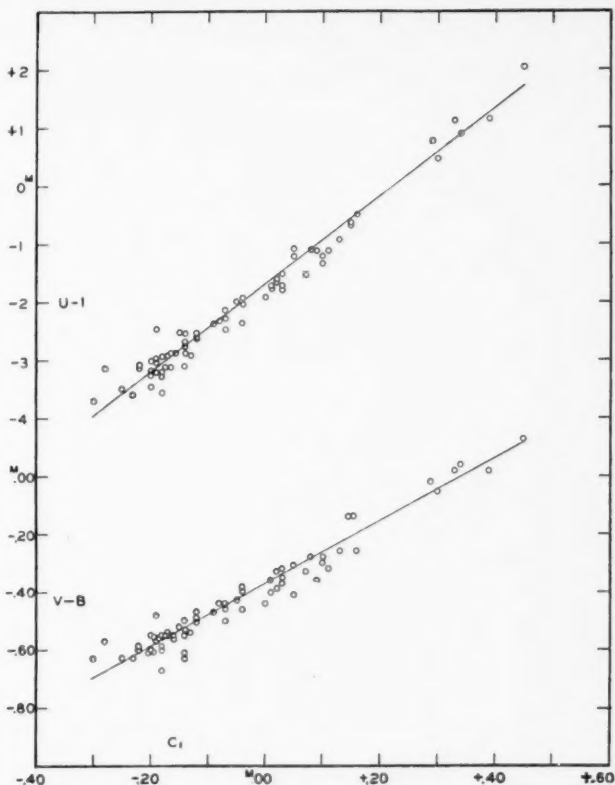


FIG. 2.—Comparison of scales

fore, assuming that there are probably no gross errors in the colors of Table 3, we proceed to derive the law of space reddening.

The method is shown in Table 5. The difference  $9 - 1$  is taken for each color of the first and ninth O stars of Table 3. This difference is divided by 1.16 to reduce to a standard value of 1.00 mag. for  $U - I$ . Then the computed values on the  $1/\lambda$  law are interpolated linearly between  $1/\lambda = 2.83$  and  $1/\lambda = 0.97$ , and the differences between the observed and the computed colors are in the last line of the table.

The same procedure was followed for 30 pairs of stars from Table 3; the results are in Table 6. Where there are several nearly normal stars, as in classes B2 and B3, a reddened star was compared with two or more whiter stars of about equal color. The mean deviations for each spectral class and the mean of all are at the end of Table 6. One difficulty in the use of filters is that, since the effective wave length transmitted depends upon the color of the source, a reddened star is measured effectively at a longer

TABLE 5  
DIFFERENCE BETWEEN A REDDENED AND A NORMAL STAR

Quantity	U	V	B	G	R	I	U-I
$1/\lambda$ .....	2.83	2.37	2.05	1.75	1.39	0.97	.....
Difference, 9-1.....	+0.52	+0.34	+0.18	-0.01	-0.17	-0.64	+1.16
Difference/ $1/\lambda$ .....	+0.45	+0.29	+0.16	-0.01	-0.15	-0.55	+1.00
Computed from $1/\lambda$ law.....	+0.45	+0.20	+0.03	-0.13	-0.32	-0.55	+1.00
Deviation from $1/\lambda$ law.....	0.00	+0.09	+0.13	+0.12	+0.17	0.00	.....

TABLE 6  
DEVIATION FROM THE  $1/\lambda$  LAW

Spectrum	Difference	U	V	B	G	R	I	U-I
O.....	9-1	0.00	+0.09	+0.13	+0.12	+0.17	0.00	1.16
	10-2	.00	+ .06	+ .06	+ .04	+ .02	.00	1.13
	11-3	.00	+ .11	+ .09	+ .09	+ .03	.00	1.21
	12-4	.00	+ .04	+ .08	+ .06	+ .02	.00	1.32
	13-5	.00	+ .03	+ .01	+ .03	.....	.00	1.20
	14-6	.00	+ .04	+ .03	+ .01	+ .02	.00	1.26
	15-7	.00	+ .06	+ .07	+ .04	+ .02	.00	1.23
	16-8	.00	+ .10	+ .13	+ .12	+ .05	.00	1.42
B0.....	10-1	.00	+ .07	+ .10	+ .05	+ .06	.00	1.59
	11-2	.00	+ .10	+ .12	+ .12	+ .06	.00	1.44
	12-3	.00	+ .03	+ .06	+ .03	+ .00	.00	1.44
	13-4	.00	+ .03	+ .05	+ .01	+ .03	.00	1.59
	14-5	.00	+ .13	+ .11	+ .11	+ .04	.00	1.93
	15-6	.00	+ .08	+ .10	+ .12	+ .08	.00	3.01
	16-7	.00	+ .06	+ .07	+ .07	+ .04	.00	3.26
	17-8	.00	+ .10	+ .13	+ .13	+ .09	.00	3.44
B1.....	18-9	.00	+ .02	+ .05	+ .06	+ .04	.00	4.03
	8-1	.00	+ .08	+ .13	+ .09	- .01	.00	1.59
	9-2, 3	.00	+ .12	+ .14	+ .13	+ .06	.00	1.90
	10-4	.00	+ .04	+ .08	+ .04	- .01	.00	1.82
	11-5	.00	+ .03	+ .04	+ .04	+ .02	.00	1.59
	12-6	.00	+ .10	+ .07	+ .12	+ .04	.00	1.73
	13-7	.00	+ .06	+ .10	+ .08	+ .06	.00	3.11
	11-1	.00	+ .04	+ .08	+ .08	+ .05	.00	1.79
B2.....	12-2, 3, ...	.00	+ .07	+ .11	+ .07	+ .04	.00	1.64
	13-4, 5	.00	+ .07	+ .10	+ .10	+ .06	.00	1.87
	14-6, 7	.00	+ .09	+ .12	+ .09	+ .04	.00	1.90
	15-8, 9	.00	+ .06	+ .10	+ .06	+ .05	.00	2.39
	16-10.....	.00	+ .08	+ .11	+ .09	+ .04	.00	3.58
B3.....	5-1, 2, 3, 4	.00	+ .01	+ .06	+ .04	+ .05	.00	2.03
O.....	Mean	.000	+ .066	+ .075	+ .064	+ .041	.000	1.24
B0.....	Mean	.000	+ .076	+ .088	+ .077	+ .049	.000	2.41
B1.....	Mean	.000	+ .072	+ .093	+ .083	+ .027	.000	1.96
B2, B3.....	Mean	0.000	+0.060	+0.097	+0.076	+0.047	0.000	2.17
Mean of all.....		0.000	+0.067	+0.088	+0.075	+0.042	0.000	1.95
Correction for filters.....		.000	+ .004	+ .008	+ .003	+ .002	.000	.....
Neglected decimals.....		0.000	-0.003	-0.001	+0.001	+0.004	0.000	.....
Final deviations.....		0.000	+0.068	+0.095	+0.079	+0.048	0.000	.....

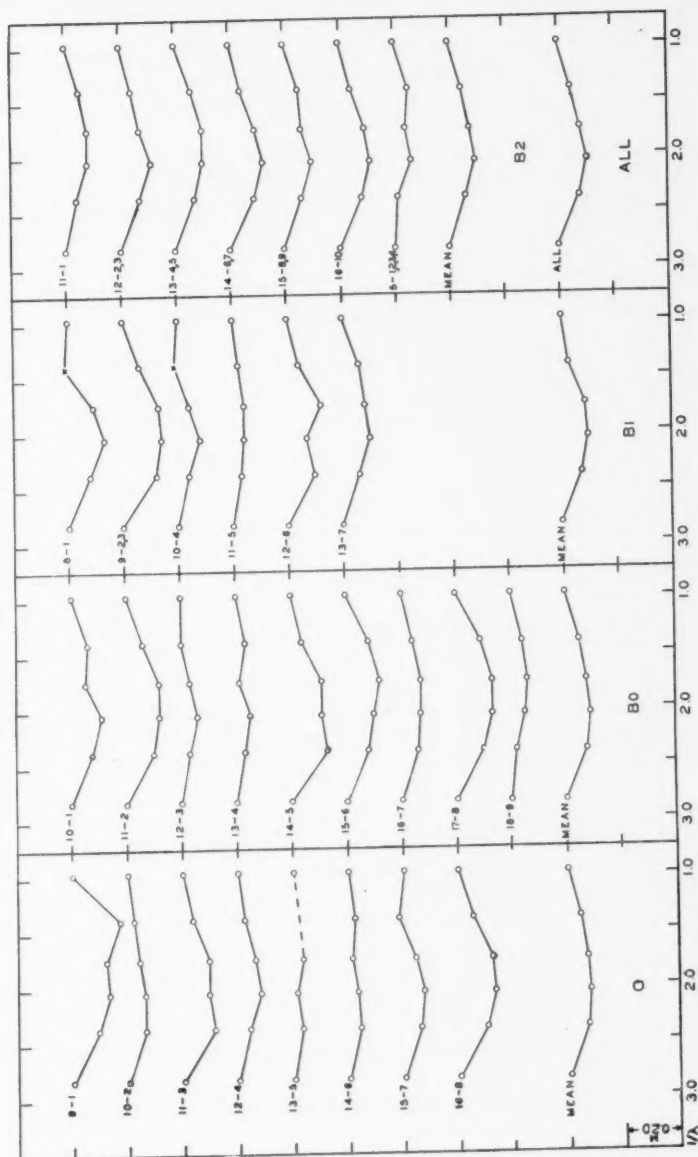


Fig. 3.—Deviations from  $1/\lambda$  law of absorption

wave length than a normal star of the same type. The proper allowance for this effect is best made by a small correction to the magnitude, indicated as "Correction for filters" at the bottom of Table 6. There is also another small correction because the interpolated values on the  $1/\lambda$  law were rounded off to 0.01 mag. When these two corrections are applied to the means, we have the final deviations from the  $1/\lambda$  law over the range of wave length here studied.

The data of Table 6 are shown graphically in Figure 3, and a glance at the curves shows no outstanding discrepancy among these stars, which are well distributed over the sky. The procedure of basing the linear relation upon the Ultra and Infra values is purely arbitrary, but the mean results would come out about the same on any basis of linear variation with  $1/\lambda$ . For instance, the discordant point for the red in the first pair is due not to the red measure but to the Infra measure of the first star, HD 14633, the bluest star of all. If we had run the adopted straight lines through the red points, this Infra point would have been a high one, but it would have been counterbalanced in the mean by low Infra points in other stars. The Infra deflection for HD 14633 was only about 1 per cent of the clear deflection, the equivalent of the clear deflection from a twelfth-magnitude O star. It would be a simple matter to go back in cases like this and spend

TABLE 7  
COMPARISON OF THREE STARS

HD	Spectrum	Quantity	U	V	B	G	R	I
194839.....	cB0	Deflection	13.1	11.8	18.5	21.7	26.9	47.5
166620.....	dK2	Deflection	10.2	15.2	25.4	24.8	27.0	32.6
16901.....	cG0	Deflection	13.9	24.7	41.7	43.2	45.7	56.1
.....	cB0-dK2	$\Delta$ mag.	-0.44	+0.11	+0.18	-0.02	-0.16	-0.57
.....	cB0-cG0	$\Delta$ mag.	-0.67	+0.07	+0.15	+0.01	-0.16	-0.55
.....	cG0-dK2	$\Delta$ mag.	+0.23	+0.04	+0.03	-0.03	0.00	-0.02

half an hour or more in measuring the discordant color of a star, using a higher resistance which requires longer times for deflections; but we have let the results stand, assuming that most errors will be averaged out in the mean.

The deviation of the selective absorption from the  $1/\lambda$  law is not a subtle phenomenon—it is conspicuous in the original galvanometer readings of every strongly reddened B star. As an illustration we give in Table 7 the deflections of three stars of about the same general color but with different spectra, a reddened B, a dwarf K, and a supergiant G star. The deflections are the original figures corrected slightly for sky background. The  $\Delta$  mags. were formed from the log deflections, referred to the mean of blue, green, and red, and then differenced between the stars. The atmospheric extinction has been ignored.

The high intensities of the Ultra and Infra of the B star are conspicuous in both the deflections and the  $\Delta$  mags. Also, the relative faintness of the Ultra in the cG0 star is a common effect where the other colors of a giant star almost match those of a dwarf. In the routine of observing, when a reddened B star comes along, the recorder at the galvanometer often thinks he has made a mistake of 5 or 10 whole divisions in a reading on the Ultra or Infra, but the regular check back on the deflections reassures him that it is only the effect of space reddening that he is seeing.

With the possibility of instrumental errors disposed of, the question remains whether there is a systematic selection of the so-called "reddened" B stars which makes them different from the normal or less reddened ones. The stars of all types from B to M are surprisingly like black bodies, giving nearly linear color-curves when log intensity or  $\Delta$  mag. is plotted against  $1/\lambda$ , despite the absorbing effects of spectral lines and bands.

The exception is the lowered intensity in the Ultra caused by strong hydrogen absorption in the A stars. This effect extends to the F stars but is not noticeable in stars earlier than B5. In Table 3 it will be noticed that nearly all the B stars in the last half of each class are marked as c stars. In other words, a star must be of high luminosity to be seen at a sufficient distance through the absorbing cloud to be strongly reddened. Nevertheless, there is the same kind of absorption all the way down the list no matter how the stars are compared. We have not been able to find any systematic difference between the color-curves of stars with sharp and nebulous lines. When two early B stars are of the same general color, they yield the same intensity over the whole spectrum. This fact may be checked anywhere in the list. Moreover, the "c" designation was added to the spectra of a number of stars after they were known to be reddened.

The great sensitivity of the index  $U - I$  to a small effect of space reddening makes it difficult to find a normal O or early B star in the summer sky. On the basis of our previous color index,  $C_1$ , more than 20 of the 69 stars, or nearly one-third, have a color excess of  $+0.05$  mag. or less; but there are only half a dozen stars with  $U - I$  within 0.20 mag. of the bluest star in each class, or fewer than 10 per cent. In fact, the only B0 star which looks normal is HD 5394,  $\gamma$  Cassiopeiae, a star one would scarcely choose for a standard of color. The bright Milky Way from Perseus through Cygnus down to the star clouds of Sagittarius is simply a region of general absorption when tested by the colors of distant early B stars. It is probable, however, that a number of normal B stars for standards can be found in the Orion region. We leave to further investigation whether the stars at the top of each class in our list are of extra high temperature or simply have less absorption than any others accessible to measurement.

In the course of the work on later-type stars, from A to M, a dozen cases of obvious space reddening among supergiants in low latitudes were found. The standards of comparison are more difficult to select for these stars than for the B stars. Nevertheless, it is obvious that the same law of reddening holds. There is the same excess of intensity in the Ultra and Infra for all reddened stars. In fact, all the evidence we have supports the conclusion that the selective absorption in space has the same quality everywhere.

The deviations from the  $1/\lambda$  law of absorption would raise, rather than lower, the ratio of total to selective absorption which we derived in previous work on colors.<sup>9</sup> But before discussing that point we can take up again the relation between the previous color index  $C_1$  and the new  $V - B$  and  $U - I$  shown in Figure 3. It is too much to expect that there will be a simple linear relation between any two pairs of colors selected for color indices, but for stars of simple spectra like the B stars, which approximate black bodies in their radiation, the different combinations of filters give results that are readily compared. If we take the slopes of the straight lines in Figure 3, neglecting the zero points, we have the ratios of scales as in Table 8. The ratio between  $U - I$  and  $V - B$  was determined independently in the same manner as the other two.

The effective wave lengths in the system  $C_1$  are  $\lambda = 4190$  and  $4760$ , or  $1/\lambda = 2.39$  and  $2.10$ , respectively, for a source of equal energy along the spectrum. The relative amounts of space absorption for the values of  $1/\lambda$  were computed from the data at the end of Table 6. The agreement between the observed and computed ratios of the new scales to that of  $C_1$  is in part accidental; and, since we are dealing with differences in  $1/\lambda$ , only about two figures are significant in the ratios. In all strictness the absorption of the optical systems of the telescopes and the energy-curves of the stars involved should be taken into account in comparing one color index with another. The colors here considered have all been reduced to outside the atmosphere.

TABLE 8  
RATIOS OF SCALES

Quantity	Observed	Computed
$\frac{V-B}{C_1}$ .....	1.09	1.13
$\frac{U-I}{C_1}$ .....	7.59	7.52
$\frac{U-I}{V-B}$ .....	7.05	6.67

The international scale of color index  $C_{\text{int}}$  is about 1.5 times the scale of  $C_1$  for stars in the North Polar Sequence. Hence,

$$\frac{U - I}{C_{\text{int}}} = \frac{7.5}{1.5} = 5.0.$$

This figure of five times the international scale is not necessarily applicable to all classes of stars, because the strong hydrogen absorption in the ultraviolet region of the A stars and the bands in the red region of the M stars introduce complications. Nevertheless, the increased leverage for color is ample to take care of many new problems for some time to come.

The final values of the observed absorption at different wave lengths and the extension to the infrared are in Table 9. The values of the absorption for U and I are taken as 1.00 mag. and 0.00 mag., respectively, and the intermediate values for the other colors are from Table 6. The absorption for  $I_1$ ,  $1/\lambda = 0.80$ , is extrapolated from B and I, since measures with a slit spectrophotometer show that the  $1/\lambda$  law holds very closely in this region out to  $I_1$ . The extrapolation on the same basis out to  $I_2$ ,  $1/\lambda = 0.00$ , gives a reasonable upper limit for the zero point of the absorption.

Interpolations in the table for the blue and yellow of  $C_1$ ,  $1/\lambda = 2.39$  and  $2.10$ , give  $A_b - A_y = E_1 = 0.130$ . Taking the photographic wave length as  $\lambda = 4250$ ,  $1/\lambda =$

TABLE 9  
ABSORPTION AT DIFFERENT WAVE LENGTHS

Quantity	U	V	B	G	R	I	$I_1$	$I_2$
$\lambda$ .....	3530	4220	4880	5700	7190	10,300	12,500	$\infty$
$1/\lambda$ .....	2.83	2.37	2.05	1.75	1.39	0.97	0.80	0.00
$A - A_1$ .....	+1.000	+0.821	+0.676	+0.498	+0.274	0.000	-0.106	-0.607

2.35, we have  $A_{\text{pg}} - A_1 = 0.813$ . If the absorption in the infrared falls off between  $I_1$  and  $I_2$ , the value of  $A_{\text{pg}}$  would lie between  $0.813 + 0.106 = 0.919$  and  $0.813 + 0.607 = 1.420$ . Hence  $A_{\text{pg}}/E_1$  would be between 7.1 and 10.9—say between 7 and 11.

In our previous discussion of absorption<sup>10</sup> from photoelectric colors we used  $A_{\text{pg}}/E_1 = 9$ , or, on the international scale,  $A_{\text{pg}}/E_{\text{int}} = 6$ ; and, until the law of selective absorption is extended farther to the infrared, there seems to be no good reason to change these figures. The present work confirms the high ratio of total to selective absorption even if there is no nonselective absorption. We may note that Greenstein and Henyey<sup>11</sup> have concluded that the nonselective absorption is practically zero, and from other considerations they derive  $A_{\text{pg}}/E_1 = 8.1 \pm 0.4$ .

We are aware of no theory of the composition of the interstellar material which will help to extrapolate the value of the absorption for longer wave lengths. Even the simple  $1/\lambda$  law requires *ad hoc* assumptions about the proportions of differently sized particles. The deviations from that law now give the theorist further material for study. One thing seems certain, since the law of space reddening is everywhere the same: some sort of equilibrium must have been reached, and the interstellar dust cloud is at least a semi-permanent part of the Galaxy.

We are indebted to Messrs. G. M. Barthold Bouricius and Willard G. Bouricius for assistance in the observations and computations for this paper. The investigation has been supported in part by grants from the Alumni Research Fund of the University of Wisconsin and from the California Institute of Technology in connection with plans for the 200-inch reflector.

<sup>10</sup> *Mt. W. Contr.*, No. 617; *Ap. J.*, 90, 213, 1939.

<sup>11</sup> *Ap. J.*, 93, 327, 1941.

## THE STRONGER LINES OF SINGLY IONIZED DYSPROSIUM AND IDENTIFICATIONS IN THE SOLAR SPECTRUM\*

ARTHUR S. KING AND CHARLOTTE E. MOORE

Mount Wilson Observatory and Princeton University Observatory

Received April 14, 1943

### ABSTRACT

Table 1 lists 527 of the stronger lines of *Dy II* in the spectral range  $\lambda\lambda$  2970–8280. A large proportion of these lines appear in the high-temperature furnace; and their furnace intensities, supplementing those in the arc and spark, indicate, in the absence of term-analysis, the relative levels from which the lines arise. The solar spectrum was examined for the presence of 95 selected lines whose laboratory behavior indicated a low-level origin. Of these, 57 were identified in the sun, in part as members of blends. Of the others, 20 are masked and 18 absent.

The laboratory part of this investigation was undertaken for the purpose of listing the stronger lines of singly ionized dysprosium and, in the absence of term-analysis, to select by means of the electric-furnace spectrum those lines which probably arise from low atomic levels. Data for the spectra of other rare earths, especially samarium,<sup>1</sup> europium,<sup>2</sup> and gadolinium,<sup>3</sup> have shown that the stronger of these low-level ionized lines may be expected to appear in the solar spectrum. From the laboratory results for dysprosium a list has been made of the solar lines which appear to be due at least in part to *Dy II*.

The spectrograms extend from  $\lambda$  2970 to  $\lambda$  8280, the second order of the 15-foot concave grating (scale, 1 mm = 1.86 Å) being used to  $\lambda$  5200, the first order from  $\lambda$  5200 to  $\lambda$  8280. The dysprosium compounds were from a collection prepared by G. Urbain. The electrodes for the arc and spark were as a rule of "spectroscopically pure" graphite, but silver electrodes were used when elimination of the CN bands was desired. For the furnace spectrum, the dysprosium was vaporized in the carbon-tube vacuum furnace at a temperature near 2600° C.

Comparison of arc and spark spectra usually served to distinguish the lines of *Dy II* from those of *Dy I*. The classification was confirmed by comparing spectrograms obtained when regions of the arc having different degrees of ionization were projected on the slit, also by furnace spectra in which the spectrum of dysprosium alone was compared with that of a mixture with cesium. The low ionization potential of cesium gave an excess of free electrons, permitting recombination and weakening the lines of *Dy II*.<sup>4</sup>

A preliminary comparison with the solar spectrum showed the types of *Dy II* lines which are likely to be present. These lines are strong in the arc and prominent in the furnace and, in general, are of reduced intensity in the spark compared with lines whose absence in the furnace indicates that they are from high levels.

Table 1 includes the lines presumably of low level and also those strong enough in the arc to be useful for identifications in spectra of stars having a higher degree of ionization than the sun. Arc, spark, and furnace intensities are given, and the table is extended to wave lengths both above and below the range where solar coincidences were found. In the near-ultraviolet the *Dy II* spectrum is very rich, and only a fraction of the lines of

\* Contributions from the Mount Wilson Observatory, Carnegie Institution of Washington, No. 681.

<sup>1</sup> W. Albertson, *Mt. W. Contr.*, No. 546; *Ap. J.*, **84**, 26, 1936.

<sup>2</sup> A. S. King, *Mt. W. Contr.*, No. 608; *Ap. J.*, **89**, 377, 1939.

<sup>3</sup> A. S. King, *Mt. W. Contr.*, No. 678; *Ap. J.*, **97**, 323, 1943.

<sup>4</sup> A. S. King, *Mt. W. Contr.*, No. 233; *Ap. J.*, **55**, 380, 1922.

fair strength are entered in Table 1. In the long-wave-length region the list is more nearly complete, only the faint lines being omitted.

The wave lengths in the first column of Table 1 are for the most part from the *M.I.T. Wave Length Tables*. Lines measured in the present investigation include those affected by blends as well as all lines for which the values of Eder<sup>5</sup> were the only ones available, as these are based on old standards. Wave lengths above  $\lambda$  5600 are chiefly those by C. C. Kiess.<sup>6</sup> An asterisk after the wave length refers to a note at the end of Table 1.

Table 2 contains lines of arc intensity 100 and higher, taken with their arc and furnace intensities from Table 1. The laboratory behavior of these lines suggested a search for them in the solar spectrum. Solar material collected by one of the writers (C. E. M.) supplements the *Revised Rowland* with many identifications of solar lines from recent material prepared for the "Revised Multiplet Table." These data proved very useful in determining whether lines in the sun nearly coincident with those in Table 2 probably belong wholly or in part to Dy II. Following three columns of laboratory data, Table 2 gives the decimal of the solar wave length, the revised solar identification, intensity in the sun, and difference between solar and arc wave lengths.

Summarizing the identifications in Table 2, we find 57 solar lines ascribed to Dy II, nearly half of them as probable members of blends. Twenty are masked by strong lines of other elements, and 18 (as a rule, lines of moderate strength) are absent. As an example of a masked line, the strong Dy II line,  $\lambda$  3968.395, probably present in the sun, would be covered by the H line of ionized calcium.

In the *Revised Rowland* 12 lines are ascribed to Dy II, most of them questioned. Of these, the identifications of 7 are confirmed in Table 2. The wave lengths of 4 agree with those of very strong lines of Dy I.<sup>7</sup> The twelfth,  $\lambda$  3544.230, is not strong enough in the laboratory to be expected in the sun.

At wave lengths greater than the questioned line,  $\lambda$  5915.168, many strong Dy II lines occur in the arc, but no solar agreements with the lines in Table 1 were found, unless  $\lambda$  7055.95 is part of a solar blend. The relatively low furnace intensities of Dy II lines in this region indicate that they are from higher levels and therefore unlikely to appear in the sun.

A solar intensity of 1 is the maximum for unblended Dy II lines, exemplified by  $\lambda$  3531.712 and  $\lambda$  4077.974. These and other very strong enhanced lines in the short-wave-length region appeared faintly in the furnace spectrum at a temperature between 2000° and 2100° C.

<sup>5</sup> *Sitzungsber. wien. Akad.*, IIa, 127, 1099, 1918.

<sup>6</sup> *Bureau of Standards Scientific Papers*, 18, 695, 1923.

<sup>7</sup> A. S. King, *Pub. A.S.P.*, 54, 201, 1942.

TABLE 1  
STRONGER LINES OF DY II

$\lambda$	Intensity			$\lambda$	Intensity		
	Arc	Spark	Furnace		Arc	Spark	Furnace
3002.58	30	25	...	3178.373	60	20	5
3003.762	40	20	2	3184.777	40	25	3
3015.074	30	25	...	3186.375	80	60	2
3015.694	60	50	2	3187.678	60	60	1
3016.96	40	60	...	3193.299	80	25	8
3026.163	150	60	25	3206.403	80	80	1-
3029.826	50	80	...	3207.120	60	60	1
3036.709	30	15	3	3208.817	80	60	2
3038.291	300	300	5	3215.189	125	125	3
3043.144	80	80	2	3216.628	150	200	4
3043.44	30	20	1	3221.499	50	50	1-
3047.563	60	50	2	3221.641	50d	25	2
3049.133	40	30	1	3223.282	80	80	2
3051.457	60	20	4	3225.084*	30	15	4
3052.324	40	60	...	3225.949	80	60	2
3060.653	80	80	1	3235.892	125	125	6
3061.375	30	30	...	3236.634*	80	80	5
3061.506	20	15	...	3240.878	30	30	...
3062.620	100	80	6	3245.123	150	150	2
3066.994	60	60	1	3248.364	50	40	1
3071.920	80	40	6	3251.260	300	300	15
3073.542	80	80	1	3251.90	50	25	1
3078.686	80	60	2	3252.19	50	50	1-
3079.341	50	40	1	3256.25	80	60	1
3082.515	50	15	3	3260.696	50	25	?
3093.108	60	20	2	3261.22	30	40	...
3095.75	40	30	...	3266.00	60	80	1-
3101.891	20	80	...	3266.207	80	125	1-
3101.935	50		4	3269.107	100	30	15
3103.246	60		4	3272.73	80	60	1-
3103.839	60	60	2	3279.692	80	60	3
3105.001	40	50	...	3280.084	250	100	25
3109.768	150	100	3	3282.774	100	150	1
3120.184	80	80	1	3287.943	50	30	1-
3126.18	50	30	1	3293.804	40	15	5
3128.409	150	125	2	3296.300	40	30	1
3135.380	500	500	10	3297.607	30	40	3
3140.645	150	150	2	3305.398	40	30	1-
3141.13	200	60	15	3305.510	50	40	1-
3142.303	40	40	1	3306.185	50	50	1-
3143.831	50	50	1	3308.793	150	100	3
3146.165	60	80	1	3308.877	300	200	8
3147.533	30	30	...	3312.716	100	50	10
3151.893	50	25	3	3316.325	150	60	20
3156.519	500	500	10	3317.115	40	30	2
3160.499	40	15	2	3319.887	400	100	60
3162.832	250	250	4	3326.188	50	25	2
3169.990	300	100	20	3327.080	30	10	1
3170.746	40	40	1	3334.14	30	25	...
3177.88	125	125	1	3339.505	50	30	15

TABLE 1 -- Continued

$\lambda$	Intensity			$\lambda$	Intensity		
	Arc	Spark	Furnace		Arc	Spark	Furnace
3340.986	200	200	2	3473.702	50	40	4
3341.420	40	10	10	3474.29	30d	50	1-
3341.880	80	30	40	3477.074	150	100	25
3347.82	40	30	...	3480.817	20	20	1
3352.696	50	60	...	3484.683	40	30	2
3353.583	125	50	25	3487.58	30d?	40	2
3356.220	40	40	...	3494.165	30	30	1
3358.596	50	15	8	3494.496	300	150	60
3359.478	40	40	1-	3496.339	50	30	5
3365.80	30	30	1	3497.841	40	25	2
3368.104	150	50	40	3498.708	100	40	15
3370.848	40	50	...	3498.939	30	15	2
3371.694	40	40	1-	3501.436	40	40	1-
3371.806	40	40	2	3504.522	80d?	80	4
3376.43	40	30	3	3505.457	50	40	5
3378.899	25	40	...	3505.83	20	10	1
3385.027	600	400	100	3506.820	150	50	30
3386.58	60	80	...	3512.563	20	20	1-
3388.863	100	60	10	3512.707	30	40	1-
3393.583	400	250	80	3517.270	60	50	3
3396.169	200	150	50	3523.983	400	300	80
3407.168	40	30	3	3531.712	2000	1500	300
3407.801	800	500	150	3534.963	200	100	50
3408.157	60	60	2	3536.024	400	400	60
3413.794	150	80	40	3538.523	300	150	100
3414.830	40	30	5	3539.376*	30	20	?
3417.140	20	20	1	3542.333	150	100	10
3418.14	20	20	1-	3544.211	25	20	3
3419.643	50	40	5	3544.355	20	20	2
3422.878	25	25	1	3546.841	100	50	30
3425.057	50	20	6	3548.202	20	20	1
3429.442	60	60	3	3550.228	300	200	60
3431.79	30	30	1-	3551.614	150	100	25
3432.575	25	15	4	3563.154	200	100	50
3434.373	250	150	60	3563.699	40	50	3
3438.952	40	40	1	3569.669	20	10	4
3440.94	60	80	2	3573.838	60	50	2
3441.453	150	60	25	3574.160	100	60	6
3445.582	300	150	80	3576.250	300	200	60
3447.001	60	40	6	3576.873	150	100	15
3449.898	30	20	5	3577.989	60	30	10
3454.326	200	150	40	3580.043	40	30	4
3454.516	40	40	2	3582.030	20	20	1
3456.566	125	80	10	3584.426	40	40	2
3460.971	300	150	60	3585.066	250	100	60
3463.876	20	10	3	3585.776	150	80	15
3468.435	60	40	4	3586.116	50	30	8
3471.145	60d	40	4	3590.072	30	25	1
3471.531	40	20	3	3590.667	25	20	1
3471.610	50	30	3	3591.423	125	80	10

TABLE 1 -- Continued

$\lambda$	Intensity			$\lambda$	Intensity		
	Arc	Spark	Furnace		Arc	Spark	Furnace
3591.815	40	40	2	3715.309	15	10	1-
3592.117	30	30	4	3716.938	20	20	2
3595.046	125	125	10	3724.447	150	80	50
3596.067	40	30	3	3747.827	100	40	30
3600.392	50d?	40	6	3748.063*	20	20	...
3602.815	30	25	2	3750.334	15	15	...
3606.126	150	100	25	3753.514	150	60	40
3612.782	20	30	1	3753.762	200	100	20
3613.078	15	20	1-	3757.372	500	300	125
3614.083	20	20	1-	3773.319	25	20	10
3618.101	20d	20	2	3779.247	25	20	1
3618.522	40	15	15	3782.888	20	10	8
3619.450	20	15	2	3785.424	30	15	8
3619.977	20	20	1	3786.177*	300	150	80
3620.154	60	40	4	3788.449*	150	80	50
3624.264	30	30	1	3791.865	50	25	20
3629.440	100	80	5	3804.152	40	20	15
3630.238	250	150	60	3806.280	50	100	...
3630.46	25	15	1	3809.035	25	20	...
3632.778*	25	20	?	3813.684	40	30	3
3633.015	15	25	1-	3816.770	200	150	10
3635.267	30	25	3	3822.591	20	15	5
3637.273	25d	15	5	3825.65*	30d	15	?
3640.253	100	60	20	3825.95	20?	30	...
3643.927*	40d	15	25	3831.643	20	15	5
3645.416	1000	800	150	3836.498*	250	150	40?
3645.860	30	20	2	3841.316	100	60	30
3646.60	15	15	1	3846.358	25	15	3
3648.807	60	50	3	3849.400*	25	25	?
3661.777	15	15	1-	3853.033	150	100	30
3664.68	60d	50	3	3866.592	30	20	10?
3665.218	30d	30	1-	3868.454*	50	30	?
3668.911	15	10	2	3869.430*	30	20	?
3671.697	20	15	1	3869.870*	60	30	20?
3672.312	125	80	10	3871.635	30	20	...
3672.695	40	20	10	3872.103*	600	500	200?
3673.152	40	15	10	3873.993*	125	80	40?
3674.093	250	60	60	3879.083	40d	40	15
3676.587	250	60	60	3882.001*	25	20	?
3694.414	25d	20	2	3888.40	15	20	...
3694.812	500	300	125	3889.013	20	10	6
3697.311	30	20	2	3895.35	25	30	...
3698.206	60	50	5	3898.535	500	400	150
3701.622	40	30	2	3904.21	20	15	3
3707.404	30	20	3	3913.95	15	20	...
3707.569	40	30	5	3914.874	80	40	8
3708.227	40	30	5	3915.601	80	40	10
3710.080	30	25	4	3923.394	30	30	1
3711.660	30	20	2	3929.348	15	20	...
3713.839	15	10	?	3931.290	20	15	...

TABLE 1 -- Continued

$\lambda$	Intensity			$\lambda$	Intensity		
	Arc	Spark	Furnace		Arc	Spark	Furnace
3931.537	150	125	30	4375.323	50	60	...
3932.228	20	20	2	4394.974	40	15	5
3934.17	20	20	...	4409.384	200	100	50
3936.03	15	15	...	4449.702	300	150	60
3942.536	50	40	5	4467.89	20	15	3
3944.692	800	600	150	4468.137	60	20	15
3946.939	30	40	...	4503.252	25	15	...
3950.399	50	50	2	4518.538	15	30	...
3954.565	40	30	2	4527.777	30	20	4
3957.802	60	60	4	4538.76	20	15	2
3968.395*	1000	800	200	4541.698	30	40	...
3978.573	250	200	30	4550.89	15	20	1
3979.461*	25	15	4?	4587.931	40	30	...
3981.938	100	80	10	4617.27	30	20	4
3983.664	150	100	50	4620.032	60	40	10
3984.226	80	50	5	4664.675	80	40	15
3991.331	30	25	...	4689.768	40	50	4
3996.699	150	100	40	4698.687*	60	60?	2
4000.454	800	600	200	4727.133	50	150	...
4011.295	30	20	2	4731.851	150	80	40
4014.713	40	25	5	4745.806	30	25	...
4027.787	30	25	...	4755.01	20	20	...
4032.480	50	50	2	4756.674	15	10	...
4050.579	100	60	30	4760.010	50	30	2
4055.159	40	25	4	4786.935	50	25	5
4073.110	150	80	50	4829.692	20	20	...
4077.974	800	500	200	4833.768	15	15	...
4087.213	25	20	2	4856.238	20	20	...
4091.533	20	15	2	4868.058	15	15	...
4103.312	600	400	150	4889.325	50	60	...
4105.051	20	15	...	4890.102	60	15	5
4111.346	125	80	40	4922.227	25	50	...
4119.325*	20	15?	...	4923.161	60	25	8
4124.626	40	20	4	4957.357	1500	500	200
4128.241	30	15	3	4974.998	15	20	...
4129.425	100	50	20	5017.996	20	15	...
4141.516	40	15	10	5090.378	50	25	5
4143.100	150	80	30	5092.206	15	15	...
4206.544*	40	20	20?	5107.979	20	20	...
4247.360	20	15	...	5129.830	15	15	...
4256.323	100	30	20	5139.594	200	80	20
4294.936	40	40	...	5145.203	15	20	...
4308.623	200	100	50	5160.998	25	25	...
4325.110	40	30	...	5164.14	25	30	...
4328.903	20	10	3	5169.699	150	60	20?
4339.633	40	50	2	5188.477	15	10	...
4358.443	60	20	15	5192.872	1000	400	150
4364.223	40	60	...	5197.663	150	80	8
4374.243	125	40	25	5246.94	20	20	...
4374.771	100	60	10	5255.03	15	20	...

TABLE 1 -- Continued

$\lambda$	Intensity			$\lambda$	Intensity		
	Arc	Spark	Furnace		Arc	Spark	Furnace
5258.392	25	15	...	6353.66	20	15	...
5272.261	80	30	2	6390.661	25	25	...
5275.314	100	100	...	6396.61*	200	200	...
5279.708	125	100	...	6427.79	15	10	...
5284.987	50	30	...	6435.66	15	15	...
5297.827	60	50	...	6441.85	10	20	...
5300.31	20	8	2	6443.71	40	40	...
5309.010	150	150	...	6468.60	50	50	...
5324.697	125	125	2	6472.04	30	20	...
5330.72	10	25	...	6483.62	250	100	...
5337.432	30	20	...	6519.16	30	20	...
5369.240	20	50	...	6532.40	10	25	...
5385.628	30	10	...	6548.28	80	40	...
5389.574	200	40	5	6594.16	50	40	...
5399.928	20	10	...	6654.27	25	25	...
5426.706	80	100	5	6700.66	40	30	...
5443.339	30	30	...	6802.20	25	25	...
5455.448	40	40	...	6807.36	20	15	...
5469.096	40	20	...	6828.41	10	10	...
5471.93	20	10	...	6897.98	100	60	4
5515.402	30	15	...	6899.34	1500	1000	40
5583.19	15	15	...	6902.11	10	10	...
5592.306	20	30	...	6906.57*	150	80	?
5597.346	20	20	...	6912.27	30	25	1
5600.71*	150d	60	20	6932.62	50	40	...
5641.524	40	15	3	6950.29	250	200	8
5660.282	10	15	...	6953.00	30	20	...
5663.93	20	10	...	7014.66	20	20	...
5695.90	30	20?	4	7055.95	250	200	15
5698.721	50	50	2	7075.15	150	100	12
5856.05	15	15	...	7100.61	15	15	...
5868.091*	150	25	6	7101.70	30	15	1
5902.45	20	20	...	7109.30*	100	60	30
5909.155	25	15	...	7141.52	15	10	...
5915.168	125	80	1	7145.11	10	10	...
5924.54	30	10	1	7149.31	20	15	...
5955.53	10	15	...	7175.16	100	80	3
5964.6*	20	15	...	7234.72*	20	?	...
5978.27	15	15	...	7273.80	50	30	...
6044.491	15	10	...	7288.26	50	30	1
6050.03	25	15	...	7345.18*	300	60	?
6063.561	20	20	...	7361.58	25	20	...
6073.774	25	25	...	7370.26	60	40	1
6074.61	20	15	...	7403.17*	30	20	?
6184.73	15	10	...	7426.99	500	200	30
6196.23	100	50	...	7451.08	40	20	1
6216.59	15	10	...	7457.05	100	60	6
6250.02	15	15	...	7516.59	100	60	8
6316.66	10	10	...	7562.96	250	200	15
6317.24	30	15	...	7577.47*	100	60	5?

TABLE 1 -- Continued

$\lambda$	Intensity			$\lambda$	Intensity		
	Arc	Spark	Furnace		Arc	Spark	Furnace
7648.12	30	25	...	8077.89	10	10	...
7666.78	60	40	2	8098.36	10	25	...
7707.38	10	10	...	8108.40	60	40	5
7711.93	40	25	1	8116.90	40	25	1
7729.78	400	300	20	8144.28	20	15	...
7739.38	15	10	...	8198.75	150	50	10
7751.61*	100d	50	?	8201.55	1000	400	150
7835.55	25	20	...	8208.30	15	10	...
7864.33	60	80	...	8216.98*	25	?	1
7940.67	20	15	...	8218.58*	40	?	3
7982.80	60	50	1	8233.55*	20	?	2
8008.68	40	25	...	8243.95*	20d	?	...
8034.94	25	15	1				
8050.05	25	15	1				
8070.88	80	40	4				

## NOTES TO TABLE 1

$\lambda$	
3225.084	Just resolved from fainter $\lambda$ 3225.156.
3236.634	Usually blended with Dy I $\lambda$ 3236.691.
3539.376	Blend Dy I to red.
3632.778	Blend impurity in furnace.
3643.927	Blend Dy I?
3748.063	Arc intensity variable. May be impurity.
3786.177	Blend Dy I to red.
3788.449	Blend Dy I to violet.
3825.65	Blend Dy I.
3836.498	} Questioned lines uncertain in furnace on account of CN band.
3882.001	
3968.395	Usually blended with Ca.
3979.481	Blend CN.
4119.325	Blend air in spark.
4206.544	Blend Dy I?
4698.687	Blend air line in spark.
5600.71	Blend Dy I?
5868.091	May be Dy I.
5964.6	Blend Dy I.
6396.61	Blend Dy I to violet.
6906.57	Blend strong Dy I to violet.
7109.30	Blend Dy I?
7234.72	Blend air line in spark.
7345.18	Blend Dy I.
7403.17	Blend Dy I to violet.
7577.47	Blend Dy I to violet.
7751.61	Blend Dy I.
8216.98	} Blend air lines in spark.
8218.58	
8233.55	
8243.95	Very wide.

TABLE 2  
LINES OF DY II IN THE FURNACE SPECTRUM,  
WITH CORRESPONDING SOLAR LINES

Laboratory			Sun				Remarks
$\lambda$	Intensity		$\lambda$	Identification	Int.	$\Delta\lambda$ Sun-Arc	
	Arc	Furnace					
3156.519	500	10	.566	.....	0	+0.047	Absent?
3169.990	300	20	70.007	Dy II	-3	+ .017	
3251.260	300	15	.257	Fe	3	- .003	Masked
3280.084	250	25	.....	.....	...	.....	Absent
3308.877	300	8	.....	.....	...	.....	Absent
3312.716	100	10	.700	Ti-Fe II	2	- .016	Masked
3316.325	150	20	.340	Mn Dy II?	-1	+ .015	
3319.887	400	60	.904	NH Dy II	0	+ .017	
3340.986	200	2	1.006	Dy II	-3	+ .020	
3353.583	125	25	.....	.....	...	.....	Absent
3368.104	150	40	.....	.....	...	.....	Absent
3385.027	600	100	.032	Dy II	0	+ .005	
3388.863	100	10	.859	Dy II Cr?	-1	- .004	
3393.583	400	80	.....	.....	...	.....	Absent
3396.169	200	50	.186	Ni	1	+ .017	Masked
3407.801	800	150	.806	Dy II	0	+ .005	
3413.794	150	40	.804	Dy II	-3	+ .010	
3434.373	250	60	.377	Dy II	-2	+ .004	
3441.453	150	25	.453	Cr	1N	.000	Masked
3445.582	300	80	.607	Cr Dy II?	2N	+ .025	
3454.326	200	40	.322	Dy II	-1	- .004	
3456.566	125	10	.581	Dy II	-3N	+ .015	
3460.971	300	60	.978	Dy II	-1	+ .007	
3477.074	150	25	6.989	Ti II-Fe	3d?	- .085	Masked
3494.496	300	60	.516	Cr II Dy II	0	+ .020	
3506.820	150	30	.842	Dy II-	0	+ .022	
3523.983	400	80	.991	Dy II	-2	+ .008	
3531.712	2000	300	.710	Dy II	1	- .002	
3534.963	200	50	.949	Dy II	-1	- .014	
3536.024	400	60	.024	CN-Dy II	-1	.000	
3538.523	300	100	.502	-Dy II	1	- .021	
3542.333	150	10	.332	Dy II	-3	- .001	
3546.841	100	30	.833	Dy II	-2	- .008	
3550.228	300	60	.223	CN Dy II	1N	- .005	
3551.614	150	25	.....	.....	...	.....	Absent
3563.154	200	50	.160	CN Dy II	-2N	+ .006	
3574.160	100	6	.159	Dy II	-3	- .001	
3576.250	300	60	.254	Ce II Dy II	-3	+ .004	
3576.873	150	15	.864	Zr II	1	- .009	Masked
3585.066	250	60	.075	CN Dy II	-2	+ .009	
3585.776	150	15	.715	Fe	6	- .061	Masked
3595.046	125	10	.021	Dy II	-3	- .025	
3606.126	150	25	.133	Dy II	-3	+ .007	
3629.440	100	5	.....	.....	...	.....	Absent
3630.238	250	60	.235	Dy II Ni?	0	-0.003	

TABLE 2 - Continued

Laboratory			Sun				Remarks
$\lambda$	Intensity		$\lambda$	Identification	Int.	$\Delta\lambda$ Sun-Arc	
	Arc	Furnace					
3640.253	100	20	.266	Nd II? Dy II	-3	+0.013	Masked Masked
3645.416	1000	150	.414	Sm II? La II DyII	-1	- .002	
3672.312	125	10	.317	Dy II	-3	+ .005	
3674.093	250	60	.063	Fe-Ni	4	- .030	
3676.587	250	60	.563	Co	2	- .024	
3694.812	500	125	.818	Dy II	-2	+ .006	Masked
3724.447	150	50	.387	Fe	6	- .060	
3747.827	100	30	.823	-Dy II	-1	- .004	
3753.514	150	40	.527	Dy II-CN?	-2	+ .013	
3753.762	200	20	.753	Dy II	-1	- .009	
3757.372	500	125	.370	Dy II	-1	- .002	Masked Masked
3786.177	300	80	.177	Fe Dy II?	4d?	.000	
3788.449	150	50	.441	Dy II CN	0	- .008	
3816.770	200	10	.747	Mn	1	- .023	
3836.498	250	40?	.503	CN	1	+ .005	
3841.316	100	30	.282	Cr	1	- .034	Masked
3853.033	150	30	.049	Ti Dy II?	-1	+ .016	Masked?
3872.103	600	200?	.064	CN	1N	- .039	
			.181	CN	0	+ .078	
3873.993	125	40?	.961	Co Fe	4	- .032	Masked
3898.535	500	150	.514	Co Ti Dy II	0	- .021	
3931.537	150	30	.590	.....	1N	+ .053	Masked?
3944.692	800	150	.686	Fe?-Dy II	1	- .006	Masked
3968.395	1000	200	.494	Ca II	700	+ .099	
3978.573	250	30	.576	Dy II	-1	+ .003	
3981.938	100	10	.....	.....	...	.....	Absent
3983.664	150	50	.670	Dy II	-1	+ .006	Masked Absent Absent
3996.699	150	40	.700	Dy II	-1	+ .001	
4000.454	800	200	.468	Fe Dy II	2	+ .014	
4050.579	100	30	.568	Dy II	-1	- .011	
4073.110	150	50	.138	Dy II	-1	+ .028	
4077.974	800	200	.977	Dy II	1	+ .003	Masked Absent Absent
4103.312	600	150	.319	Dy II	0	+ .007	
4111.346	125	40	.360	Cr	1	+ .014	
4129.425	100	20	.....	.....	...	.....	
4143.100	150	30	.....	.....	...	.....	
4256.323	100	20	.317	Dy II Fe	-1	- .006	Masked Absent
4308.623	200	50	.601	-Dy II	2Nd?	- .022	
4374.243	125	25	.228	.....	1	- .015	
4374.771	100	10	.....	.....	...	.....	
4409.384	200	50	.369	-Dy II	-1N	- .015	
4449.702	300	60	.721	Dy II-	-2	+ .019	Absent Masked Absent
4731.851	150	40	.....	.....	...	.....	
4957.357	1500	200	.309	Fe	5	- .048	
5139.594	200	20	.....	.....	...	.....	
5169.699	150	20?	.704	Dy II?-Fe II?	-3	+ .005	
5192.872	1000	150	.....	.....	...	.....	Absent
5197.663	150	8	.....	.....	...	.....	Absent
5389.574	200	5	.....	.....	...	.....	Absent
5868.091	150	6	.....	.....	...	.....	Absent
5915.168	125	1	.168	Dy II?	-3	.000	

## SOME USES OF THE DIRECT-INTENSITY MICROPHOTOMETER

ROBLEY C. WILLIAMS AND W. ALBERT HILTNER\*

Observatory of the University of Michigan

Received April 6, 1943

### ABSTRACT

Three principal uses of the direct-intensity microphotometer of the University of Michigan are discussed.

1. *Direct-intensity microphotometer.*—The sensitivity has been improved so that now it is always better than 1 per cent of the continuum of absorption spectra for plate densities between 2.0 and 0.1. The method of obtaining direct-intensity tracings from spectrograms calibrated especially for the instrument is described, as well as a method of rapid intensity analysis of spectrograms calibrated by means of "standard spots."

2. *Transmission microphotometer.*—The instrument can be used as a standard transmission microphotometer by the addition of a power amplifier, either D.C. or A.C., with rectifier and a galvanometer. A comparison of a linear intensity tracing and a transmission tracing is shown and is used to illustrate the distorted and inadequate mental picture received from the inspection of standard microphotometer tracings.

3. *Isophotometer.*—Isophotal contours of the solar corona of August 31, 1932, and of NGC 4594, 3115, and 750-751 are shown.

The direct-intensity microphotometer constructed by Williams and Hiltner<sup>1</sup> has been in operation at the Observatory of the University of Michigan for about two and one-half years. During that time its characteristics and possibilities have been explored at some length; and, as frequently happens in a development of this nature, the instrument has been found to possess a degree of versatility not realized at the time of the introductory publication describing it. This paper will describe briefly the operation of the instrument, with particular emphasis upon the many different uses to which it may be put.

The reader is referred to the detailed account<sup>2</sup> of the construction and operation of the microphotometer, but a very brief description will be offered here. The instrument has two plate carriages, both of which can be driven along the usual kind of parallel ways at equal or varying rates of travel. One carriage, called the balance carriage, can also be caused to move in a transverse direction. On the two carriages are placed the photographic plates to be analyzed and slit images of two light-sources are focused on the plates. By means of optical, electrical, and mechanical devices the balance carriage is caused to move transversely until the transmission of that part of the photograph under analysis by the slit image is equal to the transmission analyzed by the slit image on the plate held in the other carriage. The motion of the balance carriage is transferred, by means of a cam and mirror, to the motion of a recording light-beam across the face of the usual kind of microphotometer drum. Thus, if the balance carriage contains a calibrated spectrophotometric photographic wedge and the other carriage contains a spectrogram, the instrument will maintain constant balance, and the relative intensity distribution in the spectrogram can be directly recorded. The effect of the calibration spectrogram is always introduced at the right wave length, since the two carriages are driven so as to keep together in wave length. Any function of intensity, such as linear, log, or antilog intensity, can be recorded by using a properly shaped cam.

It has been found, however, that the instrument can be used in ways other than

\* Fellow of the National Research Council.

<sup>1</sup> *Pub. Obs. U. Michigan*, 8, 45, 1940.

<sup>2</sup> *Ibid.*

indicated in the above paragraph, either without modification or with only slight modification. The uses may be divided into three classes: (1) direct-intensity microphotometer, (2) transmission microphotometer, and (3) isophotometer.<sup>3</sup>

# I. DIRECT-INTENSITY MICROPHOTOMETER

## A. LINE CONTOURS

The discussion in this section will be confined to remarks additional to those of the previous publication.<sup>4</sup> These are necessitated by the increased usefulness of the instrument and by the increased excellence of its performance.

In the first place, it is found that the original negatives of the stellar spectra and of the calibrations can be used, if there is no objection to cutting the original plate. The

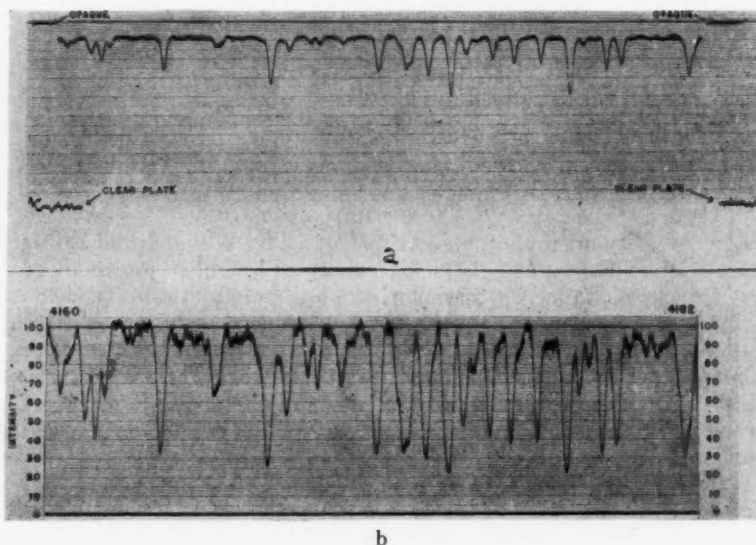


FIG. 1.—Tracings of  $\alpha$  Canis Minoris. (a) transmission; (b) direct intensity

mechanical accuracy of the instrument is considerably greater than the photographic accuracy of any emulsion, and consequently enlargements do not have to be employed. This conclusion is justified by the experience of Hiltner,<sup>5</sup> who, in the process of tracing several hundred direct-intensity-curves for which the calibration spectra were only 8 mm wide, found that the average error of tracing which could be attributed to inaccuracies in the instrument was of the order of 0.5 per cent. There is now in progress, with the collaboration of the McDonald Observatory, an atlas of direct-intensity tracings of the spectra of several typical stars, and it is being found in the course of this work that the instrument will reproduce a tracing with no variations in intensity as great as 1 per cent. Figure 1, *b*, is a sample curve from the atlas and shows a short region of the spectrum of  $\alpha$  Canis Minoris.

The sensitivity of the instrument has been increased considerably over that previously reported. Following the installation of a few minor changes in the electrical circuit, the sensitivity can be kept approximately constant, and always better than 1 per cent of the

<sup>3</sup> *Ibid.*, p. 103, 1941.

<sup>4</sup> *Ibid.*, p. 45, 1940.

<sup>5</sup> Unpublished thesis.

continuum, for all plate densities between 2.0 and 0.1. A thorough discussion of accuracy, sensitivity, "hunting," and similar phenomena will be included in the forthcoming atlas.

#### B. CONTINUOUS SPECTRA

The instrument is of considerable use as a timesaver in photometry of continuous spectra. This is an application encountered particularly in the derivation of relative energy distribution in the spectra of stars. As an example of its speed, we are able to obtain log-intensity tracings of the spectra of two stars, note and record the values of the log intensities at 40 wave lengths over a range of 2500 Å, and difference them on a magnitude scale—all within an elapsed time of 80–90 minutes.

Another example of continuous photometry illustrating a high degree of simplification is in the evaluation of the transmission of a photometric filter. Two spectrograms are taken of a continuous source of radiation, one with and one without the filter in the beam. The exposures are of equal duration, and the lamp is kept at constant temperature from one exposure to the other. A calibration spectrogram is also obtained. Direct-intensity tracings on a log-intensity scale of the spectrogram with filter and of the one without filter, when differenced, give directly the logarithm of the transmission of the filter.

#### C. USE WITH STANDARD SPOTS

It will be of interest to those whose spectrographic equipment allows only "standard spots" to be impressed as a calibration upon the spectrograms to realize that the instrument can be used as a sort of automatic Hartmann photometer to furnish "direct-intensity" tracings from plates calibrated in this inadequate fashion. This is accomplished in the following way: A set of photographic wedges is made, with light of a color similar to that employed in exposing the standard spots. The members of the set are made to differ in photographic contrast by means of variations in the development process and each wedge to have a density range greater than that encountered in the standard spots. The wedges are to be used as intermediaries, like the wedge in a Hartmann photometer. A preliminary trial is made by placing a wedge on the balance carriage and the spots on the other carriage. The position of the recording beam on the drum is noted when the instrument achieves balance for each spot. The wedge is then selected which comes closest to having a proportional relation between the position of the recording beam on the drum (measured from a fixed zero) and the known relative intensities corresponding to the spots.

The remainder of the procedure is straightforward. A tracing of the spectrogram is made, with the wedge as the "calibration spectrum" on the balance carriage. The spectrogram is then replaced by the standard spots on the other carriage, and the positions of the recording beam are impressed on the record. If these positions are nearly enough proportional to the relative intensity of the standard spots, the tracing is used directly. If not, the necessary small corrections can be made to the apparent intensities of the spectral lines. A large set of wedges, once made, does not have to be made again, and a wedge of sufficiently close correlation can always be found. It should be noted, of course, that the final tracing is no better than the original calibration, and the higher accuracy of monochromatic calibration cannot be expected from the heterochromatic standard spots.

#### II. TRANSMISSION MICROPHOTOMETER

In our previous discussions of the instrument we failed to point out that it can be used in the form of a standard microphotometer, where the function of the instrument is to measure solely the relative transmission of the exposed regions of the photographic emulsion. It is felt that this omission has led to understandable misconceptions of the general usefulness of the equipment and that a specific description of the additional use should be made.

All that is needed in the way of additional equipment is a power amplifier, either D.C. or A.C. with rectifier, and a D'Arsenval-type galvanometer. The operation of the instrument is then as follows: The analyzing beam of light traversing the balance carriage is occulted by the eyepiece, while the spectrogram is placed on the other plate carriage. If the D.C. amplifier is used, the flicker motor is not operated, and its shaft is turned to a position such as to transmit maximum light. The output of the phototube is then connected to the amplifier, and the instrument is operated like the ones developed by Beals.<sup>6</sup> In its present form, however, our instrument has no second slit, and hence its resolving-power is not expected to be as high as possible.

Figure 1, *a*, is a transmission tracing of the *same region* of the same spectrogram of  $\alpha$  Canis Minoris as is shown in Figure 1, *b*. This statement is hard to believe, but it is only a moderate example of the distorted and inadequate mental picture one gets from inspecting standard microphotometer tracings of well-exposed spectrograms. In this example the density is about normal for a good plate: 1.1 for the "continuum" and 0.4 for the centers of the absorption lines. The most obvious misrepresentations inherent in the transmission tracings are as follows: In Figure 1, *a*, one gets the impression of a fairly reliable continuum, from which he would probably measure line depths and areas, whereas, as Figure 1, *b*, shows, there is no continuum present at all. The transmission tracing practically obliterates all lines whose residual intensity, measured with respect to the top of the tracing, is greater than 80 per cent. The transmission tracing does not give adequate impressions of blends; for example, several lines in Figure 1, *a*, would not be considered blended, but it is clear from Figure 1, *b*, that they are. In view of the common practice of astronomers of obtaining general notions of spectra from transmission tracings and of the tendency to use spectra of densities as great as 2.0 (where the distortion would be many fold as great as shown here), it is our belief that the problem here discussed cannot be overemphasized.

Of course, the situation exemplified above can be improved by the use of a logarithmic amplifier<sup>7</sup> in obtaining transmission tracings, and the obliteration of the faint lines can be partially remedied by using a full-scale deflection of 1 meter or so. However, in the latter case the *relative warping* or *distortion* of the tracings persists.

### III. ISOPHOTOMETER

#### A. DIFFUSE OBJECTS

The use of the direct-intensity microphotometer in tracing isophotal contours of diffuse objects has already been described in some detail.<sup>8</sup> Suffice it to say here that, if a negative containing closed contours of equal photographic density is placed on the balance carriage and if a negative containing a given density is placed on the other carriage (and not moved), the instrument can be operated so as to trace curves of equal density on the first negative. When this tracing motion is communicated to the recording drum (preserving the proper scale), an isophotal contour is obtained. Further, if the negative placed in the stationary carriage constitutes a valid photographic calibration of the negative to be contoured, there will result isophotal contours of known intensity intervals. However, it is our experience that only a small percentage of photographs of celestial objects, such as nebulae, have ever been calibrated, and consequently most plates in the files of observatories are worthless for quantitative work with isophotal contours. We hope that the knowledge that rather complete contours of an object of uncomplicated intensity distribution can be obtained in a few hours' time may encourage astronomers to calibrate properly a greater percentage of their photographs.

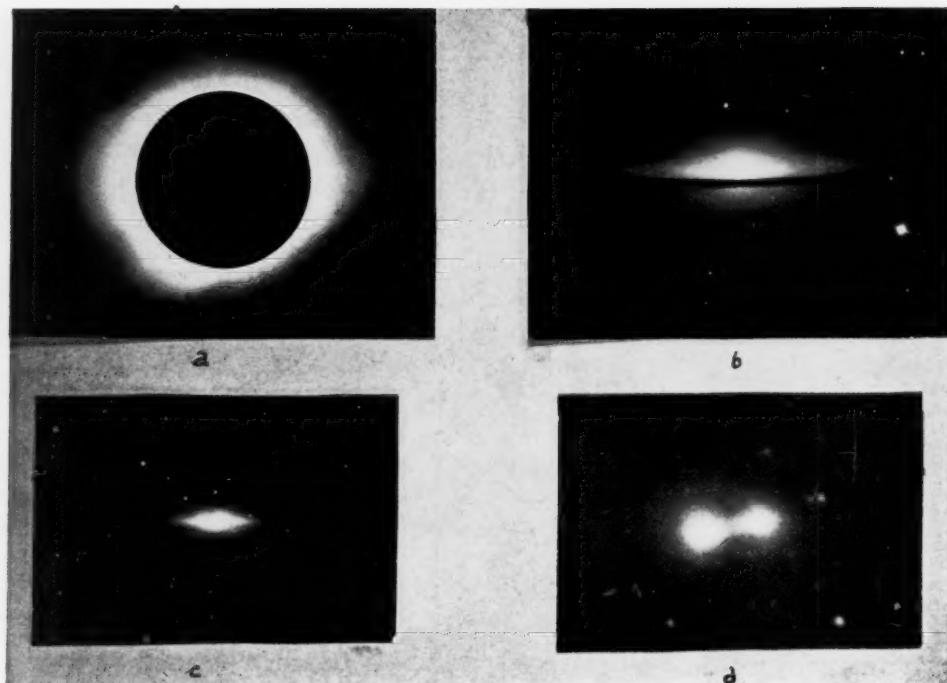
<sup>6</sup> *M.N.*, **96**, 730, 1936.

<sup>7</sup> Dimitroff and Menzel, *Harvard Ann.*, **105**, 99, 1937.

<sup>8</sup> Williams and Hiltner, *Pub. Obs. U. Michigan*, **8**, 103, 1941.

e  
e  
s  
e  
l  
e  
r  
n  
y  
n  
t  
t  
n  
e  
e  
f  
f  
e  
n  
y  
f  
t  
l  
f  
e

PLATE VI



(a) SOLAR CORONA, AUGUST 31, 1932; (b) NGC 4594; (c) NGC 3115; (d) NGC 750-751

Plate VI and Figure 2 show four typical isophotal contours obtained with the instrument. Although the original negatives were not calibrated, and hence the values of the contour intervals are not known, a few remarks of qualitative interest may be made.

The negative of the solar corona of the eclipse of August 31, 1932, was obtained by the staff of the Observatory of the University of Michigan; and, although it contains calibration marks, they are of such poor quality that it was thought best not to use them. The innermost contour represents the limb of the moon and shows the three most prominent indentations in the lunar limb at the time of totality. The most striking feature of the contours is the relative obliteration of the coronal "streamers." We would estimate

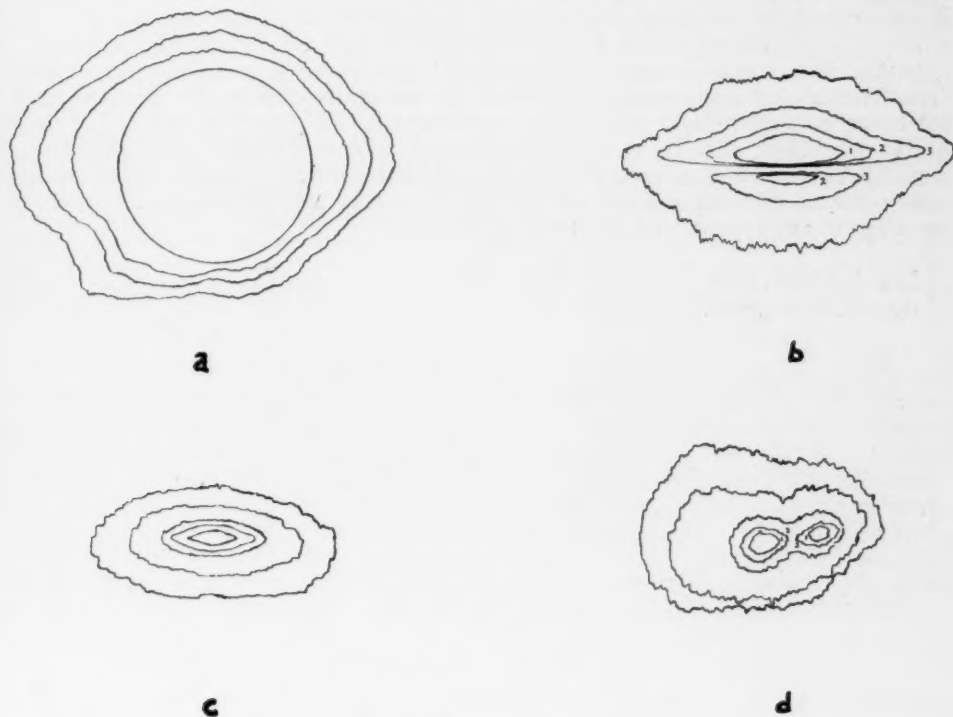


FIG. 2.—Isophotes of objects shown in Plate VI

that their intensities are no greater than twice that of the adjacent corona; but, since this brightness ratio extends all along the streamer, the eye greatly enhances its apparent contrast.

The negatives of the three nebulae were kindly loaned to us by Dr. Hubble. For each nebula the reproduction and the corresponding contour are to the same scale. NGC 4594 is a most striking example of peripheral obscuration, and this clearly shows in the contours. In fact, the intensity of the "canyon" is found to be less than that of the outermost contour. In this and the other figures, contours of the same intensity are given the same numbers.

NGC 750-751 is a well-known double nebula, whose components are probably physically connected. A complete analysis of accurately calibrated isophotal contours should assist in determining this point, since their shapes should not be the same for the case of a physically connected pair and for the case of an optical double.

The photometry of NGC 3115 has been extensively examined by Hubble<sup>9</sup> and by Oort.<sup>10</sup> The contour in Figure 2, *c*, was made to show particularly the outer regions of the nebula, and consequently the inner structure is lost. From the results of Hubble and of Oort we can obtain approximately the relative log intensities of the contours shown here; they are 2.0 1.5, 1.3, 0.9, and 0.5.

#### B. CURVE TRANSFORMATION

Since the principle of the operation of the isophotometer is that it balances the light-transmissions of the instantaneous point of analysis of objects placed on the balance carriage against some sort of calibration or comparison object placed on the other carriage, it is clear that the instrument can be made to follow the "edge" of a line. This provides a means for transforming a curve into another that is some function of the original, provided that there has been constructed a cam of the proper shape to effect the transformation. The simplest sort of useful transformation is magnification in one dimension only; for example, a curve with only minute variations in one dimension may have these greatly magnified, while the scale in the other dimension may be left unchanged or even shrunk. A corollary of this use of the instrument is its ability to check objectively and sensitively the existence of suspected faint or diffuse markings on photographs, or similar markings in any type of partially transparent object.

<sup>9</sup> *Ap. J.*, **71**, 231, 1930.

<sup>10</sup> *Ap. J.*, **91**, 273, 1940.

## NGC 5053 AND NGC 6838

JAMES CUFFEY\*

Kirkwood Observatory, Indiana University

Received April 21, 1943

### ABSTRACT

NGC 5053 and NGC 6838 are remarkable for their structural peculiarities; the former is a well-resolved globular cluster and the latter a highly condensed galactic cluster. A photometric survey, undertaken to compare these interesting objects, shows that their color-magnitude relations contain red giant branches, similar to those of typical globular clusters. In NGC 5053 the giant branch begins near  $m_r = 13.5$ ,  $C_r = 1.5$ , and its stars become steadily bluer as far as  $m_r = 15.1$ ,  $C_r = 0.9$ . Fainter than  $m_r = 15.1$ , two separate branches appear; one extends abruptly toward the blue, and the other more gradually toward the red (see Fig. 1). The color-magnitude relation indicates that, in spite of its unusual structure, NGC 5053 is correctly classified as a globular cluster. In NGC 6838, also, the giant stars are red and become bluer with decreasing brightness. In this respect, as well as in structure and richness in faint stars, NGC 6838 bears a striking resemblance to some of the globular clusters. The tendency of the color-magnitude diagrams in the very rich galactic clusters (e.g., NGC 6838 and NGC 2158) to resemble the diagrams observed in the globular clusters emphasizes again the poorly defined boundaries between the two classes of objects. The extragalactic nebulae indicate no absorption for NGC 5053. A color excess in the vicinity of 0.8 mag. seems likely for NGC 6838 and implies an absorption of 1.6 mag. The distances derived, corrected for absorption, are: NGC 5053, 16,000 parsecs, and NGC 6838, 4,000 parsecs.

NGC 5053 and NGC 6838 are of unusual interest in illustrating the poorly defined boundaries between the globular and the galactic clusters. NGC 5053, although classified for several reasons as a globular cluster, is quite unlike the typical globular cluster; it contains no densely packed nucleus, and individual stars are widely separated, even at its very center. In appearance and structure, therefore, NGC 5053 resembles the galactic, rather than the globular, clusters. It owes its classification as a globular cluster to its high galactic latitude ( $+78^\circ$ ), its richness in faint stars, and the presence of nine variables.<sup>1</sup> NGC 6838, on the other hand, is one of the richest of the galactic clusters; and its nucleus, while probably easily resolvable with larger apertures, appears on long exposures with the 36-inch reflector to approach in density the nuclei of some of the globular clusters.

### OBSERVATIONAL DETAILS

Magnitudes and red color indices ( $\lambda\lambda$  4300-6300) for 215 stars in NGC 6838 and 165 stars in NGC 5053 were obtained from Polar comparisons made with the prime-focus, 36-inch, f/5 aluminized reflector of the Goethe Link Observatory in Brooklyn, Indiana. Photographic magnitudes were measured partly on Cramer Hi-speed Special plates and partly on Eastman 103-E plates with a blue (Eastman Kodak Co. No. 43) gelatine filter; laboratory tests with a quartz spectrograph showed these combinations to possess very closely the same wave-length sensitivity. The red magnitudes are based on Eastman 103-E plates with a Ciné Red (Eastman Kodak Co. No. 28) gelatine filter.

An attempt was made to arrange the red and blue exposures in such a manner that any unknown systematic errors in the magnitudes would be the same for both magnitude systems. Blue and red exposures were taken in rapid succession on the cluster and then on the pole. The major source of error, however, in work with focal images in widely differing wave lengths and with large apertures results from the systematic difference in seeing, or image quality, between red and blue images and also between pole and cluster. This error is difficult to avoid, and little, other than the taking of numerous plates, can be

\* Lieutenant, U.S.N.R., U.S. Naval Academy, Annapolis, Md.

<sup>1</sup> Baade, *Hamburg. Mitt.*, 6, No. 29, 1928.

done to eliminate it. The largest contributions to the probable errors are due to these photometric effects, which are evident in the measures as systematic differences between plates. The observational material upon which the magnitudes are based is summarized in Table 1.

Most of the Polar comparison plates were measured twice. The probable errors of the final magnitudes, both blue and red, are  $\pm 0.05$  mag., and of the color indices,  $\pm 0.08$ .

TABLE 1

CLUSTER	NO. OF POLAR COMPARISONS				NO. OF LONG EXPOSURES	
	Red	Ext.*	Blue	Ext.*	Red	Blue
NGC 5053.....	7	0.02	8	0.05	4	5
NGC 6838.....	4	0.02	10	0.06	4	4

\* Average numerical value of extinction corrections.

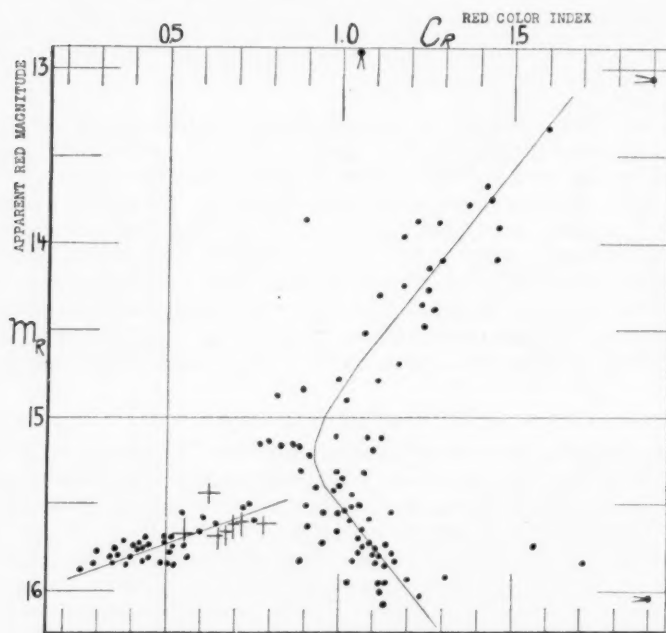


FIG. 1.—NGC 5053. Color-magnitude relation. The plus signs (+) represent variables

#### RESULTS AND CONCLUSIONS

##### NGC 5053

The color-magnitude diagram (Fig. 1), although unusual in form for the faintest stars, shows many features characteristic of a typical globular cluster. The giant red branch is similar in slope to those of Messier 13, Messier 3, and Messier 68. The faint branch extending abruptly toward the smaller color indices and the separation into two distinct branches, also, have their counterparts in Messier 3 and Messier 13. In NGC 5053 one

of the fainter branches appears to extend gradually toward red stars, unlike the corresponding branches in the other globular clusters, which extend, instead, toward blue stars (see Fig. 2). The reality of this peculiarity in the color-magnitude relation for NGC 5053 seems convincing from the present data, although it is possible that colors for stars a magnitude or two fainter might reveal the trend to be in reality toward blue stars, as in Messier 3 and Messier 13. If we neglect this relatively minor peculiarity as possibly a trend influenced by the observational limits, we conclude that the color-magnitude relation in NGC 5053 is further evidence that the cluster is correctly classified as a globular

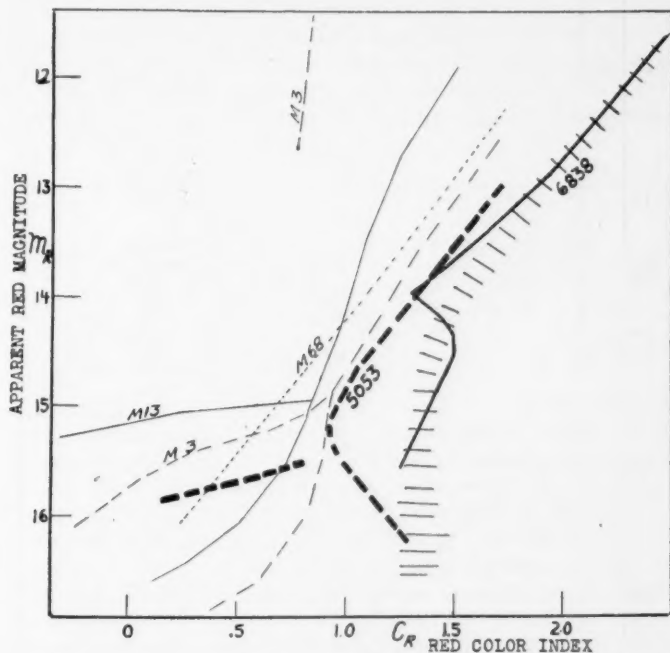


FIG. 2.—Color-magnitude relations in NGC 5053 and NGC 6838, compared with those in Messier 3, Messier 13, and Messier 68. The data for Messier 3, Messier 13, and Messier 68 were derived from Shapley's photovisual indices, using  $C_R = 1.2 C_{pv}$ . The hatched area represents the average trend in NGC 6838.

cluster. The existence of fewer stars along the giant branches follows naturally from the relatively smaller total population of the cluster.

The nine variables<sup>2</sup> are closely grouped together at the beginning of the faint blue branch. Similar concentration of variables toward particular regions in the color-magnitude relations is characteristic of other globular clusters. In NGC 5053, 8 stars not known to be variable are distributed in the color-magnitude diagram among the variables. Examination of these stars for variability on the limited number of plates at present at my disposal failed to reveal significant variation in any of them, although the results were not conclusive.

Figure 2, which compares the color-magnitude relations in several clusters, gives no evidence of lateral displacement or color excess for NGC 5053. The vertical displacements (except for NGC 6838) are due to differences in distances. Comparison of the diagrams of NGC 5053 with those of Messier 3, Messier 13, and Messier 68 leads to a dis-

<sup>2</sup> *Ibid.*

tance for NGC 5053 of  $16,000 \pm 2,000$  parsecs. No correction for absorption appears to be necessary, both because of absence of color excess and also because of the presence in near-by fields of an excess in the number of extragalactic nebulae.

The linear diameter of NGC 5053 is 30 parsecs. Baade's counts<sup>3</sup> show 3,400 stars brighter than  $m_{pg} = 21$  ( $M = +5$ ). The mean density is therefore of the order of 0.3

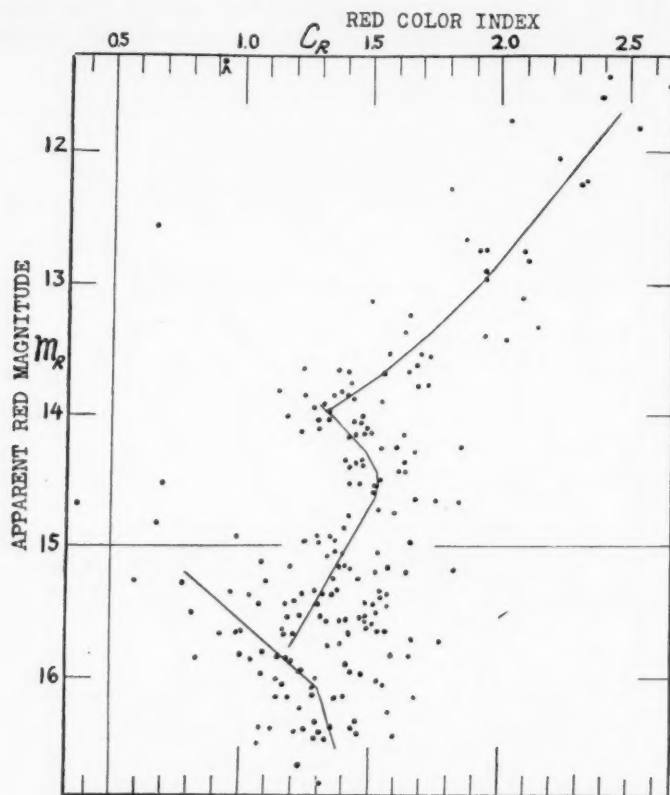


FIG. 3.—NGC 6838. Color-magnitude relation

stars per cubic parsec, decidedly less than the mean densities in ordinary galactic clusters. The poorly defined boundaries of the clusters, however, make comparison of mean densities of doubtful significance, except as exceedingly rough indications.

#### NGC 6838

NGC 6838, on long exposures, appears to be rich in faint stars and to possess a definite, congested, but probably resolvable, nucleus. The surrounding region, also, is resplendent with faint stars; and the cluster, while itself very well defined, may be in reality a condensation in a rich Milky Way star cloud. Star counts show that, after allowing for field stars, there are 3,500 cluster stars brighter than  $m_{pg} = 18.5$  ( $M = +5$ ). The extreme diameter is  $24'$ . NGC 6838, therefore, is a galactic cluster quite comparable in population and linear dimensions with the globular NGC 5053.

<sup>3</sup> *Ibid.*

In the color-magnitude diagram (Fig. 3) the giant branch is similar in slope to the corresponding branches in several of the globulars (see Fig. 2). A slight "kink" near  $m_r = 14.0$ ,  $C_r = 1.3$ , is a noticeable peculiarity. The general trend, indicated by the shaded area in Figure 2, parallels that in Messier 68.

The reality of the "kink" is confirmed, indirectly at least, by Krug's photovisual indices.<sup>4</sup> The photovisual data, however, did not reach sufficiently faint stars to show that those fainter than  $m_{pv} = 14.0$  became progressively bluer, rather than redder. Krug, erroneously assuming that he had reached the dwarf branch, along which the stars would continue to become redder, assigned the cluster to the rare Trumpler class 2f. The present red indices show that NGC 6838, although difficult to classify as other than similar to the globulars, has no relation to the 2f type of cluster.

The systematic difference between the red color indices and the photovisual indices of Krug amounts to nearly 1 mag., and there may be a zero-point error in one of the color systems. The photored indices are, in my opinion, probably reliable, since they are based upon more abundant observational material and upon plates of higher sensitivity.

TABLE 2

$R$ (Parsecs)	$D$ (Stars/Pc <sup>3</sup> )	$R$ (Parsecs)	$D$ (Stars/Pc <sup>3</sup> )	$R$ (Parsecs)	$D$ (Stars/Pc <sup>3</sup> )
1.....	6.2	4.....	1.7	10.....	0.3
2.....	5.1	5.....	1.0	15.....	0.1:
3.....	3.1	6.....	0.5		

Judged from the color-magnitude relation, the color excess for NGC 6838 is approximately 0.8 mag.; the absorption is therefore in the neighborhood of 1.6 mag. These values are not well defined and are subject to considerable uncertainty.

The distance of NGC 6838, obtained by comparison of its color-magnitude relation with those of Messier 3, Messier 13, and Messier 68 and correcting for absorption, is 4000 parsecs. The cluster's linear diameter is 28 parsecs, or very nearly that of NGC 5053. It is interesting to notice that the adopted color excess and distance place the group of stars which give rise to the "kink" mentioned above near the absolute magnitude at which the giant branches in Messier 3 and Messier 13 separate into two parts.

The true space densities at various distances from the center of NGC 6838, corrected for projection effect by means of a Plummer analysis of star counts to  $m_{pg} = 18.5$  ( $M = +5$ ), are given in Table 2. The densities are similar to those of other rich galactic clusters. They would be considerably higher, however, if allowance were made for the relatively bright limiting magnitude ( $M = +5$ ) and for the averaging effect of a necessarily large unit of volume which tended to depress the central densities.

It is a pleasure to acknowledge the kindness of Dr. Goethe Link, who placed the facilities of his observatory at my disposal, and also express appreciation for the post-doctoral fellowship at Indiana University, with which the above work was completed.

<sup>4</sup> *Zs. f. Ap.*, 13, 205-214, 1937.

## DYNAMICAL FRICTION

### III. A MORE EXACT THEORY OF THE RATE OF ESCAPE OF STARS FROM CLUSTERS

S. CHANDRASEKHAR

Yerkes Observatory

Received March 26, 1943

#### ABSTRACT

A more exact estimate of the rate of escape of stars from clusters is made than in an earlier paper by properly allowing for the dependence of the coefficient of dynamical friction on the velocity. It is found that the probability that a star will have acquired the necessary velocity of escape (assumed to be equal to twice the root mean square velocity of the stars in the system) in a time  $\tau$  (measured in units of the time of relaxation of the system) is given by

$$Q(\tau) = (1 - e^{-0.0075\tau}) .$$

On this basis, half-lives for galactic clusters of the order of  $3 \times 10^9$  years are provided for, and it is further concluded that dynamical friction provides the principal mechanism for the continued existence of galactic clusters like the Pleiades for times of the order of  $3 \times 10^9$  years.

1. *Introduction.*—In the two earlier papers of this series on “Dynamical Friction”<sup>1</sup> we have shown how stars must experience dynamical friction during their motion and how in the rate of escape of stars from clusters we can look for direct evidence for the operation of this force. However, in estimating this rate of escape of stars from clusters in II we assumed (for the sake of simplicity) that the coefficient of dynamical friction,  $\eta$ , and the diffusion coefficient,  $q$  (in the *velocity space*), were both constants. On the other hand, an explicit evaluation of the coefficient of dynamical friction on the two-body approximation for stellar encounters gave

$$\eta = 8\pi m^2 G^2 \left( \log_e \left[ \frac{D_0 |\mathbf{u}|^2}{2Gm} \right] \right) \frac{1}{|\mathbf{u}|^3} \int_0^{|\mathbf{u}|} N(v) dv . \quad (1)$$

According to this formula,

$$\eta \rightarrow \eta_0 = \text{constant as } |\mathbf{u}| \rightarrow 0 \quad (2)$$

and

$$\eta \rightarrow \text{constant } |\mathbf{u}|^{-3} \text{ as } |\mathbf{u}| \rightarrow \infty . \quad (3)$$

In view particularly of (3) it does not appear entirely satisfactory that we ignore the dependence of  $\eta$  on  $|\mathbf{u}|$ . It is therefore a matter of some importance that we make proper allowance for the variation of  $\eta$  with  $|\mathbf{u}|$  according to equation (1) in estimating the rate of escape of stars from clusters. This is the main purpose of this paper.

2. *The general theory of the rate of escape of stars from clusters allowing for the variation of  $\eta$  with  $|\mathbf{u}|$ .*—As in II, we shall suppose that, in order that a star may escape from a cluster, it is only necessary that it acquire a velocity greater than (or equal to) a certain critical velocity,  $v_\infty$ , which we may call the “velocity of escape.” On this assumption the probability that a star will have acquired the necessary velocity for escape during a certain time can be determined very simply in terms of the probability,  $p(v_0, t) dt$ , that a star having initially a velocity  $|\mathbf{u}| = v_0$  at time  $t = 0$  will acquire for the *first time* the velocity  $|\mathbf{u}| = v_\infty$  between  $t$  and  $t + dt$ . And as we have already explained in

<sup>1</sup> *Ap. J.*, 97, 255 and 266, 1943. These two papers will be referred to as “I” and “II,” respectively.

II, § 2, this probability function  $p(v_0, t)$  can be derived in turn from the spherically symmetric solution of the equation

$$\frac{\partial W}{\partial t} = \text{div } u (q \text{ grad } u W + \eta W u), \quad (4)$$

which satisfies the boundary conditions

$$W(|u|, t) = 0 \text{ for } |u| = v_\infty \text{ for all } t > 0 \quad (5)$$

and

$$W(|u|, t) \rightarrow \frac{1}{4\pi v_0^2} \delta(|u| - v_0) \text{ as } t \rightarrow 0, \quad (6)$$

where  $\delta$  stands for the usual  $\delta$ -function of Dirac.

For the case under discussion we have (I, eq. [36])

$$\eta = 8\pi N m^2 G^2 \left( \log_e \left[ \frac{D_0 \overline{|u|^2}}{2Gm} \right] \right) \frac{1}{|u|^3} [\Phi(j|u|) - j|u|\Phi'(j|u|)], \quad (7)$$

where  $\Phi$  and  $\Phi'$  denote, respectively, the error function and its derivative. Further, in equation (7),  $j$  is the parameter which occurs in the assumed Maxwellian distribution of velocities:

$$\frac{j^3}{\pi^{3/2}} e^{-j^2|u|^2} du; \quad j = \left( \frac{3}{2\overline{|u|^2}} \right)^{1/2}. \quad (8)$$

The formula (7) for  $\eta$  can be written more conveniently as

$$\eta = \eta_0 \nu(j|u|), \quad (9)$$

where

$$\eta_0 = 8\pi N m^2 G^2 \left( \log_e \left[ \frac{D_0 \overline{|u|^2}}{2Gm} \right] \right) \left( \frac{3}{2\overline{|u|^2}} \right)^{3/2} \frac{4}{3\pi^{1/2}} \quad (10)$$

and

$$\nu(\rho) = \frac{3\pi^{1/2}}{4} \rho^{-3} [\Phi(\rho) - \rho\Phi'(\rho)]. \quad (11)$$

With  $\nu(\rho)$  defined in this manner,

$$\nu(\rho) \rightarrow 1 \text{ as } \rho \rightarrow 0 \quad (12)$$

and

$$\nu(\rho) \sim \frac{3\pi^{1/2}}{4} \rho^{-3} \text{ as } \rho \rightarrow \infty. \quad (13)$$

Again, since  $q$  and  $\eta$  are quite generally related according to

$$q = \frac{1}{3} \overline{|u|^2} \eta, \quad (14)$$

we have

$$q = \frac{1}{3} \overline{|u|^2} \eta_0 \nu(j|u|). \quad (15)$$

The function  $\nu(\rho)$  is tabulated in Table 1.

Returning to equation (4), we now introduce a change of the independent variables  $u$  and  $t$ . Let

$$\tau = \eta_0 t; \quad u = \left( \frac{2}{3} \overline{|u|^2} \right)^{1/2} p. \quad (16)$$

Equation (4) now takes the dimensionless form

$$\frac{\partial W}{\partial \tau} = \text{div}_{\mathbf{p}} \left[ \frac{1}{2} \nu (|\mathbf{p}|) \text{grad}_{\mathbf{p}} W + \nu (|\mathbf{p}|) W \mathbf{p} \right]. \quad (17)$$

For a spherically symmetric solution  $W(|\mathbf{p}|, \tau)$  equation (17) reduces to

$$\rho \frac{\partial w}{\partial \tau} = \frac{\partial}{\partial \rho} \left[ \nu(\rho) \left\{ \frac{1}{2} \rho \frac{\partial w}{\partial \rho} + \left( \rho^2 - \frac{1}{2} \right) w \right\} \right], \quad (18)$$

TABLE 1  
THE FUNCTIONS  $\nu(\rho)$  AND  $-d \log \nu/d\rho$

$\rho$	$\nu(\rho)$	$-\frac{d \log \nu}{d\rho}$	$\rho$	$\nu(\rho)$	$-\frac{d \log \nu}{d\rho}$
0.00	1.00000	0.0000	1.45	0.33133	1.3062
0.05	0.99850	0.0600	1.50	.31026	1.3206
0.10	0.99402	0.1199	1.55	.29035	1.3323
0.15	0.98661	0.1795	1.60	.27157	1.3413
0.20	0.97634	0.2389	1.65	.25392	1.3477
0.25	0.96332	0.2979	1.70	.23734	1.3515
0.30	0.94770	0.3563	1.75	.22183	1.3528
0.35	0.92962	0.4141	1.80	.20732	1.3518
0.40	0.90927	0.4712	1.85	.19379	1.3486
0.45	0.88684	0.5274	1.90	.18117	1.3432
0.50	0.86257	0.5827	1.95	.16943	1.3358
0.55	0.83666	0.6369	2.00	.15852	1.3267
0.60	0.80936	0.6899	2.05	.14839	1.3159
0.65	0.78090	0.7417	2.10	.13898	1.3036
0.70	0.75152	0.7921	2.15	.13025	1.2901
0.75	0.72145	0.8409	2.20	.12216	1.2754
0.80	0.69093	0.8881	2.25	.11466	1.2597
0.85	0.66016	0.9336	2.30	.10770	1.2433
0.90	0.62936	0.9772	2.35	.10126	1.2262
0.95	0.59872	1.0188	2.40	.09528	1.2087
1.00	0.56842	1.0584	2.45	.08973	1.1907
1.05	0.53861	1.0958	2.50	.08458	1.1726
1.10	0.50944	1.1309	2.55	.07980	1.1544
1.15	0.48104	1.1636	2.60	.07536	1.1361
1.20	0.45350	1.1939	2.65	.07123	1.1179
1.25	0.42692	1.2216	2.70	.06739	1.0999
1.30	0.40137	1.2468	2.75	.06381	1.0820
1.35	0.37689	1.2693	2.80	.06048	1.0645
1.40	0.35354	1.2891	2.85	0.05737	1.0472

where we have written

$$\rho = |\mathbf{p}| \quad \text{and} \quad w = W \rho. \quad (19)$$

According to equations (5) and (6), we require a solution of equation (18) which satisfies the boundary conditions

$$w(\rho, \tau) = 0 \quad \text{for both} \quad \rho = 0 \quad \text{and} \quad \rho = \rho_{\infty} \quad \text{for all} \quad \tau > 0 \quad (20)$$

and

$$w(\rho, \tau) \rightarrow \frac{1}{4\pi\rho_0} \delta(\rho - \rho_0) \quad \text{as} \quad \tau \rightarrow 0. \quad (21)$$

Now, equation (18) is separable in the variables  $\rho$  and  $\tau$ . Accordingly, we write

$$w = e^{-\lambda\tau}\phi(\rho), \quad (22)$$

where  $\lambda$  is, for the present, an unspecified constant; we then obtain for  $\phi$  the differential equation

$$\frac{d}{d\rho} \left[ \nu(\rho) \left\{ \frac{1}{2}\rho \frac{d\phi}{d\rho} + (\rho^2 - \frac{1}{2})\phi \right\} \right] + \lambda\rho\phi = 0. \quad (23)$$

If we now let

$$\phi = e^{-\rho^2/2}\psi, \quad (24)$$

equation (23) reduces to

$$\frac{d^2\psi}{d\rho^2} + \frac{d \log \nu}{d\rho} \frac{d\psi}{d\rho} + \left[ 2 \frac{\lambda}{\nu(\rho)} + 3 - \rho^2 - \frac{d \log \nu}{d\rho} \left( \frac{1}{\rho} - \rho \right) \right] \psi = 0. \quad (25)$$

It is now seen that, in order that a solution of the foregoing equation may vanish both at  $\rho = 0$  and at  $\rho = \rho_\infty$ , it is necessary that  $\lambda$  take one of an infinite enumerable set of discrete values

$$\lambda_1, \lambda_2, \dots, \lambda_n, \dots, \quad (26)$$

which may properly be called the "characteristic values" of the problem. Further, if

$$\psi_1, \psi_2, \dots, \psi_n, \dots \quad (27)$$

denote the solutions of equation (25) which satisfy the boundary conditions (20) at  $\rho = 0$  and at  $\rho = \rho_\infty$  and belong, respectively, to the values  $\lambda_1, \lambda_2, \dots, \lambda_n, \dots$ , then it can be readily verified that these solutions form a complete set of orthogonal functions. Without loss of generality we can therefore suppose that these functions are all properly normalized. Consequently, in terms of the fundamental solutions

$$w_n = e^{-\lambda_n\tau} e^{-\rho^2/2} \psi_n(\rho) \quad (28)$$

which satisfy the boundary conditions (20) we can construct solutions which will satisfy any further arbitrary boundary condition for  $\tau = 0$ . Thus, the solution

$$w = \frac{1}{4\pi\rho_0} e^{-(\rho^2 - \rho_0^2)/2} \sum_{n=1}^{\infty} e^{-\lambda_n\tau} \psi_n(\rho) \psi_n(\rho_0) \quad (29)$$

clearly satisfies the boundary condition (21) for  $\tau = 0$ . Corresponding to the solution (29) for  $w$ , we have

$$W = \frac{1}{4\pi\rho\rho_0} e^{-(\rho^2 - \rho_0^2)/2} \sum_{n=1}^{\infty} e^{-\lambda_n\tau} \psi_n(\rho) \psi_n(\rho_0). \quad (30)$$

Using the foregoing solution for  $W$ , we can write down the probability function  $p(\rho_0, \tau)$ . For, since

$$p(\rho_0, \tau) = -2\pi\rho_\infty^2 \nu(\rho_\infty) \left( \frac{\partial W}{\partial \rho} \right)_{\rho=\rho_\infty}, \quad (31)$$

we have

$$p(\rho_0, \tau) = \frac{\rho_\infty}{2\rho_0} \nu(\rho_\infty) e^{-(\rho_\infty^2 - \rho_0^2)/2} \sum_{n=1}^{\infty} e^{-\lambda_n\tau} \left( -\frac{d\psi_n}{d\rho} \right)_{\rho=\rho_\infty} \psi_n(\rho_0). \quad (32)$$

To obtain the total probability  $Q(\rho_0, \tau)$  that a star having initially a velocity corresponding to  $\rho_0$  will have acquired during the time  $\tau$  a velocity corresponding to  $\rho_\infty$ , we have simply to integrate equation (32) from 0 to  $\tau$ . Thus,

$$Q(\rho_0, \tau) = \int_0^\tau p(v_0, \tau) d\tau; \quad (33)$$

or, using equation (32), we have

$$Q(\rho_0, \tau) = \frac{\rho_\infty}{2\rho_0} \nu(\rho_\infty) e^{-(\rho_\infty^2 - \rho_0^2)/2} \sum_{n=1}^{\infty} \frac{1}{\lambda_n} (1 - e^{-\lambda_n \tau}) \left( -\frac{d\psi_n}{d\rho} \right)_{\rho=\rho_\infty} \psi_n(\rho_0). \quad (34)$$

Finally, to obtain the expectation,  $Q(\tau)$ , that an "average" star will have acquired the necessary velocity for escape during a time  $\tau$ , we must average the foregoing expression over all  $\rho_0$ . The final result can therefore be expressed in the form

$$Q(\tau) = \sum_{n=1}^{\infty} Q_n(\tau), \quad (35)$$

where

$$Q_n(\tau) = A_n (1 - e^{-\lambda_n \tau}) \quad (36)$$

and

$$A_n = \frac{1}{2\lambda_n} \rho_\infty \nu(\rho_\infty) e^{-\rho_\infty^2/2} \left( -\frac{d\psi_n}{d\rho} \right)_{\rho=\rho_\infty} \left[ \frac{e^{\rho_0^2/2}}{\rho_0} \psi_n(\rho_0) \right]. \quad (37)$$

**3. Numerical results.**—Now, since in a star cluster the root mean square velocity of escape is twice the root mean square velocity of the stars in the system,<sup>2</sup> it is clear that the values of  $\rho_\infty$  which come under discussion are in the general neighborhood of

$$\rho_\infty = \sqrt{6} \sim 2.45. \quad (38)$$

As we shall see presently, for these values of  $\rho_\infty$ ,  $Q(\tau)$  can be represented with ample accuracy by the first term on the right-hand side of equation (35). Accordingly, it would be sufficient to specify the lowest characteristic value of  $\lambda$  (for a given  $\rho_\infty$ ) and the normalized characteristic function  $\psi_1$  belonging to it. For this purpose the following procedure appears suitable:

First we assign a value for  $\lambda$  and look for a solution  $\Psi(\rho)$  of equation (25) whose behavior near the origin can be described by a series expansion of the form

$$\Psi = \rho + a_3 \rho^3 + a_5 \rho^5 + \dots \quad (39)$$

For any prescribed value of  $\lambda$  the coefficients  $a_3$ ,  $a_5$ , etc., can be successively determined from the differential equation (25) for  $\Psi$ . Thus  $a_3$  and  $a_5$  are found to be

$$\left. \begin{aligned} a_3 &= -\frac{1}{6} (3 + 2\lambda), \\ a_5 &= \frac{1}{24} [2.2 - 1.2\lambda + \frac{1}{6} (3 + 2\lambda) (0.6 + 2\lambda)]. \end{aligned} \right\} \quad (40)$$

The higher coefficients can be similarly found, but the explicit formulae in terms of  $\lambda$  have no particular interest. However, it is clear that, starting a solution near the origin with a series expansion of the form (39), we can continue it for larger values of  $\rho$  by

<sup>2</sup> Cf., e.g., S. Chandrasekhar, *Principles of Stellar Dynamics*, pp. 206–207, University of Chicago Press 1942.

standard numerical methods until we reach the first zero  $\rho_\infty(\lambda)$  of  $\Psi$ . Conversely, for the value of  $\rho_\infty$  thus determined, the solution  $\Psi$  satisfies the necessary boundary conditions at the origin and at  $\rho = \rho_\infty$ . The initially assigned value of  $\lambda$  is therefore the lowest characteristic value of  $\lambda$  for this value of  $\rho_\infty$ . If we now let  $a$  denote the normalizing factor for the solution  $\Psi$  determined in this fashion, we can express  $A_1$  (cf. eq. [37]) alternatively in the form

$$A_1 = \frac{a^2}{2\lambda} \rho_\infty \nu(\rho_\infty) e^{-\rho_\infty^2/2} \left( -\frac{d\Psi}{d\rho} \right)_{\rho=\rho_\infty} \left[ \frac{e^{\rho_0^2/2}}{\rho_0} \Psi(\rho_0) \right]. \quad (41)$$

Now, it is found that, for the values of  $\rho_\infty$  in the neighborhood of 2.45,  $\lambda$  is very small and  $A_1$  is very close to unity. Thus, for  $\lambda = 0.0075$ , a numerical integration of equation (25) gave

$$\rho_\infty = 2.4518; \quad A_1 = 0.9966 \quad (\lambda_1 = 0.0075). \quad (42)$$

Accordingly, for this case, equation (35) takes the explicit form

$$Q(\tau) = 0.9966 (1 - e^{-0.0075\tau}) + \sum_{n=2}^{\infty} A_n (1 - e^{-\lambda_n \tau}) \quad (\rho_\infty = 2.4518). \quad (43)$$

Since  $Q(\tau)$  must, by definition, approach unity as  $\tau \rightarrow \infty$ , it is clear that

$$\sum_{n=2}^{\infty} A_n = 0.0034 \quad (\rho_\infty = 2.4518). \quad (44)$$

Again, since  $\lambda_2$  must be in the neighborhood of 2 (cf. II, p. 270) and the higher characteristic values still larger, it is evident that, for  $\tau > 5$ , sufficient accuracy will be provided by

$$Q(\tau) = 1 - e^{-0.0075\tau} \quad (\tau \gtrsim 5). \quad (45)$$

The situation for other values of  $\rho_\infty$  is quite similar, as is apparent from Table 2, where the results for a few values of  $\lambda$  are collected together.

TABLE 2

THE RATE OF ESCAPE OF STARS FROM CLUSTERS INCLUDING DYNAMICAL FRICTION  
AND ALLOWING FOR ITS DEPENDENCE ON  $|u|$

$\lambda$	$\rho_\infty$	$\nu(\rho_\infty)$	$-\Psi'(\rho_\infty)$	$a^2$	$\left[ \frac{e^{\rho_0^2/2}}{\rho_0} \Psi(\rho_0) \right]$	$Q_1(\tau)$
0.0025	2.6642	0.07011	0.4077	2.3083	0.9891	$1.0000 (1 - e^{-0.0025\tau})$
.0050	2.5320	.08148	.5183	2.3458	.9813	$0.9978 (1 - e^{-0.0050\tau})$
.0075	2.4518	.08954	.5932	2.3787	.9748	$0.9966 (1 - e^{-0.0075\tau})$
.0100	2.3936	.09601	.6503	2.4089	.9689	$0.9941 (1 - e^{-0.0100\tau})$
0.0125	2.3476	0.10156	0.6969	2.4373	0.9634	$0.9921 (1 - e^{-0.0125\tau})$

4. *The half-life of a cluster.*—From our results of § 3 it follows that for  $\tau \gtrsim 5$  we can write

$$Q(\tau) = 1 - e^{-\lambda_1 \tau} \quad (\tau = \eta_0 t) \quad (46)$$

for the values of  $\rho_\infty$  which come under discussion. Since  $Q(\tau)$  gives the expectation that an average star will have escaped during a time  $\tau$  (in units of  $\eta_0^{-1}$ ), we can properly regard  $1/\lambda_1\eta_0$  as a measure of the half-life of the cluster. Thus,

$$\text{Half-life of the cluster} = (\lambda_1\eta_0)^{-1}, \quad (47)$$

where  $\eta_0$  is defined in equation (10). The precise value of  $\lambda_1$  will depend, of course, on circumstances; but it is clear that greatest interest attaches to a value of  $\rho_\infty \simeq 2.45$ . For this value of  $\rho_\infty$  we have found that  $\lambda_1 \simeq 0.0075$ , so that the half-life of the cluster may be defined by

$$\text{Half-life of the cluster} = 133\eta_0^{-1}. \quad (48)$$

For the Pleiades,  $\eta_0^{-1}$  is of the order of  $2 \times 10^7$  years, so that its half-life is of the order of  $3 \times 10^9$  years. In judging this value it should be remembered that, when dynamical friction is ignored, a half-life for the Pleiades of the order of only  $5 \times 10^7$  years is predicted, while our own earlier calculations in II, in which we ignored the dependence of the coefficient of dynamical friction on  $|\mathbf{u}|$ , gave half-lives which are about seven to eight times shorter than those indicated by our present calculations. More explicitly, we have found that (cf. II, eqs. [28] and [62])

$$\left. \begin{aligned} Q(\tau) &\simeq 1.3(1 - e^{-0.82\tau}) && \text{(dynamical friction ignored),} \\ Q(\tau) &= (1 - e^{-0.059\tau}) && \text{(dynamical friction included, but the dependence of } \eta \text{ on } |\mathbf{u}| \text{ ignored),} \\ Q(\tau) &= (1 - e^{-0.0075\tau}) && \text{(dynamical friction included and the dependence of } \eta \text{ on } |\mathbf{u}| \text{ allowed for).} \end{aligned} \right\} \quad (49)$$

There can thus be hardly any doubt that dynamical friction provides the principal mechanism for the continued existence of the galactic clusters like the Pleiades for times of the order of  $3 \times 10^9$  years. But, even with dynamical friction properly allowed for, it will be hard to account for such clusters' half-lives of the order of  $10^{10}$  years. This, in turn, provides another strong argument in favor of the "short-time scale."

The results of Table 2 allow us also to infer something about the relative rates of escape of stars of different masses: for stars with masses appreciably different from the average value,  $\rho_\infty$  may be expected to change according to <sup>3</sup>

$$\rho_\infty(m) = \left(6 \frac{m}{\bar{m}}\right)^{1/2}. \quad (50)$$

From Table 2 we now see that even a 10 per cent increase of  $\rho_\infty$  prolongs the half-lives by a factor of the order 3, while a similar decrease in  $\rho_\infty$  shortens the half-life by a factor of the order 2. The general conclusion to be drawn from this is simply that a cluster loses its less massive members rather more rapidly than the average ones, while the more massive members continue to remain, on the average, for longer times. We hope to return to these questions in greater detail on a later occasion.

In conclusion, I wish to record my indebtedness to Mrs. T. Belland, who undertook most of the numerical work involved in the preparation of this paper, and in particular for the care with which she performed the necessary numerical integrations.

<sup>3</sup> *Ibid.*, pp. 209-213.

## A SPECTROSCOPIC STUDY OF THE REGION OF THE DOUBLE CLUSTER IN PERSEUS

WILLIAM P. BIDELMAN

Yerkes Observatory

Received April 14, 1943

### ABSTRACT

Spectral classes and spectroscopic absolute magnitudes have been derived from low-dispersion spectrograms for 153 early-type stars in the vicinity of the double cluster in Perseus. The material is complete to apparent magnitude 7.5 over a large region ( $10^\circ \times 15^\circ$ ) about the double cluster and symmetrical with respect to the galactic circle; it is complete, also, to magnitude 8.5 over an area of  $6^\circ$  diameter symmetrical about the double cluster. A few stars have been taken which make the material complete to apparent magnitude 9.5 in a small region near the center of each cluster.

True distance moduli have been found for all stars later than O8 by using the photoelectric colors measured by Stebbins, Huffer, and Whitford. The results indicate that (1) there is a pronounced clustering of early-type supergiants in the direction of, and at the distance of, the  $\eta$  and  $\chi$  Persei cluster, and (2) the diameter of this cluster of supergiants is considerably larger than that usually ascribed to the double cluster and may be estimated as about  $5^\circ$ .

The variation in selective and total interstellar absorption across the field studied is discussed, and a reproduction shows the effect on star density caused by the considerable absorption suffered by these stars. On the bases of spectroscopic absolute magnitude, radial velocity, and interstellar line intensity, a considerable number of the stars investigated are attributed to the  $\eta$  and  $\chi$  Persei cluster, and the most probable distance of the cluster is found to be 1920 parsecs. There is an appreciable difference between the distance as found from spectroscopic absolute magnitudes and that obtained from the galactic-rotation effect on the radial velocity of the cluster members. This discrepancy in distance, however, represents a discrepancy in distance modulus of only about 0.6 mag., which may be due to an error in the absolute magnitudes ascribed to these supergiants. The cluster may, of course, have a small peculiar velocity.

Many of the stars between apparent magnitudes 8.5 and 9.5 show the diffuse lines characteristic of rapidly rotating stars, and a number of the fainter stars show emission. It is shown that highly luminous stars of other types, such as the irregular M-type variables, appear in the same region about the double cluster. The Russell-Hertzsprung diagram for early-type stars attributed to the cluster is plotted, using the data of this investigation and that of Trumpler.

### I. INTRODUCTION

It has long been known that the region of  $\eta$  and  $\chi$  Persei, though not a particularly brilliant section of the Milky Way, contains an extraordinarily large number of early-type stars of high luminosity. In R. E. Wilson's catalogue of nonvariable c stars<sup>1</sup> we find, for example, 23 early-type supergiants in this region, most of them within  $2^\circ$  or  $3^\circ$  of the double cluster. Twenty of these are attributed to the  $\eta$  and  $\chi$  Persei cluster.

In a discussion of the *Henry Draper Catalogue* stars of type B3 or earlier, Struve<sup>2</sup> emphasized a "very thick" clustering of B stars in Perseus and suggested that we are here dealing with an actual grouping in space—a suggestion which was further strengthened by the discovery that these stars possess interstellar calcium lines of comparable intensity. As such, these stars were used as a calibration point for a relation between K intensity and distance, the distance adopted being that of the cluster as determined by Trumpler.<sup>3</sup>

Shapley<sup>4</sup> tabulated probable members of this group of stars and plotted a Russell-Hertzsprung diagram on the assumption that all these stars belong to the  $\eta$  and  $\chi$  Persei system. The resulting distribution is of great interest, for it shows a large dispersion in absolute magnitude for each spectral class; it is clear that, if it is possible to plot in the

<sup>1</sup> *A. J.*, **93**, 212, 1941.

<sup>2</sup> *A. N.*, **231**, 17, 1927.

<sup>3</sup> *A. J.*, **67**, 353, 1928.

<sup>4</sup> *Star Clusters* ("Harvard Monographs," No. 2), 1930.

same diagram these very luminous stars and those obviously belonging to the cluster, we have an accurate means of calibrating the absolute magnitudes of early-type supergiants.

However, it is by no means certain that we may consider all the stars which Shapley plots as a physical group. For one thing, as Oosterhoff<sup>5</sup> points out, the apparent diameters of the two clusters are of the order of 30', while the supergiants are spread over an area of a number of square degrees. The common radial velocity shown by many of these stars is not conclusive evidence of cluster membership, for any distant star in this direction will show a large negative velocity due to the galactic rotation effect; and the peculiar velocity of the stars might bring the galactic rotation velocity fairly close to that of the cluster stars. Of course, a radial velocity differing widely from -40 km/sec definitely excludes a star from cluster membership.

The presence of very luminous and presumably highly massive stars at the edges of galactic clusters is not a common characteristic of those known at present. Further, another sort of evidence would appear to negate the cluster hypothesis for these stars. Merrill, in his "Regional Study of Interstellar Sodium,"<sup>6</sup> plots D-line equivalent widths against distances uncorrected for absorption for many of these supergiants. The stars fall at apparent distances of 1000-3000 parsecs, and the sodium intensity increases somewhat with distance. The introduction of differential interstellar absorption, however, tends to bring these stars closer together; and, since D-line intensity increases with color excess, according to Evans,<sup>7</sup> these observations may not be in disagreement with the idea that these stars are in reality at the same distance.

Because of the great importance of knowing which of these supergiants can be considered as members of the  $\eta$  and  $\chi$  Persei cluster and because proper-motion data do not appear to be capable of deciding this question as yet, a program of spectroscopic absolute-magnitude determination has been embarked on for a fairly large number of stars in the region of the double cluster. With the recent work of Morgan, Keenan, and Kellman<sup>8</sup> we have for the first time a comprehensive system of absolute-magnitude and spectral-class criteria for early-type supergiants; using this system, the principal aim of this investigation is to determine, if possible, which of these stars can be considered physical members of the  $\eta$  and  $\chi$  Persei clusters. In what follows we shall refer to the Morgan-Keenan-Kellman investigation as the "*Atlas*."

## II. THE OBSERVATIONS

The stars have been classified and their luminosities determined on low-dispersion slit spectrograms; a majority of the stars were taken with the identical equipment used in establishing the criteria discussed in the *Atlas*. The brighter stars were taken at the Yerkes Observatory with a dispersion of 125 Å/mm at  $H\gamma$ , while the fainter stars were taken at the McDonald Observatory with the  $f/2$  glass Schmidt spectrograph camera, giving a dispersion of 76 Å/mm at  $H\gamma$ . The plates used at Yerkes were Cramer Hi-Speed and Eastman 103a-0, while at McDonald, since film is necessary, owing to the curvature of the field, Agfa Super-Plenachrome Press film was used; the last named was ammoniated before use.

Standard stars given in the *Atlas* were used; in general, at least three luminosity classes were represented for each spectral type, and in several classes stars were taken both in luminosity class Ia and Ib to test the accuracy which can be obtained. Standard stars were taken at both observatories, so that the classification could be made by directly comparing standard stars with program stars. The spectra at Yerkes were obtained with the optimum width, as described in the *Atlas*; at McDonald it proved impossible to attain the desired width with reasonable exposure times, so that the spectra taken there are probably not of quite so good quality as those at Yerkes. Nevertheless, the width of

<sup>5</sup> *Leiden Ann.*, 17, Part I, 1937.

<sup>6</sup> *Ap. J.*, 86, 28, 1937.

<sup>7</sup> *Ap. J.*, 93, 275, 1941.

<sup>8</sup> *An Atlas of Stellar Spectra* ("Astrophysical Monographs"), 1943.

the spectra obtained there exceeds considerably that usually employed for spectral classification from slit spectra.

Since accurate color excesses are lacking for many stars included in this investigation, it was decided to obtain only one good spectrum for each star. Unless the object proved of special interest, the classifications were based solely on this. Underexposed, badly guided, or otherwise imperfect plates were not used at all, as a poor plate can contribute nothing of value to data obtained from a good one. It has, of course, been impossible to avoid using some plates which are not of sufficiently good quality for great accuracy; and in the case of broad-line stars, in particular, there is some doubt as to the classification. This has usually been indicated in the tables by a colon following the classification. The remarks which follow the tables, in so far as they refer to the appearance of the spectra, are merely indications of interesting features of these stars; it should be borne in mind that they refer to what can be seen on the dispersion used. The small dispersion used at Yerkes is of great value in minimizing rotation broadening, while the somewhat larger dispersion used at McDonald shows it much more clearly. Despite this fact, a few of the stars taken at Yerkes show considerable broadening. The plates and films used are not red-sensitive, so that no data on the behavior of  $H\alpha$  was obtained.

### III. THE OBSERVING PROGRAM

Although the  $h$  and  $\chi$  Persei clusters are only some  $40^\circ$  distant from the anticenter, because of their small galactic latitude ( $-3^\circ$ ), we should expect an appreciable number of "background" supergiants in their vicinity, because early-type supergiants are known to be highly concentrated to the galactic plane. To evaluate the number of "field" supergiants in the region of the double cluster, stars were observed over a fairly large area. A region (which we shall call "Region I") was chosen running from  $95^\circ$  to  $110^\circ$  in galactic longitude and from  $+5^\circ$  to  $-5^\circ$  in galactic latitude. All stars classified in the *Henry Draper Catalogue* as type A2 or earlier and between 5.0 and 7.5 photometric magnitude were observed at Yerkes.

A second region (which we shall call "Region II") was chosen by plotting all stars of type A2 or earlier and between photographic magnitudes 5.0 and 8.5 in the Yale zone catalogues<sup>9, 10</sup> on a right ascension and declination chart, made with a scale corresponding to  $\delta = 60^\circ$ , and then drawing a circle of radius  $3^\circ$  about the center of the double cluster. The area thus chosen is not strictly circular but is sufficiently symmetrical about the cluster for our purposes. All stars falling within this circle were observed, those fainter than eighth magnitude in general at the McDonald Observatory.

Region III consists of the vicinity of the clusters themselves and comprises an area about  $37'$  square centered on each cluster. These two squares are the regions considered by Oosterhoff<sup>5</sup> in his study of the double cluster and also include those areas studied by Trumpler<sup>11, 12</sup> and Zug.<sup>13</sup> All stars in Region III were observed which are brighter photographically than 9.50, according to Oosterhoff. These stars were all taken at the McDonald Observatory.

A few stars were also observed which, although they lie outside the regions chosen, are contained in Shapley's table.<sup>4</sup>

### IV. AUXILIARY DATA USED

The only quantities directly determined in this investigation are spectral classes and absolute magnitudes. However, to derive distances from the observed data we also need accurate apparent magnitudes and very accurate color-excess data.

<sup>9</sup> *Trans. Yale Obs.*, 4, 1925; 7, 1930.

<sup>10</sup> The photographic magnitudes used are in *Contr. Columbia Obs.*, No. 30, 1937; No. 31, 1938.

<sup>11</sup> *Pub. Allegheny Obs.*, 6, No. 4, 1929.

<sup>12</sup> *Pub. A.S.P.*, 38, 350, 1926.

<sup>13</sup> *Lick Obs. Bull.*, No. 454, 1933.

The apparent magnitudes used in this investigation have been derived from a variety of sources. It is well known that the photometric magnitudes given in the *Henry Draper Catalogue* are not uniformly accurate; the revision of the magnitudes of bright stars published recently as the "Harvard Photovisual Magnitudes of Bright Stars"<sup>14</sup> does, however, provide magnitudes on a uniform system; and, as all the stars taken in Region I have *Mimeogram* magnitudes, these have been used. The absolute magnitudes have, however, been derived using the preliminary calibration curve given in the *Atlas*, and they are visual magnitudes. The calibration was made using the Harvard photometric magnitudes of bright stars, and so it was necessary to investigate the relation between the Harvard photometric system and that of the *Harvard Mimeogram* referred to above. A plot of the two magnitude systems for those stars in Region I used in this work shows that, while there is little systematic difference for the dwarf stars, the supergiants appear to be systematically fainter by about 0.1 mag. in the photometric system than in the photovisual system. This conclusion was checked by comparing the magnitudes of early-type supergiants of the *Atlas*, where a systematic difference in the same sense of 0.07 mag. was found. Thus, a correction of  $-0.1$  mag. was applied to the absolute magnitudes of the supergiants of Region I, whereas no change was made in the case of stars of lower luminosity.

Since many stars observed in Region II do not have Harvard Photovisual System magnitudes, those used are the regular Harvard photometric (two-decimal) magnitudes, if available; if not, the magnitudes given in the catalogue of Stebbins, Huffer, and Whitford<sup>15</sup> are used. These magnitudes were obtained by photoelectric measures, using the Harvard photometric magnitudes as standards. The visual magnitudes of the remaining stars were taken from the *Henry Draper Catalogue* and are simply the reduced *Bonner Durchmusterung* magnitudes. The probable error of these magnitudes has been found by Stebbins, Huffer, and Whitford to be about 0.3 mag.

The magnitudes of the stars in Region III, with one exception, have been taken from the work of H. Vogt,<sup>16</sup> whose scale and zero point were set by reference to the Potsdam magnitudes of the Pleiades and some stars belonging to the double cluster. Since it appears that there is a difference in zero point, Potsdam *minus* Harvard, of 0.28 mag.,<sup>17</sup> Vogt's magnitudes have been correspondingly reduced. One of the stars in Region III is given the magnitude listed in the *Henry Draper Catalogue*. Magnitudes for the stars not included in these three regions have been taken from the Harvard Photovisual System or the *Henry Draper Catalogue*, the correction for supergiants again having been made.

A number of the stars studied in this investigation are double, either spectroscopically or visually, and the magnitude of the brighter component has been computed from the difference in magnitude, usually taken from Aitken's *Catalogue of Double Stars*, and the distance modulus corresponding to this component has been found. In all such cases the apparent magnitude of the brighter component is tabulated.

The other auxiliary datum required for obtaining the distance of a star is the total visual absorption. It has proved invaluable to use the photoelectric colors of Stebbins, Huffer, and Whitford<sup>15</sup> for the determination of color excess; and in agreement with them we determine the total visual absorption by multiplying the color excess by 7.<sup>18</sup> Photoelectric colors are available for many of the supergiants in this region, as well as for some other B stars. The determination of color excess, however, demands information on the normal colors as well as measured colors themselves. The normal colors tabulated in "The Colors of 1332 B Stars" were determined by considering those stars near enough

<sup>14</sup> Payne-Gaposchkin, *Harvard Mimeograms*, Ser. III, No. 1, 1938.

<sup>15</sup> *Ap. J.*, **91**, 20, 1940.

<sup>16</sup> *Pub. Heidelberg*, **8**, No. 3, 1932.

<sup>17</sup> *Harvard Ann.*, **89**, 65, 1932.

<sup>18</sup> *Ap. J.*, **90**, 209, 1939.

to be presumably unreddened.<sup>19</sup> Obviously, a large percentage of these are dwarf stars, and there is no a priori reason why the supergiants should possess the same normal colors as these dwarf B and A stars.

The *Atlas* tabulates a number of very luminous early-type stars, for most of which photoelectric colors are available. Assuming the normal colors tabulated by Stebbins, Huffer, and Whitford, the color excesses were computed; and, although most of these stars have fairly large color excesses, we find, for a few of the stars, data as given in Table 1. Of these stars, perhaps  $\rho$  Leonis is the most interesting, as it has a galactic latitude of  $+54^\circ$ , and thus its true distance above the plane of the Galaxy must be such that it is practically out of the absorbing layer, which presumably lies within 250 parsecs of the galactic plane.<sup>20</sup> It must then suffer at least 0.03 mag. color excess on the photoelectric scale, so that, even allowing for a possible error in the measure or extreme transparency in that direction, as is indicated somewhat by Hubble's nebular counts,<sup>21</sup> there seems to be evidence that the normal color of a B1 supergiant is really a little bluer than that adopted heretofore, when measured photoelectrically.

TABLE 1

Type	Star	Color Excess	Type	Star	Color Excess
B1.....	$\rho$ Leo	0.01	A0.....	$\eta$ Leo	-0.05
B8.....	$\beta$ Ori	.00	A2.....	$\alpha$ Cyg	-0.05
A0.....	13 Mon	-0.03			

For the A-type supergiants tabulated above, there seems no doubt but that this is the case,  $\alpha$  Cygni supplying the best evidence of all. For this star must have suffered at least some color excess—probably 0.03 mag. or so, assuming a mean coefficient of absorption—so that even a fairly large error would not account for the discrepancy.

The stars  $\alpha$  Cygni and  $\rho$  Leonis may be exceptional, but the supergiants in the region of the Perseus cluster are equally so. On the basis of this evidence the author has adopted as normal colors for supergiants values differing from those tabulated in the list of "1332 B stars" by 0.00 at B0 and  $-0.05$  at A2, with appropriate intermediate corrections. The effect observed, if real, probably is caused by the difference in strength of the hydrogen lines in supergiant and dwarf, thus increasing toward A0.

It should be remarked that the maximum effect of this correction, at A2, will be a change of 0.35 in the distance modulus, in the sense that the distance of the star is decreased. The change, however, becomes comparable with the probable error of the measures only around B5, the earlier stars being little affected.

The photoelectric colors are used wherever available, and for stars which appear to be at roughly the distance of the cluster the color excesses have been estimated from a consideration of the change of color excess across the field, which will be discussed later in the paper. For stars appearing to be definitely closer than the cluster, i.e., dwarfs, the true distance moduli were computed, assuming a mean coefficient of absorption of 0.12 mag. per kiloparsec on the photoelectric scale. The true distances were found from a graph giving the relation between true and apparent distance for a total (visual) absorption of 0.8 mag. per kiloparsec; and, when the true distances were found, the appropriate color excess was computed, assuming uniformity of the absorbing layer.

<sup>19</sup> *Pub. Washburn Obs.*, 15, Part V, 1934.

<sup>20</sup> Stebbins, Huffer, and Whitford, "Selective Absorption in Space near the Sun," *Ap. J.*, 94, 215, 1941.

<sup>21</sup> *Ap. J.*, 79, 41, 1934.

## V. COMPARISON WITH OTHER OBSERVERS

We may compare the present spectral types with those of other observers for supergiants and less luminous stars separately. The 23 objects observed in common with the c star list of Wilson<sup>1</sup> show a mean difference of 0.7 subclass, with a negligible systematic difference. Some of the mean difference is caused by the rather liberal use of class A1 in the present work.

Neglecting 8 stars which show a difference of more than 5 subclasses, 96 nonsupergiants observed in common with the *Henry Draper Catalogue* show a mean difference of 1.5 subclasses and a systematic difference of  $\frac{1}{2}$  subclass, in the sense that the types of the present work are in general earlier than those of the Harvard observers.

Thirteen objects have been observed in common with Trumpler.<sup>12, 13</sup> These show a mean difference of 0.9 subclass and a systematic difference of 0.7 in the sense that my types are earlier than Trumpler's. Comparison with 6 dwarf emission stars in Merrill's lists<sup>22</sup> shows a mean difference of 1.2 subclass and shows that my classes are systemati-

TABLE 2  
STARS WHOSE PRESENT CLASSIFICATION DIFFERS CONSIDERABLY  
FROM THE *Henry Draper Catalogue*

Star	Class	HD Class	Remark
HD 9105.....	B5	B0p	The spectrum has changed. See note in tables
12150.....	B1	B8	
13661.....	B2e	B8	
14299.....	B2	B9	
14331.....	B0	B9	
14434.....	O7	B2	
14520.....	B1	B9	
15990.....	B3:	B9	
19820.....	O9	B5	

cally 1 subclass earlier than Merrill's. It should be said that these stars are quite difficult to classify accurately.

Twenty-two stars in the Victoria catalogue of radial velocities<sup>23</sup> give a mean difference of 0.7 subclass and a negligible systematic difference. From these comparisons we may conclude that the classes of supergiants are in good agreement with other modern determinations, that the dwarfs are classified earlier by about 0.1 spectral class than in other classifications, and that the types should be accurate to about 0.1 of a spectral class in general but that the accidental error may reach 0.2 of a spectral class occasionally. This is especially true of stars with rotational broadening and of dwarfs in the range B8-A2.

The classification of a few stars shows a considerable deviation from the *Henry Draper Catalogue*; these are given in Table 2. These stars are all fainter than magnitude 7.5 except HD 9105 and HD 19820. It is apparent that there are many more early B stars than the *Henry Draper Catalogue* would indicate.

The accuracy of the absolute magnitudes derived in this investigation is rather hard to evaluate. With the large range in absolute magnitude among the early-type stars established in recent years, the accuracy obtainable from spectroscopic criteria has somewhat decreased. Thus, although the criteria of luminosity are plainly marked for all the classes considered here except for the stars earlier than O9, the error in absolute magni-

<sup>22</sup> *Ap. J.*, 78, 87, 1933; 96, 15, 1942.

<sup>23</sup> *Pub. Dom. Ap. Obs.*, 5, 99, 1931.

tude caused by a rather small error in luminosity classification can be quite serious. In the most serious case here considered, namely A2, there is a difference of 2 mag. between luminosity classes Ia and Ib. Even with the present somewhat scanty material, this difference of luminosity class will almost certainly be noted; but accurate classification of a star within this 2-mag. range is quite difficult with the type of plates used in the present work. An uncertainty of a magnitude is to be fully expected in the absolute magnitudes of this investigation, in the case of the most luminous stars. For dwarfs with good lines the accuracy may be somewhat better.

#### VI. OBSERVATIONAL RESULTS

The observational results of this investigation are given in Tables 3, 4, 5, and 6. The content of each table is as follows:

Table 3 contains those stars observed in Region I. Columns give HD number; galactic co-ordinates, which were computed for all the stars; the photovisual magnitude, as described above; the revised spectral class and absolute visual magnitude; the color excess, as computed from the colors of Stebbins, Huffer, and Whitford or (in parentheses) estimated from position in the field or computed as described above. Column 8 gives the true distance modulus,  $m_0 - M$ , where  $m_0$  is the magnitude the star would have had were it not obscured. Then follows the radial velocity for those stars for which it is known; an asterisk in the remarks column indicates a remark following the table.

Figure 1, *a* and *b*, shows the stars in Table 3. Those stars which appear to be nearer than 500 parsecs are plotted in Figure 1, *a*; those which appear to be farther than 500 parsecs are plotted in Figure 1, *b*. In the latter diagram the stars which are considered to be members of the  $\eta$  and  $\chi$  Persei cluster are represented by filled circles.

Table 4 contains all the stars observed in Region II, with the exception of those in Table 3. The columns are the same except that equatorial co-ordinates for 1900 are given. The two-decimal magnitudes are the Harvard photometric magnitudes; the one-decimal magnitudes are from Stebbins, Huffer, and Whitford; and the one-decimal magnitudes followed by a colon are the reduced BD magnitudes.

In Figure 2 we have plotted all the stars observed in Region II which have photographic magnitudes between 5.0 and 8.5, i.e., all those in Table 4 and those in Table 3 which fall within the circle defining Region II. Those stars which are believed to be members of the double cluster are represented by filled circles. The large circles indicate the size of the two clusters as found by Trumpler for stars of the seventeenth magnitude. We may note that the material is complete for early-type stars to apparent photographic magnitude 8.5.

Table 5 contains those stars observed in Region III. Columns give: the designation; the number of the star in Oosterhoff's catalogue;<sup>5</sup> the visual magnitude, as described above; the spectral type and visual absolute magnitude; the color excess, as in the other tables; the true distance modulus; and the asterisks indicating remarks. It is considered probable that all these stars are physical members of the  $\eta$  and  $\chi$  Persei cluster.

Table 6 gives data on several stars observed but not belonging in any of the other tables.

In all the tables a dagger before the designation indicates that the star is thought to be a member of the  $\eta$  and  $\chi$  Persei cluster; a question mark indicates that the star may be a member. In the notes "ADS" refers to Aitken's *Double Star Catalogue* and "MWC" and "Mt. W." to the Mount Wilson Be star lists.<sup>22</sup>

*General conclusions.*—Some conclusions which may be drawn from the tables and figures appear to be the following:

1. Among early-type stars brighter than magnitude 7.5, i.e., those in Table 3 and Figure 1, *a* and *b*, the distribution of the stars nearer than 500 parsecs is fairly uniform, while that of the stars farther than 500 parsecs shows a marked concentration about the

TABLE 3

HD	<i>l</i>	<i>b</i>	$m_{pv}$	Sp.	$M_v$	C.E.	$m_0 - M$	<i>V</i>	Re- marks
8965.....	95°4	-1°8	7.21	B0	-3.2	0.18	9.2	+ 0.6	
9105.....	95.1	+1.3	7.39	B5	-6.6	.36	11.5	-39.9	*
9311.....	95.8	-1.3	7.17	B5	-5.7	.27	11.0	-38.1	*
9812.....	96.7	-3.2	7.45	B3	-2.2	(.08)	(9.1)		*
9878.....	96.0	+0.4	6.60	B8	0.0	(.02)	(6.5)		
10107.....	97.0	-2.7	6.89	B9	-1.8	(.05)	(8.4)		
10260.....	96.8	-0.7	6.64	B8	-1.0	.00	7.6		
10293.....	97.3	-3.1	6.31	B8	-1.0	(.03)	(7.1)		*
10362.....	96.8	-0.4	6.43	B8	-2.1	(.05)	(8.2)		
10425.....	97.0	-1.2	5.79	B8	-0.5	(.02)	(6.2)	var.	*
10543.....	97.8	-4.1	6.32	A2	+0.3	(.02)	(5.9)	+ 5.1	*
10587.....	98.0	-4.5	6.11	A1	+1.0	(.01)	(5.0)	+ 5.3	*
11606.....	98.8	-2.0	7.02	B1ne	-1.9	.11	8.2	+12.5	*
11669.....	98.4	-0.1	8.04	A0	+0.6	(.03)	(7.2)		*
11857.....	98.5	+0.4	6.04	B7	-0.8	(.03)	(6.6)		
11860.....	99.0	-1.6	6.54	A1	+1.0	(.01)	(5.5)		
11946.....	97.8	+3.2	5.20	A0	+0.6	(.01)	(4.5)	+ 5.0	*
12112.....	99.3	-1.2	6.62	A3	0.0	(.02)	(6.5)		
12279.....	98.0	+3.6	5.99	A0	+0.6	(.01)	(5.3)	-29.1	*
12301.....	98.2	+3.1	5.64	B8	-5.9	.22	10.0	-20.4	*
12365.....	99.3	-0.4	7.43	B9	-0.3	(.04)	(7.4)		
12468.....	98.2	+3.8	6.49	B9	+0.2	(.02)	(6.2)	- 4.2	*
†12953.....	100.7	-2.4	5.67	A1	-6.6	.18	11.0	-37.2	
†13267.....	101.3	-3.0	6.36	B8	-6.1	.16	11.3	-34.4	
13427.....	99.2	+3.9	7.36	A1	+1.0	(.02)	(6.2)		
†13476.....	101.2	-2.0	6.39	A2	-6.1	.26	10.7	-38	
†13841.....	102.2	-3.3	7.22	B0.5	-4.9	.15	11.1	-39.4	
†13854.....	102.2	-3.3	6.46	B1	-6.6	.18	11.8	-40.0	*
14010.....	99.8	+3.7	7.05	B9	-6.6	.26	11.8	-47.0	*
†14134.....	102.4	-3.1	6.63	B3	-6.1	.24	11.0	-43.4	*
†14143.....	102.4	-3.1	6.64	B2	-6.1	.27	10.8	-45.2	*
14171.....	100.0	+3.7	6.44	A0	+0.1	(.02)	(6.2)	-25.8	
14172.....	101.5	-0.4	6.83	A2	+1.4	(.01)	(5.4)		
†14322.....	103.1	-4.2	6.81	B8	-5.9	.17	11.5	-37	
†14433.....	102.7	-2.9	6.42	A1	-6.1	.25	10.8	-46.1	
14489.....	103.3	-4.2	5.17	A1	-6.6	.16	10.6	-16	*
†14535.....	102.9	-2.8	7.35	A2	-5.6	.31	10.8	-53	
†14542.....	102.8	-2.7	6.85	B9	-6.1	.33	10.6	-51.4	*
14817.....	101.6	+1.3	7.58	B8	0.0	(.04)	(7.3)		*
†14818.....	103.4	-3.3	6.26	B2	-6.1	.27	10.5	-47.0	*
†14899.....	103.3	-2.6	7.38	A0	-5.1	(.32)	(10.2)	-42.0	
†14956.....	103.2	-2.2	7.16	B2	-6.1	.37	10.7	-30.3	
15102.....	101.3	+2.9	7.44	A0	+0.6	(.03)	(6.6)		
15253.....	104.3	-4.1	6.86	A1	-1.1	(.04)	(7.7)		*
†15316.....	103.5	-1.9	7.12	A2	-5.6	.40	9.9	-44	*
†15497.....	103.8	-2.0	7.01	B5	-6.1	.46	9.9	-35.4	*
15640.....	103.0	+0.2	7.43	A1	+1.0	(.02)	(6.3)		*
15641.....	103.6	-1.2	8.14	A3	+1.7	(.02)	(6.3)		*
16218.....	102.6	+2.9	6.71	A0	+0.1	(.02)	(6.5)		
16230.....	102.6	+2.9	7.45	A2	+1.4	(0.02)	(5.9)		

TABLE 3—Continued

HD	<i>l</i>	<i>b</i>	<i>m<sub>DV</sub></i>	Sp.	<i>M<sub>v</sub></i>	C.E.	<i>m<sub>0</sub>-M</i>	<i>V</i>	Re- marks
16349.....	102°7	+3°0	7.23	A2	-0.2	(0.03)	(7.2)	.....	*
16524.....	105.5	-2.7	7.39	B6	-0.4	(.04)	(7.5)	.....	
16616.....	103.1	+2.9	7.22	A2	+0.3	(.03)	(6.7)	.....	
16718.....	104.7	-0.3	7.42	A0	-0.4	(.04)	(7.5)	.....	*
16727.....	106.3	-3.6	5.72	B8	0.0	(.02)	(5.6)	.....	
17198.....	107.4	-4.4	7.42	A0	+0.6	(.03)	(6.6)	.....	*
17217.....	106.7	-2.9	6.92	A2	+0.8	(.02)	(6.0)	.....	
17505.....	104.9	+1.6	7.15	O7	.....	.24	.....	-17	*
17581.....	105.9	-0.3	6.29	A3	+1.7	(.01)	(4.5)	-4.8	*
17743.....	108.6	-4.9	6.91	B8	0.0	(.03)	(6.7)	.....	*
18352.....	105.4	+2.8	6.86	B2	-1.5	.12	7.5	-1.5	
18439.....	108.4	-2.4	7.02	A2	+0.8	(.02)	(6.1)	.....	
18473.....	106.3	+1.5	7.27	A1	0.0	(.03)	(7.1)	-1.6	*
18537.....	109.9	-4.8	5.42	B8	-0.5	.00	5.9	-4.1	*
18538.....			6.94						
18876.....	105.0	+4.7	7.37	B7	-1.4	(.06)	(8.4)	-2.9	
19243.....	105.7	+4.3	6.49	B2ne	-1.5	.26	6.2	-24.7	*
19536.....	106.9	+3.0	7.14	A0	+0.1	(.03)	(6.8)	+12.8	*
19820.....	107.8	+2.3	7.43	O9	-4.2	.32	9.4	-4.2	*
20041.....	109.3	+0.4	5.82	A0	-6.6	.33	10.1	-13	*
20536.....	107.2	+4.8	6.63	B9	-0.8	(.03)	(7.2)	-8.3	
21203.....	108.9	+3.8	6.69	B9	+0.2	(.02)	(6.4)	+3.8	*
21427.....	109.6	+3.3	6.36	A1	0.0	(0.02)	(6.2)	+13.1	*

## . NOTES TO TABLE 3

HD No.

9105. MWC 13. This interesting star, which had bright  $H\beta$ ,  $H\gamma$ , and  $H\delta$  at the time of the Harvard observations and which also showed several other lines in emission, appears to be a very luminous supergiant. Bright  $H\alpha$  has been noted for many supergiants, but it is definitely peculiar for a supergiant to show as many bright lines as this star did at one time. See *Pub. A.S.P.*, **34**, 180, 1922, for a discussion of this star by Merrill and Humason. The star now has a sharp-line spectrum with strong interstellar H and K lines.
9311. ADS 1209.
9812. ADS 1262.
10293. ADS 1334.
10425. ADS 1344. Radial velocity varies from -4 to -51 km/sec. See *Dom. Ap. Obs.*, **1**, 287, 1921.
10543. ADS 1359.
11606. MWC 21. The lines are very broad and  $H\beta$  is weakly bright.
11669. ADS 1531. The lines show considerable broadening.
11946. ADS 1571.
12279. Spectroscopic binary?
12301. A note in Miss Payne's c star catalogue indicates emission lines in this star, but nothing extraordinary is seen on my spectra.
12468. Spectroscopic binary?
13854. MWC 31. Emission at  $H\alpha$  according to Merrill.
14010. ADS 1759.
14134. MWC 32. Emission at  $H\alpha$  according to Merrill.
14143. ADS 1766. This star probably has emission at  $H\alpha$  according to Merrill.
14489. ADS 1802. This star is 9 Persei, an A1 supergiant which agrees in luminosity and position with the cluster stars but which is not a member, if the radial velocity is constant.
14817. ADS 1833.
14818. MWC 45. Emission at  $H\alpha$  according to Merrill.
15253. ADS 1878.

NOTES TO TABLE 3—*Continued*

- 15316, 15497. These stars, although not having distance moduli quite as large as the other cluster stars, are considered to be cluster members because of their large color excess, which introduces uncertainty in the distance, and because their radial velocities and positions agree well with the other members of the double cluster. Nevertheless, they are neither included in the computation of the distance of the cluster nor plotted in the Russell-Hertzprung diagram of cluster members.
15640. ADS 1932.
15641. ADS 1933.
16349. The  $\text{Si II}$  lines are abnormally strong, the star in this respect resembling  $\theta$  Aurigae. However, this object differs from  $\theta$  Aurigae in showing more faint lines, evidently corresponding to a later type and, in addition, possessing a normal K line for its type. This star is undoubtedly somewhat above the main sequence.
16718. ADS 2058.
17198. ADS 2115.
17505. ADS 2161. The velocity is variable; see Plaskett, *Dom. Ap. Obs.*, 5, 18, 1931.
17581. The metallic lines seem a little too strong for the K line in this star. This object may be peculiar as the HD type is A0 with the remark that "a line at about  $\lambda$  4174 is very strong." This line does not appear extraordinarily strong on my spectra. Harper, in *Dom. Ap. Obs.*, 4, 39, 1927, gives the velocity-curve of this object, which is a spectroscopic binary, and a table of line intensities.
17743. ADS 2185.
18473. The  $\text{Si II}$  lines are abnormally strong, and the spectrum generally resembles  $\theta$  Aurigae. Unlike HD 16349, the K line here is weak or absent. This star was announced as a spectroscopic binary with a range of 63 km/sec in *Pub. David Dunlap Obs.*, 1, No. 3, 1939, and the presence of strong  $\text{Si II}$  lines noted. According to the above, the star is a spectrum variable also.
- 18537-8. ADS 2270. The stars were not observed separately.
19243. MWC 61.  $H\beta$  appears as a very weak absorption, while the other hydrogen lines are very broad. The helium spectrum, however, appears fairly sharp.
19536. Probably a spectroscopic binary, according to *Pub. David Dunlap Obs.*, 1, No. 3, 1939.
19820. This star is an O-type double-line binary. The orbit has been computed by Pearce, in *Dom. Ap. Obs.*, 4, 67, 1927. It is also an Algol type eclipsing variable of small range, CC Cassiopeiae.
20041. ADS 2424.
21203. ADS 2538.
21427. ADS 2563.

double cluster in Perseus ( $l = 102.5^\circ$ ,  $b = -3^\circ$ ). Since the material is complete to apparent photometric magnitude 7.5, there can be no doubt that there is a real clustering of supergiants in the direction of the  $h$  and  $\chi$  Persei cluster.

2. By reference to the spectroscopic distance moduli and radial velocities of these stars, one sees that there is good evidence that most of these stars in the *direction* of the cluster actually are members of a physical group at approximately the same *distance*. Thus we are entitled to speak of a "cluster of supergiants" in the direction of the double cluster in Perseus.

3. Among early-type stars between magnitude 7.5 and 8.5, i.e., those in Table 4, there are a number of stars whose positions with respect to the double cluster and whose distance moduli indicate an extension of the cluster of supergiants to fainter magnitudes. Also, there are a number of stars in Table 4 whose membership in the cluster is not certain but distinctly possible.

4. For fainter stars which are almost certainly true members of the double cluster, i.e., those in Table 5, we find distance moduli which agree within the limits of error with those found for the stars belonging to the cluster of supergiants. We will further see that the distance of all these stars in the three regions agrees well with the distance of the  $h$  and  $\chi$  Persei cluster, as judged from the main sequence observed by Trumpler.

5. The diameter of the cluster of early-type stars presumably associated with the double cluster exceeds considerably that heretofore adopted for the double cluster. The diameter of the "extended cluster" surrounding  $h$  and  $\chi$  Persei may be estimated as close to  $5^\circ$ , in comparison with that of the cluster as defined by fainter stars, which is judged to be about  $1\frac{1}{2}^\circ$ . There seems to be little doubt that the double cluster in Perseus is surrounded by a group of very luminous early-type stars whose presence can hardly be incidental.

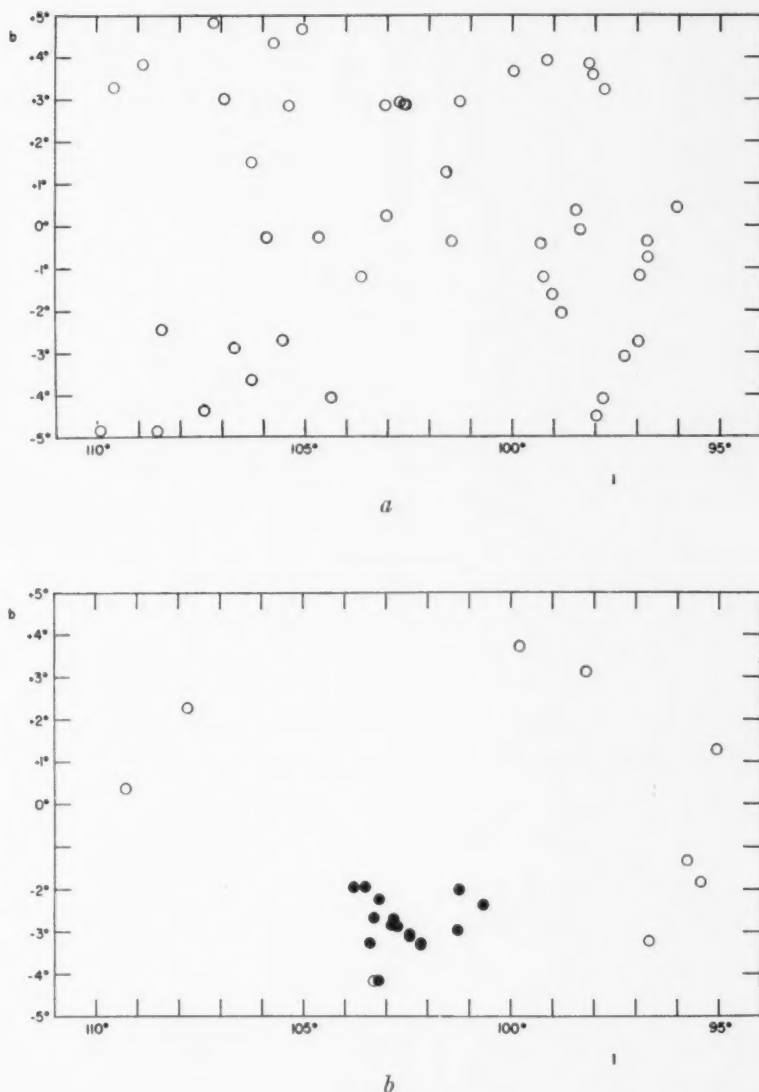


FIG. 1.—Stars with spectra as early as A2 in the *Henry Draper Catalogue* and with photometric magnitudes between 5.0 and 7.5 in the region shown. Fig. 1, *a*, shows those stars which have spectroscopic absolute magnitudes which put them within 500 parsecs, while Fig. 1, *b*, shows those stars with distances greater than 500 parsecs. In the second plot those stars considered to be members of the  $h$  and  $\chi$  Persei cluster are represented by filled circles. The galactic co-ordinates of the double cluster are:  $l = 102.5^\circ$ ,  $b = -3^\circ$ . The only open circle near the double cluster represents the star 9 Persei.

TABLE 4

HD	R.A.	Dec.	$m_v$	Sp.	$M_v$	C.E.	$m_0 - M$	V	Re- marks
11866.....	1 <sup>h</sup> 51 <sup>m</sup> 5	57°22'	8.1:	A2	+1.4	(0.02)	(6.6)	.....	
?12150.....	1 54.2	57 43	8.4:	B1	-3.8	(.19)	(10.9)	.....	
12709.....	1 59.4	56 50	8.0:	B3	-2.2	(.10)	(9.5)	.....	
†12856.....	2 0.9	56 38	8.6	B0.5ne	-3.5	.16	11.0	.....	*
12928.....	2 1.5	58 23	8.6:	B8	0.0	(.05)	(8.2)	.....	
12994.....	2 2.1	56 34	8.2:	B8n	-0.5	(.06)	(8.3)	.....	*
†13051.....	2 2.6	56 31	8.7	B0.5	-3.9	.15	11.6	.....	*
13088.....	2 3.0	58 41	8.0:	A1	+1.0	(.03)	(6.8)	.....	
13268.....	2 4.6	55 41	8.1	O7n	.....	.11	.....	.....	*
†13402.....	2 5.9	59 4	8.2:	B0	-4.8	(.25)	(11.2)	.....	
13412.....	2 6.0	58 20	8.2:	Ap	.....	.....	.....	.....	*
†13621.....	2 7.8	54 51	8.06	B0.5	-4.8	(.18)	(11.6)	.....	*
13633.....	2 7.9	58 1	7.96	B8	-1.0	(.06)	(8.5)	.....	*
13661.....	2 8.1	54 4	8.6:	B2ne	-2.5	(.13)	(10.2)	.....	*
13669.....	2 8.2	55 20	8.51	B5n:	-2.4	(.12)	(10.1)	.....	*
13716.....	2 8.6	57 18	8.4	B0.5	-4.8	.16	12.1	-60.1	
13717.....	2 8.6	55 8	8.01	B9	-0.8	(.06)	(8.4)	var.	*
†13744.....	2 8.9	57 50	7.8	A1	-5.3	.32	10.9	-51	
†13745.....	2 8.9	55 32	7.96	O9.5	-4.8	.14	11.8	-32	
?13831.....	2 9.7	56 17	7.9	O9.5:	-2.6	.09	9.9	-31	
†13866.....	2 10.0	56 15	7.4	B2	-4.2	.14	10.6	-48.8	
?13890.....	2 10.2	56 19	8.9:	B1ne	-4.8	(.14)	(12.7)	.....	*
13910.....	2 10.4	56 54	8.2:	A0n	+0.6	(.04)	(7.3)	-1	*
13970.....	2 10.8	56 11	8.6	B1n	-1.9	.14	9.5	-27	*
†14052.....	2 11.4	56 45	7.98	B1	-4.8	(.24)	(11.1)	-41	
?14053.....	2 11.4	56 33	8.3	B3	-5.6	.14	12.9	-49	
14183.....	2 12.6	59 4	8.0:	A2	+1.4	(.02)	(6.5)	.....	
14210.....	2 12.8	56 52	8.12	B9	-0.8	(.06)	(8.5)	-39	
14299.....	2 13.6	59 9	8.6:	B2	-2.5	(.15)	(10.0)	.....	
?14331.....	2 13.9	55 22	8.81	B0	-4.8	(.17)	(12.4)	.....	
†14357.....	2 14.1	56 25	8.24	B2	-4.2	(.22)	(10.9)	-40	
†14434.....	2 14.8	56 27	8.4	O7n	.....	.14	.....	.....	*
†14443.....	2 14.9	56 42	7.81	B2	-4.8	(.24)	(10.9)	-39	
14581.....	2 16.3	56 24	8.35	B9	-1.8	(.10)	(9.4)	.....	
14646.....	2 16.8	57 24	8.8:	A0	+0.6	(.04)	(7.9)	-12	
14722.....	2 17.4	53 46	8.2:	B2	-1.5	(.08)	(9.1)	.....	*
14795.....	2 18.0	59 33	7.52	B6	-0.4	(.04)	(7.6)	.....	*
14825.....	2 18.3	57 44	7.88	A3	+1.7	(.02)	(6.0)	+2	*
14827.....	2 18.3	54 48	7.51	A0	-1.4	(.06)	(8.5)	.....	*
14864.....	2 18.8	57 3	8.6:	A0	-0.4	(.06)	(8.6)	.....	
14871.....	2 18.9	55 38	8.0:	B5	-0.6	(.05)	(8.2)	.....	
14947.....	2 19.5	58 25	8.04	O5e	.....	.....	.....	-53.7	*
15090.....	2 20.8	56 8	8.5:	A1	+1.0	(.03)	(7.3)	.....	
15124.....	2 21.1	56 49	8.2:	B3:	-1.1	(.07)	(8.8)	.....	
15332.....	2 23.0	56 13	8.1:	A1	+1.0	(.03)	(6.9)	.....	*
15485.....	2 24.5	54 50	8.5:	A3	+1.7	(.03)	(6.6)	.....	
†15642.....	2 25.8	54 54	8.6	O9.5n	-3.4	.05	11.6	.....	*
†236970.....	2 26.2	55 52	9.3:	Comp.	-5.1	(.50)	(10.9)	.....	*
†15690.....	2 26.3	57 5	8.2:	B2	-5.6	.39	11.1	.....	*
15963.....	2 28.9	57 38	7.98	Bp	.....	.....	.....	.....	*

TABLE 4—Continued

HD	R.A.	Dec.	$m_v$	Sp.	$M_v$	C.E.	$m_0 - M$	$V$	Re- marks
15990.....	2 <sup>h</sup> 29 <sup>m</sup> 1	55° 30'	8.2:	B3:	-1.1	(.07)	(8.8)	.....	*
16012.....	2 29.3	57 17	8.2:	B9	+0.2	(.04)	(7.7)	.....	
16040.....	2 29.5	55 29	8.7:	B9	-0.8	(.07)	(9.0)	.....	
†16310.....	2 32.0	58 38	8.4:	B0.5	-6.0	(.45)	(11.2)	.....	
16576.....	2 34.4	55 4	7.87	A3	+1.7	(.02)	(6.0)	.....	
16964}.....	2 38.1	56 8	{8.3:	A1	+0.5	(.04)	(7.5)	.....	*
16965}.....			{8.6:	A0n	+0.6	(0.04)	(7.7)	.....	

## NOTES TO TABLE 4

- HD No.
12856. MWC 25.  $H\beta$  appears as a strong emission line. All other lines in the spectrum, with the exception of H and K, appear extremely diffuse.
12994. The Balmer series is strongly winged and somewhat broadened.
13051. MWC 27.  $H\beta$  and  $H\gamma$  show no trace of emission on my spectra but are somewhat weaker than in ordinary stars. The lines are not noticeably broadened.
13268. All lines somewhat broad.
13412. The spectrum shows strong lines corresponding to a type of around F0, while the K line would give a type of around A5. The star is probably a metallic-line star.
13621. ADS 1714.
13633. ADS 1717.
13661. MWC 29.  $H\beta$  is fairly strong in emission, and all lines are somewhat broad.
13669. The helium lines are quite broad.
13717. The radial velocity varies from -8 to -59 km/sec.
13890. Mt. W. 249.  $H\beta$  shows a very weak emission, and all lines are weak and diffuse. This star is classed as a fairly high-luminosity object because of the strength of  $\lambda$  3995.
13910. The hydrogen lines are strong and appear rotationally broadened.
13970. ADS 1748. All lines are broad, and the Balmer series seems rather weak.
14434. This star, which is classed B2 in the *Henry Draper Catalogue*, appears to be classified for the first time as an O star. The lines  $\lambda$  4541 and  $\lambda$  4471 are of approximately equal intensity, while  $\lambda$  4686 is considerably stronger than  $\lambda$  4640. All lines are quite weak and diffuse except the strong interstellar lines.
14795. The hydrogen lines seem very strong for the class, and this star may be below the main sequence in luminosity.
14825. ADS 1832.
14827. ADS 1829.
14947. This O star resembles  $\zeta$  Puppis in the relative intensity of  $\lambda$  4686 and  $\lambda$  4640 in emission. There is a possibility that  $H\beta$  has a very weak P Cygni emission component. See Plaskett, *Dom. Ap. Obs.*, 2, 287, 1924.
15332. ADS 1893.
15642. All lines appear weak and ill-defined.
15690. ADS 1937.
16576. ADS 2040.
236970. ADS 1934. This is a double of 0.8" distance, and the spectra obtained are composite, of types around A2 and B2. The star is mentioned in the Mount Wilson discovery list of Be stars (*Ap. J.*, 96, 15, 1942) as one in which bright  $H\alpha$  is present according to objective prism observations. When it was first taken, in Texas, only the region to the red of  $H\gamma$  was well exposed, owing to the faintness and great redness of the object. This part of the spectrum matches well with  $\alpha$  Cygni, except for the weakness of  $H\beta$ ; and it was not until the whole spectral range was observed at Yerkes that the composite character of the spectrum was noted. Since the helium lines are fairly sharp, the observations seem capable of explanation in terms of both components of the double; but, since the difference in magnitude is given as 0.9 mag. in Aitken's catalogue, the author asked Dr. Van Biesbroeck to re-estimate the difference, which he kindly did. He finds  $\Delta M = 0.5$  mag., and also noted that the star appeared about as red as a G star. It is probable, then, that we are dealing with two stars—at least one possessing emission at  $H\alpha$  and weak  $H\beta$ . The helium line  $\lambda$  4009, however, appears somewhat peculiar, as in some shells; and it is possible that the brighter component of the double is a shell star. The Si II lines do not appear noticeably weak; but, if the fainter component were of type B also, it could strengthen these lines, which are weak in typical shells.

## NOTES TO TABLE 4—Continued

15963. This star appears in Miss Payne's c star list as cA0 and as such has been included in other lists. It shows a Cygni-like metallic lines and extremely sharp Balmer lines. However, there is evidence of an underlying broad hydrogen absorption under these sharp lines, and the helium lines  $\lambda 4026$  and  $\lambda 4009$  appear and are very broad. There is no doubt from the appearance of the spectrum that the "cA0" spectrum is produced in a shell surrounding an early-type B star. In support of the shell interpretation is the fact that the  $Si\ II$  and  $Mg\ II$  lines are conspicuously weaker in this star than in typical supergiants. See a note on this star in *A. J.*, 97, 452, 1943.
16012. The lines appear rather broadened.
- 16964-5. ADS 2094. The fainter component of this double has quite broad lines.

## VII. THE INTERSTELLAR ABSORPTION IN THE REGION OF THE DOUBLE CLUSTER

The region of the double cluster is one fairly poor in stars, in consideration of the galactic latitude. On the reproduction of the cluster in the *Barnard Atlas*,<sup>24</sup> one sees no

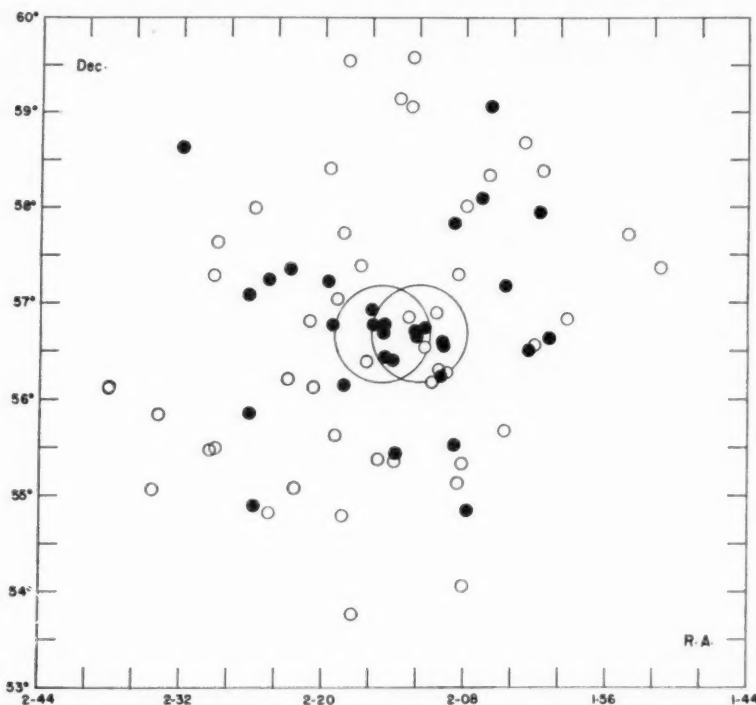


FIG. 2.—Stars with spectra as early as A2 in the *Henry Draper Catalogue* or the *Henry Draper Extension* and with photographic magnitudes between 5.0 and 8.5 in a region symmetrical about the double cluster. Those stars which are considered to be members of the  $\eta$  and  $\chi$  Persei cluster are represented by filled circles, while the large circles indicate the size of the two clusters as found by Trumpler for stars of the seventeenth magnitude.

particularly striking evidence of interstellar absorption; only one of Barnard's dark markings is found on that plate. One would judge by this reproduction that the  $\eta$  and  $\chi$  Persei cluster is about at the edge of the Milky Way, for the star density falls off fairly rapidly to the upper left-hand part of the plate. That, however, is the direction toward the galactic circle.

<sup>24</sup> "A Photographic Atlas of Selected Regions of the Milky Way," 1927.

TABLE 5

Designation	Oosterhoff No.	$m_v$	Sp.	$M_v$	C.E.	$m_0 - M$	Re- marks
†BD 56°473	49	8.91	B1n	-4.3	(0.17)	(12.0)	*
†HD 13900	146	9.0	B1n	4.3	(.15)	(12.2)	*
†HD 13969	339	8.70	B1	4.3	.13	12.1	
†BD 56°502	717	8.97	B1	3.8	(.22)	(11.2)	
†BD 56°511	847	8.91	B3	4.8	(.23)	(12.1)	
†BD 56°526	1133	9.23	B1n	4.5	(.24)	(12.0)	*
†BD 56°527	1132	8.55	B2n	4.2	(.24)	(11.1)	*
†HD 14250	1586	8.65	B2n	3.6	(.24)	(10.6)	*
†HD 14321	1781	8.96	B2	3.6	(.22)	(11.0)	
†HD 14422	2138	8.59	B1ne	3.8	(.28)	(10.4)	*
†BD 56°574	2296	8.38	B2n	4.8	(.24)	(11.5)	*
†BD 56°575	2299	8.88	B0.5	3.9	(.24)	(11.1)	
†BD 56°576	2311	8.99	B2	3.6	(.24)	(10.9)	
†HD 14476	2361	8.59	B0.5	3.9	.22	11.0	
†BD 56°578	2371	9.05	B3n	4.8	(.25)	(12.1)	*
†HD 14520	2541	9.09	B1	-3.8	(0.25)	(11.1)	*

NOTES TO TABLE 5

## Designation

- BD 56°473. Mt. W. 248. All lines quite diffuse.  
 HD 13900. Lines somewhat diffuse.  
 BD 56°526. All lines quite diffuse.  
 BD 56°527. Lines somewhat diffuse. Radial velocity -39 km/sec.  
 HD 14250. Lines somewhat diffuse.  
 HD 14422. MWC 37.  $H\beta$  is strong in emission, while the other hydrogen lines in absorption have a peculiar appearance. All the lines in the spectrum are weak, though not especially diffuse.  
 BD 56°574. Lines quite diffuse.  
 BD 56°578. Lines somewhat diffuse.  
 HD 14520. ADS 1810.

TABLE 6

HD	R.A.	Dec.	$m_v$	Sp.	$M_v$	C.E.	$m_0 - M$	Re- marks
13590	2 <sup>h</sup> 7 <sup>m</sup> 6	63° 34'	8.0	B2	-1.5	0.22	8.0	*
14708	2 17.3	53 46	9.2	B9:	+0.2	(.06)	(8.6)	
15240	2 22.2	56 38	8.5	A1	+1.0	(.03)	(7.3)	
?16778	2 36.3	59 24	7.69	A2	-5.6	.49	9.9	*
?17145	2 40.0	57 15	8.0	B8	-6.5	.45	11.4	
?17378	2 42.2	56 40	6.24	A4	-6.6	(.45)	(9.7)	*
18458	2 53.0	59 16	8.8	B8	0.0	(0.06)	(8.4)	

NOTES TO TABLE 6

## HD No.

13590. The lines appear somewhat broadened, although the star is listed in the c-star catalogue of Miss Payne. This star, as well as HD 16778 and HD 17145, was included in the program because Shapley's list of probable cluster members contains it.  
 16778. The radial velocity is -36 km/sec.  
 17378. This star has a Draper type of F5p, and a remark indicates that the spectrum is thought to be composite, consisting of an F5 and A2 component. It is called cA8 in Wilson's c-star list. The spectrum resembles the supergiant  $\phi$  Cassiopeiae, which is F5p in the *Henry Draper Catalogue* but A5 according to the system of the *Atlas*, except that its K line appears to be definitely weaker than  $\phi$  Cassiopeiae. Also, with respect to the rest of the metallic lines this star appears to be intermediate between the supergiants  $\alpha$  Cygni and  $\phi$  Cassiopeiae, and is thus classified as an A4 supergiant. The Balmer lines are at least as sharp as those of  $\phi$  Cassiopeiae, indicating great luminosity.

Reference to the *Ross-Calvert Atlas*<sup>25</sup> shows very clearly that the small field covered by the Barnard plate is deceiving, for the cluster certainly is well in the middle of the Milky Way. Plate 6 of "The Northern Milky Way," by S. I. Bailey,<sup>26</sup> shows clearly the true relation of the cluster to the Milky Way; on this plate it is evident that the decrease in star density on the Barnard plate is due to an absorbing lane running practically parallel to the galactic circle and only  $1\frac{1}{2}^\circ$  or so from the double cluster.

The effect of this absorbing lane on the stellar distribution in the region is strikingly brought out by Plate VII, which has been taken from a 3-hour exposure taken by the author with the 10-inch Bruce telescope. For the reproduction of this plate I am indebted to Dr. W. W. Morgan. The absorption is seen to extend quite uniformly across the field, from slightly to the south of the double cluster; and even at a distance of only a few degrees from the cluster the absorption is very heavy, for there are numerous places where no stars show at all.

Hubble's nebular surveys<sup>21</sup> show that the edge of the zone of avoidance of the extragalactic nebulae runs very close to the double cluster; nebulae have been found at galactic co-ordinates ( $100^\circ, -5^\circ$ ) and ( $110^\circ, -5^\circ$ ) on the southern side of the Milky Way. However, while the area to the south of the Milky Way is quite transparent, the zone of avoidance extends far above the galactic circle on the northern side. Stebbins, Huffer, and Whitford<sup>18</sup> showed that the region of the double cluster is one of obscuration and also that there is a strong gradient of absorption extending from  $\eta$  and  $\chi$  Persei to the galactic circle. In support of this,  $\chi$  Persei is found to be considerably redder than  $\eta$  Persei.

This conclusion has been emphasized by Miss Pishmish,<sup>27</sup> who showed that Oosterhoff's effective wave lengths and magnitudes give evidence of a differential absorption suffered by the two clusters. Oosterhoff<sup>5</sup> found that a region near  $\eta$  Persei (in the direction of the lower right-hand corner of Plate I) contains a much larger number of "white" stars, as shown by effective wave length, than any other part of the area he studied.

The present material, by enabling us to pick out those stars near the region which are at approximately the same distance, permits a new evaluation of the effect of selective absorption in this region. One may easily establish, by taking the color excesses from Tables 3, 4, and 5, that a strong gradient of selective absorption across the field is indeed present. From the present material there does not appear to be such a large difference between the two clusters as Miss Pishmish found, but perhaps she obtained a large effect due to selecting the opposite sides of the two clusters and thus emphasizing the greater transparency of  $\eta$  away from the galactic circle.

One should remember that the slightly different normal colors of supergiants which the author has used have an effect of increasing the color excesses throughout the region. The rather great value of the interstellar absorption and the rapid, although probably fairly uniform, change across the field demand accurate measurement of the colors of the stars if we desire to use them to calibrate our supergiant absolute-magnitude scale.

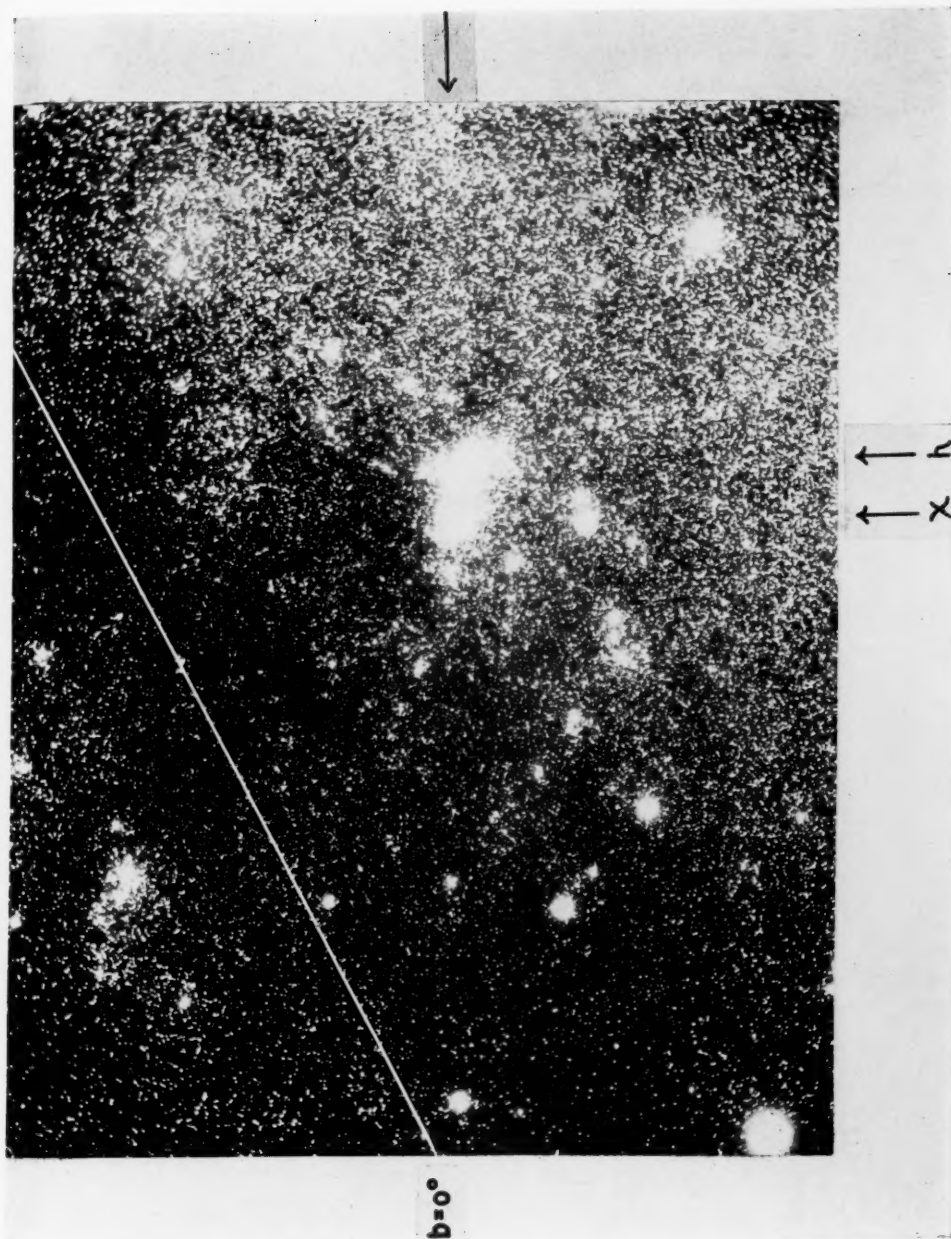
#### VIII. THE DISTANCE OF THE CLUSTER

On the basis of the present material the distance of the cluster surrounding  $\eta$  and  $\chi$  Persei and the double cluster itself may be found in several ways: (a) by the absolute magnitudes of the stars brighter than magnitude 7.5 (Region I); (b) by the absolute magnitudes of the stars between magnitude 7.5 and 8.5 (Region II); (c) by the absolute magnitudes of those stars which almost certainly belong to the cluster (Region III); (d) by the main sequences of the Russell-Hertzsprung diagrams of the two clusters observed by Trumpler;<sup>12,13</sup> and (e) by the radial velocities of the brighter stars, assuming the effect to be due to galactic rotation.

<sup>25</sup> "Atlas of the Milky Way," 1936.

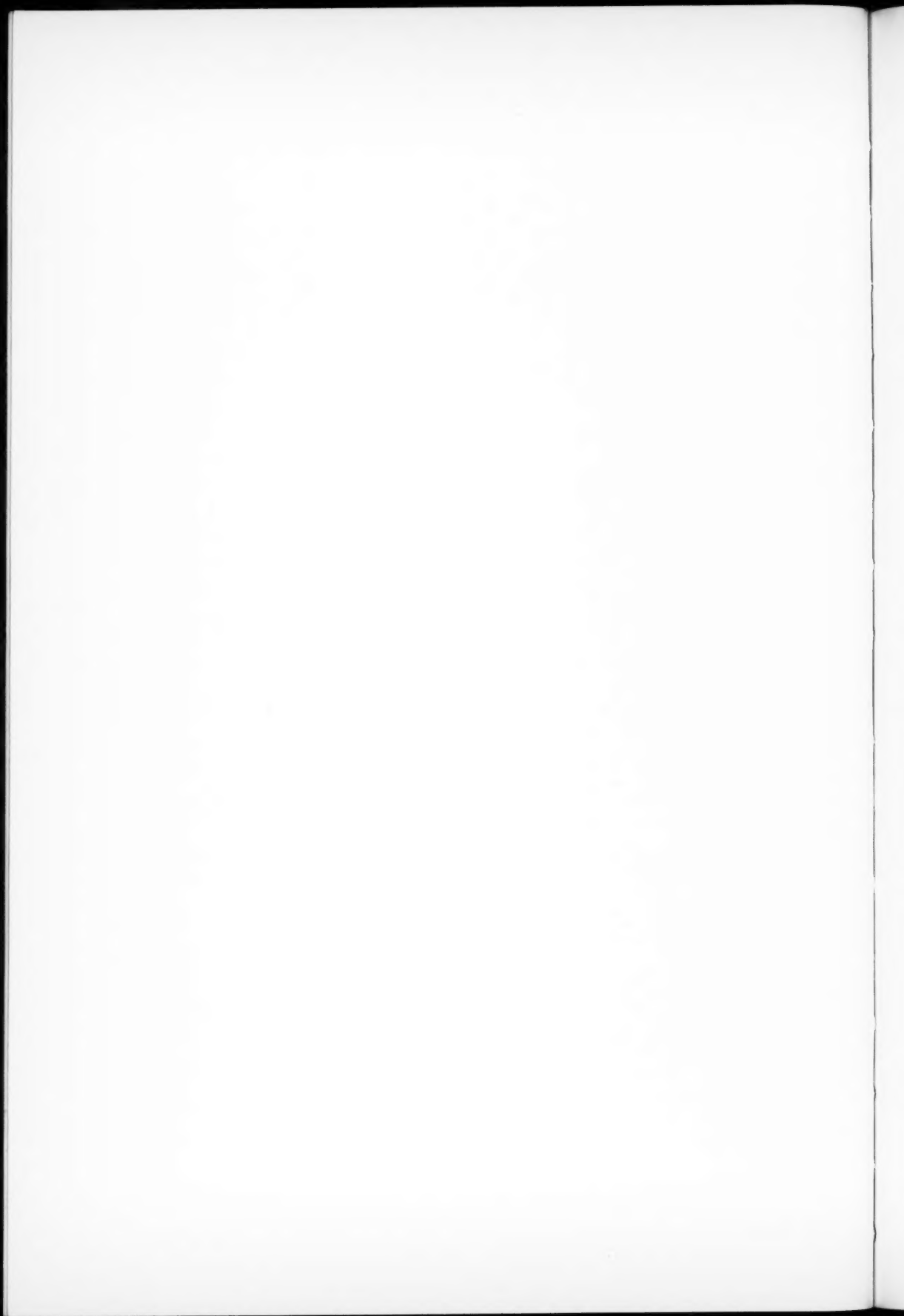
<sup>26</sup> *Harvard Ann.*, 80, 83, 1917.

<sup>27</sup> *Harvard Bull.*, No. 915, 27, 1941.



THE MILKY WAY IN THE REGION OF THE h AND x PERSEI CLUSTER

The galactic circle is indicated, and the scale may be judged from the galactic latitude of the cluster,  $-3^\circ$ . The decrease in star density toward the upper left-hand corner of the plate is striking. The symmetrical bright areas about the brighter stars are not considered as evidence of nebulosity.



Deciding definitely on the cluster membership of a star is difficult, since there are no observable criteria which guarantee membership. Consequently, the question of cluster membership has been decided principally on the grounds of spectroscopic absolute magnitude and radial velocity. For all stars plotted in Figure 2, i.e., material complete for early-type stars brighter than photographic magnitude 8.5 in the region covered, a frequency-curve of distance modulus was plotted, using  $\frac{1}{2}$ -mag. intervals in distance modulus. This curve is fairly uniform except near distance modulus 11.0, where there is a considerable excess; and this was assumed as a provisional value of the distance modulus of the cluster of supergiant stars surrounding the double cluster. With the aid of this provisional value and with consideration of radial velocities whenever available and the intensity of the interstellar K line, the stars marked in the tables with daggers were determined to be probable cluster members. Those with question marks may possibly be cluster members. On this basis we may have left out several true members, but it was felt desirable to compute the distance of the cluster from only those stars which are quite certainly members. We then find the following results:

- a) From 14 stars in Table 3 we find a mean  $m_0 - M$  of 10.9 mag.
- b) From 15 stars in Table 4 we find a mean  $m_0 - M$  of 11.1 mag.
- c) From all the stars in Table 5 we find a mean  $m_0 - M$  of 11.4 mag. There can be little doubt that all these stars belong to the cluster, because of their close similarity in absolute magnitude, spectral class, and interstellar line appearance. The absolute magnitudes are, however, somewhat difficult to estimate, owing to the wide spectral lines of many of these stars.
- d) The Russell-Hertzsprung diagram for  $\eta$  Persei was plotted from the data given by Zug,<sup>13</sup> using Trumpler's classes and Zug's magnitudes. Although the dispersion is considerable, the average of the B9 stars is about apparent photographic magnitude 12.1. When Oosterhoff's magnitudes are used for the same cluster, the dispersion is somewhat reduced, and the average of the B9 stars is at about 12.0. Using Trumpler's<sup>12</sup> magnitudes and spectra for  $\chi$  Persei, we find the average of the B9 stars at about 12.5 photographic. Although the exact value of the difference is in considerable doubt, as the scatter is large and the spectral composition may not be the same for both clusters, the effect is in the direction remarked by Miss Pishmish. Since we wish the corresponding visual magnitudes, we must correct both for normal color index, which we assume to be  $-0.2$  mag., and for the coloring effect of the interstellar absorption suffered. Following Stebbins, Huffer, and Whitford, we assume that the latter is given by two times the photoelectric color excess; and, if we adopt a color excess of 0.22 for  $\eta$  Persei and 0.25 for  $\chi$  Persei, we obtain for the apparent visual magnitude of the B9 stars 11.8 and 12.2 for  $\eta$  and  $\chi$  Persei, respectively.

We must now adopt a visual absolute magnitude for the B9 stars in the double cluster. This value must be uncertain to some extent because we cannot be sure that the "main sequence" stars in the cluster occur at the same absolute magnitudes as for stars in general, without spectra of stars which have not been studied in this work. But in general it is clear that the average of the B9 stars should not be given the absolute magnitude corresponding to class V on the system of the *Atlas*, for what is commonly termed "main sequence" is generally a mixture of stars of luminosity class III, IV, and V. The author has adopted  $-0.5$  as the visual absolute magnitude to use in this connection, suggested by Dr. W. W. Morgan. Using this value and applying the total visual absorption correction, we arrive at true distance moduli of 10.7 for  $\eta$  Persei and 11.0 for  $\chi$  Persei.

- e) Using radial velocities with probable errors no greater than  $\pm 2$  km/sec for the stars which are considered certain members of the cluster, we find the average radial velocity of  $-41.9$  km/sec. For the average of these stars we adopt a correction of  $+3$  km/sec for the local solar motion. Taking Oort's constant  $A$  as 18 km/sec/kiloparsec,<sup>28</sup> we deter-

<sup>28</sup> Chandrasekhar, *Principles of Stellar Dynamics* ("Astrophysical Monographs"), 1942.

mine the distance of these stars as 2180 parsecs, which corresponds to a  $m_0 - M$  of 11.7.

Since it is difficult to estimate the relative reliability of the various distance determinations made on the basis of spectroscopic absolute magnitudes, we have taken the mean of the first four values as the "spectroscopic distance." This distance, computed from  $m_0 - M = 11.1$ , comes out as 1660 parsecs. Hence there is a considerable discrepancy in distance, though only a fairly small one in distance modulus, between the spectroscopic and the radial velocity determinations. It is perhaps of importance that the distance obtained from the stars in Table 5 agrees the best with that obtained from the radial velocities. In fact, in so far as the stars above the main sequence in  $h$  and  $\chi$  Persei are concerned, we may bring the two distance determinations into agreement by increasing the absolute magnitudes of our supergiants and giants by about 0.6 mag. (undoubtedly a permissible correction), by decreasing the color excesses somewhat, or by lowering somewhat the ratio between total and selective absorption. On the other hand, a peculiar motion of about  $-9$  km/sec on the part of the entire  $h$  and  $\chi$  Persei system would again bring the two distance determinations into agreement. This latter situation is, however, unlikely in view of the high masses of these stars.

Wilson<sup>1</sup> finds a discrepancy of the same order as the above between the distance of the cluster as judged from absolute magnitudes and radial velocities. Further, Evans<sup>7</sup> finds that the distance of  $h$  and  $\chi$  Persei found from the strength of the interstellar lines is considerably smaller than that found from the radial velocities, which possibly indicates a peculiar motion of the stars. However, he says that the stellar and interstellar velocities agree in giving the same distance, which shows that the peculiar motion of the stars must be small, if we assume that the interstellar medium has little peculiar velocity.

It appears to the author as though the most probable cause of the discrepancy is an error in the absolute magnitudes, which may be caused either by a systematic error in the luminosity classes of this work or by a systematic error, for the most luminous stars, in the preliminary reduction curves used. At any rate, such an error would be fairly small, and we may conclude that the current estimates of the absolute magnitudes of early-type supergiants are probably not too high.

Taking the mean of the distances determined from the absolute magnitudes and the radial velocities, we obtain  $r = 1920$  parsecs. With this distance the projected distance of the centers is 14 parsecs; the radius of each cluster 7 parsecs, according to Oosterhoff;<sup>5</sup> the radius of each cluster 17 parsecs, according to Trumpler's work on  $h$  Persei;<sup>11</sup> and the total diameter of the "extended cluster" of supergiants 167 parsecs, assuming an apparent diameter of  $5^\circ$ .

#### IX. OTHER CONSIDERATIONS

*Interstellar calcium intensity.*—As would be expected for distant stars, the majority of the early-type stars in this region show a strong interstellar K line. In fact, among all the stars observed as B5 or earlier, the K line is weak only in the following stars: HD 8965, 9812, 13590, 13661, 13669, 14722, 18352, and absent only in HD 11606 and 14871. All stars attributed to the cluster have interstellar lines of about the same intensity. A few early-type stars which were classified as of low luminosity have quite strong interstellar lines. Those showing the greatest discrepancy are HD 13831 and 13970, the lines of both of which are somewhat broad.

*The broad-line stars in  $h$  and  $\chi$  Persei.*—Trumpler<sup>12</sup> showed that in the cluster  $\chi$  Persei the Be stars are limited to a rather small range in absolute magnitude. These stars are, in general, somewhat fainter than those considered in the present work. It is of interest, however, to note that of the stars in Table 5, 8 stars, or one-half, have lines to some degree diffuse. It seems quite probable that we observe here an interval of absolute magnitude in which the stars are subject to rapid rotation, without, however, the speed of rotation being such that emission occurs. With decreasing absolute magnitude the rotational

speed apparently increases. The double cluster thus contains two types of emission stars: supergiants bright at  $H\alpha$  and rapidly rotating giants and dwarfs usually bright at both  $H\alpha$  and  $H\beta$  and often showing practically continuous spectra at  $H\gamma$ .<sup>29</sup>

*Later-type members of the double cluster.*—It is interesting to consider whether supergiants of later type are also present in the "extended cluster" of supergiants surrounding  $\eta$  and  $\chi$  Persei. Evidence confirming this supposition is shown in Keenan's work<sup>30</sup> on the luminosities of the M-type variables of small range. Figure 3 is plotted from Keenan's table and shows only the more luminous supergiants; the grouping about the position of the double cluster is very conspicuous. It is of importance in the present connection that 2 of the 5 supergiants in this grouping are at as much as  $2^\circ$  from  $\eta$  and  $\chi$  Persei. The hypothesis of cluster membership for these stars is confirmed to some extent by the radial

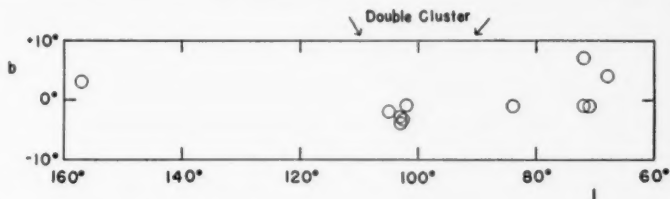


FIG. 3.—Distribution of the most luminous supergiants among the M-type variables of small range according to Keenan, *A. p. J.*, **95**, 461, 1942. Since "the material is reasonably complete down to the ninth apparent magnitude" over this area, the clustering of five of these objects close to the double cluster in Perseus is undoubtedly significant.

velocities of Joy.<sup>31</sup> There is a cF8 star attributed in Wilson's catalogue to the double cluster, but its radial velocity of  $-26.2$  km/sec excludes it.

From the work of Joy<sup>32</sup> on the radial velocities of Cepheid variables one sees that several of these stars may be, from radial velocity and absolute magnitude evidence, members of the grouping of supergiants around the double cluster. The possible members of this group include VX Persei, UX Persei, UY Persei, and SZ Cassiopeia.

It is well known that there is an extraordinarily rich clustering of faint Be stars in the region of the double cluster. The plot of the galactic distribution of faint Be stars in the paper of Merrill and Burwell<sup>22</sup> shows clearly that this clustering has an extension comparable with that found from the early-type supergiants. Of course, some of the stars are the same, since many supergiants have bright  $H\alpha$ ; but the clustering is marked over a fairly large region for stars much fainter than those considered here. Although the absolute magnitudes of the emission stars are more uncertain than those of normal stars, and we therefore cannot say definitely that these stars are at the distance of the cluster, it would be unusual if this rich apparent clustering were not the reflection of a physically connected group of stars.

*The Russell-Hertzsprung diagram for the brighter stars of  $\eta$  and  $\chi$  Persei.*—Figure 4 is the absolute magnitude-spectral class diagram obtained by using those stars of Tables 3, 4, and 5 and those given in the lists of Trumpler and Zug which are considered to be members of the  $\eta$  and  $\chi$  Persei cluster. Ordinates are the visual apparent magnitudes which the stars would have were there no interstellar absorption; these were obtained by use of the photoelectric color excesses, and for the fainter stars by considering both color

<sup>29</sup> Beals (J. R.A.S., Canada, **34**, 190, 1940) has found that 5 of the supergiants studied in the present work, HD 12953, 13841, 14134, 14143, and 14818 are P Cygni stars. Since 2 of these stars were not discovered to be emission stars by the Mount Wilson observers, it appears that the majority of highly luminous early-type stars show slight P Cygni characteristics at some times.

<sup>30</sup> *A. p. J.*, **95**, 461, 1942.

<sup>31</sup> *A. p. J.*, **96**, 344, 1942.

<sup>32</sup> *A. p. J.*, **89**, 356, 1939.

excess and normal color index. The ordinate scale thus differs only in zero point from the visual absolute magnitudes; this would not be so if we merely plotted apparent magnitudes, because of the differential interstellar absorption suffered by the stars. For the stars in Table 3 Harvard photometric magnitudes have been used. The stars represented by the larger filled circles have been observed in this investigation, and the author's classes have been used; those stars represented by the smaller filled circles were studied by Trumpler and Zug. Actually, all of the stars listed by Zug are included; but for Trum-

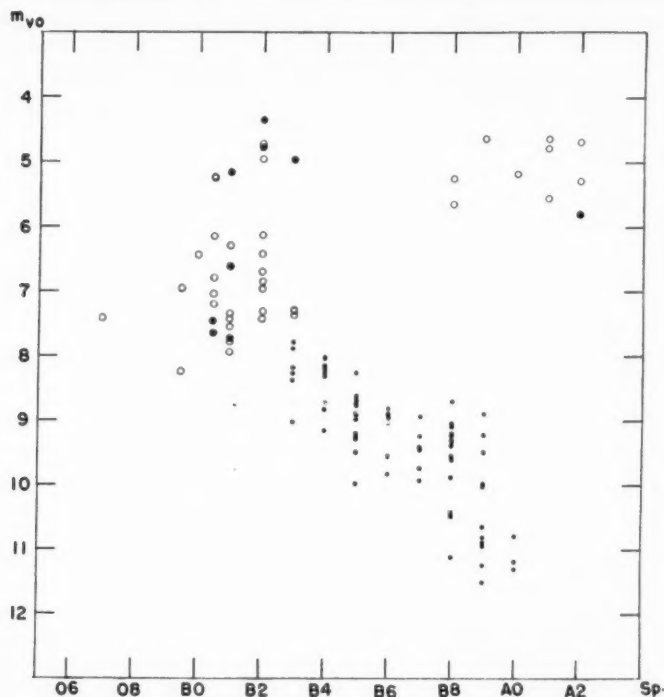


FIG. 4.—Russell-Hertzsprung diagram for stars considered to be members of the double cluster. The ordinates are the visual magnitudes which the stars would have were there no interstellar absorption. The larger circles represent stars studied in the present work, the smaller, filled circles those stars classified by Trumpler. Large filled circles denote emission stars, the five most luminous stars having sharp lines and bright  $H\alpha$  and the four less luminous stars having broader lines and usually  $H\beta$  also in emission. Several of the stars studied by Trumpler also belong to the latter class. Two supergiants, HD 15316 Sp. A2, and HD 15497, Sp. B5, although probably cluster members, are omitted because of their abnormally high color excess and the consequent uncertainty in the correction for absorption. The two open circles at (A1, 4.6) and (B0.5, 6.2) should also be filled, as Beals has found these stars to be P Cygni stars.

pler's stars, only those which he lists (the brighter stars) have been used. Hence the lower part of the diagram refers exclusively to stars in  $h$  Persei. However, the diagrams are similar for  $h$  and  $\chi$  Persei and differ only in zero point, which is probably caused by the different amount of interstellar absorption in the two. The larger filled circles refer to stars showing emission, either supergiants with emission at  $H\alpha$  or lower-luminosity stars with emission at several hydrogen lines.

There is some uncertainty in the position in the diagram of the fainter stars, owing to uncertainty in color excess. However, if we assume a distance modulus of 11.1 (as found from the spectroscopic evidence, with little uncertainty), we can transform the diagram

into one involving absolute magnitudes. Doing this, we see that the stars near class A0 are more or less around the main sequence but that the stars around B1 average considerably above it, being largely members of luminosity class III. Of course, there may be fainter stars in the cluster of early spectral class which have been heretofore unrecognized. Barring this, there is little doubt that the "main sequence" turns upward very sharply in this cluster in the earliest spectral classes. The same effect has been noted for galactic clusters before by Trumpler.<sup>33</sup>

If the distance is assumed to be given correctly by the radial velocities, then the main sequence of the cluster stars must be somewhat above that of stars in general.

In connection with the Russell-Hertzsprung diagram, it must be remembered that, while our data on the upper part of the diagram are essentially complete, aside from the possibility that several more of the stars listed in the Tables 3, 4, 5, and 6 may be cluster members, the faint stars have been observed over only a very small area about the centers of the two clusters. It seems quite likely, however, that there are few normal giants of spectral class around A0 in the cluster.

*Dynamical considerations.*—It is rather difficult to compute the quantities of dynamical interest for the  $\eta$  and  $\chi$  Persei cluster, since we do not know the number of stars or the total mass. For our present purpose we assume (for one cluster) the number of cluster stars as 1000 and the total mass as 2500 solar masses. Also, for dynamical purposes it probably is more correct to use the smaller value of the radius suggested by Oosterhoff,<sup>5</sup> as most of the stars are within this limit.

From the formulae given by Chandrasekhar<sup>28</sup> we find the following:

- a) The dispersion of the residual velocities equals 0.88 km/sec.
- b) The time of relaxation equals  $1.3 \times 10^8$  years. It follows from the work of Chandrasekhar, who has recently shown that clusters can hold their members for times of the order of one hundred times the time of relaxation, that we cannot picture the supergiants in the region of the double cluster as having "escaped" from it in a time of the order of the age of the universe.
- c) The average density of the clusters is about 1.7 solar masses per cubic parsec, which shows that the small clusters, with radii of 7 parsecs, will be stable, even considering the tidal action of galactic rotation, if the distribution of potential within the clusters can be approximated to that of a homogeneous ellipsoid.

However, the above considerations do not indicate whether the stars situated at great distances from the center of the double cluster are primarily subject to its influence, or, if they are, whether they will continue to be so. This matter is closely linked with the problem of the stability of star clouds and leads to the question of maintenance of fluctuations of density in the Galaxy.

The writer wishes to thank Dr. O. Struve for the privilege of being at the Yerkes Observatory, Dr. W. W. Morgan for suggesting the problem and for valuable advice, and also Dr. S. Chandrasekhar and Dr. H. F. Weaver for helpful discussions of several questions.

<sup>33</sup> *Lick Obs. Bull.*, No. 420, 1930.

# A STUDY OF THE RADIAL VELOCITY OF $\beta$ CEPHEI

BURKE SMITH

Yerkes Observatory

Received April 3, 1943

## ABSTRACT

The study is based on measurements of 91 Yerkes plates taken in 1940-1942 and presents a review of all published radial-velocity measurements of this star. The average period of  $\beta$  Cephei is slowly lengthening, the increase amounting to 0.43 sec. during the last twenty-five years. From the form of the velocity-curve of the center of mass it appears to be probable that  $\beta$  Cephei is the bright component of a binary with a period of about 50 years and an eccentricity equal to 0.66. An abrupt change in the length of  $P$  occurred coincident with the close approach of the two components at periastron in 1914-1916. After periastron the period began to lengthen and is now best represented by  $P = 0.1904886$  day. There is no conclusive evidence of a change in ionization or excitation with phase. The amplitude of the radial velocity of the  $H\beta$  line was observed to be somewhat greater than that of the mean of all measured lines, and this also seems to hold for  $H\gamma$ . No other lines were found which show a similar effect.

The star  $\beta$  Cephei (Sp. B1s) was found to have a variable radial velocity by Frost and Adams<sup>1</sup> in 1902 from observations secured with the Bruce spectrograph of the Yerkes Observatory. In 1906 Frost<sup>2</sup> determined that the period of velocity variation was about

TABLE 1  
WAVE LENGTHS OF STELLAR LINES USED FOR RADIAL-VELOCITY MEASUREMENTS

Element	$\lambda$	Element	$\lambda$	Element	$\lambda$	Element	$\lambda$
He I.....	3964.732	O II.....	4119.221	O II.....	4416.975	O II.....	4638.854
O II.....	3973.263	He I.....	4120.860	He I.....	4437.552	O II.....	4661.65
N II.....	3994.996	He I.....	4143.759	He I.....	4471.508	O II.....	4699.21
He I.....	4009.270	N II.....	4236.983	Mg II.....	4481.228	O II.....	4705.355
He I.....	4026.218	C II.....	4267.15	Si III.....	4552.622	O II.....	4710.04
O II.....	4069.788	O II.....	4317.139	Si III.....	4567.841	He I.....	4713.200
O II.....	4072.164	O II.....	4319.664	Si III.....	4574.758	H $\beta$ .....	4861.327
O II.....	4075.868	H $\gamma$ .....	4340.466	O II.....	4590.971	He I.....	4921.930
O II.....	4085.124	O II.....	4366.896	O II.....	4596.174		
Si IV.....	4088.862	He I.....	4387.931	N II.....	4630.537		
Si IV.....	4116.103	O II.....	4414.909	Si IV.....	4631.38		

4½ hours. In the succeeding years many investigations have been made of the radial velocity and light-variations.<sup>3</sup> As was pointed out by Struve and Swings<sup>4</sup> this star is typical of a small group of B-type stars with variable radial velocity whose periods are less than ½ day and whose velocity ranges are so small that they can hardly be explained in terms of binary motion.

## RESULTS OF MEASUREMENTS OF 1940-1942 YERKES PLATES

The present study includes results of measurements of 91 spectrograms taken at Yerkes with the Bruce spectrograph attached to the 40-inch refractor, during the years 1940, 1941, and 1942, together with a review of all previously published results. During the interval 1906-1942 the star has gone through some seventy thousand complete cycles.

<sup>1</sup> *A. p. J.*, 15, 340, 1902.

<sup>2</sup> *A. p. J.*, 24, 259, 1906.

<sup>3</sup> Crump, *A. p. J.*, 79, 246, 1934.

<sup>4</sup> *A. p. J.*, 94, 99, 1941.

Of the 91 Yerkes plates which were measured, 64 were one-prism Eastman Process plates (dispersion 30 Å/mm at  $\lambda$  4500) and the remainder three-prism Cramer Hi-speed and Ia-0 plates (dispersion 10 Å/mm at  $\lambda$  4500). They were generally of very good qual-

TABLE 2  
RADIAL-VELOCITY MEASUREMENTS

Date	Julian Day	Number of Lines Measured	Length of Exposure in Minutes	Radial Velocity (Km/Sec)	Date	Julian Day	Number of Lines Measured	Length of Exposure in Minutes	Radial Velocity (Km/Sec)
One-Prism Plates					One-Prism Plates—Continued				
1940 Sept. 21....	242+ 9893.544	12	20	+ 4.5	1942 July 2....	0542.694	31	30	+14.6
	.563	30	30	- 5.8		.718	28	30	+ 2.9
	.587	27	32	-15.5		.741	28	30	-11.2
	.613	28	37	-15.5		.764	30	30	-20.6
	.660	31	36	-10.4		.786	26	25	-30.3
	.685	17	42	+12.7		.806	32	25	-22.0
	.715	30	37	+14.2		.826	31	25	-11.0
	.753	20	39	- 8.5		.846	28	25	- 0.4
	.785	28	40	-18.3	1942 Aug. 12....	0583.671	28	29	+17.8
1940 Sept. 22....	9894.550	28	30	-17.9		.694	25	29	- 0.5
	.576	24	29	-15.6		.710	28	29	-12.1
	.602	28	30	- 3.8		.740	30	30	-13.3
	.629	28	31	+ 6.7		.773	25	29	- 9.9
	.652	19	25	+21.2	Three-Prism Plates				
	.685	32	33	+ 5.7	1941 July 7....	0182.841	7	15	+10.6
	.710	30	28	-15.9		.849	14	15	+13.9
	.734	27	29	-26.2		.872	13	15	+17.5
	.757	27	31	-21.6		.886	12	15	+10.5
	.782	28	33	-14.1		.898	17	15	- 0.9
	.806	30	30	+ 2.6	1941 July 24....	0199.721	18	45	-21.0
1940 Sept. 23....	9895.531	19	30	-16.5		.755	25	45	- 8.2
	.553	30	31	- 3.3		.791	20	45	+15.5
	.579	29	33	+ 8.3		.864	21	45	- 2.0
	.604	31	30	+15.6		.900	20	50	-22.3
	.628	28	30	+ 6.4	1941 July 26....	0201.608	14	40	-18.6
	.655	30	30	- 4.7		.635	17	40	-23.1
	.679	31	30	-18.3		.667	21	40	- 8.2
	.702	30	30	-20.3		.700	19	45	+ 9.1
	.726	30	32	-14.6		.730	16	35	+15.0
	.750	26	31	+ 1.9		.758	20	35	+ 9.5
	.774	22	30	+15.9		.788	20	45	- 9.3
1940 Oct. 1....	9903.517	19	25	-20.2		.837	20	35	-17.4
	.537	23	25	-18.1		.865	23	40	- 2.7
	.560	28	33	- 4.3		.896	20	40	+12.5
	.610	23	35	+17.5	1941 Aug. 10....	0216.740	22	35	+10.9
1940 Oct. 2....	9904.534	17	24	+ 5.0		.781	21	40	+17.8
	.554	26	28	+10.9		.820	18	55	-10.1
	.581	24	36	+ 8.9		.860	20	50	-18.0
	.605	26	26	- 0.8		.896	20	45	-14.5
	.630	30	28	-15.9	1941 Aug. 12....	0218.633	17	50	+ 5.6
	.651	31	28	-20.5		.671	19	50	+16.0
	.671	30	26	-16.8					
	.693	32	27	- 3.8					
	.714	31	30	+ 4.3					
	.737	26	28	+ 9.9					
	.761	30	29	+10.6					
1942 June 19....	243+ 0529.672	28	30	- 9.3					
	.695	28	30	+ 0.4					
	.718	30	30	+14.3					
	.745	26	30	+17.1					
	.774	20	30	+ 8.3					

ity. Table 1 gives the laboratory wave lengths used in reducing the stellar lines. A total of 41 such lines was measured, extending from  $\lambda$  3964.73 to  $\lambda$  4921.93. Of these lines, 32 were visible on the one-prism plates and 24 on the three-prism plates. The wave

lengths were taken from the works of H. Kühnborn<sup>5</sup> and O. Struve.<sup>6</sup> An average of 27 lines were measured on the one-prism plates and 18 lines on the three-prism plates. The range in probable errors of radial-velocity measurements was  $\pm 1.0$  to  $\pm 2.8$  km/sec for the one-prism plates and  $\pm 0.8$  to  $\pm 2.0$  km/sec for the three-prism plates.

Table 2 gives the results of measurements of radial velocities for each plate, with the time of mid-exposure in Julian days, the number of lines measured, and the length of exposure. Radial-velocity-curves were drawn for each set of measurements, and in some cases the observational material was sufficient to extend the curve over almost two complete cycles.

Figure 1 shows four typical radial-velocity-curves, plotted with the center of mass, or  $\gamma$ -axis, as a common base and the intersection of the descending branch of the velocity-curve with the  $\gamma$ -axis as a common point. It will be noted that these curves show distinct variations in shape. The upper branches of the curves are generally similar, but the lower branches tend to vary somewhat and are occasionally broad and shallow. In con-

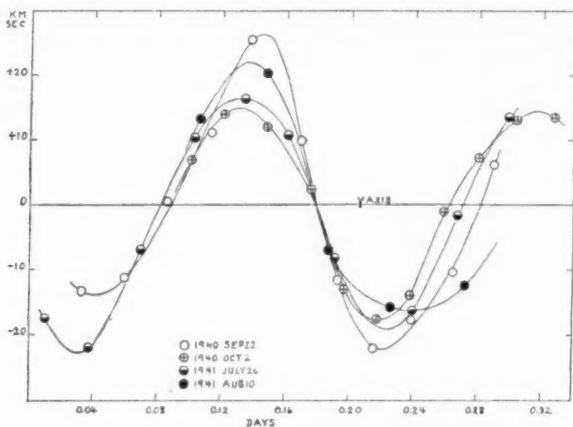


FIG. 1.—Radial velocity-curves of  $\beta$  Cephei

sequence, the observed values of  $K$  and  $P$  tend to vary from cycle to cycle. It is found that the observed value of  $\gamma$  also varies, and it is therefore not desirable to combine two or more cycles into a single curve. For this reason, in determining  $P$ ,  $K$ , and  $\gamma$  from the 1940–1942 plates only those observations were used which were sufficient in number to enable a determination of these elements to be made without combining observational material obtained on different nights.

#### THE AVERAGE PERIOD

Crump<sup>7</sup> found an average period of 0.1904795 day for the interval 1906–1912. Table 3 shows the departures of the observed times of maximum radial velocity from those computed with  $P = 0.1904795$  day, for epochs extending over the interval 1906–1942. Where published data permitted, the observed epochs were established independently by plotting velocity-curves. This was done because in the literature in many cases observations on different dates have been combined to form a composite velocity-curve, and the epoch was determined from the composite curve. The time of observed maximum,  $M_o$ , minus

<sup>5</sup> Veröff. d. Univ. Sternwarte, Berlin-Babelsberg, 12, No. 1, 1938.

<sup>6</sup> *Ap. J.*, 74, 225, 1931.

<sup>7</sup> *Pub. Detroit Obs., U. of Michigan*, 2, 144, 1916.

TABLE 3

DEPARTURES OF OBSERVED MAXIMUM RADIAL VELOCITIES FROM  
THOSE COMPUTED WITH  $P=0.1904795d$

DATE	$M_o$			$M_c$		$M_o - M_c$	AUTHORITY	REFER- ENCE
	Epoch of Observed Max. Radial Velocity (Julian Days)	$M_o$ in Days Elapsed from First Epoch	Observed No. of Cycles with $P =$ 0.1904795d	Computed Time of Max. in Days				
	241+							
1906 May 28	7359.702	0.000	0	0.000	0.000		Crump	3, 1
1906 May 28	7359.898	0.196	1	0.190	+ .006		Crump	3, 1
1906 June 22	7384.872	25.170	132	25.143	+ .027		Crump	3, 1
1906 July 6	7398.766	39.064	205	39.048	+ .016		Frost, Crump	2, 1
1906 Aug. 27	7450.586	90.884	477	90.859	+ .025		Davis, Crump	3, 1
1907 May 20	7716.672	356.970	1874	356.958	+ .012		Crump	3, 1
1907 May 20	7716.862	357.160	1875	357.149	+ .011		Crump	3, 1
1907 May 27	7723.725	364.023	1911	364.006	+ .017		Crump	1, 3
1907 July 29	7786.769	427.067	2242	427.055	+ .012		Frost, Crump	2, 1
1907 Aug. 2	7790.767	431.065	2263	431.055	+ .010		Crump	3, 1
1907 Oct. 28	7877.623	517.921	2719	517.914	+ .007		Crump	3, 1
1907 Nov. 11	7891.728	532.026	2793	532.009	+ .017		Crump	3, 1
1908 June 15	8108.866	749.164	3933	749.156	+ .008		Frost, Crump	3, 2, 1
1908 June 29	8122.767	763.065	4006	763.061	+ .004		Frost, Crump	3, 2, 1
1912 Apr. 29	9522.815	2163.113	11356	2163.085	+ .028		Crump	3, 1
1912 {Aug. 23 Nov. 21}	9638.813	2279.111	11965	2279.087	+ .024		Crump, Kohl	4, 5, 1
	242+							
1914 June 1	0285.676	2925.974	15361	2925.955	+ .019		Davis, Crump	3
1914 June 1	0285.866	2926.164	15362	2926.146	+ .018		Davis, Crump	3
1914 Oct. 9	0415.922	3056.220	16045	3056.243	- .023		Gerasimovič, Be- lopolsky	6
1914 Oct. 13	0419.920	3060.218	16066	3060.243	- .025		Gerasimovič, Be- lopolsky	6
1914 Oct. 21	0427.927	3068.225	16108	3068.243	- .018		Gerasimovič, Be- lopolsky	6
1916 Sept. 12	1119.370	3759.668	19738	3759.684	- .016		Belopolsky	7
1916 Sept. 25	1132.322	3772.620	19806	3772.636	- .016		Belopolsky	7
1917 Sept. 16	1488.342	4128.640	21675	4128.643	- .003		Belopolsky	7
1917 Oct. 7	1509.293	4149.591	21785	4149.595	- .004		Belopolsky	7
1917 Oct. 31	1533.286	4173.584	21911	4173.596	- .012		Belopolsky	7
1918 May 15	1729.854	4370.152	22943	4370.171	- .019		Henroteau, Hobe, Mendenhall	8
1919 Sept. 1	2203.794	4844.092	25431	4844.084	+ .008		Crump	3
1919 Sept. 17/20	2219.600	4859.898	25514	4859.894	+ .004		Van Arnam	5, 9
1920 {Jan. 19 Feb. 3}	2343.612	4983.910	26165	4983.896	+ .014		Henroteau, Hen- derson	5, 10
1921 Nov. 6	3000.586	5640.884	29614	5640.860	+ .024		Hobe, Mendenhall	8
1921 Nov. 6	3000.764	5641.062	29615	5641.050	+ .012		Hobe, Mendenhall	8
1922 {Feb. 16 Apr. 18}	3102.693	5742.991	30150	5742.957	+ .034		Henroteau	5, 11
1922 {Aug. 26 Sept. 4}	3293.551	5933.849	31152	5933.817	+ .032		Van Arnam	5, 10
1923 Mar. 8	3487.662	6127.960	32171	6127.916	+ .044		Henroteau	5, 11
1923 Mar. 8	3487.869	6128.167	32172	6128.106	+ 0.061		Henroteau	5, 11

TABLE 3—Continued

DATE	$M_o$			$M_c$	$M_o - M_c$	AUTHORITY	REFERENCE
	Epoch of Observed Max. Radial Velocity (Julian Days)	$M_o$ in Days Elapsed from First Epoch	Observed No. of Cycles with $P = 0.1904795d$	Computed Time of Max. in Days			
	242+						
1923 Mar. 14. . . .	3493.769	6134.067	32203	6134.011	+0.056	Henroteau	5, 11
1923 Mar. 16. . . .	3495.841	6136.139	32214	6136.107	+ .032	Henroteau	5, 11
1923 Mar. 26. . . .	3505.759	6146.057	32266	6146.011	+ .046	Henroteau	5, 11
1923 Mar. 28. . . .	3507.837	6148.135	32277	6148.107	+ .028	Henroteau	5, 11
1926 June 15. . . .	4690.950	7331.248	38488	7331.175	+ .073	Mendenhall	8
1926 July 12. . . .	4709.786	7350.084	38587	7350.032	+ .052	Mendenhall	8
1926 July 12. . . .	4709.995	7350.293	38588	7350.223	+ .070	Mendenhall	8
1926 July 28. . . .	4725.796	7366.094	38671	7366.033	+ .061	Mendenhall	8
1926 Aug. 8. . . .	4736.864	7377.162	38729	7377.080	+ .082	Mendenhall	8
1926 Aug. 11. . . .	4739.904	7380.202	38745	7380.128	+ .074	Mendenhall	8
1926 Aug. 14. . . .	4742.961	7383.259	38761	7383.176	+ .083	Mendenhall	8
1926 Oct. 7. . . .	4796.863	7437.161	39044	7437.082	+ .079	Mendenhall	8
1926 Oct. 24. . . .	4813.613	7453.911	39132	7453.844	+ .067	Mendenhall	8
1927 Jan. 7. . . .	4888.656	7528.954	39526	7528.893	+ .061	Mendenhall	8
1928 Aug. 21. . . .	5480.704	8121.002	42634	8120.903	+ .099	Duncan-Mitchell	5, 12
1928 Sept. 10. . . .	5500.866	8141.164	42740	8141.094	+ .070	Mendenhall	8
1929 Oct. 26. . . .	5912.579	8552.877	44901	8552.720	+ .157	Crump	3
1929 Oct. 26. . . .	5912.785	8553.083	44902	8552.910	+ .173	Crump	3
1929 Nov. 15/16. . .	5931.580	8571.878	45001	8571.768	+ .110	Crump	3
1930 Oct. 19. . . .	6268.549	8908.847	46770	8908.726	+ .121	Crump	3
1931 Aug. 26. . . .	6580.570	9220.868	48408	9220.732	+ .136	Kohl	5
1931 Sept. 11. . . .	6595.610	9235.908	48487	9235.779	+ .129	Crump	3
1931 Nov. 4. . . .	6650.284	9290.582	48774	9290.447	+ .135	Kohl	5
1932 Sept. 5. . . .	6955.630	9595.928	50377	9595.786	+ .142	Crump	3
1932 Sept. 5. . . .	6955.824	9596.122	50378	9595.976	+ .146	Crump	3
1940 Sept. 21. . . .	9893.702	12534.000	65801	12533.742	+ .258	B. Smith	
1940 Sept. 22. . . .	9894.658	12534.956	65806	12534.694	+ .262	B. Smith	
1940 Sept. 23. . . .	9895.603	12535.901	65811	12535.647	+ .254	B. Smith	
1940 Sept. 23. . . .	9895.790	12536.088	65812	12535.837	+ .251	B. Smith	
1940 Oct. 1. . . .	9903.612	12543.910	65853	12543.647	+ .263	B. Smith	
1940 Oct. 2. . . .	9904.564	12544.862	65858	12544.599	+ .263	B. Smith	
1940 Oct. 2. . . .	9904.751	12545.049	65859	12544.790	+ .259	B. Smith	
	243+						
1941 July 7. . . .	0182.866	12823.164	67319	12822.890	+ .274	B. Smith	
1941 July 24. . . .	0199.810	12840.108	67408	12839.843	+ .265	B. Smith	
1941 July 26. . . .	0201.730	12842.028	67418	12841.747	+ .281	B. Smith	
1941 July 26. . . .	0201.910	12842.208	67419	12841.938	+ .270	B. Smith	
1941 Aug. 10. . . .	0216.770	12857.068	67497	12856.795	+ .273	B. Smith	
1942 June 19. . . .	0529.734	13170.032	69140	13169.753	+ .279	B. Smith	
1942 July 2. . . .	0542.680	13182.978	69208	13182.706	+ .272	B. Smith	
1942 Aug. 12. . . .	0583.664	13223.962	69423	13223.659	+0.303	B. Smith	

## NOTES FOR TABLE 3

1. *A. p. J.*, 15, 340, 1902.
2. *A. p. J.*, 24, 259, 1906.
3. *A. p. J.*, 79, 246, 1934.
4. *Pub. Detroit Obs.*, 2, 144, 1916.
5. Kohl, *A. N.*, 248, No. 22, 1933.
6. Gerasimovič, *Bull. de l'Observatoire central de Russie, Poulkovo*, 7, No. 8, 1917.
7. *Bull. acad. sci. de Russie*, 12, 1783, 1918.
8. Mendenhall, *Lick Obs. Bull.*, No. 418.
9. Van Arnem; *Pub. Dom. A. p. Obs., Victoria*, 4, 171, 1929.
10. *Pub. Dom. Obs.*, 5, 77, 1922.
11. *Pub. Dom. Obs.*, 9, 36, 1925.
12. *A. p. J.*, 70, 127, 1929.

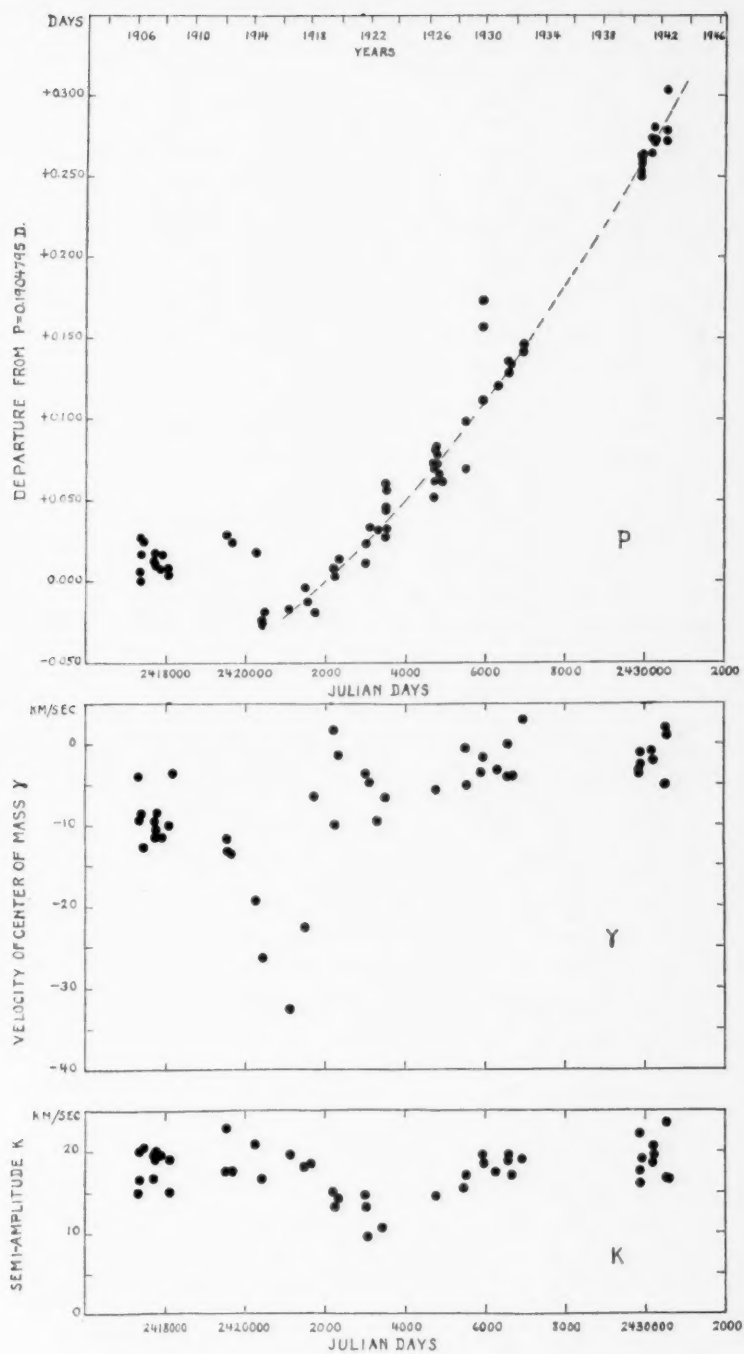


FIG. 2.—Secular changes in  $P$ ,  $\gamma$ , and  $K$

the time of computed maximum,  $M_c$ , gives the departure as shown in Table 3. The second column gives the time of observed maximum,  $M_o$ , in Julian days, established in this way for each date. The epoch JD 2417359.702 (1906, May 28), was taken as the first epoch, and the third column shows the elapsed time in days from this epoch. The fourth column gives the observed number of cycles, based on  $P = 0.1904795$  day, while the fifth column gives the computed maxima,  $M_c$ , in days, using a whole number of cycles from the fourth column. The values  $M_o - M_c$  are shown in the sixth column.

Figure 2 shows  $M_o - M_c$  plotted against days elapsed from the first epoch as taken from Table 3. It will be noted that there was an abrupt change in  $P$  during the years 1914-1916 (JD 2420200-2421000). After 1916 for a few years the average period was 0.35-0.40 sec. longer than the average for 1906-1912. However, it is evident from Figure 2 that there has been a slow progressive increase in  $P$  during the years. The amount of this increase as determined from the slope of the curve is approximately as shown in the accompanying tabulation.

Date	Departure from $P = 0.1904795$ day
JD 2421500 (1917) . . . . .	+0.0000041d = 0.35 sec.
JD 2430600 (1942) . . . . .	+0.0000091d = 0.78 sec.

It thus appears that the average value of  $P$  has increased by about 0.43 sec. during the last twenty-five years, or at the rate of 1.7 sec. per century. It is not possible, from the limited data, to say whether this increase is taking place at a constant rate. If we take into account both the abrupt change which occurred in 1914-1916 and the slow progressive change since that time, the period now seems to be best represented by  $P = 0.1904886$  day.

#### VELOCITY OF CENTER OF MASS AND SEMI-AMPLITUDE

Table 4 shows the velocity of the center of mass,  $\gamma$ , and the semi-amplitude,  $K$ , as derived from the observational material for the entire interval 1906-1942. Where there was not enough material available to plot velocity-curves, the values given by the various investigators, which in many cases were based on a combination of two or more cycles, were taken from the literature.

The results are plotted in the lower half of Figure 2. While the points are scattered and there are uncertainties in the data due to the number of sources from which they were obtained, the general distribution of points indicates a binary system of which  $\beta$  Cephei is the brighter component, with periastron in 1915. Gerasimovič<sup>8</sup> and Mendenhall<sup>9</sup> noted the possibility of a binary, and Mendenhall thought the period would be of the order of twenty years. It now appears that the period is fifty years or more, as the maximum value of  $\gamma$  seems not to have been reached until some time around 1935-1940.

With an assumed period of fifty years the following approximate elements of the orbit of the brighter star have been derived:

$$\begin{aligned}
 P_1 &= 50 \text{ years ,} & T_1 &= 1915.0 , \\
 K_1 &= 16.0 \text{ km/sec ,} & \gamma_1 &= -7.4 \text{ km/sec ,} \\
 e_1 &= 0.66 , & a \sin i &= 20.13 \text{ A.U. ,} \\
 \omega_1 &= 187^\circ , & \frac{m_2^3 \sin^3 i}{(m_1 + m_2)^2} &= 3.3 \odot .
 \end{aligned}$$

<sup>8</sup> *Bull. de l'Observatoire central de Russie, Poulkovo*, 7, No. 8, 1917.

<sup>9</sup> *Lick Obs. Bull.*, No. 418.

TABLE 4  
VELOCITY OF CENTER OF MASS  $\gamma$  AND SEMI-AMPLITUDE  $K$

Date	Julian Day	$\gamma$ (Km/Sec)	$K$ (Km/Sec)	Observatory*	Date	Julian Day	$\gamma$ (Km/Sec)	$K$ (Km/Sec)	Observatory*
1906 May 28.....	241+	— 4.0	15.0	Yerkes	1922 Feb. 16}	242+			
June 22.....	7359	— 9.2	20.0	Yerkes	Apr. 18}.....	3102	— 4.8	13.1	Ottawa(†)
July 6.....	7384	— 8.6	16.6	Yerkes	Aug. 26, 27}				
Aug. 27.....	7398	— 12.7	20.5	Yerkes	Sept. 4}.....	3293	— 9.6	9.5	Victoria
1907 May 20.....	7716	— 11.5	16.7	Yerkes	1923 Mar. 5, 28..	3484	— 6.8	10.6	Ottawa
May 20.....	7716	— 9.5	19.5	Yerkes	1926 June 23}				
July 29.....	7786	— 8.2	19.0	Yerkes	Dec. 31}.....	4796	— 5.7	14.6	Lick
Aug. 2.....	7790	— 10.5	20.0	Yerkes	1928 Aug. 22.....	5480	— 0.7	15.5	Mt. Wilson
Nov. 11.....	7891	— 11.5	19.5	Yerkes	Sept. 10.....	5500	— 5.0	17.0	Lick
1908 June 15.....	8108	— 10.0	15.0	Yerkes	1929 Oct. 26, 27..	5913	— 3.5	19.7	Yerkes
June 29.....	8122	— 3.5	19.0	Yerkes	Nov. 15, 16..	5931	— 1.5	18.2	Yerkes
1912 Apr. 29.....	9522	— 11.7	17.5	Yerkes	1930 Oct. 19.....	6269	— 3.1	17.4	Yerkes
May 13.....	9536	— 13.1	22.8	Yerkes	1931 Aug. 26.....	6580	— 4.0	18.8	Babelsberg
Aug. 8.....					Sept. 11.....	6596	0.0	19.5	Yerkes
Oct. 1.....	9638	— 13.5	17.5	Ann Arbor	Nov. 4.....	6650	— 4.0	17.0	Babelsberg
Nov. 21.....					1932 Sept. 5.....	6956	+ 3.0	19.0	Yerkes
1914 June 1.....	242+	— 19.3	21.0	Yerkes	1940 Sept. 21.....	9893	— 3.6	17.8	Yerkes
Oct. 9, 21.....	0415	— 26.1	16.8	Poulkovo	Sept. 22.....	9894	— 3.9	22.1	Yerkes
1916 Sept. 12, 30}					Sept. 23.....	9895	— 3.8	19.1	Yerkes
Oct. 1, 29, 30}	1119	— 32.7	19.6	Poulkovo	Oct. 1.....	9903	— 1.3	19.0	Yerkes
1917 Sept. 16}.....	1489	— 22.5	18.0	Poulkovo	Oct. 2.....	9904	— 2.8	16.1	Yerkes
Oct. 31}.....					1941 July 24.....	243+	— 1.3	20.7	Yerkes
1918 May 15.....	1729	— 6.3	18.3	Lick	July 26.....	0200	— 1.3	18.5	Yerkes
1919 Sept. 1, 2...	2203	+ 1.8	15.0	Yerkes	Aug. 10.....	0217	— 2.3	19.5	Yerkes
Sept. 17, 21.....	2219	— 10.1	13.1	Victoria	1942 June 19.....	0530	+ 1.7	16.7	Yerkes
1920 Jan. 19}.....	2343	— 1.1	14.3	Ottawa†	July 2.....	0542	— 5.3	23.5	Yerkes
Feb. 3}.....					Aug. 12.....	0584	+ 0.7	16.7	Yerkes
1921 Nov. 6.....	3000	— 3.6	14.8	Lick					

\* References to the literature are given in Table 3.

† A correction of +9.4 km/sec has been added to the Ottawa 1920–1922 radial velocities (see J. H. Moore, *Pub. Lick Obs.*, 18, xii, n. a).

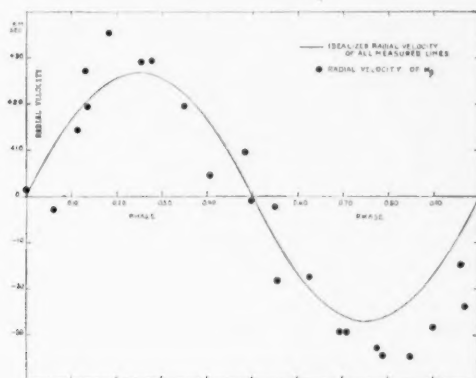


FIG. 3.—Velocities from  $H\beta$

It is significant that the time of nearest approach of the two components in 1915 was very nearly coincident with the time of sudden change in the average period of  $\beta$  Cephei noted above.

The semi-amplitude,  $K$ , reached a minimum of about 10 km at JD 2423000 and shows no indication of being periodic, except that there are frequent fluctuations somewhat similar to those of  $\gamma$ .

#### THE SPECTRUM

From a careful inspection of all recent plates no conclusive evidence was found of a change in ionization or excitation with phase.<sup>10</sup> The ionized helium lines  $\lambda$  4541.61 and  $\lambda$  4685.75 are visible on a few plates, but no definite correlation of visibility of these lines with phase was found. Slight changes in the appearance of lines with phase were noted as follows: On some plates, especially in the case of three-prism plates, certain lines give the appearance, at times, of being blended or double, although one cannot be sure that the effect is real. Nevertheless, a distinctly greater number of such apparent blends was noted (ratio, 2 to 1) during the second half of the cycle (phase 0.50–1.00) than during the first half. This may be due to the lines in the first half of the cycle being, in general, sharper than those in the second half. The dispersion of the Yerkes plates is not sufficient to answer this question.

#### RADIAL VELOCITY OF HYDROGEN LINES

The amplitude of the radial velocity of  $H\beta$ , as measured on three-prism plates, was observed to be greater than that of the mean of all measured lines. This effect is shown in Figure 3, in which the velocity of  $H\beta$  is plotted relative to an idealized radial-velocity-curve representing the mean of all measured lines. It is believed that this same effect holds true for  $H\gamma$ , which is visible only on the one-prism plates, but on account of the lower dispersion the effect is less definitely determined. No other lines were found which show a similar effect.

I am indebted to Messrs. O. Struve, J. A. O'Keefe, J. L. Greenstein, R. E. Williamson, and R. G. Hall for the use of spectrograms obtained by them at the Yerkes Observatory during 1940–1942. Grateful acknowledgment is also made to Dr. Struve for having suggested this investigation and for his kind advice and encouragement.

<sup>10</sup> See note on spectrum of  $\beta$  Cephei by Struve and Ogorodnikoff, *Pub. A.A.S.*, 7, 105, 1933.

## SPECTROGRAPHIC OBSERVATIONS OF PECULIAR STARS. VI\*

P. SWINGS AND O. STRUVE  
McDonald and Yerkes Observatories

Received April 15, 1943

### ABSTRACT

Large changes have recently been observed in the spectrum of T Coronae Borealis. Many absorption lines were measured on spectrograms of January, 1943. The high members of the Balmer series consist of two emission components separated by a central absorption; the blue component is appreciably stronger than the red. Several  $He\ I$ ,  $Ca\ II$ , and  $Si\ I$  lines have similar profiles;  $[Ne\ V]$  and  $[Fe\ VII]$  were weakly present in January, 1943. AX Persei is increasing in excitation, while Z Andromedae is declining, following its peak in the summer of 1942. HD 45677 has changed since 1939. In 1943 the  $H$  absorption cores were much weaker than in 1939, and the  $H$  emission lines showed only red components. The shell-absorption lines of  $Ca\ II$  had also become weak. Thirty-one Be stars from the Mount Wilson catalogues have been observed. The stars MWC 47, MWC 120, MWC 158, Mt. W. 265, and Mt. W. 275 present interesting shell-absorption spectra. The star MWC 93 has lost most of the expanding-shell characteristics observed by Merrill between 1928 and 1930.

### I. NEW OBSERVATIONAL DATA ON PECULIAR BRIGHT-LINE STARS

*Nova T Coronae Borealis*.—A considerable change has occurred in the early-type part of the composite spectrum of T CBr since it was last described<sup>1</sup> on the basis of spectrograms taken in January, 1942. In 1940, 1941, and 1942 the Balmer lines were present in emission up to  $H\ 21$ . On our spectrograms of January 28 and 29, 1943 (Pl. VIII), all the Balmer lines from  $H\ 14$  to  $H\ 9$  show violet and blue emission components, separated by an absorption component. The violet emission component is stronger than the red. In  $H\ 15$ ,  $H\ 16$ , and the higher members (up to  $H\ 23$ ) the red component is not observed. The regions of  $H\ 8$ ,  $H\epsilon$ , and  $H\delta$  are complex because of the presence of other emission lines, but  $H\gamma$  and  $H\beta$  are present only in emission.

Previously the  $He\ I$  lines were all bright. In January, 1943, the  $He\ I$  lines  $2p^3P^0-13$ ,  $12$ ,  $11$ ,  $10$ ,  $9$ ,  $8$ ,  $7$ , and  $6d^3D$  and  $2s^1S-5p^1P^0$  were pure absorption features. The case of  $\lambda\ 3889$  and  $\lambda\ 3965$  is not clear because of the proximity of strong emissions, but  $\lambda\ 4026$  ( $2p^3P^0-5d^3D$ ) and  $\lambda\ 4121$  ( $2p^3P^0-5s^3S$ ) are triple, like the ultraviolet Balmer lines. The line  $\lambda\ 4471$  ( $2p^3P^0-4d^3D$ ) has a violet emission and a weak absorption. The line  $Ca\ II\ 3934$  is also triple, whereas  $Si\ I\ 3906$  has two emission components but no apparent central absorption deeper than the continuous background;  $Si\ II\ 3856$  and  $3863$  are present as weak and broad emissions.

Besides the pure emission of  $He\ II\ 4686$ ,  $[O\ II]$ ,  $[O\ III]$ ,  $O\ III$  (fluor.),  $N\ III$  (fluor.),  $[Ne\ III]$ , and  $Fe\ II$  (and  $[Fe\ II]?$ ), previously reported, the spectrum now shows a trace of  $[Ne\ V]\ 3426$ . There is also a weak emission on the violet edge of  $He\ I\ 3587$ ; this emission must be attributed to  $[Fe\ VII]\ 3586.3$ . The two  $[S\ II]$  lines are weakly present.

Hence the excitation of the nebular region seems to be higher than it was previously, but the absorption characteristics suggest lower excitation. Such changes are reminiscent of the analogous case of Z And, which is an object of similar geometrical and dynamical complexity.

The pattern near  $\lambda\ 3889$  is rather complex. It consists essentially of a strong emission (6E) at  $\lambda\ 3887.1$ , due to  $He\ I$ ; of a second emission (4E) at  $\lambda\ 3888.1$ , due to  $H\ 8$ , sepa-

\* Contributions from the McDonald Observatory, University of Texas, No. 72. This work was interrupted in March, 1943, by the departure of Dr. Swings on a war-research assignment.

<sup>1</sup> *Ap. J.*, **96**, 254, 1942. For previous accounts see *Ap. J.*, **94**, 291, 1941; *Pub. A.S.P.*, **52**, 199, 1940. Spectrograms taken by Dr. John Titus on April 16 and 18, 1943, show that the shell absorptions had almost disappeared and the spectrum had, with minor differences, returned to its former stage. Judging from Minkowski's description (*Pub. A.S.P.*, **55**, 101, 1943), which reached us after this article had been completed, the absorption lines were strongest about March 1.

rated from *He* I by 85 km/sec; of a weak absorption due to *H* 8 and *He* I; and of a broad emission (2E $\eta$ ) centered around  $\lambda$  3890.8 and due to *H* 8, *He* I, and [*Fe* v]. Similarly, the pattern near  $\lambda$  3965, due to *He* I, [*Ne* III], *Ca* II, and *H*  $\epsilon$  is very complex.

The radial velocities measured on our spectrogram of January 28, 1943, are as follows:

*Hydrogen*.—Violet emission (using all lines from *H* 16 to *H*  $\epsilon$ , but excluding *H* 8:

$$V_{\text{v em}} = -71.3 \text{ km/sec ;}$$

central absorption (from the eight lines *H* 16 to *H* 9):

$$V_{\text{abs}} = +24.0 \text{ km/sec ;}$$

red emission (from the six lines *H* 14 to *H* 9):

$$V_{\text{r em}} = +116.6 \text{ km/sec ;}$$

emission at *H*  $\gamma$ :

$$V_{\gamma} = +32.2 \text{ km/sec .}$$

*Helium I*.—Violet emission (from  $\lambda\lambda$  4026, 4121, and 4471):

$$V_{\text{v em}} = -70.9 \text{ km/sec ;}$$

absorption (from the pure absorption lines  $\lambda\lambda$  3497, 3513, 3540, 3554, 3587, 3614, 3634, and 3705):

$$V_{\text{abs}} = +24.5 \text{ km/sec ;}$$

central absorption (from  $\lambda$  4026 and  $\lambda$  4121):

$$V_{\text{c abs}} = +55.1 \text{ km/sec ;}$$

red emission (from  $\lambda$  4026 and  $\lambda$  4121):

$$V_{\text{r em}} = +175.7 \text{ km/sec .}$$

*Calcium II* (*K*).—

$$V_{\text{v em}} = -125 \text{ km/sec ;}$$

$$V_{\text{abs}} = -13 \text{ km/sec ;}$$

$$V_{\text{r em}} = +117 \text{ km/sec .}$$

*Silicon I*.—

$$V_{\text{v em}} = -85 \text{ km/sec ;}$$

$$V_{\text{r em}} = +60 \text{ km/sec ;}$$

*Pure emission lines*.—

$$\text{Fe II: } V_{\text{em}} = +44 \text{ km/sec ;}$$

$$\text{Si II: } V_{\text{em}} = -3 \text{ km/sec ;}$$

$$\text{O III (fluor.): } V_{\text{em}} = -1 \text{ km/sec ;}$$

$$[\text{Ne III}]: V_{\text{em}} = +5 \text{ km/sec ;}$$

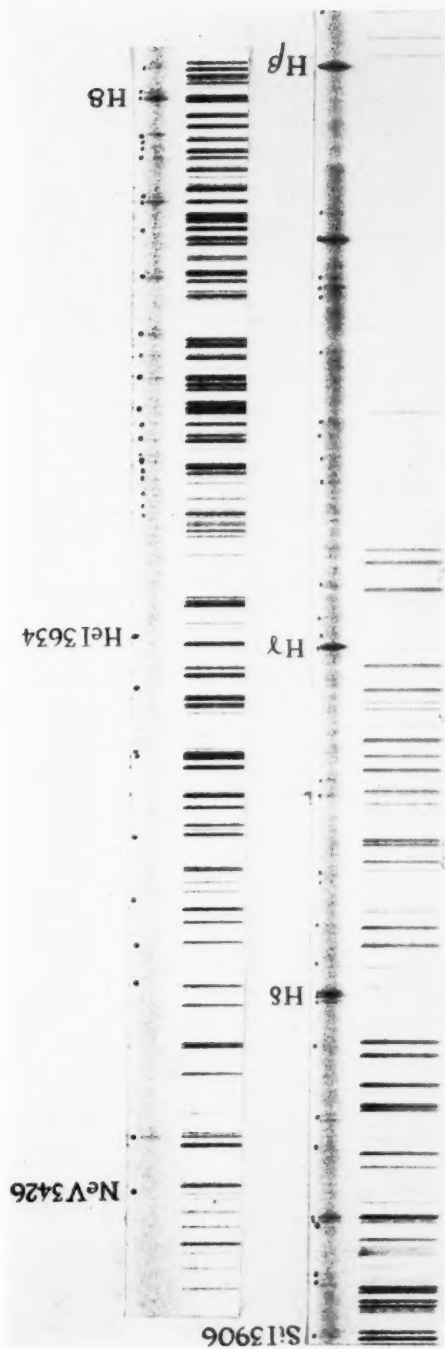
$$[\text{Fe VII}]: V_{\text{em}} = +27 \text{ km/sec .}$$

It will be interesting to follow the spectroscopic transformation now taking place in T CBr, and it is important in this connection that an accurate light-curve be obtained.

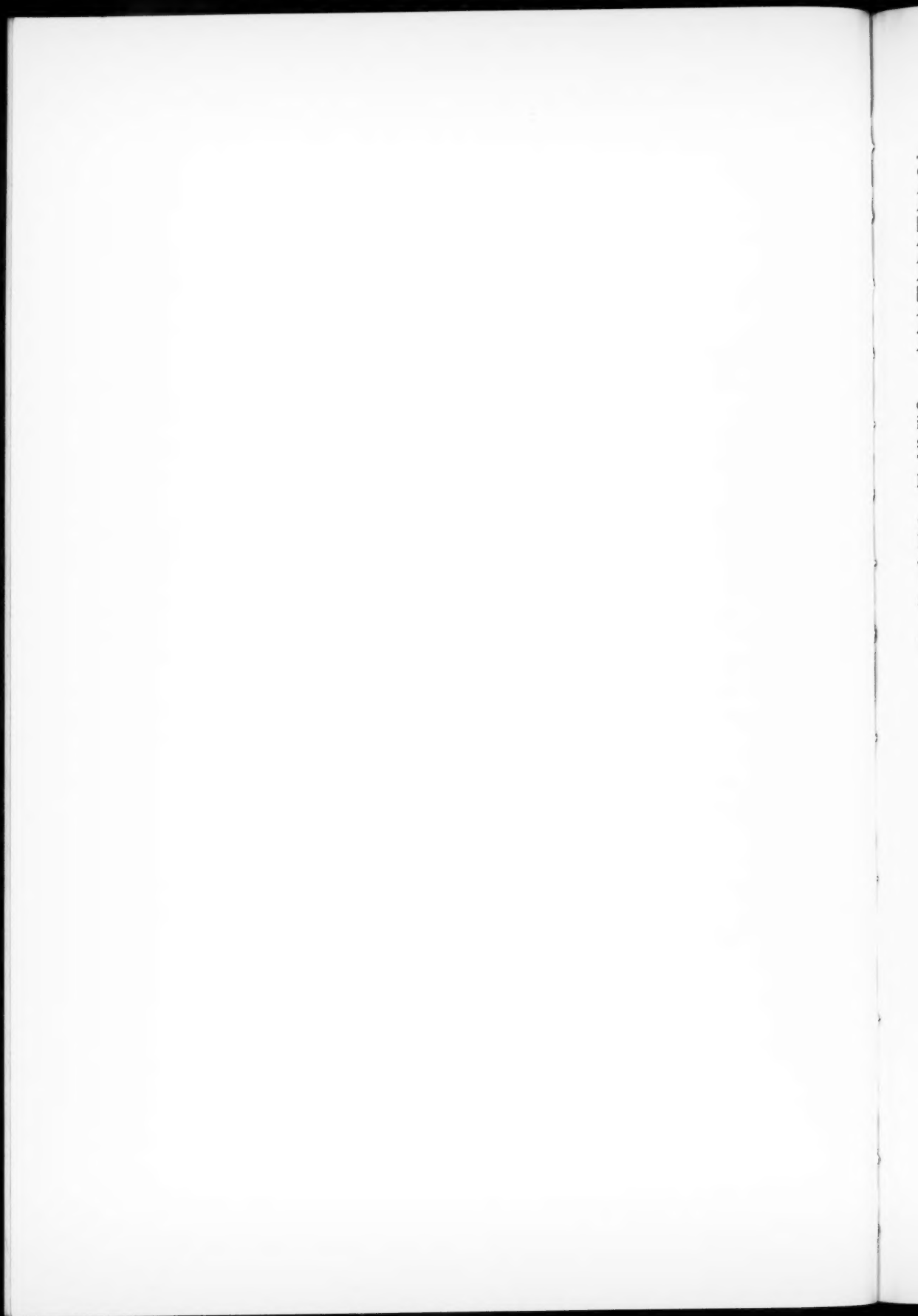
The lines marked with a dot in Plate VIII are as follows:

	<i>Top</i>	
[ <i>Ne</i> v] 3426 em	<i>H</i> 18 abs	<i>H</i> 11
<i>O</i> III 3444 em	<i>H</i> 17 abs	<i>H</i> 10
<i>He</i> I 3499 abs	<i>H</i> 16	<i>He</i> I 3820 abs
<i>He</i> I 3512 abs	<i>He</i> I 3705 abs	<i>H</i> 9
<i>He</i> I 3530 abs	<i>H</i> 15	<i>Si</i> II 3856 em
<i>He</i> I 3554 abs	<i>Cr</i> II 3713	<i>Si</i> II 3862 em
[ <i>Fe</i> VII] 3586 em	<i>H</i> 14	<i>He</i> I 3868 abs
<i>He</i> I 3587 abs	[ <i>O</i> II] 3726 em	[ <i>Ne</i> III] 3869 em
<i>He</i> I 3614 abs	<i>H</i> 13	<i>H</i> 8 + <i>He</i> I
<i>He</i> I 3634 abs	<i>H</i> 12	[ <i>Fe</i> v] 3891 em
<i>H</i> 19 abs	<i>O</i> III 3760 em	<i>Si</i> I 3906 em

PLATE VIII



SPECTRUM OF T CORONAE BOREALIS ON JANUARY 28, 1943



## Bottom

Si I 3906 em	He I 4121 abs + em	Fe II 4508 em
Ca II 3934 abs + em	He I 4144 em	Fe II 4520, 4523 em
Fe II 3938 em	Fe II 4173 em	Fe II 4584 em
He I 3965 abs	Fe II 4179 em	Fe II 4629 em
[Ne III] 3967 + Ca II em	Fe II 4233 em	N III 4634 em
He abs + em	[Fe II] 4244 em	N III 4640 em
He I 4009 em	H $\gamma$ em	He II 4686 em
He I 4026 abs + em	Fe II 4352 em	He I 4713 em
[S II] 4068 em	[O III] 4363 em	H $\beta$ em
N III 4097 em	He I 4388 abs	He I 4922 abs + em
H $\delta$ em	He I 4471 em	
N III 4103 em	Fe II 4489, 4491 em	

*AX Persei*.—Some differences between the spectrograms of January, 1943, and those of January, 1942, are worth mentioning. There has been a considerable change in the intensity ratio of the He I triplets and singlets, in the sense that the singlets were much stronger in January, 1943, than they were in January, 1942, or even in November, 1942. This is especially striking when one compares the triplet line  $\lambda$  4471 with the singlet line  $\lambda$  4388. This type of variation has been discussed previously.<sup>2</sup>

The [Fe VII] lines are of about the same intensity as they were in January, 1942, and the [Fe V] lines are still present, although weaker than in January or July, 1942. The line [Ne III] is much weaker than it was in January, February, and July, 1942; it has even declined in intensity since November, 1942. On the other hand, the ratio [Ne V]/O III (fluor.) is larger than it was in July, 1942, but it is similar to those of January, February, and November, 1942.

On the whole, AX Per has increased in excitation since last summer, continuing the fluctuations which have been observed since 1939.

*Z Andromedae*.—Following the peak in excitation reached last summer,<sup>3</sup> *Z Andromedae* has continued its slow decline in excitation. The lines of [Fe VII] and [Fe V] were still present in January, 1943, but they were weaker than in July, 1942, or even than in November, 1942. The intensity ratio [Ne V]/O III (fluor.) was much smaller than in July or even in November, 1942.

Incidentally, this intensity ratio [Ne V]/O III (fluor.) should be used only with caution, since its variation may not necessarily be related to a variation in excitation. It is known<sup>4</sup> that the intensity of the fluorescence lines of O III is sensitive to the velocity and density gradients in the envelope. The atmospheres of objects like *Z And* or *AX Per* expand rather slowly, as is shown by the sharp character of the emission lines; yet even small changes in velocity or density distribution may affect the efficiency of the mechanism of monochromatic fluorescence.

*HD 45677 = MWC 142*.—This star has been described by Merrill<sup>4</sup> and by the present writers.<sup>5</sup> The spectrum has greatly changed since 1939. At that time the emission lines of H were double, with  $V/R = 0.5$ . The emission could be seen as far as He. Beginning with H $\gamma$ , the higher members of the Balmer series had strong central cores, characteristic of absorption shells; and these could be seen as far as H 29 or H 30. The Ca II K line was very strong and sharp, but the Ca II H line was exceedingly weak. This important observation, reminiscent of a similar observation in HD 190073<sup>6</sup> proves that in MWC 142 the shell absorption of Ca II is effectively obscured by the emission of He.

<sup>2</sup> Swings and Struve, *Ap. J.*, **96**, 254, 1942; **97**, 194, 1943.

<sup>3</sup> *Ap. J.*, **97**, 194, 1943.

<sup>5</sup> *Ap. J.*, **91**, 598, 1940.

<sup>4</sup> *Ap. J.*, **67**, 405, 1928.

<sup>6</sup> *Ap. J.*, **96**, 475, 1942.

It will be recalled that in HD 190073 the weakening of the  $\text{Ca II H}$  was explained as being produced by  $H\epsilon$  wing absorption in the reversing layer. The radial velocities of several relevant absorption lines measured on a plate of December 2, 1939, at 10<sup>h</sup>01<sup>m</sup> U.T. are as follows:

$H\epsilon$ .....	-0.2 km/sec
$H 8$ .....	-3.5
$H 9$ .....	-3.8
$\text{Ca II K}$ .....	+7.9

They show that the excessive weakness of  $\text{Ca II H}$  is probably not caused by differential motion of the  $\text{Ca II}$  and  $H$  atoms, causing a blending with the core of  $H\epsilon$ . The relative velocity of 10 km/sec corresponds to only one-twelfth of the normal separation between  $\text{Ca II H}$  and  $H\epsilon$ . It is clear that only the weak violet emission component of  $H\epsilon$  can be responsible for the phenomenon.

It is doubtful that mere mechanical superposition of the normal absorption line of  $\text{Ca II H}$  with the weak emission wing of  $H\epsilon$  could produce the observed weakening. Hence it is probable that the  $\lambda$  3968 transition of  $\text{Ca II}$  is somehow suppressed by a physical cause. If the shell rotated like a solid body, all emission of  $H\epsilon$ , as seen from the calcium atoms, would be concentrated in a narrow line at  $\lambda$  3970, and there could be no such effect. But differential rotation might shift an appreciable fraction of the  $H\epsilon$  quanta, as seen from the calcium atoms, to  $\lambda$  3968, in which case these quanta would cause an excess of emissions in the line  $\text{Ca II H}$  and correspondingly tend to suppress the absorption line.

In 1943 the absorption cores of the  $H$  lines, though still very narrow, had become quite weak and could be seen only to  $H 15$ . The emission lines of  $H$  have strong red components, but the violet components are vanishingly weak. Instead, there appears to be a second, weaker, and slightly more diffuse absorption component on the violet side of the main core. The line  $\text{Ca II K}$  is sharp but very much weaker than in 1939, and there may be a normal absorption line of  $\text{Ca II H}$  blended with the violet absorption component of  $H\epsilon$ .

The narrow emission lines of  $\text{Fe II}$ ,  $[\text{Fe II}]$ , etc., are essentially similar to those observed by Merrill on plates taken between 1923 and 1927.<sup>7</sup> On our plates the intensity of the blend  $\text{Fe II } 4352 + [\text{Fe II}] 4353$  is similar to that of  $[\text{Fe II}] 4359$ , while Merrill gives intensities 1 and 3, respectively. Our plates also show emission between  $H\gamma$  and  $\lambda$  4352, which may be  $[\text{Fe II}] 4347$ , observed by Merrill in  $\eta$  Carinae<sup>8</sup> but not in HD 45677. The ultraviolet emission lines, measured on the plates of March, 1943, and uncorrected for the radial velocity of the star, are as shown in the accompanying table.

$\lambda$	Int.	$\lambda$	Int.	$\lambda$	Int.	$\lambda$	Int.
3334.69 .....	0	3422.35 .....	1	3442.10 .....	3	3483.65 .....	1
3348.78 .....	1	3423.73 .....	1	3452.56 .....	0	3494.57 .....	0
3359.78 .....	2	3436.25 .....	0	3474.54 .....	0		
3408.09 .....	1	3439.10 .....	5	3482.64 .....	0		

The strongest line,  $\lambda$  3439.10, has also been observed as a strong emission in B 1985 and WY Gem. If, as is likely, the line is due to  $\text{Mn II}$ , it shows a very pronounced enhancement relative to the  $\text{Mn II}$  lines of higher excitation potential. Such an effect is well known in the case of  $\text{Fe II}$ .

<sup>7</sup> *Ap. J.*, **67**, 408, 1928.

<sup>8</sup> *Ap. J.*, **67**, 392, 1928.

TABLE 1  
OBSERVATIONS OF Be STARS

Star	Dates of Observation 1943	Description
MWC 47.....	I 29	This spectrum was classified by Merrill as B8ea, while the <i>Henry Draper Catalogue</i> gives "B" with the remark "perhaps B0." The spectrum is that of a typical shell. The <i>H</i> lines have sharp, deep cores superposed over very faint, broad, Stark-effect wings. The <i>He I</i> lines are exceedingly broad and shallow, due to rotation; <i>Fe II</i> is weak and fairly sharp. The ultraviolet lines of <i>Si II</i> are visible and are fairly narrow. They must belong to the shell and show, by comparison with <i>Fe II</i> , that the dilution factor is not very small. The lines of <i>Ca II</i> are sharp and fairly strong; <i>Mg II</i> 4481, though faint, is present and is much narrower than <i>He I</i> . It must also come from the shell
MWC 51.....	I 29	<i>Hβ</i> is fairly strong in absorption. Merrill had found <i>Hα</i> bright and <i>Hβ</i> continuous. The spectrum shows many faint, metallic lines, including <i>Fe I</i> , while <i>Mg II</i> and <i>Fe II</i> are relatively weak; <i>Ca II</i> is fairly strong
MWC 76.....	I 28	Probably no change. Spectrum B3ne
MWC 79.....	III 3, 4	The spectrum is B3ne. There is no emission at <i>Hβ</i> , but the corresponding absorption line is faint; the lines of <i>He I</i> and <i>H</i> are strong and broad
MWC 82.....	I 21, 23	No change
MWC 91.....	I 25	The emission lines are fairly narrow, and the absorption lines are intermediate between <i>n</i> and <i>s</i> ; <i>Hδ</i> shows a narrow emission line, but <i>He I</i> is in absorption
MWC 93.....	I 20, 28	The appearance of this spectrum suggests that the expanding shell observed by Merrill ( <i>Ap. J.</i> , <b>77</b> , 103, 1933) between 1928 and 1930 has disappeared. Our plates show very strong emission lines of <i>H</i> which can be seen to <i>H 11</i> or <i>H 12</i> . They are not very sharp and may be double. The violet absorption wing is somewhat stronger than the red, suggesting a possible vestige of the strong violet cores observed by Merrill in 1928-1930; <i>Ca II K</i> is present as a very weak narrow line, while on Merrill's plates it was strong; <i>Mg II</i> 4481 is weak and fairly narrow. There are no lines of <i>He I</i> or of <i>Fe II</i>
MWC 100.....	I 21, 23, 25	The appearance of this spectrum agrees with Merrill's description ( <i>Ap. J.</i> , <b>79</b> , 343, 1934). The sharp lines originate in a shell, while the broad <i>He I</i> lines come from a normal B3n star
MWC 103.....	I 25	No change. The <i>H</i> lines are very broad and shallow, but the <i>He I</i> lines are fairly narrow. The star is of moderate luminosity
MWC 114.....	III 6	<i>Hβ</i> is strong in emission, but <i>Hγ</i> is seen only in absorption. Probably no change
MWC 116.....	I 29	No change
MWC 120.....	I 28	Probably no change. The sharp absorption cores of <i>Hβ</i> , <i>γ</i> , <i>δ</i> , etc., are probably produced in a shell. There is a suspicion of a broad, shallow line of <i>He I</i> 4026. The lines of <i>Fe II</i> are very sharp in absorption, while <i>Mg II</i> 4481 is somewhat broader and rather fainter than should be expected for class A0; <i>Si II</i> is very faint and somewhat broad; <i>Ca II</i> is strong and sharp. The broad Stark-effect wings of <i>H</i> show that the star is not a supergiant
MWC 146.....	III 9	<i>Hβ</i> and <i>Hγ</i> are in emission; the interstellar <i>Ca II</i> lines are very strong
MWC 147.....	III 9	The emission lines of <i>H</i> are strong and extend to <i>H 15</i> ; they are fairly narrow, as are also the absorption lines of <i>He I</i> . The absorption lines of <i>H</i> and <i>He I</i> are weak. The type is B3e
MWC 153.....	III 8	<i>Hβ</i> is weak in emission. The type is B3ne

TABLE 1—*Continued*

Star	Dates of Observation 1943	Description
MWC 158.....	III 8	This remarkable variable spectrum has been described by Merrill ( <i>Ap. J.</i> , <b>73</b> , 348, 1931). Our plate shows double emission lines of $H\beta$ and $H\gamma$ with $V/R=2$ for $H\beta$ and $V/R=1$ for $H\gamma$ . From $H\gamma$ to about $H 25$ the Balmer lines have sharp cores, characteristic of absorption shells. The lines of $He I$ , $Mg II$ , and $Si II$ are broadened by rotation but are narrower than the over-all widths of the $H$ emission lines. There is no indication of $He I$ lines originating from metastable levels being produced in the shell. On the contrary, the weak absorption lines of $Fe II$ , already observed by Merrill, and the lines $Ti II$ 3685, 3759, 3761, and probably $Mg I$ 3832 and 3838 are very sharp and must come from the shell. The unusual feature of this shell is that the rotational broadening of the $He I$ absorption lines, though appreciable, is probably less than that of the $H$ emission lines. MWC 158 is the first case in which this has been observed. It suggests that the $He I$ lines originate in the deeper strata of the shell. The $Ca II$ lines are very strong and sharp and probably originate at least in part within the shell
MWC 175.....	III 9	$H\beta$ , $\gamma$ , $\delta$ , $\epsilon$ , are in emission. The bright lines and the $He I$ absorption lines are fairly narrow, though the latter do not justify the designation "s"
MWC 176.....	I 28	The bright lines of $H$ are strong and can be seen to $H 8$ or $H 9$ . The higher members of the Balmer series are broad, shallow, and faint absorption lines
MWC 184.....	III 10	$H\beta$ is strong in emission, but $H\gamma$ and $H\delta$ are nearly continuous. The higher members of the Balmer series are exceptionally weak and shallow
MWC 187.....	III 10	Probably no change
MWC 188.....	III 10	Probably no change
MWC 189.....	I 20	This spectrum is classified by Merrill as B(5)ne. He reported $H\beta$ as a weak emission line, while $H\gamma$ and $H\delta$ were continuous. The <i>Henry Draper Catalogue</i> gives the type simply as "B" and adds that "the spectrum is nearly continuous." On our plate $H\beta$ is nearly continuous, but $H\gamma$ , $H\delta$ , and the higher $H$ lines are peculiarly weak and shallow, broadened perhaps more by rotation than by Stark effect; $He I$ is present and is appreciably broadened by rotation. Some lines of $O II$ are weakly present. Of special interest are two well-marked absorption lines at $\lambda$ 4640 and $\lambda$ 4650. If they are due to $O II$ , their intensity is abnormally great. It is more probable that they are due to $N III$ and $C III$ ; but, surprisingly, $Si III$ and $Si IV$ are not prominent. The spectrum is abnormal; and the weakness of the $H$ absorption lines, which are fainter than the stronger lines of $He I$ , cannot in this case signify high luminosity because the interstellar $Ca II$ lines in this 8.1-mag. star are not strong enough for a supergiant. The spectrum merits further study. It is probable that it has changed since Merrill's observations
MWC 190.....	I 20	Probably no change, though our plate shows emission at $H\delta$ , superposed over broad absorption. The type is B2ne, and the higher members of the Balmer series are broad, shallow, and faint
MWC 191.....	III 9	Probably no change. The bright lines at $H\beta$ and $H\gamma$ are unusually narrow, and the absorption lines of $He I$ are fairly narrow. The type is B3se
MWC 194.....	I 23	The plate is underexposed, but $H\beta$ is strong in emission
Mt.W. 247.....	I 29	Probably no change. Our plates show emission at $H\beta$ and possibly at $H\gamma$ and $H\delta$ . The $H$ absorption lines are strong and do not suggest high luminosity. The last discernible member of the Balmer series is $H 17$ . This suggests that the star is on the main sequence ( <i>Ap. J.</i> , <b>91</b> , 365, 1940) or below it. We should be inclined, however, to assign to this star type B5ne, instead of type B8e. There are no indications of an absorption shell

TABLE 1—Continued

Star	Dates of Observation 1943	Description
Mt.W. 257.....	I 30	No change. The <i>He I</i> lines are very weak; <i>Ca II</i> K is sharp but is probably interstellar
Mt.W. 265.....	I 28	Probably no change. The <i>H</i> lines have violet-displaced cores of considerable intensity, suggesting that there is an expanding shell; <i>Ca II</i> K is double, with the violet component the stronger; <i>Mg II</i> 4481 is present but probably does not share the violet displacement of the <i>H</i> and <i>Ca II</i> lines. The lines of <i>Si II</i> are very weak and look diffuse. Merrill has already remarked upon the similarity of this star to HD 31293. Other similar objects are 17 Leporis and HD 190073. The structure of <i>Ca II</i> K bears a definite resemblance to that of HD 190073
Mt.W. 275.....	I 21, 24	<i>Hβ</i> is a narrow emission line. The other <i>H</i> lines show narrow cores superposed over broad Stark-effect wings. The <i>He I</i> lines are greatly broadened by rotation; <i>Mg II</i> 4481 and the <i>Si II</i> lines are weak and of intermediate width. A few lines of <i>Fe II</i> are weakly present and are very sharp; <i>Ca II</i> K is sharp and strong. The sharp absorption features indicate a shell, but the central intensities of the sharp <i>H</i> cores are not so low as is usually the case. The <i>Mg I</i> lines, which are surprisingly strong in many shells, are probably present and are sharp. The rotational broadening of the <i>He I</i> lines corresponds to about 300 km/sec
Mt.W. 277.....	III 8	<i>Hβ</i> and <i>Hγ</i> are in emission. The plate is underexposed
Mt.W. 287.....	I 21	<i>Hβ</i> and <i>Hγ</i> are in emission. The higher <i>H</i> lines are broad and shallow. <i>H</i> 14 or <i>H</i> 15 is the last member seen in absorption. The type is B5ne. The interstellar <i>Ca II</i> K line is either absent or very weak

Table 1 is a continuation of our observations of Be stars.<sup>9</sup> The stars designated by their MWC numbers refer to the Mount Wilson catalogue of Be stars. Those listed by their Mt. W. numbers will be found in several later lists published by Merrill from Mount Wilson. These stars have not yet been supplied with MWC numbers.

<sup>9</sup> *A p. J.*, 97, 219, 1943.

## THE SPECTRUM OF 48 LIBRAE (HD 142983)\*

OTTO STRUVE

Yerkes and McDonald Observatories

Received April 15, 1943

### ABSTRACT

The star 48 Librae shows a strong metallic absorption spectrum which has developed during the last ten or twenty years. This spectrum shows appreciable dilution in the intensities of  $Mg\ II$  and  $Si\ II$ . The  $H$  lines consist of sharp cores superposed over broad wings.  $H\beta$  and  $H\alpha$  are bright. The sharp-line spectrum is attributed to a shell which resembles in the relative intensities of  $Ni\ II$ ,  $Fe\ II$ ,  $Cr\ II$ , and  $Mn\ II$  the shell of Pleione as observed in 1940. But the Balmer jump in the shell of 48 Librae is much more conspicuous than in Pleione. The shell of 48 Librae is fairly transparent in the ordinary photographic region but is essentially opaque on the violet side of  $\lambda\ 3650$ . The strong shell lines are sharp but unsymmetrical, while the weaker lines, especially of  $Ti\ II$  and  $Fe\ I$ , are somewhat diffuse. This suggests stratification. The emission lines of  $H$  have shown a marked variation in  $V/R$ . The radial velocity is variable.

The spectrum of 48 Librae is at the present time that of a typical shell surrounding a normal, rapidly rotating B star. The star is listed as No. 239 in the Mount Wilson catalogue of Be and Ae stars<sup>1</sup> and is there classified as Apea. The *Henry Draper Catalogue* lists it as B3p with the remark: "The spectrum is peculiar in combining sharply defined hydrogen lines with wide and ill-defined helium lines. In this respect it resembles the spectrum of  $\epsilon$  Capricorni." It is evident that the spectrum has undergone a change, since in recent years the metallic lines have been very strong, and the type now more nearly resembles A2 or A5 than B3. Although at the time of the Harvard observations the sharp hydrogen lines already gave indications of a shell, the metallic lines have greatly increased in intensity since that time. Emission at  $H\beta$  was found by Struve on plates taken in 1904, but  $Fe\ II\ 4549$  was only suspected as a weak, narrow absorption line.<sup>2</sup> In 1915 the narrow metallic lines were again suspected, but the remarkable development of the metallic spectrum shown in Plates IX and X probably took place between 1924, when the star was observed at the Chilean station of the Lick Observatory, with the remark "good hydrogen lines,"<sup>3</sup> and 1930, when Merrill classified it as A3sea.<sup>4</sup> In 1935 Struve and Wurm<sup>5</sup> found that the broad  $He\ I$  lines were weak, while sharp  $Fe\ II$  was fairly strong;  $Mg\ II$  was probably present as a very weak line, broader than  $Fe\ II$ , but not as broad as  $He\ I$ . It is quite certain that in 1935 the metallic lines were not nearly as strong as they are at the present time. Incidentally, in 1935 the red component of the bright line at  $H\beta$  was stronger than the violet component. In recent years the violet component has been the stronger of the two.

Although in the past 48 Librae had shown little or no indication of variation in the radial velocity,<sup>6</sup> Merrill and Sanford found that "between 1935 and 1939 the velocity derived from the displacements of the metallic lines and the ultraviolet members of the Balmer series decreased about 100 km/sec and then returned to its previous value. The Balmer lines  $H\beta$ ,  $\gamma$ ,  $\delta$  were displaced only about one-half as much. The velocities from both groups of lines are now (1940) showing a tendency toward algebraically higher values."<sup>7</sup>

The observations discussed in this paper were started at the Yerkes Observatory in

\* Contributions from the McDonald Observatory, University of Texas, No. 73.

<sup>1</sup> *Ap. J.*, **78**, 96, 1933.

<sup>2</sup> *Ap. J.*, **76**, 210, 1932.

<sup>3</sup> *Pub. Lick Obs.*, **16**, 233, 1928.

<sup>4</sup> *Ap. J.*, **74**, 195, Pl. VIII, 1931.

<sup>5</sup> *Ap. J.*, **88**, 91, Pl. IV, 1938.

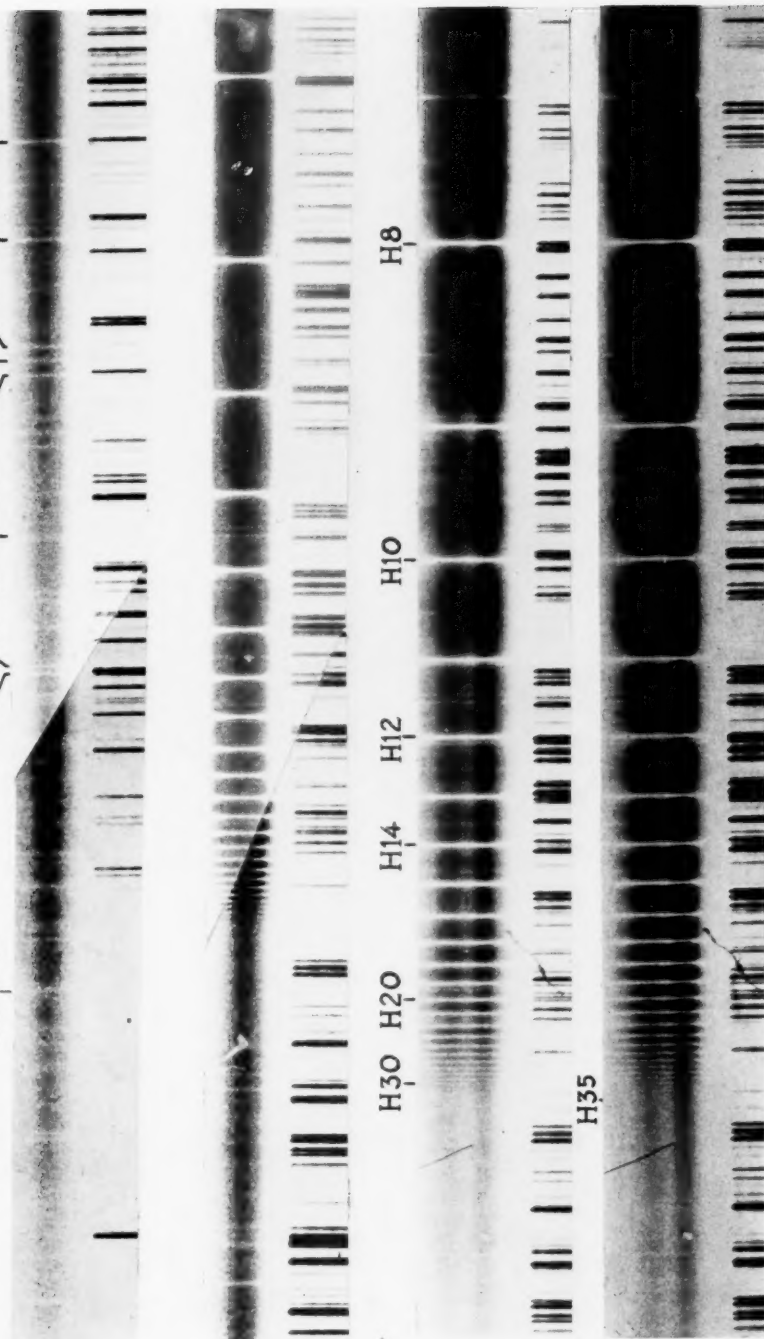
<sup>6</sup> *Pub. Lick Obs.*, **18**, 125, 1932.

<sup>7</sup> *Pub. A.S.P.*, **52**, 279, 1940.

PLATE IX

Ti II 3349 Ni II Cr II 3409 Cr II 3433 Ni II Fe II Ni II Fe II 3493 Ni II 3514

Ti II 3349



ULTRAVIOLET SPECTRA OF 48 LIBRAE IN MARCH, 1943  
The two spectra at the bottom are reproductions of the same original

PLATE X

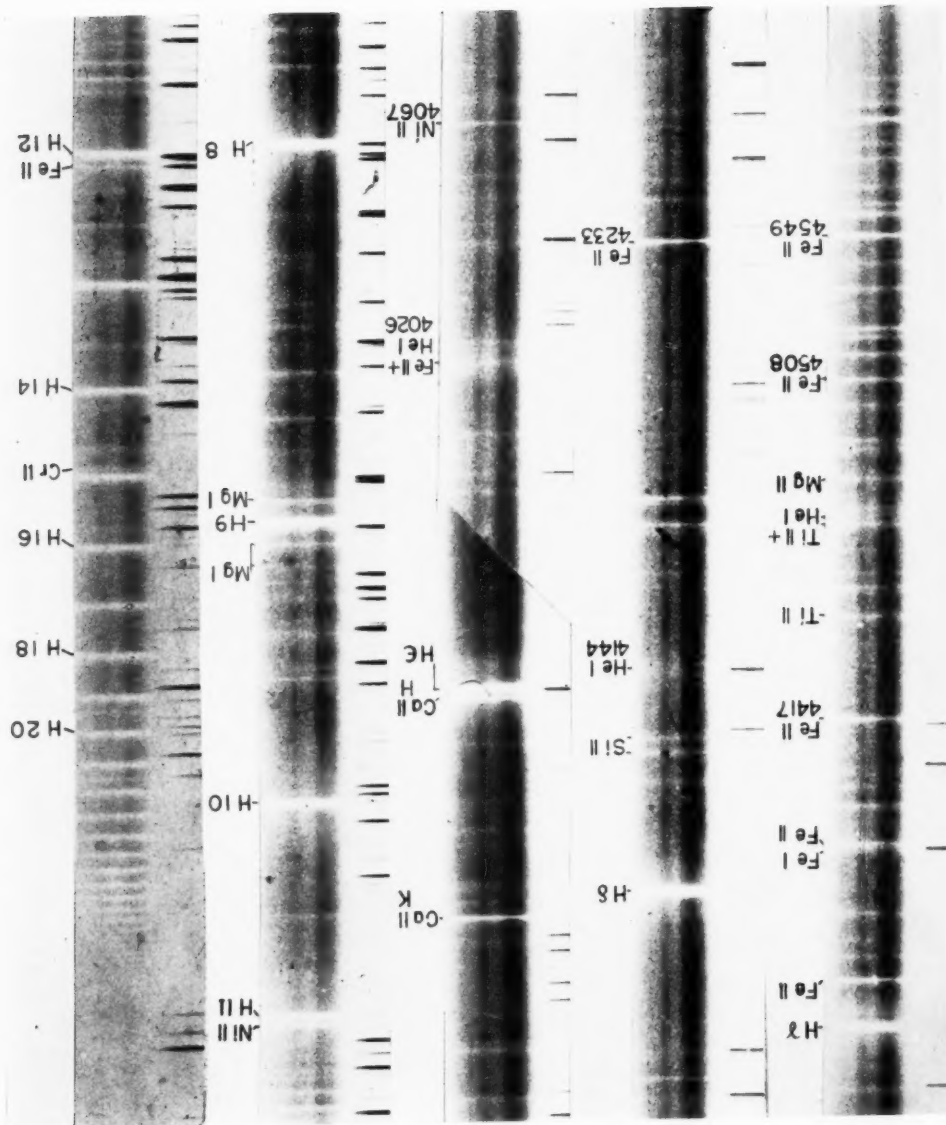


TABLE 1  
LIST OF LINES IN THE SPECTRUM OF 48 LIBRAE IN 1943

Wave Length	Int.	Identification
3289.48	1	<i>Fe</i> II 89.35 (7), <i>V</i> II 89.39 (100)
3295.68	4	<i>Fe</i> II 95.81 (6), <i>Fe</i> II 95.24 (4), <i>Cr</i> II 95.42 (30)
3297.98	1	<i>Fe</i> II 97.89 (5)
3299.85	0	<i>Fe</i> II 99.77 (1)
3303.18	1	<i>Fe</i> II 02.86 (4), <i>Fe</i> II 03.47
3307.05	1	<i>Cr</i> II 07.04 (50), <i>Cr</i> II 06.95 (50)
3312.25	1n	<i>Cr</i> II 12.18 (40), <i>Cr</i> II 11.93 (40)
3314.05	0	<i>Fe</i> II 14.00 (1), <i>Cr</i> II 14.57 (35), <i>Cr</i> II 14.06 (18)
3315.42	0	<i>Ti</i> II 15.32 (100), <i>Cr</i> II 15.29 (12)
3321.57	0n	<i>Fe</i> II 21.49 (1), <i>Ti</i> II 21.70 (125), <i>V</i> II 21.54 (150)
3323.07	2	<i>Fe</i> II 23.07 (8), <i>Ti</i> II 22.94 (300)
3324.41	1	<i>Cr</i> II 24.35 (50), <i>Cr</i> II 24.06 (25), <i>Cr</i> II 24.10 (20)
3329.13	1n	<i>Fe</i> II 29.07 (2), <i>Ti</i> II 29.46 (200)
3332.14	0	<i>Ti</i> II 32.11 (125)
3335.40	2n	<i>Cr</i> II 35.28 (40), <i>Ti</i> II 35.19 (150), <i>Cr</i> II 35.46 (30)
3336.62	1n	<i>Cr</i> II 36.33 (40)
3338.44	0	<i>Fe</i> II 38.52 (3)
3340.20	3n	<i>Cr</i> II 39.80 (50), <i>Ti</i> II 40.34 (100), <i>Cr</i> II 39.90 (20)
3342.37	2n	<i>Cr</i> II 42.51 (50), <i>Ti</i> II 41.87 (300)
3343.72	1	<i>Ti</i> II 43.77 (70)
3346.68	1n	<i>Ti</i> II 46.73 (60)
3348.03	2	<i>Cr</i> II 47.84 (40)
3349.39	3	<i>Ti</i> II 49.41 (400), <i>Ti</i> II 49.03 (800)
3350.66	1	<i>Ni</i> II 50.42 (5)
3352.94	1	<i>Cr</i> II 53.12 (20)
3356.85	1n	<i>Cr</i> II 57.40 (40), <i>Fe</i> II 56.26 (2)
3358.53	3	<i>Cr</i> II 58.50 (75), <i>Fe</i> II 58.25 (3)
3360.17	2n	<i>Fe</i> II 60.10 (3), <i>Cr</i> II 60.29 (100)
3361.64	3n	<i>Ti</i> II 61.21 (600), <i>Cr</i> II 61.77 (30)
3363.84	1n	<i>Cr</i> II 63.71 (12)
3366.77	0n	<i>Fe</i> II 66.96 (3)
3368.01	5	<i>Cr</i> II 68.05 (150)
3369.27	0n	<i>Fe</i> II 69.35 (3), <i>Cr</i> II 69.05 (18)
3372.53	1n	<i>Ti</i> II 72.80 (400)
3374.10	6	<i>Ni</i> II 73.98 (4)
3377.75	0n	<i>Cr</i> II 78.34 (25)
3379.80	2n	<i>Cr</i> II 79.82 (60)
3383.17	1n	<i>Ti</i> II 83.76 (300), <i>Cr</i> II 82.68 (60)
3387.84	3nn	<i>Ti</i> II 87.84 (125), <i>Fe</i> II 88.13 (2)
3390.96	2n	<i>Cr</i> II 91.43 (35), <i>Fe</i> II 91.30 (1)
3393.87	3n	<i>Cr</i> II 94.32 (35), <i>Ti</i> II 94.57 (200)
3396.06	1	<i>Cr</i> II 95.62 (15)
3398.29	1nn	<i>Ni</i> II 97.82 (1), <i>Fe</i> II 98.35 (4)
3401.93	2n	<i>Ni</i> II 01.76 (2), <i>Ti</i> II 02.42 (90), <i>Cr</i> II 02.43 (25)
3403.39	3	<i>Cr</i> II 03.32 (100)
3407.31	6	<i>Ni</i> II 07.30 (8)
3408.80	6	<i>Cr</i> II 08.76 (150)
3414.00	0n	<i>Fe</i> II 14.14 (2)
3416.00	2n	<i>Fe</i> II 16.02 (5)
3421.11	2n	<i>Cr</i> II 21.20 (75)

TABLE 1—Continued

Wave Length	Int.	Identification
3422.72	4n	<i>Cr</i> II 22.74 (125)
3425.65	0	<i>Fe</i> II 25.58 (3)
3428.76	0	<i>Cr</i> II 28.94 (7)
3433.46	4n	<i>Cr</i> II 33.30 (75)
3436.16	2	<i>Fe</i> II 36.11 (5)
3438.73	1n	<i>Mn</i> II 38.98 (20)
3441.87	2	<i>Mn</i> II 41.98 (100), <i>Fe</i> I 40.61 (500)
3444.11	1n	<i>Ti</i> II 44.31 (150)
3446.40	0	<i>Co</i> II 46.40 (100)
3451.36	3	<i>Fe</i> II 51.23 (2), <i>Fe</i> II 51.32 (2), <i>Fe</i> II 51.61 (2)
3454.19	3	<i>Ni</i> II 54.16 (5)
3456.76	3n	<i>Fe</i> II 56.93 (5), <i>Cr</i> II 57.62 (30), <i>Ti</i> II 56.39 (125), <i>V</i> II 57.15 (300)
3459.84	1nn	<i>Cr</i> II 59.29 (25), <i>Mn</i> II 60.31 (75)
3461.36	1n	<i>Ti</i> II 61.50 (125)
3465.59	4	<i>Ni</i> II 65.62 (1), ( <i>Ti</i> II 65.56 (60))
3468.59	4	<i>Fe</i> II 68.68 (8)
3471.44	5	<i>Ni</i> II 71.35 (2), <i>Cr</i> II 72.07 (25)
3473.70	1nn	<i>Fe</i> II 73.82 (2), <i>Mn</i> II 74.04 (50), <i>Mn</i> II 74.12 (40)
3475.19	1n	<i>Cr</i> II 75.13 (20)
3477.17	0	<i>Ti</i> II 77.18 (100)
3482.63	1n	<i>Mn</i> II 82.90 (40), ( <i>Cr</i> II 82.58 (12))
3488.32	0nn	<i>Mn</i> II 88.68 (40), ( <i>Cr</i> II 89.07 (2))
3490.85	1	<i>Ti</i> II 91.05 (70), <i>Fe</i> I 90.57 (400)
3493.39	7	<i>Fe</i> II 93.47 (10)
3495.45	3	<i>Fe</i> II 95.45 (4), <i>Cr</i> II 95.56 (20), <i>Fe</i> II 95.62 (4), <i>Ni</i> II 95.6 (pred)
3497.30	1	<i>Mn</i> II 97.54 (25), <i>Mn</i> II 96.81 (20), <i>V</i> II 97.03 (200)
3499.80	1	<i>Fe</i> II 99.88 (4)
3501.64	1	<i>Co</i> II 01.73 (200), ( <i>Cr</i> II 01.53 (1))
3504.68	2	<i>Ti</i> II 04.89 (150), <i>V</i> II 04.43 (400)
3507.29	1	<i>Fe</i> II 07.39 (3), ( <i>Fe</i> II 08.21 (1))
3510.64	1nn	<i>Ti</i> II 10.84 (125)
3514.00	10	<i>Ni</i> II 13.93 (8), ( <i>Fe</i> I 13.82 (400))
3516.60	2n	<i>Fe</i> II 15.82 (12)
3520.21	1	<i>Ti</i> II 20.25 (18), <i>V</i> II 20.02 (120)
3523.96	0n	Pleione
3526.31	2	<i>Fe</i> I 26.04 (80), <i>Fe</i> I 26.17 (50), <i>Fe</i> I 26.68 (80)
3530.36	0n	<i>V</i> II 30.76 (500), ( <i>Cr</i> II 30.72 (1)), ( <i>Cr</i> II 30.05 (1))
3532.81	0n	( <i>Ti</i> II 33.87 (35))
3535.50	1n	<i>Ti</i> II 35.41 (125), <i>Fe</i> II 35.63 (2), <i>Mg</i> II 35.04 (8)
3538.63	0n	<i>Mg</i> II 38.86 (6), ( <i>Cr</i> II 38.47 (1))
3544.77	1	<i>V</i> II 45.19 (1000)
3548.08	0nn	( <i>Fe</i> II 49.03 (1))
3554.32	0	<i>Fe</i> II 54.50 (1)
3561.11	1nn	<i>Ti</i> II 61.57 (20), <i>Cr</i> II 60.91 (1)
3565.41	1nn	<i>Cr</i> II 65.31 (5)
3569.94	0n	<i>Fe</i> I 70.10 (300)
3575.12	0	( <i>Ti</i> II 73.74 (40))
3576.76	9	<i>Ni</i> II 76.76 (3)
3580.91	1nn	<i>Fe</i> I 81.19 (1000), ( <i>Sc</i> II 80.93 (40))
3585.44	3n	<i>Cr</i> II 85.31 (60), <i>Cr</i> II 85.54 (40)

TABLE 1—Continued

Wave Length	Int.	Identification
3589.53	2	<i>V</i> II 89.74 (1000), ( <i>Sc</i> II 89.63 (12))
3596.08	0nn	<i>Ti</i> II 96.05 (125)
3603.66	1n	<i>Cr</i> II 03.80 (40), <i>Cr</i> II 03.86 (20), <i>Cr</i> II 03.61 (20)
3608.74	2	<i>Ni</i> II 08.7 (pred), <i>Fe</i> I 08.86 (500)
3613.04	1n	<i>Cr</i> II 13.26 (15), <i>Cr</i> II 13.21 (20)
3615.00	1	<i>Fe</i> II 14.87 (5)
3618.55	0	<i>Fe</i> I 18.77 (400), <i>V</i> II 18.92 (200)
3621.30	4	<i>Fe</i> II 21.27 (60), <i>V</i> II 21.20 (150)
3624.74	3	<i>Ti</i> II 24.83 (125), <i>Fe</i> II 24.89 (5), <i>Fe</i> II 24.69 (2)
3627.89	0	<i>Fe</i> II 7.17 (1), <i>V</i> II 27.71 (60)
3631.55	3n	<i>Cr</i> II 31.49 (50), <i>Cr</i> II 31.72 (40), <i>Fe</i> I 31.46 (500)
3634.91	0	( <i>Ti</i> II 5.64 (pred)), Pleione, $\alpha$ Cyg
3658.56	1	<i>H</i> 34 58.64
3659.48	1	<i>H</i> 33 59.42
3660.32	1	<i>H</i> 32 60.28
3661.20	2	<i>H</i> 31 61.22
3662.24	3	<i>H</i> 30 62.26
3663.55	3	<i>H</i> 29 63.40
3664.78	4	<i>H</i> 28 64.70
3666.14	5	<i>H</i> 27 66.10
3667.76	6	<i>H</i> 26 67.68
3669.44	6	<i>H</i> 25 69.47
3671.54	8	<i>H</i> 24 71.48
3673.84	8	<i>H</i> 23 73.76
3676.40	9	<i>H</i> 22 76.36
3677.76	2n	<i>Cr</i> II 77.69 (40), <i>Cr</i> II 77.86 (50), <i>Cr</i> II 77.93 (30)
3679.40	9	<i>H</i> 21 79.35
3682.88	10	<i>H</i> 20 82.81
3685.22	2	<i>Ti</i> II 85.19 (700), ( <i>Cr</i> II 84.25 (25))
3686.88	10	<i>H</i> 19 86.83
3691.58	10	<i>H</i> 18 91.56 (2)
3697.22	10	<i>H</i> 17 97.15 (3)
3700.90	0n	<i>Fe</i> I 01.09 (300)
3703.86	11	<i>H</i> 16 03.86 (4)
3706.07	1n	<i>Ca</i> II 06.03 (40), <i>Ti</i> II 06.23 (125)
3707.13	0	( <i>Fe</i> I 07.82 (80)), ( <i>Fe</i> I 07.92 (80))
3708.97	0n	<i>Fe</i> I 09.25 (600)
3712.04	12	<i>H</i> 15 11.98 (5)
3712.88	2	<i>Cr</i> II 2.97 (35)
3713.93	1	
3715.22	2n	<i>V</i> II 15.48 (1200), <i>Cr</i> II 15.19 (20), <i>Cr</i> II 15.45 (20)
3717.43	0n	( <i>V</i> II 18.16 (60)), ( <i>Fe</i> I 18.41 (80))
3719.88	1n	<i>Fe</i> I 19.93 (1000), ( <i>Cr</i> II 19.72 (1))
3722.02	12	<i>H</i> 14 21.95 (6)
3723.28	1	<i>Cr</i> II 23.40 (15)
3725.15	0n	<i>Fe</i> II 25.30 (3)
3727.26	2n	<i>Cr</i> II 27.37 (40), <i>V</i> II 27.35 (1000), <i>Fe</i> II 27.04 (m), <i>Fe</i> I 27.62 (200)
3732.89	1n	<i>V</i> II 32.76 (800)
3734.44	12	<i>H</i> 13 34.37 (8)
3737.03	2n	<i>Ca</i> II 36.90 (50), <i>Fe</i> I 37.13 (1000)

TABLE 1—Continued

Wave Length	Int.	Identification
3738.32	2n	<i>Cr</i> II 38.38 (25)
3741.58	3	<i>Ti</i> II 41.64 (200)
3743.48	0	<i>Fe</i> I 43.36 (200)
3745.67	2n	<i>V</i> II 45.81 (800), <i>Fe</i> I 45.56 (500)
3748.64	5	<i>Fe</i> II 48.49 (8), <i>Fe</i> I 48.26 (500)
3750.19	12	<i>H</i> 12 50.15 (10)
3751.93	0	( <i>V</i> II 50.88 (600))
3754.54	2nn	<i>Cr</i> II 54.59 (20)
3755.54	1	<i>Fe</i> II 55.56 (4)
3757.66	2n	<i>Ti</i> II 57.69 (100), <i>Fe</i> I 58.23 (700)
3759.40	4	<i>Fe</i> II 59.46 (6), <i>Ti</i> II 59.29 (400)
3761.42	4	<i>Ti</i> II 61.32 (300)
3763.00	1	<i>Fe</i> II 62.89 (5)
3763.87	1	<i>Fe</i> I 63.79 (500), ( <i>Fe</i> II 64.09 (pred))
3765.66	0n	<i>Cr</i> II 65.62 (8)
3766.93	1n	<i>Fe</i> I 67.19 (500)
3768.40	1	
3769.54	7	<i>Ni</i> II 69.46 (5)
3770.72	14	<i>H</i> 11 70.63 (15)
3773.77	1n	
3774.99	1nn	<i>Y</i> II 74.34 (300)
3776.19	0n	<i>Ti</i> II 76.06 (60)
3778.22	0	<i>V</i> II 78.36 (100), <i>Fe</i> II 78.37 (pred)
3778.93	0n	<i>Cr</i> II 78.69 (6), ( <i>Cr</i> II 79.06 (1))
3783.34	3	<i>Fe</i> II 83.35 (4)
3786.18	0	( <i>Fe</i> I 86.68 (125))
3786.70	0n	<i>V</i> II 87.23 (150), ( <i>Fe</i> I 87.88 (500))
3790.06	1	
3797.94	14	<i>H</i> 10 97.91 (20)
3799.33	1	
3814.16	2n	<i>Fe</i> II 14.12 (4)
3815.56	1n	<i>Fe</i> I 15.84 (700), <i>V</i> II 15.38 (200)
3816.29	1n	
3817.98	0n	<i>Y</i> II 18.35 (60)
3820.18	2nn	<i>Fe</i> I 20.43 (800), <i>He</i> I 20.87
3821.71	1n	<i>Fe</i> II 21.97 (pred)
3824.92	2n	<i>Fe</i> II 24.91 (4)
3827.29	2n	<i>Fe</i> II 27.08 (4), <i>Fe</i> I 27.82 (200)
3829.24	2n	<i>Mg</i> I 29.35 (100)
3830.69	1n	
3832.27	4	<i>Mg</i> I 32.31 (250)
3835.42	14	<i>H</i> 9 35.40 (40)
3838.21	4	<i>Mg</i> I 38.26 (300), <i>Fe</i> II 38.04 (?)
3840.36	1n	<i>Fe</i> I 40.44 (400), <i>Fe</i> I 41.05 (500)
3843.32	0	<i>Sc</i> II 43.00 (20), <i>Zr</i> II 43.03 (30)
3844.63	1	Pleione
3845.28	1	<i>Fe</i> II 45.18 (3)
3847.22	0	<i>V</i> II 47.32 (100)
3848.68	1	( <i>Mg</i> II 48.24 (10))
3849.64	3	<i>Ni</i> II 49.58 (2), ( <i>Fe</i> I 49.97 (500))

TABLE 1—*Continued*

Wave Length	Int.	Identification
3850.74	1	<i>Fe</i> I 50.82 (200)
3852.54	1	<i>Fe</i> I 52.57 (150)
3853.89	0n	<i>Si</i> II 53.67 (3)
3855.89	5	<i>Si</i> II 56.03 (8)
3859.70	1n	<i>Fe</i> I 59.91 (1000)
3860.96	0	<i>Fe</i> II 60.91 (3)
3862.50	2	<i>Si</i> II 62.59 (6)
3864.05	1	<i>Fe</i> II 63.95 (1)
3865.58	1	<i>Cr</i> II 65.59 (75), <i>Fe</i> I 65.53 (600)
3866.63	1	<i>V</i> II 66.74 (60), <i>Cr</i> II 66.54 (7), <i>Cr</i> II 66.01 (5)
3872.62	1n	<i>Fe</i> I 72.50 (300), <i>Fe</i> II 72.76 (2)
3875.62	0	$\alpha$ Cyg
3878.48	2n	<i>Fe</i> I 78.57 (300), <i>Fe</i> I 78.02 (400), <i>V</i> II 78.71 (300)
3886.12	1n	<i>Fe</i> I 86.28 (600)
3889.14	18	<i>H</i> 8 89.05 (60)
3892.07	1	( <i>S</i> II 92.32 (35)), ( <i>Cr</i> II 93.31 (1))
3894.86	0n	<i>Fe</i> I 95.66 (400)
3899.36	3	<i>V</i> II 99.14 (200)
3899.90	0	<i>Fe</i> I 99.71 (500)
3900.40	3	<i>Ti</i> II 00.54 (100), <i>Al</i> II 00.68 (200)
3902.98	2n	<i>V</i> II 3.27 (250), <i>Fe</i> I 02.95 (500)
3905.70	2	<i>Cr</i> II 5.64 (25), <i>Si</i> I 05.53 (20)
3906.09	3	<i>Fe</i> II 06.04 (5), ( <i>Fe</i> I 06.48 (300))
3908.18	0	( <i>Fe</i> I 07.94 (100))
3910.29	1	( <i>Cr</i> II 11.32 (3))
3912.03	1	
3913.52	4n	<i>Ti</i> II 13.46 (70), ( <i>Fe</i> I 13.63 (100))
3914.58	2	<i>Fe</i> II 14.48 (2), <i>V</i> II 14.33 (250)
3916.52	0	<i>V</i> II 16.42 (200), ( <i>La</i> II 16.07 (300))
3918.58	1	<i>Fe</i> II 18.51 (pred)
3921.21	0	<i>Fe</i> I 20.26 (500), ( <i>C</i> II 20.68 (200))
3922.57	0	<i>Fe</i> I 22.91 (600)
3927.92	0	<i>Fe</i> I 27.92 (500)
3930.26	2n	<i>Fe</i> I 30.31 (600), <i>Fe</i> II 30.31 (pred)
3932.40	1n	<i>Ti</i> II 32.02 (30)
3933.40	1b	( <i>Ca</i> II 33.67 (600))
3933.68	8	<i>Ca</i> II 33.67 (600)
3936.03	2	<i>Fe</i> II 35.94 (6)
3937.05	0	( <i>Cr</i> II 36.95 (1))
3938.17	1n	<i>Fe</i> II 38.29 (2)
3938.72	2n	<i>Fe</i> II 38.97 (4)
3940.37	0	<i>Fe</i> I 40.82 (150)
3942.55	0	<i>Fe</i> I 42.44 (100)
3943.37	1n	( <i>Al</i> I 44.03 (2000)), ( <i>Cr</i> II 43.64 (1))
3945.12	1n	( <i>Cr</i> II 45.11 (1)), ( <i>Fe</i> II 45.21 (pred))
3946.44	0	( <i>Fe</i> I 47.00 (50))
3947.34	2n	<i>O</i> I 47.33 (300)
3949.46	1	<i>Fe</i> I 49.96 (150)
3950.76	1	<i>Fe</i> I 51.17 (150)
3951.90	1n	<i>V</i> II 51.97 (500)

TABLE 1—Continued

Wave Length	Int.	Identification
3958.61	0	<i>Cr</i> II 58.07 (2), <i>Zr</i> II 58.22 (150)
3960.95	2n	<i>Fe</i> II 60.89 (3), ( <i>Al</i> I 61.53 (3000))
3964.74	0n	<i>He</i> I 64.73 (50), ( <i>Fe</i> I 64.52 (80))
3966.66	0n	<i>Fe</i> I 66.07 (100)
3968.46	7	<i>Ca</i> II 68.47 (500)
3970.06	18	<i>He</i> 70.08 (80)
3973.12	1nn	<i>V</i> II 73.64 (300)
3974.48	1n	<i>Fe</i> II 74.16 (3), <i>Fe</i> II 75.03 (2)
3977.48	0n	<i>Fe</i> I 77.74 (300), <i>V</i> II 77.73 (60)
3979.50	1n	<i>Cr</i> II 79.51 (20)
3981.25	1n	<i>Fe</i> I 81.77 (150), ( <i>Fe</i> II 81.66 (pred))
3982.59	0	<i>Y</i> II 82.59 (100)
3997.03	0n	<i>V</i> II 97.13 (200), <i>Fe</i> I 97.40 (300)
3998.92	1	<i>Zr</i> II 98.97 (30), ( <i>S</i> II 98.79 (60))
4002.40	2nn	<i>Fe</i> II 02.53 (3), <i>Fe</i> II 02.07 (2)
4004.58	0	<i>Fe</i> II 04.15 (pred)
4005.43	2	<i>V</i> II 05.71 (800), <i>Fe</i> I 05.25 (250)
4007.39	0	<i>Fe</i> II 07.72 (pred)
4012.46	2n	<i>Fe</i> II 12.47 (1), <i>Ti</i> II 12.39 (50), <i>Cr</i> II 12.50 (30)
4015.41	1n	<i>Ni</i> II 15.48 (1)
4023.36	1nn	<i>V</i> II 23.39 (600)
4024.71	3nn	<i>Fe</i> II 24.55 (5), <i>Fe</i> I 24.74 (120)
4026.87	0	( <i>He</i> I 26.19 (5))
4028.25	2n	<i>Ti</i> II 28.35 (80)
4029.70	1	( <i>Zr</i> II 29.68 (20)), ( <i>Fe</i> I 29.64 (80))
4033.01	1n	<i>Fe</i> II 32.95 (3), <i>Mn</i> I 33.07 (400)
4035.47	0n	<i>V</i> II 35.63 (400)
4037.85	1n	<i>Cr</i> II 38.03 (25)
4044.12	1	<i>Fe</i> II 44.01 (m)
4045.64	2n	<i>Fe</i> I 45.81 (400), ( <i>Zr</i> II 45.63 (15))
4048.92	1n	<i>Fe</i> II 48.83 (3), ( <i>Zr</i> II 48.68 (25)), ( <i>Cr</i> II 49.14 (18))
4051.70	1	<i>V</i> II 51.34 (100), ( <i>Fe</i> II 51.21 (pred))
4053.71	1	<i>Ti</i> II 53.84 (25), <i>V</i> II 53.59 (60), ( <i>Cr</i> II 54.11 (8))
4055.35	0	( <i>Cr</i> II 56.07 (4))
4057.57	2	<i>Fe</i> II 57.46 (2)
4063.41	1n	<i>Fe</i> I 63.69 (400)
4067.16	4	<i>Ni</i> II 67.05 (3), ( <i>Fe</i> I 66.98 (100))
4069.06	0	$\alpha$ Cyg
4070.90	0n	<i>Cr</i> II 70.90 (10)
4071.88	1n	<i>Fe</i> I 71.74 (300)
4075.71	1	( <i>Cr</i> II 75.63 (pred)), ( <i>Si</i> II 75.45 (2))
4077.29	1	<i>Sr</i> II 77.71 (500), <i>Fe</i> II 77.16 (3), <i>La</i> II 77.35 (300)
4093.17	0	<i>Fe</i> II 93.24 (0)
4101.90	20	<i>H<math>\delta</math></i> 01.74 (100)
4110.99	1	<i>Cr</i> II 11.01 (18)
4118.38	0	<i>Fe</i> I 18.55 (200)
4122.60	2n	<i>Fe</i> II 22.64 (4)
4124.92	1nn	<i>Fe</i> II 24.79 (1)
4128.19	3n	<i>Si</i> II 28.05 (8), <i>Fe</i> II 28.73 (3)
4130.91	3n	<i>Si</i> II 30.88 (10), <i>Fe</i> I 32.06 (300)

TABLE 1—Continued

Wave Length	Int.	Identification
4132.22	1	<i>Cr</i> II 2.41 (7)
4134.47	1n	<i>Fe</i> I 34.68 (150)
4137.00	1	<i>Fe</i> I 37.00 (100)
4144.34	1nn	<i>Fe</i> I 43.87 (400), ( <i>He</i> I 43.76 (15))
4150.46	0n	<i>Cr</i> II 51.00 (5), ( <i>Fe</i> I 50.26 (50))
4160.90	1	<i>Cr</i> II 61.05 (2), <i>Ti</i> II 1.54 (30)
4163.82	3	<i>Ti</i> II 63.65 (150)
4167.73	0	<i>Mg</i> I 67.39 (6), <i>Mg</i> I 67.65 (5)
4171.75	1n	<i>Ti</i> II 71.90 (70), ( <i>Cr</i> II 71.92 (3))
4173.43	5	<i>Fe</i> II 73.45 (8)
4176.26	0	<i>Fe</i> I 75.64 (100), <i>Fe</i> I 76.57 (100)
4177.66	2	<i>Fe</i> I 77.60 (100), <i>Fe</i> II 77.70 (pred), ( <i>Y</i> II 77.54 (125))
4178.89	5	<i>Fe</i> II 78.85 (8)
4183.40	0n	<i>V</i> II 83.43 (250)
4188.09	1n	<i>Fe</i> I 87.80 (200)
4190.02	1	<i>Ti</i> II 90.24 (5)
4191.89	1	<i>Ni</i> II 92.02 (1)
4199.36	0n	<i>Fe</i> I 99.10 (300)
4202.25	1n	<i>V</i> II 02.34 (150), <i>Fe</i> I 02.03 (400)
4204.16	0	<i>V</i> II 05.08 (250)
4215.75	0	<i>Sr</i> II 15.52 (400)
4219.67	0	<i>Fe</i> I 19.36 (250)
4224.68	1	<i>Cr</i> II 24.85 (20)
4227.75	0n	<i>Fe</i> I 27.43 (300), ( <i>Al</i> II 27.98 (20))
4233.19	10	<i>Fe</i> II 33.17 (11)
4235.72	0	<i>Fe</i> I 35.94 (300)
4238.75	1n	<i>Fe</i> I 38.82 (200)
4242.25	3n	<i>Cr</i> II 42.38 (30)
4246.53	2n	<i>Sc</i> II 46.83 (500)
4250.07	0	<i>Fe</i> I 50.13 (250)
4252.72	1n	<i>Cr</i> II 52.62 (10)
4254.30	1	<i>Cr</i> I 54.35 (5000)
4255.79	1	$\alpha$ Cyg
4258.33	2n	<i>Fe</i> II 58.15 (3), ( <i>Zr</i> II 58.05 (12))
4261.92	2n	<i>Cr</i> II 61.92 (20)
4264.71	1	
4269.46	1n	<i>Cr</i> II 69.28 (10)
4273.18	1	<i>Fe</i> II 73.32 (3)
4275.47	1n	<i>Cr</i> II 75.57 (30)
4284.01	1n	<i>Cr</i> II 84.21 (20)
4287.54	1n	<i>Ti</i> II 87.88 (30)
4289.91	4n	<i>Ti</i> II 90.23 (60), <i>Cr</i> I 89.72 (3000)
4293.98	4	<i>Ti</i> II 94.12 (60), <i>Fe</i> I 94.13 (700)
4296.64	5	<i>Fe</i> II 96.57 (6)
4300.08	4	<i>Ti</i> II 00.05 (100)
4301.83	1	<i>Ti</i> II 01.93 (50)
4303.19	5	<i>Fe</i> II 03.17 (8)
4306.63	0n	<i>Al</i> II 7.16 (20)
4307.68	3n	<i>Fe</i> I 07.91 (1000), <i>Ti</i> II 07.91 (100)
4310.06	0n	$\alpha$ Cyg

TABLE 1—*Continued*

Wave Length	Int.	Identification
4312.74	3n	<i>Fe</i> II 13.03 (1), <i>Ti</i> II 12.87 (100)
4314.75	4n	<i>Fe</i> II 14.29 (4), <i>Ti</i> II 14.98 (100), <i>Fe</i> I 15.09 (500)
4316.63	0	<i>Ti</i> II 16.80 (35)
4320.73	1n	<i>Ti</i> II 20.96 (40), <i>Sc</i> II 20.75 (40)
4325.42	4	<i>Fe</i> I 25.76 (1000), <i>Sc</i> II 25.01 (40)
4330.89	0nn	<i>Ti</i> II 30.24 (40), <i>Ti</i> II 30.71 (30)
4333.33	0n	Pleione
4337.50	1n	<i>Ti</i> II 37.92 (125)
4340.52	20	<i>Hγ</i> 40.47 (200)
4343.69	1nn	<i>Ti</i> II 44.29 (50)
4345.88	1n	
4351.83	6	<i>Fe</i> II 51.76 (9)
4357.57	3n	<i>Fe</i> II 57.57 (4)
4361.58	2nn	<i>Fe</i> II 61.25 (2)
4363.43	0	<i>Cr</i> II 62.93 (3)
4368.22	3n	<i>O</i> I 68.30 (1000), <i>Fe</i> II 68.26 (1)
4370.92	0	( <i>Zr</i> II 70.95 (7))
4374.01	0n	<i>Sc</i> II 74.46 (25), <i>Ti</i> II 74.82 (35)
4383.96	2n	<i>Fe</i> I 83.55 (1000)
4385.52	5	<i>Fe</i> II 85.38 (7)
4390.58	1nn	<i>Ti</i> II 90.03 (25), <i>Fe</i> I 90.95 (100), <i>Mg</i> II 90.58 (10)
4394.95	3	<i>Ti</i> II 95.04 (150)
4399.72	2n	<i>Ti</i> II 99.77 (100)
4403.00	1	<i>Fe</i> II 02.87 (2)
4404.41	0	<i>Fe</i> I 04.75 (1000)
4411.52	1n	<i>Ti</i> II 11.08 (100)
4414.00	0	<i>Fe</i> II 13.60 (0)
4416.93	5n	<i>Fe</i> II 16.82 (7), ( <i>Ti</i> II 17.72 (80))
4421.66	1nn	<i>Ti</i> II 21.95 (35)
4425.15	1	
4430.77	1	<i>Fe</i> I 30.62 (200)
4434.01	0	<i>Mg</i> II 33.99 (8)
4436.39	0	<i>Mg</i> II 36.48 (5)
4443.57	4n	<i>Ti</i> II 43.80 (125)
4445.57	0n	$\alpha$ Cyg
4449.76	2	<i>Ti</i> II 50.49 (50), <i>Fe</i> II 49.66 (1)
4451.53	3	<i>Fe</i> II 51.54 (4)
4455.34	2n	<i>Fe</i> II 55.26 (3)
4461.74	1n	<i>Fe</i> I 61.65 (300), ( <i>Zr</i> II 61.22 (10))
4464.06	1	<i>Ti</i> II 64.46 (40), <i>V</i> II 64.32 (40)
4468.53	3	<i>Ti</i> II 68.50 (150)
4470.47	0	<i>Ti</i> II 70.86 (25)
4472.56	3nn	<i>Fe</i> II 72.96 (2), <i>He</i> I 71.48 (100)
4480.88	3n	<i>Mg</i> II 81.33 (100), <i>Fe</i> II 80.69 (1)
4483.29	0n	<i>S</i> II 83.42 (100), <i>S</i> II 83.63 (50)
4489.02	3n	<i>Fe</i> II 89.18 (4), <i>Ti</i> II 88.32 (125)
4491.41	3n	<i>Fe</i> II 91.40 (5)
4496.43	0	<i>Fe</i> II 95.52 (pred)
4499.73	0	<i>Fe</i> II 99.71 (0)
4501.12	3	<i>Ti</i> II 01.28 (100)

TABLE 1—Continued

Wave Length	Int.	Identification
4508.24.....	6	<i>Fe</i> II 08.28 (8)
4515.29.....	6	<i>Fe</i> II 15.34 (7)
4520.24.....	5	<i>Fe</i> II 20.22 (7)
4522.62.....	6	<i>Fe</i> II 22.63 (9)
4528.30.....	1n	<i>Fe</i> I 28.62 (600), <i>V</i> II 28.51 (300)
4529.98.....	1n	<i>Ti</i> II 29.46 (40)
4533.91.....	3n	<i>Fe</i> II 34.17 (2), <i>Ti</i> II 33.97 (150)
4538.58.....	1nn	
4541.47.....	3	<i>Fe</i> II 41.52 (4)
4543.45.....	1	( <i>Ti</i> II 44.01 (20))
4549.49.....	10	<i>Fe</i> II 49.47 (10), <i>Ti</i> II 49.63 (200), <i>Fe</i> II 49.21 (4)
4552.10.....	0	$\alpha$ Cyg
4555.70.....	5n	<i>Fe</i> II 55.89 (8), <i>Cr</i> II 55.02 (20)
4558.60.....	4	<i>Cr</i> II 58.66 (100)
4563.79.....	3n	<i>Ti</i> II 63.77 (200), ( <i>V</i> II 64.59 (200))
4566.20.....	1	<i>Cr</i> II 65.78 (10)
4571.75.....	3	<i>Ti</i> II 71.98 (300)
4576.16.....	3	<i>Fe</i> II 76.33 (4)
4579.83.....	1n	<i>Fe</i> II 80.05 (1), <i>Fe</i> II 79.52 (1)
4583.71.....	10	<i>Fe</i> II 83.83 (11)
4588.27.....	4	<i>Cr</i> II 88.22 (75)
4591.94.....	1	<i>Cr</i> II 92.09 (20)
4595.96.....	3	( <i>A</i> I 96.10 (1000)), ( <i>Fe</i> II 95.68 (pred))
4616.58.....	1	<i>Cr</i> II 16.64 (18)
4618.59.....	3	<i>Cr</i> II 18.83 (35)
4620.68.....	2	<i>Fe</i> II 20.51 (3)
4625.05.....	0	<i>Fe</i> I 25.05 (100), <i>Fe</i> II 25.55 (tr)
4629.18.....	8	<i>Fe</i> II 29.34 (7)
4634.05.....	3	<i>Cr</i> II 34.11 (25)
4635.21.....	3	<i>Fe</i> II 35.33 (5)
4641.02.....	1n	<i>Fe</i> II 40.84 (0)
4656.87.....	1	<i>Fe</i> II 56.97 (1)
4662.76.....	0	<i>Al</i> II 63.05 (50)
4666.99.....	2	<i>Fe</i> II 66.75 (2)
4670.19.....	1	<i>Sc</i> II 70.40 (300), <i>Fe</i> II 70.17 (0)
4731.29.....	3	<i>Fe</i> II 31.44 (3)
4823.61.....	3	<i>Cr</i> II 24.13 (75)
4861.68.....	20	<i>H</i> $\beta$ 61.33 (500)

April, 1940. Their purpose was to provide material for a physical study of the shell, similar to other studies carried out at Yerkes and McDonald observatories, and at the same time to follow the changes in radial velocity discovered by Merrill and Sanford.

The spectrum as photographed at the McDonald Observatory in March, 1943, is shown in Plates IX and X. It is characterized by the great strength and the unusual sharpness of the shell lines of *H*. I have measured them to *H* 34 and believe the illustration shows *H* 35. This exceptional extension of the Balmer series, which surpasses that of supergiants like  $\alpha$  Cygni and of shells like  $\zeta$  Tauri and Pleione, is not an indication of exceptionally great luminosity, as one is tempted to infer from the work of Unsöld and Struve on ordinary and supergiant stars.<sup>8</sup> The correlation found in that work can be used only for normal stars, not for the tenuous shells of stars like 48 Librae. Table 1

<sup>8</sup> *A p. J.*, 91, 365, 1940.

gives the entire list of lines which I have measured between  $\lambda$  3289 and  $\lambda$  4862. It should be compared with the list of lines of Pleione—another remarkable example of a shell spectrum.<sup>9</sup>

The spectrum of 48 Librae differs in several important points from that of Pleione. Its *H* lines are very much stronger, as are also its lines of *Ni* II. The lines of *Fe* II and *Cr* II are similar in the two shells, while *Ti* II and *Mn* II are much weaker in 48 Librae. In the relative intensities of the lines of different atoms, 48 Librae resembles the spectrum of Pleione as observed in 1940; but all lines of 48 Librae are now much stronger than were those of Pleione in 1940. Moreover, Pleione has shown a gradual change in the relative intensities of the different atoms, with *Ti* II and *Mn* II becoming much stronger in 1941 and 1942, respectively. There has been no such evolution in 48 Librae, at least since 1940.

The *H* lines of the shell are superposed over broad wings, characteristic of strong Stark widening. The underlying star is thus a main-sequence B star. Relative to Pleione, the broad wings are more conspicuous in 48 Librae, which may indicate less continuous absorption in the shell or a stronger underlying line. The sharp shell lines are approximately symmetrical with the broad wings.

The contours of the sharp shell lines are not symmetrical: they are shaded toward the violet and have steep edges on their red sides. This must be caused by the distribution of turbulent motions in the shell and may account for the anomalous velocities measured by Merrill and Sanford and for those presented in this paper. The line *Ca* II K is also unsymmetrical. This is visible on Plate X, which was obtained with the moderate dispersion of 20 Å/mm at  $\lambda$  3930 on a Process film.

A plate on emulsion Eastman 103a0 was obtained with the coudé spectrograph on May 16, 1943, the linear dispersion being 3.0 Å/mm at  $\lambda$  4360. Three sections of a tracing of this plate, made with the Beals microphotometer of the Yerkes Observatory, are shown in Figure 1. All moderately strong lines of *Fe* II and *Ti* II are unsymmetrical—in the same sense as are the *H* lines and *Ca* II K. The *Mg* II line  $\lambda$  4481 is very slightly unsymmetrical, suggesting an overlap of a symmetrical, rounded contour with an unsymmetrical contour having a sharp minimum. The weaker lines of *Ti* II ( $\lambda$  4321) and *Fe* I ( $\lambda$  4326) are symmetrical and have rounded bottoms. These lines give the appearance of a moderate amount of rotational broadening, in contradistinction to the unsymmetrical lines whose pointed contours do not suggest rotation.

The unsymmetrical lines present an interesting astrophysical problem. The measured velocities in Table 1 refer to the centers of gravity of the lines, the contours being completely redistributed by the spectrograph. It is probable that the sharp minima of the stronger *Fe* II lines show little relative motion with respect to the star as a whole. The violet wings extend approximately 1.8 Å from these sharp minima. This corresponds to a velocity of expansion of the order of 120 km/sec. But a uniformly expanding reversing layer shows a contour which is shaded in the opposite sense, as was first shown by Shapley and Nicholson. Hence, we cannot attribute the effect to the geometrical factor which arises when the radius of the shell is but slightly in excess of the radius of the photosphere, and we must assume that the observed range in velocities actually exists within the shell. If this is correct, we have here a situation which resembles that in 17 Leporis, where the absorption lines are also often shaded toward the violet, when they are not actually double. Apparently the distribution of velocities in the shells of both stars is such that the shading is toward the violet.

This presupposes that the unsymmetrical appearance of the stronger *Fe* II and *Ti* II lines is not caused by the superposition of red-displaced emission lines. Although no *Fe* II or *Ti* II emission can be seen in 48 Librae, they are sometimes observed in 17 Leporis. It is possible that the red wings of the lines in question are appreciably modified by

<sup>9</sup> Struve and Swings. *Ast. J.*, **97**, 426, 1943.

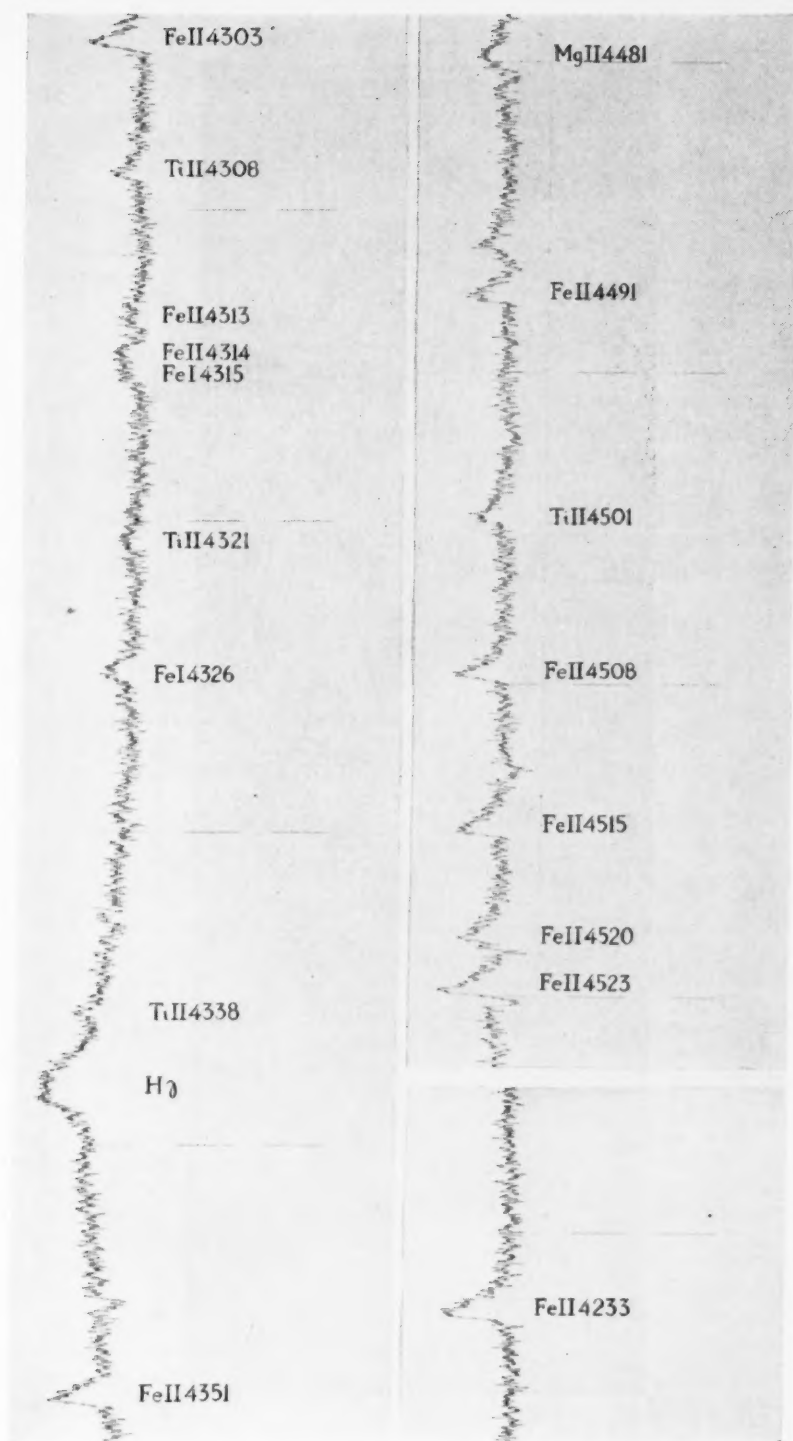


FIG. 1.—Tracings of sections of spectrogram of 48 Librae taken May 16, 1943

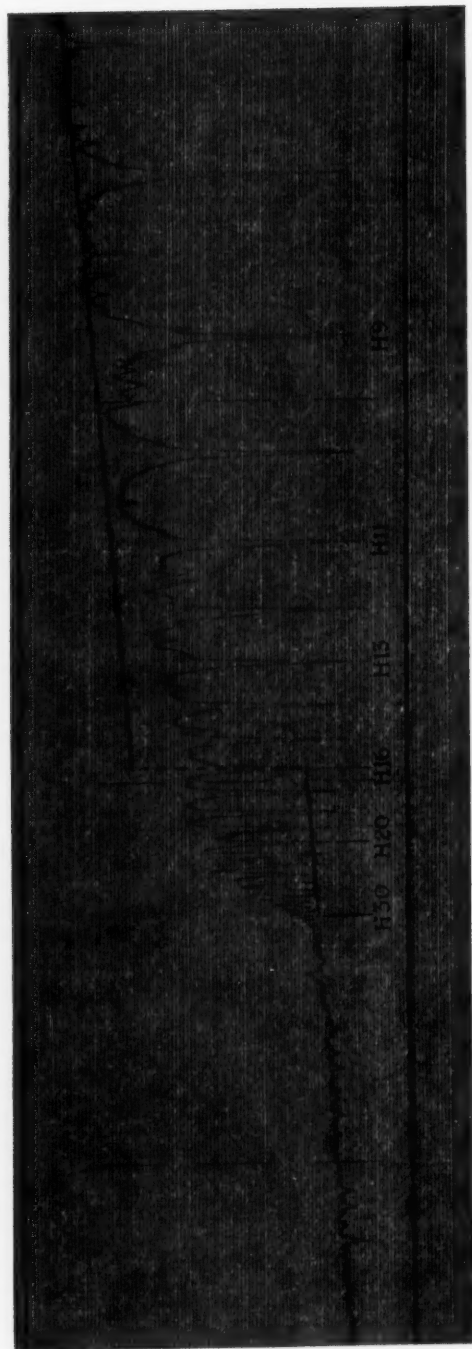


FIG. 2.—Tracing of spectrogram of 48 Librae taken in March, 1943

emission. Nevertheless, the violet contours are so characteristically pointed—more like an *H* line broadened by Stark effect than a metallic line broadened by rotation—that I am inclined to prefer the interpretation in terms of a large range in velocities of expansion within the shell.

The “jump” at the Balmer limit is very steep. It is illustrated in the tracing in Figure 2. The jump, as measured at  $\lambda$  3700 by means of the calibration marks, is  $D = \Delta \log_{10} F_{\nu} = 0.35$ . This is considerably more than was observed by Barbier, Chalonge, and their collaborators in stars of type B3 or B5 ( $D = 0.17$  and  $0.25$ , respectively)<sup>10</sup> but is less than observed by them in type A0 ( $D = 0.47$ ). The Balmer jump in 48 Librae is produced mostly in the shell. In this respect the star is quite different from Pleione, where the Balmer jump was small.

The broad *He I* lines are easily visible in the ordinary photographic region, although they are blended with sharp metallic lines produced in the shell. These *He I* lines are similar in width to those observed in 1935 and before. It is difficult to decide whether they have become fainter as a result of continuous absorption in the shell. However, since on the Process film used for Plate X  $\lambda$  4472 ( $2^3P^0 - 4^3D$ ),  $\lambda$  4144 ( $2^1P^0 - 6^1D$ ), and  $\lambda$  4026 ( $2^3P^0 - 5^3D$ ) are conspicuous through their enormous widths, it is to be expected that under normal conditions  $\lambda$  3820 ( $2^3P^0 - 6^3D$ ),  $\lambda$  3705 ( $2^3P^0 - 7^3D$ ), and  $\lambda$  3634 ( $2^3P^0 - 8^3D$ ) would also be seen, especially on the more contrasty Process plate used for Plate IX. However, only a trace of  $\lambda$  3820 is seen. The usual absorption intensities in B-type stars are:

LINE	INTENSITY	
	$\gamma$ Pegasi	$\beta$ Cephei
He I 3820 . . . . .	15	10
3705 . . . . .	10	10
3634 . . . . .	6	7

The complete absence of  $\lambda$  3634 in 48 Librae is probably a good indication that the underlying *He I* line is effectively blotted out by the increased continuous absorption on the violet side of the Balmer limit.

Although the shells are known to be more tenuous than the reversing layers of normal supergiant stars, the Balmer jump does not take place abruptly; this shows that, even at the low densities prevailing in this shell, Stark broadening is not altogether negligible.

There appears to be a marked tendency for many weak lines to be nebulous in appearance. A similar tendency has been observed in Pleione, and probably in other shells; but it has not heretofore been possible to isolate this effect from the confusing influence of blends, except in the case of 14 Comae Berenices, where it is very conspicuous.<sup>11</sup> Table 1 shows many unblended lines which are conspicuously nebulous in character. In a general way it appears that all strong shell lines are narrow and sharp (although slightly unsymmetrical, as in the case of *H*). The high members of the Balmer series are sharp, though weak. The other weak lines, especially of *Fe I* and *Ti II*, are nebulous, though I am not prepared to say that they are more nebulous than weak lines of *Fe II* and *Cr II*. However, none of these lines even approaches the *He I* lines in diffuseness. I suggest that we are looking into a shell which rotates with conservation of angular momentum, so that the strong lines come principally from the slowly rotating outermost layers, while the weak lines come from deeper layers which rotate more rapidly. This interpretation applies also to such stars as 14 Comae and  $\zeta$  Tauri.

<sup>10</sup> *Ap. J.*, 97, 445, 1943.

<sup>11</sup> *Ap. J.*, 94, 305, 1941.

The lines of  $Si$  II and  $Mg$  II are relatively stronger than they are in Pleione and in other shells. These lines are somewhat nebulous, but not more so than are the weaker lines of  $Ti$  II and  $Fe$  I. If 48 Librae is compared with  $\alpha$  Cygni, the lines of  $Si$  II and  $Mg$  II are seen to be noticeably weakened through the effect of geometrical dilution, but this effect is smaller than in Pleione. Both  $Mg$  II and  $Si$  II are produced in the lower strata of the shell and not in the reversing layer where the broad lines of  $He$  I and the wings of  $H$  are produced.

We again notice the great strength of  $Mg$  I—a feature already observed in other shells. I believe that the most reasonable explanation of this effect lies in the weakening of the three ultraviolet  $Mg$  I lines—the only ones thus far observed systematically in shells—in the wings of  $H$  9, even in such supergiants as  $\alpha$  Cygni. There can be no question that the wing formation is conspicuous in these stars and must give rise to increased opacity.

The ultraviolet spectrum, to the violet of  $\lambda$  3650, is deficient in lines and shows to a very marked degree the weakening of lines by continuous  $H$  absorption. This weakening is most conspicuous in the case of  $Ti$  II. These lines have been almost completely obliterated on the violet side of  $\lambda$  3650, when they are compared with the same lines in Pleione. On the other hand, in the ordinary photographic region the lines of  $Ti$  II are only slightly fainter in 48 Librae than they are in Pleione. This effect is so conspicuous that its absence in the case of  $Ni$  II becomes extremely striking. These lines are very strong all over the spectrum, and there is no indication of any weakening by continuous  $H$  absorption. The lines of  $Fe$  II and  $Cr$  II behave in an intermediate manner. We conclude that the shell is stratified, with  $Ni$  II—producing exceptionally sharp lines—at the top, where it is least affected by continuous  $H$  absorption, and  $Ti$  II (and probably  $Mn$  II) in the deeper layers, where the lines are subject to more rotational broadening and to greater weakening by  $H$ .

The great depth of the  $H$  cores already observed in Pleione is conspicuously present in the case of 48 Librae. We again conclude that the explanation lies in the small amount of re-emission which is thrown into the observed beam within the frequencies of the Balmer lines.

The star 48 Librae presents, therefore, a notable paradox: to the violet of  $\lambda$  3650 the shell is essentially opaque; and the continuous spectrum must, therefore, arise very largely within the shell. This is inferred from (a) the absence of  $He$  I lines, (b) the large Balmer jump, and (c) the weakening of shell lines of  $Ti$  II. But in the ordinary photographic region the shell is sufficiently transparent to permit us to see the rotationally broadened lines of  $He$  I and the wings of the  $H$  lines. Hence, within these wave lengths the continuous spectrum is mostly that of the B-type star. With a filter for light of  $\lambda < 3650$  and a sufficiently high magnification, the object would look like a disk the size of the shell, while with a filter for  $\lambda > 3650$  the diameter of the object would correspond to that of a main-sequence B star. We have in this case no accurate determination of the size of the shell, but the dilution effect and the great sharpness of the  $H$  lines suggest a structure which may not be very different in size from that of an early-type supergiant.<sup>12</sup> The paradox consists of the fact that for light of  $\lambda < 3650$  we observe in effect a supergiant, while for light of a few hundred angstroms longer wave lengths we observe a main-sequence star. In reality, the transition may not be quite so extreme. But it is difficult to escape the conclusion that 48 Librae is in some respects an object intermediate between an A-type supergiant and a B-type main-sequence star.

There are, unfortunately, no other observations which would confirm or disprove this intermediate character of 48 Librae. Nor are we aware of any recent observations of the magnitude or color index of this star. The interpretation of the continuous spectrum would be, at best, a complicated procedure. The ultraviolet spectrum corresponds to a

<sup>12</sup> See the corresponding discussion of the shell of Pleione in *Ap. J.*, 93, 451, 1941.

lower temperature, but it comes from a larger area than the continuous spectrum at  $\lambda > 3650$ . Prior to the origin of the shell the entire spectrum must have been that of a normal B star.

Caution must also be exercised in the interpretation of the geometrical dilution. If we compare the *Si* II and *Mg* II lines with neighboring lines of *Fe* II, *Ti* II, and *Cr* II (whose lower levels are metastable) in 48 Librae and in  $\alpha$  Cygni, we estimate that the dilution effect produces a weakening of these lines by a factor of perhaps 3 in the equivalent widths. In several other shells the corresponding weakening was estimated to be of the order of 10 or even 100. Does this mean that the shell of 48 Librae is smaller, or is it a consequence of the greater ultraviolet opacity of this shell? To answer this question we would have to compute the density of radiation in those wave lengths which are required to feed the atoms into the lower (nonmetastable) levels of the lines of *Si* II and *Mg* II.

It is probably premature to consider this problem at the present time. For the two *Si* II lines,  $\lambda$  4128 and  $\lambda$  4131 ( $3^2D - 4^2F^0$ ), we require either direct transitions from the ground level, through the absorption of  $\lambda$  1265 and  $\lambda$  1261, or recombination from the doubly ionized state, which requires an energy of 16.3 volts. In both regions the shell should be very transparent, so far as continuous *H* absorption is concerned.<sup>13</sup> This would suggest that the dilution is correctly shown by the estimated factor and that the shell is relatively small. It is difficult to apply the usual formula for the dilution factor

$$W = \frac{1}{2} \left\{ 1 - \sqrt{1 - \frac{R^2}{r^2}} \right\}$$

unless we assume that for  $\alpha$  Cygni  $W = 0.5$  and, hence, for 48 Librae

$$W = 0.17 .$$

In that case we find

$$\frac{r}{R} = 1.3 .$$

The effective thickness of the shell, where *Si* II and *Mg* II originate, is about one-third of the radius of the B-type star, and presumably the entire shell may be two or three times thicker.

We cannot trust these figures to give us more than a general idea of the order of magnitude of the tenuous structure which we are discussing.

The interpretation of the ionization of the shell encounters great difficulties when we compare 48 Librae and Pleione. Assuming, for the moment, that both shells are uniform, we conclude that the shell of 48 Librae contains more *H* atoms in the second energy-level, per square centimeter, than does the shell of Pleione. But the latter contains more *Mn* II and *Ti* II per square centimeter and less *Ni* II than 48 Librae. This would suggest higher ionization in 48 Librae, since the ionization potential of *Ni* II is 18.2 volts, while the potentials of *Ti* II and *Mn* II are 13.6 and 15.7 volts, respectively. But the ionization potential of *H* is 13.5 volts—almost identical with that of *Ti* II. Hence, in terms of the ordinary theory of ionization, the observations can only be reconciled by assuming that (a) the composition of the two shells is not the same or (b) conditions of excitation and ionization are influenced by physical dilution factors of the type we have discussed elsewhere. In the case of Pleione we have already encountered insurmountable difficulties in the application of the theory of ionization to the evolution of the line intensities.<sup>14</sup> In that shell the gradual strengthening of *Mn* II and *Ti* II went parallel with a strengthening of the Balmer absorption lines.

<sup>13</sup> See Unsöld's convenient diagrams of  $\kappa'_v/P_e$  for  $T = 28,150^\circ$ , in *Zs. f. Ap.*, 21, 229, 1942.

<sup>14</sup> *Ap. J.*, 97, 439, 1943.

TABLE 2  
RADIAL VELOCITIES OF 48 LIBRAE

DATE	U.T.	VELOCITY			OBSERVATORY QUALITY
		All Lines	<i>Fe</i> II, <i>Si</i> II, <i>Ti</i> II, <i>Cr</i> II, <i>Sc</i> II, <i>Mg</i> II	<i>H</i>	
1940 April 28.....	8:02	+ 4.8	.....	+ 4.8	Y poor
1941 Feb. 10.....	11:23	+21.6	+23.8	+ 6.3	Y good
Feb. 16.....	10:32	+26.3	+28.9	+15.7	Y poor
Mar. 13.....	9:36	+26.3	+28.2	+17.8	Y poor
April 7.....	8:57	+20.4	+21.4	+14.3	Y good
April 24.....	7:33	+22.1	+21.7	+24.7	Y good
April 25.....	7:01	+22.4	+23.0	+18.7	Y good
1942 Feb. 12.....	11:40	+16.3	+16.2	+17.2	Y good
Feb. 20.....	10:30	+12.9	+12.1	+17.6	Y good
April 14.....	7:44	+10.8	+10.5	+12.5	Y good
May 26.....	7:05	+12.5	+11.5	+14.3	Y poor
June 20.....	3:58	+22.4	+20.7	+25.7	Y poor
June 30.....	2:40	+ 4.5	+ 4.1	+ 7.7	Y good
July 12.....	2:36	+ 9.9	+ 9.5	+13.9	Y good
July 27.....	2:38	+10.4	+ 9.5	+17.6	Y good
1943 Feb. 16.....	10:39	- 5.8	- 7.3	+ 4.9	Y good
Feb. 19.....	11:47	+ 3.2	+ 1.8	+ 6.1	Y poor
Feb. 25.....	10:58	- 9.5	-10.8	+ 2.2	Y good
Mar. 2.....	10:23	- 3.4	- 8.5	- 0.3	M good
Mar. 4.....	10:47	- 6.9	-10.5	- 3.3	M good
Mar. 7.....	10:45	+ 3.4	+ 3.4	.....	M good
Mar. 9.....	11:10	+ 1.6	- 2.3	+ 4.3	M good
Mar. 11.....	11:20	- 2.2	- 2.9	+ 1.7	M good
Mar. 13.....	10:53	- 0.6	- 1.0	+ 1.2	M good
Mar. 21.....	9:12	- 9.8	-10.3	- 4.4	Y good
Mar. 22.....	9:47	- 5.7	- 7.2	+ 6.2	Y good
April 1.....	7:54	- 7.9	- 9.7	+ 4.2	Y good
April 8.....	7:45	-11.9	-13.4	- 0.7	Y good
April 8.....	8:59	-11.3	-12.8	- 2.4	Y good
April 14.....	9:22	-12.4	-13.2	- 7.2	Y good
April 15.....	8:51	- 9.6	-11.2	+ 1.2	Y good
April 21.....	7:32	- 5.5	- 6.5	+ 0.9	Y good
May 1.....	6:22	- 7.5	- 8.4	- 1.3	Y good
May 10.....	7:25	- 1.9	- 4.0	- 0.9	M good
May 16.....	7:57	- 4.6	- 4.6	- 4.8	M good
May 25.....	5:10	- 9.6	- 9.6	-10.6	Y poor
May 28.....	3:39	- 7.7	- 8.1	- 4.4	Y good
June 8.....	3:10	-17.5	-18.6	- 9.5	Y good
June 9.....	2:36	-18.0	-19.5	- 6.8	Y good
June 9.....	3:43	-13.1	-15.0	+ 0.3	Y good
June 11.....	5:28	-13.3	-13.8	- 5.9	Y good

The  $H$  emission lines have shown marked changes in  $V/R$ . The estimated values for  $H\beta$  are summarized as follows:

Average Time	No. of Obs.	V/R	Average Time	No. of Obs.	V/R
1935 June.....	1	0.5	1942 April.....	7	2.0
1940 April.....	1	2.0	1943 March.....	5	1.4
1941 April.....	5	3.0	1943 May.....	5	1.5

The width of bright  $H\beta$ , measured between the violet edge of the violet component and the red edge of the red component, corresponds to a rotational velocity of about 240 km/sec. The broad absorption lines of  $He\ I$ , as photographed in 1935, when they were relatively little blended with sharp metallic lines, give a rotational velocity of about 300 km/sec.

The radial velocities are listed in Table 2. The Balmer lines measured on the Yerkes plates consisted of  $H\epsilon$ ,  $H\delta$ ,  $H\gamma$ , and  $H\beta$ . On the McDonald plates some twenty ultra-violet  $H$  lines were usually measured. There were appreciable variations from year to year, but it seems profitable to postpone their discussion until the Mount Wilson results have been published in detail.

## RECENT PROGRESS IN ASTROPHYSICS

### EDLÉN'S IDENTIFICATION OF THE CORONAL LINES WITH FORBIDDEN LINES OF *Fe* x, xi, xiii, xiv, xv; *Ni* xii, xiii, xv, xvi; *Ca* xii, xiii, xv; *A* x, xiv<sup>1</sup>

For seventy years the line spectrum of the solar corona has been observed at practically all eclipse expeditions. Since 1936 it has been also obtained with coronagraphs. There are more than twenty lines present in the inner corona, some of them quite conspicuous, especially a green line ( $\lambda$  5303), two red ones ( $\lambda$  6375 and  $\lambda$  6702), two in the infrared ( $\lambda$  10,747 and  $\lambda$  10,798), and one in the ultraviolet ( $\lambda$  3388). The green line is the strongest of all. These lines have been measured very often; they are not as sharp as the nebular lines but have rather a diffuse character. Their behavior has been examined at different eclipses; the monochromatic images of the corona in various wave lengths have been compared; the intensity decrease of the lines with increasing distance from the limb is not identical for all lines; and, finally, certain coronal lines have been observed in Nova RS Ophiuchi in 1932 and in 1942. From all these observations the coronal lines have been classified in a number of groups, probably belonging to specific excitations. The most reliable of such groupings was made by Lyot.<sup>2</sup> Yet, despite the considerable amount of data accumulated on the coronal lines, no satisfactory identification was available until quite recently. All possibilities based on the usual (i.e., normal or ionized once, twice, or three times) atoms or molecules had failed. Neither forbidden lines, Raman effects, nor peculiar types of excitation could provide an interpretation of the corona.<sup>3</sup> After Bowen had succeeded in 1927 in interpreting the strongest nebular radiations, the coronal lines remained the most spectacular spectroscopic mystery in astronomy. This problem has now been solved by the Swedish physicist B. Edlén.<sup>1</sup> Among the other less spectacular unidentified astronomical spectra, several have been interpreted in the course of the last four years: sharp interstellar absorption lines as due to molecules of *CH*, *CN*, and *CH*<sup>+</sup>; the  $\lambda$  4050 group of emission features in comets as due to *CH*<sub>2</sub>; and numerous lines in early-type objects as due to permitted or forbidden transitions in *Fe* iii, v, vi, and vii. Hence, at the present time the only important spectroscopic features which still remain unidentified are the diffuse interstellar absorption lines and certain emission bands of supernovae. The present review is concerned with Edlén's discovery. It has appeared to me that some historical remarks might not be out of place since I have collaborated with Edlén in several other spectroscopic investigations and since the first list of coincidences with coronal wave lengths was communicated to me by Edlén in June, 1939. Edlén had been thinking of the corona problem for many years. In 1934 we had spent three months together discussing all possibilities existing at that time. In 1937 we started our joint investigation of the *Fe* iii spectrum with a slight hope that it might be of some help in identifying the coronal lines! In 1939 W. Grotrian<sup>4</sup> pointed out<sup>5</sup> that the term separations  $3s^23p^5\ ^2P_{1/2} - ^2P_{1/2}$  of *Fe* x and  $3s^23p^4\ ^3P_1 - ^3P_2$  of *Fe* xi, as determined in the extreme ultraviolet by Edlén,<sup>6</sup> coincide

<sup>1</sup> B. Edlén, *Arkiv f. Matem., Astr. och Fys.*, **28**, B, No. 1, 1941; *Zs. f. Ap.*, **22**, 30, 1942.

<sup>2</sup> *C.R.*, **202**, 1259, 1936; *ibid.*, **203**, 1327, 1936; *L'Astronomie*, **51**, 203, 1937; *C.R.*, **206**, 648, 1938; *M.N.*, **99**, 580, 1939.

<sup>3</sup> P. Swings, *Scientia*, **33**, 69, 1939.

<sup>4</sup> *Naturwiss.*, **27**, 214, 1939.

<sup>5</sup> Throughout this review the levels are named in the order: initial level minus end level, as in Edlén's paper.

<sup>6</sup> *Zs. f. Phys.*, **103**, 536, 1936; *ibid.*, **104**, 188 and 407, 1937.

with the wave numbers of the two coronal lines  $\lambda$  6374 and  $\lambda$  7892. This remark by Grotrian came at about the time Edlén was preparing his report on the spectra of novae in their nebular stages which was to be presented at the Paris conference on novae. Edlén became deeply interested in Grotrian's remark. From his unpublished measurements of the spectra of *Ca* XII and *Ca* XIII he found that the separations in the  $2s^22p^5$  and  $2s^22p^4$  configurations of these two ions also coincided within the experimental errors with two fainter coronal lines ( $\lambda$  3328 and  $\lambda$  4086). Assuming the identifications of *Fe* X and XI, *Ca* XII and XIII, to be correct, Edlén proceeded with the prediction of the forbidden lines of *Fe* XIII, XIV, *Ni* XII, etc., and found a number of coincidences which at that time (June–July, 1939) already seemed too remarkable to be due purely to coincidences. I had the privilege of seeing this first table and of discussing it with Edlén

TABLE 1  
THE EXPERIMENTAL BASIS FOR THE DIRECT IDENTIFICATION OF CORONAL LINES

Transitions	$\lambda$ (Vacuum Spark)	$\nu$ $\text{Cm}^{-1}$	Level Separations	$\nu$ Corona
<i>Fe</i> X $3s^23p^5-3s^23p^44s$ :				
$^2P_{1/2}-^2P_{3/2}$ .....	95.338 (1)	1,048,900}	15,714	
$^2P_{3/2}-^2P_{5/2}$ .....	96.788 (2)	1,033,186}		
$^2P_{1/2}-^2P_{3/2}$ .....	96.122 (4)	1,040,345}	15,660	
$^2P_{3/2}-^2P_{5/2}$ .....	97.591 (0)	1,024,685}		
Av.....			15,687	15,683
<i>Fe</i> XI $3s^23p^4-3s^23p^34s$ :				
$^3P_2-^3D_2$ .....	87.025 (1 <sup>+</sup> )	1,149,095}	12,667	
$^3P_1-^3D_2$ .....	87.995 (0)	1,136,428}		
$^3P_2-^3S_1$ .....	89.185 (1 <sup>+</sup> )	1,121,265}	12,679	
$^3P_1-^3S_1$ .....	90.205 (1)	1,108,586}		
Av.....			12,673	12,668
<i>Ca</i> XII $2s^22p^6-2s2p^6$ :				
$^2P_{1/2}-^2S_{1/2}$ .....	141.036 (8)	709,039}	30,028	30,039
$^2P_{3/2}-^2S_{1/2}$ .....	147.273 (6)	679,011}		
<i>Ca</i> XIII $2s^22p^4-2s2p^5$ :				
$^3P_2-^3P_2$ .....	161.748 (1d)	618,246}	24,464	24,465
$^3P_1-^3P_2$ .....	168.412 (00d)	593,782}		

in June–July, 1939, while he was spending a few weeks in my laboratory in Belgium on his way to and from the Paris meeting. Yet he refrained from mentioning his results at the conference even when he was questioned on the problem of coronal lines in novae: modestly, he wanted to study the matter further. The first announcement in a scientific periodical appeared in 1941 under the title "An Attempt To Identify the Emission Lines in the Spectrum of the Solar Corona."<sup>1</sup> A complete account has now been published in the *Zeitschrift für Astrophysik*, **22**, 30, 1942. A few typewritten copies of this last paper have been received in this country from the author.

#### I. WAVE-NUMBER COINCIDENCES WITH DIRECTLY OBSERVED TERM SEPARATIONS

The coincidences between the level separations of *Fe* X and XI and *Ca* XII and XIII, as determined in the laboratory by Edlén<sup>6</sup> and the wave numbers of coronal lines, are listed in Table 1.

The level separations are necessarily rather uncertain, since they are determined

through lines of very short wave lengths. Other transitions of *Fe* x and xi of longer wave lengths may eventually provide better laboratory values of the ground-term separations. As for the calcium lines of Table 1, they represent the largest wave lengths in which the ground terms are involved.

Although the coincidences of Table 1 are rather impressive, they cannot quite make the identification conclusive, owing to the present unavoidable relatively wide tolerances. The decisive fact is that, assuming the identifications of  $\lambda\lambda$  6374 (*Fe* x), 7892 (*Fe* xi), 3328 (*Ca* xii), and 4086 (*Ca* xiii) to be correct, an almost complete identification of the coronal spectrum can be consistently carried through, as will be shown below. First, it should be noticed that the [*Fe* vii] lines which have been observed in several novae and peculiar stars do not appear in the corona. Besides, the ground configuration of *Fe* ix gives only one single level and *Fe* ix has no metastable state. As for *Fe* viii, the splitting of the ground term  $^2D$  is too small to give any astronomically observable transition. Hence, as far as iron is concerned, the investigation should be concerned with *Fe* x and higher stages of ionization. Similar considerations apply to other atoms, especially nickel. A survey of possible level separations shows that coronal transitions should be searched for mainly within the configurations  $3s^23p$ ,  $3s^23p^2$ ,  $3s^23p^4$ , and  $3s^23p^5$  of the elements in the iron group.<sup>7</sup> Because of the relative cosmical abundances, iron should be expected first; nickel next.

## II. TERM INTERVALS IN THE CONFIGURATIONS

### $3s^23p$ , $3s^23p^2$ , $3s^23p^4$ , AND $3s^23p^5$ OF *Fe* AND *Ni*

The configurations  $3s^23p$  and  $3s^23p^5$  give rise to a  $^2P$  term only, whose splitting can be easily and accurately extrapolated according to the regular doublet law. Hence, this splitting varies with the atomic number  $Z$  as  $(Z - \sigma)^4$ , the screening constant  $\sigma$  being nearly constant. The data for the  $3s^23p$  and  $3s^23p^5$  sequences are collected in Table 2. The linear variation of  $\sqrt{\zeta}$ ,  $\zeta$  being two-thirds of the term separation, appears clearly.

In the  $3s^23p$  sequence, the splitting could be determined up to *Sc* ix by lines of the  $3s^23p^k - 3s3p^{k+1}$  type of transition, and correspondingly up to *V* vii for  $3s^23p^5$ . These transitions have considerably longer wave lengths than other combinations with the ground term, particularly for the higher stages of ionization. Hence, they will provide the most accurate values for the level separations. The separations for *Cr* viii, *Mn* ix, *Fe* x, and *Co* xi, directly derived from the transitions  $3s^23p^5 - 3s^23p^4s$  observed in the laboratory by Edlén,<sup>6</sup> are not of comparable accuracy and therefore are not included in Table 2.

From Table 2 it appears clearly now that the forbidden transitions between the two sublevels of the  $^2P$  term of *Fe* xiv, *Ni* xvi, *Fe* x, and *Ni* xii agree in wave numbers with four of the coronal lines—the [*Fe* xiv] transition giving the strong green line. It will be shown later that the intensity ratios of homologous lines of iron and nickel are in accordance with the relative cosmical abundance of these elements, simultaneously indicating the degree of ionization of the coronal matter.

The extrapolation problem is more complex for the configurations  $3s^23p^2$  and  $3s^23p^4$ , which, in order of increasing energy, furnish respectively the following levels:  $^3P_0$ ,  $^3P_1$ ,  $^3P_2$ ,  $^1D_2$ ,  $^1S_0$  and  $^3P_2$ ,  $^3P_1$ ,  $^3P_0$ ,  $^1D_2$ ,  $^1S_0$ . The  $^1S_0$  level lies too high above  $^1D_2$  to give observable lines. But, besides the transitions between the  $^3P$  components which are analogous to those of the  $3s^23p$  or  $3s^23p^5$  configurations, we have also to consider the transitions from  $^1D_2$  to  $^3P$ . It will be apparent from what follows that coronal lines might be expected especially for the following transitions:  $^1D_2 - ^3P_2$ ,  $^3P_2 - ^3P_1$ ,  $^3P_1 - ^3P_0$  of  $3s^23p^2$ , and  $^1D_2 - ^3P_1$ ,  $^3P_1 - ^3P_2$  of  $3s^23p^4$ .

<sup>7</sup> The  $3s^23p^3$  configuration (*Fe* xii and *Ni* xiv) cannot produce forbidden lines of appreciable intensity, as will be shown later.

For a provisional extrapolation of these differences, one might assume the  $^3P$  splittings proportional to  $(Z - \sigma)^4$ , and the  $^1D - ^3P$  intervals proportional to  $Z$ . However, deviations from these simple relations become increasingly large because of the successive change from  $LS$  to  $JJ$  coupling when  $Z$  increases along an isoelectronic sequence. Hence, use had to be made of the more complicated theoretical formulae for intermediate coupling. The reviewer will not go into the details of the practical procedure followed by Edlén in applying these theoretical formulae to his extrapolation problem, but it

TABLE 2  
COMPARISON OF THE GROUND-TERM SPLITTINGS IN THE ISOELECTRONIC SEQUENCES  
 $3s^23p$  ( $Al\ I, Si\ II, \dots$ ) AND  $3s^23p^5$  ( $Cl\ I, A\ II, \dots$ ).  $\zeta = \frac{2}{3}\Delta\nu$

$Z$	Ion	$(^3P_1 - ^3P_0)$ $\text{Cm}^{-1}$	$\sqrt{\zeta}$	Diff.	Ion	$(^3P_1 - ^3P_0)$ $\text{Cm}^{-1}$	$\sqrt{\zeta}$	Diff.
13	$Al\ I$	112.04	2.939					
14	$Si\ II$	287.3	3.720	0.781				
15	$P\ III$	559.6	4.395	.675				
16	$S\ IV$	950.2	5.017	.622				
17	$Cl\ V$	1492	5.616	.599	$Cl\ I$	881	4.923	
18	$A\ VI$	2210	6.195	.579	$A\ II$	1432	5.559	0.636
19	$K\ VII$	3131	6.759	.564	$K\ III$	2162	6.162	.603
20	$Ca\ VIII$	4305	7.319	.560	$Ca\ IV$	3115	6.751	.589
21	$Sc\ IX$	5759	7.871	.552	$Sc\ V$	4325	7.327	.576
22	$Ti\ X$				$Ti\ VI$	5825	7.894	.567
23	$V\ XI$				$V\ VII$	7657	8.452	.558
24	$Cr\ XII$			.543	$Cr\ VIII$			
25	$Mn\ XIII$				$Mn\ IX$			.553
26	$Fe\ XIV$	18,852.5*	10.588		$Fe\ X$	15,683.2*	10.112	
27	$Co\ XV$			0.538	$Co\ XI$			0.545
28	$Ni\ XVI$	27,762*	11.664		$Ni\ XII$	23,626*	11.203	

\* Coronal lines.

should be stressed that the results of the extrapolation are of an accuracy similar to that for  $3s^23p$  and  $3s^23p^5$ . The only difficulty concerns  $Fe\ XIII$ , in which case it is impossible to decide, from the extrapolated wave numbers only, how to allot the two very close infrared coronal lines to  $^3P_1 - ^3P_0$  or to  $^3P_2 - ^3P_1$ . However, a definite identification will be possible on the basis of intensity considerations. The  $^3P_1 - ^3P_0$  and  $^3P_2 - ^3P_1$  transitions of  $Ni\ XV$  correspond respectively to the coronal lines  $\lambda\ 6702$  and  $\lambda\ 8024$ . The interval  $^1D_2 - ^3P_2$  of  $Fe\ XIII$  corresponds to the strong ultraviolet coronal line  $\lambda\ 3388$ . The same transition of  $Ni\ XV$  falls outside the observable spectral range.

Figure 1 illustrates the relative level positions for the various isoelectronic sequences considered; the transitions actually observed in the corona are indicated by arrows and

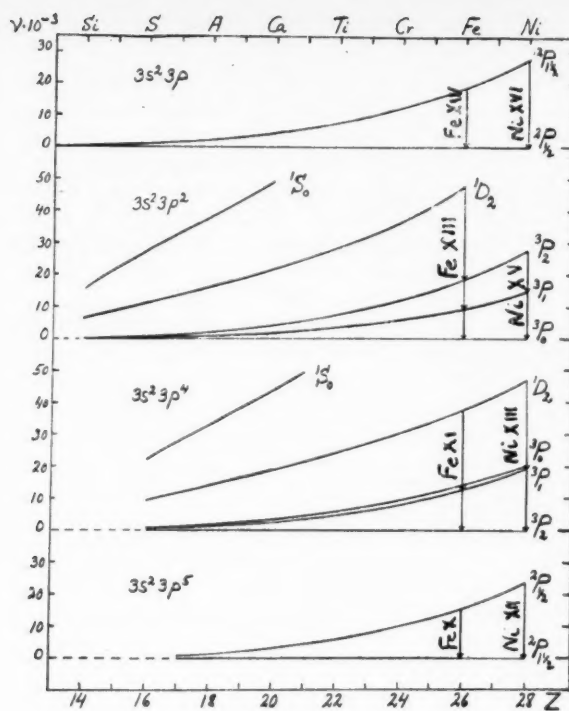


FIG. 1

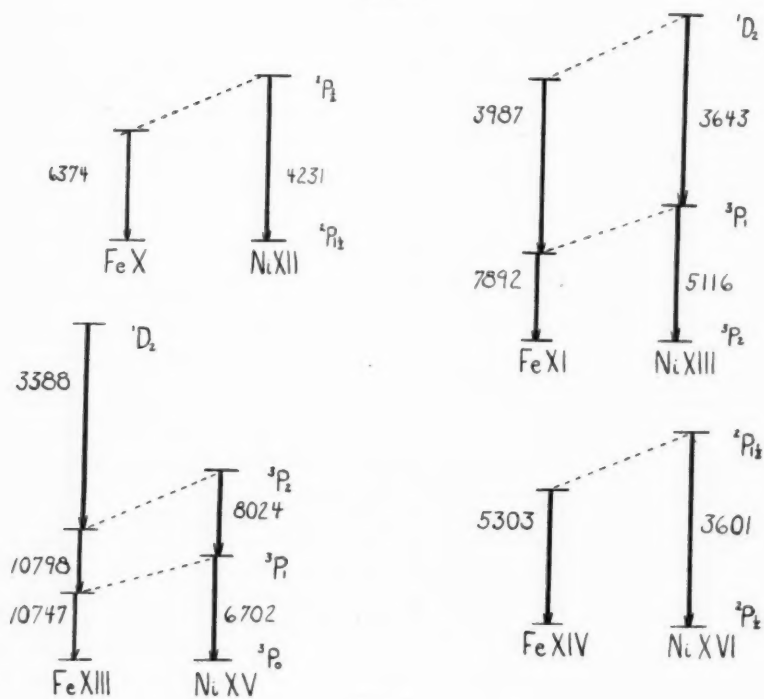


FIG. 2

are also shown in Figure 2. All in all, at the present stage, 13 coincidences have been observed between the wave numbers of coronal lines and those of transitions in the ground configurations  $3s^23p$ ,  $3s^23p^2$ ,  $3s^23p^4$ , and  $3s^23p^5$  of *Fe* and *Ni*. These 13 coronal lines account for more than nine-tenths of the total intensity of the coronal line emission.

The next step is a discussion of the observed intensities in order to ascertain whether these are compatible with the theoretical transition probabilities, with the cosmical abundances of the elements, and with definable ionization and excitation conditions in the corona.

### III. LINE INTENSITIES

There is no initial state of the ions considered for which more than one transition has been identified in the corona. Hence, the intensity ratios of the various forbidden lines depend upon the physical conditions. In this connection it should be remembered that

TABLE 3  
TRANSITION PROBABILITIES  $A$

TRANSITION	IRON			NICKEL		
	Ion	$\nu \times 10^{-3}$	$A$ (in $\text{Sec}^{-1}$ )	Ion	$\nu \times 10^{-3}$	$A$
$3s^23p^5\ ^2P_{1/2} - ^2P_{1/2}$	<i>Fe</i> X	15.68*	69	<i>Ni</i> XII	23.63*	237
$3s^23p^4\ ^1D_2 - ^3P_1$	<i>Fe</i> XI	25.08*	9.5	<i>Ni</i> XIII	27.44*	18
$\ ^1D_2 - ^3P_2$		37.74	92		46.98	257
$\ ^3P_0 - ^3P_1$		(1.71)	0.25		(0.65)	0.01
$\ ^3P_0 - ^3P_2$		(14.38)	0.02†		(20.19)	0.06†
$\ ^3P_1 - ^3P_2$		12.67*	44		19.54*	157
$3s^23p^2\ ^1D_2 - ^3P_2$	<i>Fe</i> XIII	29.51*	87	<i>Ni</i> XV	(35.47)	229
$\ ^1D_2 - ^3P_1$		38.77	72		(47.93)	221
$\ ^3P_2 - ^3P_1$		9.26*	9.7		12.46*	22
$\ ^3P_2 - ^3P_0$		18.56	0.01†		27.38	0.05†
$\ ^3P_1 - ^3P_0$		9.30*	14		14.92*	57
$3s^23p\ ^2P_{1/2} - ^2P_{1/2}$	<i>Fe</i> XIV	18.85*	60	<i>Ni</i> XVI	27.76*	193

\* Coronal lines.

† These are electric quadrupole probabilities; all other values of  $A$  are magnetic dipole probabilities.

considerable variations in the intensity ratios of the coronal lines have been repeatedly observed, as already mentioned in the beginning.

The intensity of a forbidden transition of probability  $A_1$  and wave number  $\nu$  may be expressed in arbitrary units by the classical formula

$$I = \frac{\eta \nu A_1}{A_1 + A_2 + A_3 + \dots + B + C}, \quad (1)$$

where  $\eta$  is the number of ions arriving in the initial metastable state per second;  $A_1$ ,  $A_2$ ,  $A_3$ , are the probabilities of the various spontaneous transitions from the initial state; and  $B$  and  $C$  are the probabilities of de-excitation by collision and radiative absorption.

It is possible to determine fairly accurately the probabilities of the transitions considered here. For all lines observed in the corona the probabilities of the electric quadrupole are extremely small, compared with the probabilities of the magnetic dipole. Edlén bases his determinations on recent investigations by S. Pasternack<sup>8</sup> and by Shortley, Aller, Baker, and Menzel.<sup>9</sup> The values adopted are listed in Table 3. The fol-

<sup>8</sup> *Ap. J.*, 92, 129, 1940.

<sup>9</sup> *Ap. J.*, 93, 178, 1941.

lowing additional remarks should be made. For *Fe* XI the total probabilities of transitions from  $^1S_0$  are:

	$A$
$^1S_0 - ^1D_2$	14
$^1S_0 - ^3P_0$	0
$^1S_0 - ^3P_1$	910
$^1S_0 - ^3P_2$	3

Similar values are obtained for *Fe* XIII, *Ni* XIII, and *Ni* XV. Hence, we may assume that practically all ions arriving in  $^1S_0$  will be transferred to  $^3P_1$ . For *Fe* XI the probability of  $^1D_2 - ^3P_0$  is only 0.002, i.e., vanishingly small compared with the other  $^1D - ^3P$  transitions; this is also true for the other ions *Fe* XIII, *Ni* XIII, and *Ni* XV.

De-excitation by absorption of radiation is probably unimportant, since the next higher configuration,  $3s3p^{k+1}$ , combining with the ground configuration,  $3s^23p^k$ , corresponds to an excitation potential of about 35 volts in all the *Fe* ions and somewhat more in the *Ni* ions. In any case, the de-exciting radiation must be of wave length shorter than  $\lambda$  400, and the intensity of the solar radiation in this spectral region is probably extremely small.

It is further assumed by Edlén that de-excitation of the metastable levels by electron collisions ( $^3P_0$  excluded) can be neglected in comparison with the spontaneous transitions. Such an assumption is extremely probable. If de-excitations by electron collisions were much in excess relative to the de-excitations by radiative emission, a Boltzmann distribution would result; and, because of the high electron temperature ( $T_e \approx 250,000^\circ$ ; motivated below), the number of ions in the various levels of the ground configuration would be approximately proportional to their statistical weights. Consequently, the line intensities in a given ion would be proportional to  $(2J + 1) A \nu$ . In *Fe* XIII, for example, the intensity ratios of the transitions  $^1D_2 - ^3P_2$ ,  $^3P_2 - ^3P_1$ ,  $^3P_1 - ^3P_0$  would be given approximately as 128:4.6:3.9, while the observed intensity ratios for the corresponding coronal lines  $\lambda\lambda$  3388, 10,798, and 10,747 are 16:35:55, according to B. Lyot.<sup>2</sup> Such a discrepancy is too large to be attributed to observational uncertainties.

Other evidence is provided by estimating the probability of collisional de-excitation of a metastable level, following a method similar to the treatment of the [O III] problem in the nebulae by Hebb and Menzel<sup>10</sup> and by Menzel, Aller, and Hebb.<sup>11</sup> Hebb and Menzel derived by wave mechanics certain parameters  $\Omega$  ( $A$ ,  $B$ ) with which to express the collisional cross-sections for transitions, upward as well as downward, between two levels  $A$  and  $B$ . In the case of the  $2s^22p^2$  configuration of O III, numerical values of  $\Omega$  were given for all level combinations. Edlén noticed that the parameter  $\Omega'$  defined by

$$\Omega'(A, B) \times (2J_A + 1)(2J_B + 1) = \Omega(A, B) \quad (2)$$

is approximately equal for all the [O III] transitions, and he made the simplifying plausible assumption that  $\Omega'$  may be considered as a constant characteristic for a certain ion and configuration.

Assuming an electron density  $N_e$  and a Maxwellian velocity distribution of the electrons corresponding to a temperature  $T_e$ , the formula of Hebb and Menzel gives the following probability for a collisional de-excitation of a metastable level:

$$B = 8.54 \times 10^{-6} N_e T_e^{-1/2} \Omega' \Sigma (2J + 1), \quad (3)$$

the  $\Sigma$  being taken over all the lower levels.

In comparing the probabilities  $A$  and  $B$ , the fact that the electron density in the corona ( $N_e^{\text{cor}} \approx 10^8 \text{ cm}^{-3}$ , according to Baumbach<sup>12</sup>) is higher than in most nebulae

<sup>10</sup> *Ap. J.*, **92**, 408, 1940.

<sup>11</sup> *Ap. J.*, **93**, 230, 1941.

<sup>12</sup> *A.N.*, **263**, 121, 1937.

( $N_e^{\text{neb}} \simeq 10^4 \text{ cm}^{-3}$ ) is compensated by the much greater transition probabilities of the coronal transitions and also, to a lesser extent, by the higher electron temperature of the corona. The values of the ratio of the number of collisional de-excitations to the number of spontaneous transitions were estimated, assuming  $\Omega' = 0.5$ ; they indicate that, except in the case of  $^3\text{P}_0$ , the spontaneous transitions have a decided predominance over the collisional de-excitations.

Next we have to estimate the numbers of excitations per cubic centimeter and per second into certain levels. Edlén computes these numbers in the case of an excitation by collisions of electrons having a Maxwellian velocity distribution corresponding to the temperature  $T_e$ . But he mentions the fact that the conditions for an excitation by radiation are considerably more favorable in the corona than they are in nebulae. In the first place, the ratio between exciting and excited intensity is of a much higher order of magnitude; and, in the second place, the corresponding transition probabilities are roughly  $10^4$  times greater. No attempt is being made to estimate the amount of an eventual radiative excitation.

The number of excitations per cubic centimeter and per second in a certain level with inner quantum number  $J$  and excitation energy  $\nu$  may be approximately given as

$$n = W N_{\text{ion}}, \quad (4)$$

where  $N_{\text{ion}}$  is the total number per cubic centimeter of the ions in question and where (from the results of Hebb and Menzel)

$$W = 8.54 \times 10^{-6} N_e T_e^{-1/2} \Omega' (2J+1) e^{-1.45\nu/T_e}, \quad (5)$$

$\Omega'$  being the same quantity as considered before. For  $T_e = 250,000^\circ$  and  $N_e = 10^8 \text{ cm}^{-3}$ , we get

$$n = 1.71 (2J+1) e^{-1.45\nu/250,000} \Omega' N_{\text{ion}}. \quad (6)$$

The factor  $e^{-1.45\nu/250,000}$  for all the considered levels lies between 0.5 and 0.9 and thus plays only a minor role. If we adopt, as before,  $\Omega' \simeq 0.5$ ,  $n$  turns out to be of the same order of magnitude as  $N_{\text{ion}}$ , which means that, on the average, each metastable level is being excited about once per second in every ion. All the values of the factor

$$n' = 1.71 (2J+1) e^{-1.45\nu/250,000} \quad (7)$$

are between 1.0 and 7.5. For ions with several metastable levels an addition to the population of the lower levels is caused by "cascading" from the upper levels. The corresponding enrichment factors  $a$  are easily determined from the transition probabilities.

The values of  $n'$  and of  $\eta' = an'$  are given in Table 4. Assuming  $B = C = 0$ , formula (1), giving the intensity of a line in arbitrary units, now becomes

$$I = \eta' \nu \frac{A}{\Sigma A} \Omega' N_{\text{ion}}, \quad (8)$$

where  $\nu$  and  $A$  refer to the transition considered, and  $\eta'$  and  $\Sigma A$  refer to its initial level.

In case several transitions are observed in the same ion, the quantities  $\eta' \nu (A/\Sigma A)$  should represent their relative intensities. This can be tested in the case of  $\text{Fe XI}$ ,  $\text{Fe XIII}$ , and  $\text{Ni XIV}$  and is satisfactorily confirmed by the observed intensities when considering the observational uncertainties. From the extrapolated term separations alone, it was impossible to decide how each one of the two close infrared lines  $\lambda 10,747$  and  $\lambda 10,798$  is to be identified with the separate transitions  $^3\text{P}_1 - ^3\text{P}_0$  and  $^3\text{P}_2 - ^3\text{P}_1$ . The assignment was primarily made to correspond with the intensity ratio of the analogous  $\text{Ni XV}$  lines. This is now confirmed by the intensity estimates based on formula (8).

Next comes the comparison of intensities of lines belonging to different kinds of ions. Let  $N_A$  be the number of atoms of the element  $A$  per cubic centimeter,  $n_A$  be the rela-

tive number referred to 100 atoms of *Fe*, and *X* be the relative abundance of a certain ionization stage. Then  $N_{\text{ion}}$  is equal to  $XN_A$  and proportional to  $Xn_A$ . The intensity may thus be expressed:

$$I = \eta' \nu \frac{A}{\Sigma A} n_A \Omega' X. \quad (9)$$

We provisionally assume  $n_{Fe} = 100$  and  $n_{Ni} = 5.2$ , as has been found in meteorites.<sup>13</sup>

TABLE 4  
VALUES OF  $n'$  AND  $\eta' = an'$  FOR THE METASTABLE LEVELS OF THE *Fe* AND *Ni* IONS

LEVEL	IRON			NICKEL		
	Ion	$n'$	$\eta'$	Ion	$n'$	$\eta'$
$^2P_{1/2}$ .....	<i>Fe</i> X	3.1	3.1	<i>Ni</i> XII	2.9	2.9
$^1S_0$ .....	<i>Fe</i> XI	1.0	1.0	<i>Ni</i> XIII	0.9	0.9
$^1D_2$ .....		6.5	6.5		6.1	6.1
$^3P_0$ .....		1.5	1.5		1.5	1.5
$^3P_1$ .....		4.7	8.0		4.5	5.7
$^1S_0$ .....	<i>Fe</i> XIII	1.0	1.0	<i>Ni</i> XV	0.8	0.8
$^1D_2$ .....		6.0	6.0		5.4	5.4
$^3P_2$ .....		7.5	10.8		7.0	9.8
$^3P_1$ .....		4.8	19.2		4.6	17.9
$^2P_{1/2}$ .....	<i>Fe</i> XIV	5.9	5.9	<i>Ni</i> XVI	5.6	5.6

TABLE 5  
CALCULATED AND OBSERVED INTENSITIES\*

CON- FIGU- RATION	TRANSI- TION	IRON					NICKEL				
		Ion	$A/\Sigma A$	$I'$	$I$ (Obs.)	$R = I \text{ Obs.}/I'$	Ion	$A/\Sigma A$	$I'$	$I$ (Obs.)	$R = I \text{ Obs.}/I'$
$3s^23p^5$	$^2P_{1/2} - ^2P_{1/2}$	<i>Fe</i> X	1	43	8.1 (18)	0.19 (0.42)	<i>Ni</i> XII	1	3.1	2.6 ...	0.84 ....
$3s^23p^4$	$^1D_2 - ^3P_1$	<i>Fe</i> XI	0.09	14	0.7 ...	0.05 ....	<i>Ni</i> XIII	0.06	0.5	faint ...	.....
	$^3P_0 - ^3P_2$	<i>Fe</i> XI	0.07	1.4	...	...		0.9	1.2	...	...
	$^3P_1 - ^3P_2$		1	70	... (13)	... (0.19)		1	5.2	4.3 (2.2)	0.83 (0.42)
$3s^23p^2$	$^1D_2 - ^3P_2$	<i>Fe</i> XIII	0.55	87	16 ...	0.18 ....	<i>Ni</i> XV	0.51	4.5	uv	.....
	$^3P_2 - ^3P_1$		1.00	89	... (35)	... (0.39)		1.00	5.6	... (0.5)	... (0.09)
	$^3P_1 - ^3P_0$		1	160	... (55)	... (0.34)		1	12	5.4 (2.0)	0.45 (0.17)
$3s^23p$	$^2P_{1/2} - ^2P_{1/2}$	<i>Fe</i> XIV	1	100	100 (100)	1 (1)	<i>Ni</i> XVI	1	7.2	2.1 ...	0.29 ....

\* The observed intensities quoted first in the sixth and eleventh columns are from W. Grotrian (*Zs. f. Ap.*, **2**, 106, 1931; **7**, 26, 1933); the second are intensities by Lyot, reduced on a scale similar to Grotrian's.

Let us introduce  $I'$  proportional to  $\eta' \nu (A/\Sigma A) n_A$  and normalized to 100 for  $\lambda 5303$ . All the other values of  $I'$  are immediately obtained as

$$I' = 0.89 \times 10^{-5} \eta' \nu \frac{A}{\Sigma A} n_A. \quad (10)$$

The values of  $I'$  are given in Table 5. The ratio  $R = (I_{\text{obs}}/I')$  is proportional to  $\Omega'x$ .

<sup>13</sup> V. M. Goldschmidt, *Norske Videnskaps Akademie Skrifter. I. Mat. Naturv.-Klasse*, No. 4, 1938.

We may assume equal values of  $\Omega'$  for isoelectronic ions of *Fe* and *Ni*. In comparing isoelectronic ions the ratio of the *R*-values will thus be equal to the ratio of the values of *X*. It is clear at once from Table 5 that an ionization maximum appears at about the stages XIII or XIV. Probably over 95 per cent of the atoms are found in the stages from *x* to XVI; about half of them in the stages XIII and XIV.

Table 5 shows that for both *Fe* XI and *Ni* XIII the intensity of the  ${}^3P_0-{}^3P_2$  transition is not zero. The extrapolated wave numbers are accurate enough to exclude any identification with hitherto observed coronal lines. Their absence may be due to observational difficulties; yet it may also be caused by collisional de-excitation of  ${}^3P_0$ , as the previously estimated probability of collisional de-excitation indicates.

The transitions  $3s23p\ ^1D_2-{}^3P_0$  and  $3s23p\ ^2P_2-{}^3P_0$  fall within the observable range; but their estimated intensities are too small, and no trace of line is found at their predicted wave lengths.

On the whole, the conclusion of this discussion is that the proposed identifications are compatible with the observed intensity ratios of the coronal lines.

#### IV. OTHER IONIZATION STAGES OF *Fe* AND *Ni*

From the foregoing considerations it is clear that transitions between levels of the ground configurations of *Fe* X, XI, XIII, XIV, and of *Ni* XII, XIII, XV, XVI, provide most of the coronal identifications. Although *Fe* XII and *Ni* XIV must be quite abundant in the corona, we should not expect any coronal lines to be attributed to them because of the relative positions of the levels of their  $3s23p^3$  configuration. The term  ${}^2D$  is too high, relative to the ground level  ${}^4S$ ; and the splittings of  ${}^2D$  and  ${}^2P$  are too small to produce observable lines. Only  ${}^2P_{1/2}-{}^2D_{3/2}$  could fall within the observable range, but this transition has a vanishingly low probability. The lower stages of ionization have already been considered previously. Their absence is in accordance with the degree of ionization already estimated for the corona. As for *Fe* XV, XVI, and XVII and the corresponding *Ni* ions, their ground configurations give only one single level  ${}^1S_0$  or  ${}^2S_{1/2}$ . Stages higher than *Fe* XVII are improbable, since the ionization increases quite abruptly when passing from *Fe* XVII to *Fe* XVIII when the *L* shell is broken up.

While no further transition within the ground configuration of *Fe* and *Ni* ions can thus be expected, we may still consider the second lowest configuration of *Fe* XV and *Ni* XVII in which two metastable levels occur, viz.,  $3s3p\ ^3P_0$  and  ${}^3P_2$ . These levels cannot combine with the ground level  $3s2\ ^1S_0$  under any circumstances, but the transition between  ${}^3P_2$  and  ${}^3P_1$  is possible through magnetic dipole radiation. From Edlén's study of the ultraviolet spectrum of *Fe* XV the wave number of the  $3s3p\ ^3P_2-{}^3P_1$  transition may be estimated as  $14,120\text{ cm}^{-1}$ , which is close enough to the only remaining infrared line ( $\nu = 14,161\text{ cm}^{-1}$ ;  $\lambda\ 7059$ ). This identification is very probable. The excitation energy, 31.9 volts, is considerably higher than for the previously identified transitions; but this does not constitute any objection if the electron temperature is of the order of from  $200,000^\circ$  to  $400,000^\circ$ .

Nine metastable states with excitation energies of the order of 50 volts also occur in *Fe* IX and *Ni* XI. They belong to the  $3s23p^53d$  configuration; and a number of combinations may arise between them, some of them falling in the observable region. Their wave lengths cannot be predicted at present. Yet it seems not excluded that some faint coronal lines might be explained as such transitions in *Fe* IX and *Ni* XI.

#### V. FORBIDDEN LINES OF OTHER HIGHLY IONIZED ATOMS

Considering the great intensity of certain transitions of *Fe* and *Ni*, it appears reasonable to search for the corresponding transitions of the neighboring metals. But, although the wave numbers can be accurately predicted with the aid of the *Fe* and *Ni* identifications, no coincidence appears. This, however, may be explained readily if the chemical

composition of the corona is similar to that of the solar atmosphere or, for that matter, of the meteorites.

Assuming relative abundances of the metals similar to those found by V. M. Goldschmidt<sup>13</sup> in the meteorites, and taking into account the ionization conditions, a few

TABLE 6

ESTIMATED WAVE LENGTHS AND INTENSITIES OF SOME TRANSITIONS NOT YET OBSERVED

Transition	$\lambda_{\text{air}}$	Intensity	Transition	$\lambda_{\text{air}}$	Intensity
<i>Co</i> xv $^2P_{1/2} - ^2P_{3/2}$ .....	4349.4	0.4	<i>Cr</i> xii $^2P_{1/2} - ^2P_{3/2}$ .....	8159	0.6
<i>Mn</i> xiii $^2P_{1/2} - ^2P_{3/2}$ .....	6539	0.7	<i>Co</i> xiv $^3P_1 - ^3P_0$ .....	8448	0.3
<i>S</i> xii $^2P_{1/2} - ^2P_{3/2}$ .....	7536	2			

TABLE 7

COMPARISON OF THE GROUND-TERM SPLITTINGS IN THE ISOELECTRONIC SEQUENCES  $2s^22p$  (*B* I, *C* II, ...) AND  $2s^22p^6$  (*F* I, *Ne* II, ...).  $\zeta = \frac{2}{3}\Delta\nu$

<i>Z</i>	Ion	$(^3P_{1/2} - ^3P_{3/2})$ $\text{Cm}^{-1}$	$\sqrt{\zeta}$	Diff.	Ion	$(^3P_{1/2} - ^3P_{3/2})$ $\text{Cm}^{-1}$	$\sqrt{\zeta}$	Diff.
5.....	<i>B</i> I	15.1	1.787					
6.....	<i>C</i> II	64.0	2.555	0.768				
7.....	<i>N</i> III	174.5	3.285	.730				
8.....	<i>O</i> IV	386.5	4.007	.722				
9.....	<i>F</i> V	746	4.722	.715	<i>F</i> I	404.0	4.051	
10.....	<i>Ne</i> VI	1316	5.442	.720	<i>Ne</i> II	782	4.778	0.727
11.....	<i>Na</i> VII	2139	6.145	.703	<i>Na</i> III	1364	5.491	.713
12.....	<i>Mg</i> VIII	3304	6.851	.706	<i>Mg</i> IV	2226	6.207	.716
13.....	<i>Al</i> IX	4900	7.560	.709	<i>Al</i> V	3440	6.920	.713
14.....	<i>Si</i> X				<i>Si</i> VI	5097	7.635	.715
15.....	<i>P</i> XI				<i>P</i> VII	7268	8.343	.708
16.....	<i>S</i> XII	(13,266)		0.712	<i>S</i> VIII	10,081	9.054	.711
17.....	<i>Cl</i> XIII				<i>Cl</i> IX	13,641	9.765	.711
18.....	<i>A</i> XIV	22,935?	11.120		<i>A</i> X	(18,063)		.710
19.....					<i>K</i> XI	23,475	11.185	
20.....					<i>Ca</i> XII	30,028	11.895	0.710

additional weak lines might possibly be expected. They are listed in Table 6, the intensities being estimated on the basis of  $I = 100$  for the green line.

Considering that two coronal lines have been satisfactorily attributed to forbidden transitions in *Ca* XIII ( $2s^22p^4$ ) and *Ca* XII ( $2s^22p^6$ ), we should examine the other possible

transitions within configurations  $2s^22p^k$ . The laboratory data for the splitting of  $^2P$  of  $2s^22p$  and  $2s^22p^5$  are collected in Table 7.

In the  $2s^22p^5$  sequence,  $K\ x1$  does not provide any identification; this is due to the low abundance of  $K$  (about one-tenth of  $Ca$ ). But the splitting for  $A\ x$ , which is accurately determined, coincides with the wave number of the occasionally observed coronal line  $\lambda\ 5536$ . Although the cosmic abundance of argon is not known, the identification of  $\lambda\ 5536$  is quite plausible. Neon has been shown by Unsöld<sup>14</sup> to be a very abundant element; hence we may also expect argon to be fairly abundant.

The extrapolation to  $A\ xiv$  in the sequence  $2s^22p$  gives a wave number quite close to that of the faint coronal line  $\lambda\ 4359$ , but this coincidence may not be significant. The same transition in  $S\ xii$  (approximately  $\lambda\ 7536$ ) is more likely expected than  $A\ xiv$  but is not observed.

In the  $2s^22p^4$  configuration, only  $^3P_1 - ^3P_2$  of  $Ca\ xiii$  can be found in the corona; the corresponding transition of  $A\ xi$  is estimated at  $\lambda\ 6919$ .

In the  $2s^22p^2$  sequence, the extrapolated value of  $^3P_1 - ^3P_0$  or  $^3P_2 - ^3P_1$  for  $Ca\ xv$  is approximately  $17,700\text{ cm}^{-1}$ . This is close to the line  $\lambda\ 5694$  observed by Lyot. But this identification is also questionable, since the ionization potential of  $Ca\ xiv$  is considerably higher than for any other coronal ion. On the other hand, Lyot<sup>2</sup> found the line to have an exceptional character.

No forbidden or permitted line of  $Si$ ,  $Mg$ ,  $C$ ,  $N$ ,  $O$ , or  $Ne$  is possible in the corona under the actual ionization conditions.

Finally, the lines of  $H$  and  $He\ ii$  might be present in the corona. The hitherto observed intensity of these lines has been ascribed to the chromosphere or to prominences.

#### VI. CONCLUSION

The main results are collected in Table 8. The wave lengths of the coronal lines are from Mitchell's compilation<sup>15</sup> and from Lyot's later measurements. The intensities are from Grotrian (col. 3) and Lyot (reduced values, col. 4). The sixth column gives the transition probability: all the identified lines are due to magnetic dipole radiation. The seventh and eighth columns give the excitation potential and the ionization potential of the next preceding ionization stages. Only four coronal lines ( $\lambda\lambda\ 3454, 4567, 3801$ , and  $4311$ ) remain unidentified, the latter two being very faint.

In the light of the present identifications a physical significance may be attributed to the determinations of width of the coronal lines. As shown by Lyot and by Waldmeier, the line profiles are symmetrical and entirely explainable by the Doppler effect of a Maxwellian velocity distribution. The kinetic temperature derived from the observed widths agrees as to the order of magnitude with the temperature estimated from the established degree of ionization. The identifications agree perfectly with the classification of coronal lines in groups which, according to Lyot, appear strengthened or weakened in certain coronal regions.

Edlén's identification of the coronal lines has opened an immense new field in solar and stellar physics. A first theoretical attempt at explaining the origin of the high-energy coronal particles has recently been published by H. Alfvén.<sup>16</sup> In normal times Edlén's discovery would have already inspired many other theoretical investigations. There is not the slightest doubt that it will affect the whole orientation of solar research for years to come. In the inner corona Grotrian<sup>17</sup> found the mean velocity of the scattering electrons to be  $4.10^8\text{ cm sec}^{-1}$ ; in thermal equilibrium this corresponds to  $350,000^\circ$ .

<sup>14</sup> *Zs. f. Ap.*, 21, 22, 1941.

<sup>15</sup> *Handb. d. Ap.*, Vols. 4 and 7.

<sup>16</sup> *Arkiv f. Matem., Astr. och Fys.*, 27, A, No. 25, 1941.

<sup>17</sup> *Zs. f. Ap.*, 8, 155, 1934.

The intensity of the *He* II lines in the flash spectrum is much too great to be acceptable at a temperature  $T \simeq 6000^\circ$ .<sup>18</sup> There is no doubt that the superexcitation observed in the corona results from the same physical factors as the small density gradient and the large turbulence.

Waldmeier's<sup>19</sup> numerous investigations with the coronagraph of Arosa (Switzerland) take an additional significance on the basis of their relation with Edlén's work.

TABLE 8

THE EMISSION LINES IN THE SOLAR CORONA: OBSERVATIONAL DATA AND IDENTIFICATIONS

$\lambda$	$\nu$ $\text{cm}^{-1}$	Intensity		Identification	$A_m$ $\text{Sec}^{-1}$	E.P.	I.P.*
3328.....	30039	1.0	.....	<i>Ca</i> XII $2s^22p^6\ ^2P_{1/2} - ^2P_{1/2}$	488	3.72	589
3388.1.....	29507	16	.....	<i>Fe</i> XIII $3s^23p^2\ ^1D_2 - ^3P_2$	87	5.96	325
3454.1.....	28943	2.3	.....	.....	.....	.....	.....
3601.0.....	27762	2.1	.....	<i>Ni</i> XVI $3s^23p\ ^2P_{1/2} - ^2P_{1/2}$	193	3.44	455
3642.9.....	27443	.....	.....	<i>Ni</i> XIII $3s^23p^4\ ^1D_2 - ^3P_1$	18	5.82	350
3800.8.....	26303	.....	.....	.....	.....	.....	.....
3986.9.....	25075	0.7	.....	<i>Fe</i> XI $3s^23p^4\ ^1D_2 - ^3P_1$	9.5	4.68	261
4086.3.....	24465	1.0	.....	<i>Ca</i> XIII $2s^22p^4\ ^3P_1 - ^3P_1$	319	3.03	655
4231.4.....	23626	2.6	.....	<i>Ni</i> XII $3s^23p^6\ ^2P_{1/2} - ^2P_{1/2}$	237	2.93	318
4311.....	23190	.....	.....	.....	.....	.....	.....
4359.....	22935	.....	.....	? <i>A</i> XIV $2s^22p\ ^2P_{1/2} - ^2P_{1/2}$	108	2.84	682
4567.....	21890	1.1	.....	.....	.....	.....	.....
5116.03.....	19541.0	4.3	2.2	<i>Ni</i> XIII $3s^23p^4\ ^3P_1 - ^3P_2$	157	2.42	350
5302.86.....	18852.5	100	100	<i>Fe</i> XIV $3s^23p\ ^2P_{1/2} - ^2P_{1/2}$	60	2.34	355
5536.....	18059	.....	.....	<i>A</i> X $2s^22p^6\ ^2P_{1/2} - ^2P_{1/2}$	106	2.24	421
5694.42.....	17556.2	.....	1.2	? <i>Ca</i> XV $2s^22p^2\ ^3P_1 - ^3P_0$	95	2.18	814
6374.51.....	15683.2	8.1	18	<i>Fe</i> X $3s^23p^6\ ^2P_{1/2} - ^2P_{1/2}$	69	1.94	233
6701.83.....	14917.2	5.4	2.0	<i>Ni</i> XV $3s^23p^2\ ^3P_1 - ^3P_0$	57	1.85	422
7059.62.....	14161.2	.....	2.2	<i>Fe</i> XV $3s3p\ ^3P_2 - ^3P_1$	.....	31.7	390
7891.94.....	12667.7	.....	13	<i>Fe</i> XI $3s^23p^4\ ^3P_1 - ^3P_2$	44	1.57	261
8024.21.....	12458.9	.....	0.5	<i>Ni</i> XV $3s^23p^2\ ^3P_2 - ^3P_1$	22	3.39	422
10746.80.....	9302.5	.....	55	<i>Fe</i> XIII $3s^23p^2\ ^3P_1 - ^3P_0$	14	1.15	325
10797.95.....	9258.5	.....	35	<i>Fe</i> XIII $3s^23p^2\ ^3P_2 - ^3P_1$	9.7	2.30	325

\* The ionization potential refers to the next lower ionization stage.

This applies also to other solar research carried on by Kiepenheuer in Germany, by Lyot in France, by the Harvard, Mount Wilson, and Michigan groups in this country, and by others. A discussion of all these other solar investigations related in some way to the corona problem lies beyond the scope of the present review.

P. SWINGS

McDONALD OBSERVATORY

February 3, 1943

<sup>18</sup> A. Unsöld, *Physik der Sternatmosphären*, p. 420, Berlin, 1938.

<sup>19</sup> *Zs. f. Ap.*, 19, 21, 1939; 20, 172, 1940; 20, 317, 1941; 20, 323, 1941; 21, 120, 1942.

## V. G. FESSENKOFF'S DYNAMICAL THEORY OF THE ZODIACAL LIGHT

The latest issue of the *Astronomical Journal of the Soviet Union* to reach this country<sup>1</sup> contains an article by Professor Fessenkoff on the origin of the cloud of diffuse matter in the solar system which gives rise to the phenomena of the zodiacal light and the zodiacal band. The author states that the problem consists in accounting for clouds of cosmic dust whose density decreases somewhat more rapidly than the inverse distance from the sun and whose oblateness is of the order of 4/5. In accordance with the work of Robertson, the author believes that the particles which at any one time form the zodiacal light fairly rapidly fall into the sun through the braking action of the solar radiation and are replaced by new particles from a source which has not previously been identified. The disintegration of comets by a planet proceeds at too slow a rate and, moreover, leads to a greatly flattened system, which is contrary to the observations. Fessenkoff advances the hypothesis that the dust particles are produced from collisions between sporadic interstellar meteors and asteroids. In support of this idea he advances the well-known fact that photometric, as well as radiometric, observations of the moon and of Mercury show their surfaces to be covered with a thick layer of dust whose origin he attributes to the gradual shattering of surface rocks by meteors. The formation of dust appears to be a process which is going on continually on all members of the solar system which are devoid of gaseous atmospheres. But, while a massive planet or satellite retains the dust on its surface, a small asteroid is more than likely to lose it. Since the integrated exposed surface of all the asteroids is enormously larger than that of a major planet, the process of dust formation must be especially efficient within the ring of the asteroids. The dust particles created in each collision enter the solar system with different velocities and in different directions. Fessenkoff assumes that all directions are equally probable, as seen from the moving asteroid, and that the distribution of velocities relative to the asteroid is given by an expression of the form

$$A e^{-K^2(v_0 - v_m)^2},$$

where  $A$  and  $K^2$  are constants. The problem is to compute the density of the dust cloud for any point in the neighborhood of the sun, after the process has been in operation for a length of time greatly in excess of the orbital period of the asteroid.

The dust cloud must have spherical symmetry. Hence the density at any point can be considered as the sum of the partial densities of the cloud elements arranged on a circle perpendicular to the axis of symmetry and resulting from a single element of the orbit of the asteroid. In principle, the method of finding  $\rho$  consists in the following: We consider the elliptical orbit of a particle and neglect the hyperbolic orbits because they contribute to the density of the element  $P$  only once, while elliptical orbits contribute many times. Let the absolute value of the velocity of the particle be  $v_1$  and the velocity relative to the moving asteroid  $O$  be  $v_0$ . Since the initial co-ordinates of the particle are those of  $O$ , the orbit of the particle is determined for each value of  $v_1$  by two parameters  $c_1$  and  $c_2$ . The density of the cloud at  $P(x, y, z)$  is proportional to the elementary volume,  $V$ , whose base is given by the four points  $x(c_1, c_2)$ ,  $y(c_1, c_2)$ ,  $z(c_1, c_2)$ ,  $x(c_1 + \Delta c_1, c_2)$ ,  $y(c_1 + \Delta c_1, c_2)$ ,  $z(c_1 + \Delta c_1, c_2)$ ,  $x(c_1, c_2 + \Delta c_2)$ ,  $y(c_1, c_2 + \Delta c_2)$ ,  $z(c_1, c_2 + \Delta c_2)$ ,  $x(c_1 + \Delta c_1, c_2 + \Delta c_2)$ ,  $y(c_1 + \Delta c_1, c_2 + \Delta c_2)$ ,  $z(c_1 + \Delta c_1, c_2 + \Delta c_2)$ , and whose height is  $v$ . If the probabilities of the values  $c_1$  and  $c_2$  are  $p_1$  and  $p_2$ , then the density is proportional to

$$\rho \sim \sum \frac{p_1 p_2}{a^{3/2} V}.$$

<sup>1</sup> Although the issue is labeled Volume 19, Part 4, on the outside cover, it really should be Volume 20, Part 2. The journal was formerly printed in Moscow. The last issue appeared at Alma Alta in August, 1942. The editor is V. G. Fessenkoff.

Fessenkoff solves the problem numerically for the plane of the orbit of  $O$  and for the axis perpendicular to this plane passing through the sun. He adopts several values of  $v_0$  expressed in terms of the circular velocity of the asteroid  $u$ . If the value of  $v_0$  is small, the particles remain in the vicinity of  $O$  and do not approach the sun (because in that case  $v_1 \approx u$ ). When  $v_0$  is of the order of  $u$ , the density near the sun changes approximately as  $r^{-1}$ . The density reaches a minimum at  $r = 0.8r_0$ , where  $r_0$  is the radius of the orbit of  $O$ ; it then rises to infinity at  $r = r_0$  and finally decreases asymptotically to zero. The final determination of the density of the cloud involves an integration over all values of  $v_0$ .

The results of the computations in the plane of the orbit of  $O$  are shown in Figure 1. The density is plotted as the ordinate (in relative units), while the distance  $r$  is plotted

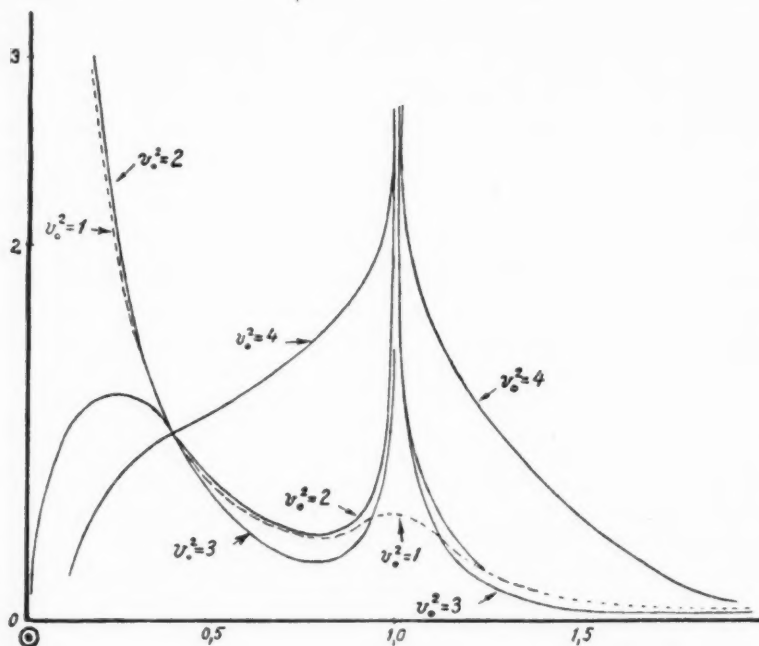


FIG. 1

as the abscissa. The curves are labeled with the corresponding values of  $v_0^2$  in units of  $u$ . In the direction normal to the orbit the density distribution is computed in a similar manner and gives a decrease which represents the observations satisfactorily if the distribution of  $v_0$  is suitably chosen.

Fessenkoff concludes that the data are sufficient to show that the dust cloud will form an oblate spheroid (with the sun at its center) which is surrounded by a dense ring of particles in the zone of the asteroids. He identifies the spheroid with the conical displays of the zodiacal light and the ring with the uniform zodiacal band which is visible along the entire ecliptic throughout the night. But he points out that, to obtain the required large values of  $v_0$ , which must greatly exceed  $u$  and, moreover, must be confined within fairly narrow limits, places severe restrictions upon the properties of the colliding meteors. He emphasizes that his theory neglects the effects of the solar radiation.

O. S.

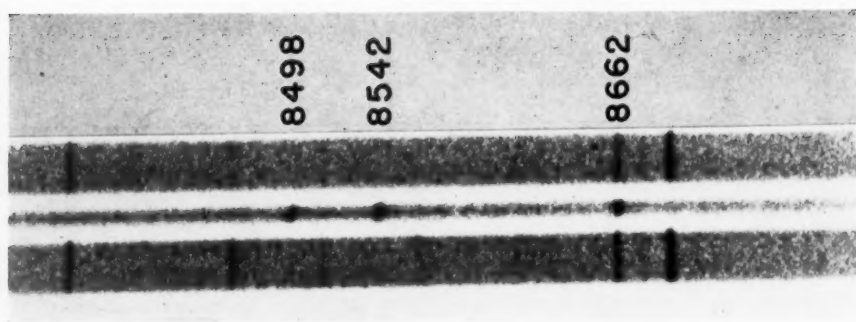
June 15, 1943

is  
x-  
e  
e  
y  
it  
e  
es

1.  
d

u.  
ur  
s-  
m  
of  
s-  
le  
e-  
d  
g

PLATE XI



*Ca II* EMISSION IN  $\nu$  SAGITTARI  
3<sup>h</sup>18<sup>m</sup>–8<sup>h</sup>02<sup>m</sup> U.T., September 6, 1942; iron-arc comparison spectrum

## NOTES

### CALCIUM II EMISSION IN $\nu$ SAGITTARII

The spectral peculiarities of  $\nu$  Sagittarii in the ultraviolet and photographic regions of its spectrum are well known, owing to the work of Greenstein,<sup>1</sup> Plaskett,<sup>2</sup> and W. W. Morgan.<sup>3</sup> The infrared spectrum of this star was examined on September 6, 1942, 5<sup>h</sup>40<sup>m</sup> U.T., with a grating spectrograph giving a dispersion of 65 Å/mm, attached to the 100-inch telescope at Mount Wilson. The Ca II triplet arising from the transition 3d<sup>2</sup>D—4p<sup>2</sup>P and having components at  $\lambda\lambda$  8498, 8542, and 8662 Å was found to be composed of very strong emission lines, as shown in Plate XI. The H and K lines of Ca II arising from the transition 4s<sup>2</sup>S—4p<sup>2</sup>P, however, are always observed as absorption lines. The emission lines appear to be about one and one-half times as wide as lines of comparable intensity in the comparison spectrum, but precise measures are difficult. If the emission character of the lines is due to the fluorescence mechanism suggested by Wyse,<sup>4</sup> Lyman  $\alpha$  must be an extremely bright emission line. This, however, would not be surprising in view of the star's other peculiarities, which include a bright H $\alpha$  and a variable bright H $\beta$ .

The radial velocity of the star as determined from the Ca II emission lines is  $-6 \pm 3$  km/sec. The radial velocity determined from the spectroscopic-binary orbit computed by R. E. Wilson<sup>5</sup> is  $-35$  km/sec. The phase of the observation, 62<sup>d</sup>84, places the star just past minimum radial velocity. The cause of the discrepancy between the observed and the computed values is, at present, not known.

It is hoped that observations of this star may be continued with the new IV-N plates, which have a very fine grain and are approximately twenty-five times as fast as the I-P plate used for the observation described above.

HAROLD F. WEAVER\*

YERKES OBSERVATORY

April 1943

<sup>1</sup> *Ap. J.*, **91**, 438, 1940.

<sup>2</sup> *Pub. Dom. Ap. Obs., Victoria*, **4**, 103, 1928.

<sup>3</sup> *Pub. Yerkes Obs.*, **7**, Part III, 1935; *Ap. J.*, **79**, 513, 1934.

<sup>4</sup> *Pub. A.S.P.*, **53**, 184, 1941.

<sup>5</sup> *Lick Obs. Bull.*, **8**, 132, 1914.

\* National Research Fellow.

## REVIEWS

*The Origin of the Carolina Bays.* ("Columbia Geomorphic Studies," No. 4.) By DOUGLAS JOHNSON. New York: Columbia University Press, 1942. Pp. xiii+341+46 figs.+6 tables. \$4.50.

The following statement of the publisher concerning the forenamed work will serve as an introduction to this review.

The Atlantic coastal plain in North and South Carolina is literally peppered with curious craters. The discovery was first made at the end of the nineteenth century, and various hypotheses have been offered as to the cause of them. Within the last ten years, however, interest in these new land forms has increased tremendously, chiefly on account of the fact that aerial photographs have revealed hundreds of these craters where topographic maps have shown but one or two. It is believed that there are literally hundreds of thousands of these craters in this particular area.

The most spectacular, or at least the most highly publicized, theory of their origin has to do with meteorites, and this despite the fact that the area of most abundant meteorites is considerably west of the coastal plain. These craters are, in the main, elliptical or ovoid. Their axial relationships [i.e., their prevailing northwest-southeast orientation] are uniform enough to be significant. All in all, the theory has been accepted popularly that these were caused by a hailstorm of meteorites that struck the Earth at an angle.

The author of this book, however, offers a new hypothesis, and one that must be considered in its entirety before it can be dismissed or before any other hypothesis can be accepted.

The new hypothesis is called "the artesian-solution-lacustrine-aeolian hypothesis" or, for short, "the hypothesis of complex origin." The gist of it (as stated on p. 154 of the volume) is "that artesian springs, rising through moving groundwater and operating in part by solution, produced broad shallow basins occupied by lakes, about the margins of which beach ridges were formed by wave action and dune ridges by wind action."<sup>1</sup>

The contents of the book are presented in fifteen chapters, entitled: (i) "Introduction," (ii) "Nature of the Bays," (iii) "Scientific Studies of the Bays," (iv) "Hypotheses Based on Supposed Terrestrial Origin of the Bays," (v) "Hypothesis of Ancient Meteorite Scars," (vi) "Hypothesis of Recent Meteorite Scars," (vii) "Further Tests of Meteoritic Hypothesis," (viii) "Magnetic Tests of the Meteoritic Hypothesis," (ix) "The Hypothesis of Complex Origin," (x) "Competence of the Hypothesis of Complex Origin," (xi) "The Artesian Phase of the Hypothesis," (xii) "The Solution Phase of the Hypothesis," (xiii) "The Lacustrine Phase of the Hypothesis," (xiv) "The Aeolian Phase of the Hypothesis," and (xv) "Possible Weaknesses of the Hypothesis."

In chapter x, "Competence of the Hypothesis of Complex Origin," some twenty-nine distinct facts about the Carolina bays, few, if any, of which, according to the author, are adequately accounted for under the meteoritic hypothesis, are considered in detail and are plausibly explained by the hypothesis of complex origin. Professor Johnson cautiously observes, however (on pp. 219-220), that "the artesian-solution-lacustrine-aeolian hypothesis of bay origin may in time suffer amputation of some of its parts or may eventually give place to some other and very different explanation. But, if so, it should not be through lack of a conscious effort to subject it to critical tests. That the hypothesis has so well supported the severe test applied to it in the present chapter entitles it to some measure of confidence."

On page 317 the author combines "empirical and genetic methods" and, in the light of his hypothesis, formulates the following definition of the term "oval bay":

*The particular "bays" which have attracted public attention and which are the subject of present discussion are more or less oval, comparatively shallow basins, usually though not always oriented in directions more or less nearly approximating northwest-southeast, generally containing marshes or lakes or both but sometimes dry, normally produced by artesian-spring excavation and by solution operating in conjunction but sometimes by one or the other operating independently, commonly though not necessarily occupied formerly if not now by lakes the waves of which smoothed the contours of the basins and often built beach ridges and bars about portions of their borders, and frequently though not always partially surrounded by rims of sand transported from the basins by wind action.*

<sup>1</sup> The italics here and in a subsequent quotation are the author's—not the reviewer's.

He adds that

if the foregoing definition seems unduly complicated, the writer would remind the reader that the bays appear to have had a complex and, within certain limits, variable origin and to present a certain degree of variability in their characteristics. If Nature sometimes moves in complex as well as in mysterious ways her wonders to perform, man can only record the complexity and do his best to solve the mystery. The foregoing definition states as concisely and as accurately as the writer can the essential nature of the oval bays.

It cannot be denied that Professor Johnson has made out a very strong case against the meteoritic hypothesis of the origin of the Carolina bays and an equally strong one in favor of his artesian-solution-lacustrine-aeolian hypothesis; the hypothesis of complex origin is not just an alternative or a concurrent explanation of the genesis of the bays; if true, it obviously completely supplants the older hypothesis.

The procedure employed in this able and exhaustive study admirably exemplifies the method of multiple hypotheses. Regardless of whether Professor Johnson's hypothesis of complex origin is correct in every particular, it seems to the reviewer decisively, though negatively, to answer the question of the meteoritic origin of the Carolina bays and thus to remove the investigation of these remarkable topographical features from the province of meteoritics and to fix it solely in the domain of geomorphology.

FREDERICK C. LEONARD

*Department of Astronomy  
University of California, Los Angeles*

*Revista, Serie A: Mathematicas y fisica teorica*, Vols. 1 and 2. Ed. Universidad Nacional de Tucuman, Tucuman, Argentina, 1940 and 1941. Pp. 334 (Vol. 1); 369 (Vol. 2).

The National University of Tucuman, Argentina, has started a new series of their *Revistas*, Serie A, devoted to mathematics and theoretical physics. The scope of the first two volumes, issued in 1940 and 1941, is illustrated by their tables of contents: Elie Cartan, "Sur des familles d'hypersurfaces isoparamétriques des espaces sphériques à 5 et à 9 dimensions"; Tullio Levi-Civita, "Formule di Green e di Stokes"; B. Gross, "Sobre a teoria da hereditariedade dielétrica"; I. F. Ritter, "Solution of Schwarz' Problem concerning Minimal Surfaces"; E. Persico, "Deduzione del principio di equivalenza elettromagnetica dalla legge di Laplace"; Max Steck, "Das Newton'sche Kraft-axiom in der Mechanik der Elektronenwellen"; Guido Fubini, "Equazioni differenziali per i periodi di un integrale iperellittico"; J. H. Van Vleck, "Electronic Conduction and the Equilibrium of Lattice Oscillators"; Guido Fubini, "On Hyperautomorphic Functions"; Su Buchin, "A Note on the Planar Point of a Surface"; J. Rey Pastor, "Espacios D"; Alberto E. Sagastume Berra, "Determinantes y ecuaciones lineales en cuasi-cuerpos"; Su Buchin, "Some Arithmetical Invariants of a Curve in Projective Space of  $n$  Dimensions"; Chuan-Chih Hsiung, "On the Curvature Form and the Projective Curvatures of Curves in Space of Four Dimensions"; M. M. Haimovici, "Sur la géométrie intrinsèque des surfaces non holonomes  $V_3$ "; Guido Ascoli, "Sulla decomposizione degli operatori differenziali lineari in fattori lineari e sopra alcune questioni geometriche che vi si riconnettono"; P. Erdős, "On a Conjecture of Steinhaus"; Alejandro Terracini, "Superficies con proyecciones parabólicas"; Félix Cernuschi, "Una generalización de la mecánica estadística de Fermi-Dirac" and "Nota sobre la fórmula de Halley para el equilibrio de sedimentación"; Gino Fano, "Su alcune particolari reti di quadriche dello spazio ordinario"; Lucien Godeaux, "Sur les points unis symétriques des involutions cycliques appartenant à une surface algébrique"; Federico Enriques, "Sopra le involuzioni irregolari appartenenti a una superficie algebrica"; Francesco Tricomi, "Sul teorema di Hadamard sui determinanti"; Gyula v. Sz. Nagy, "Ueber ganze Funktionen mit lauter reellen Nullstellen"; S. Finikoff, "Couple de surfaces en correspondance biunivoque dont les axes homologues relativement à la base de la correspondance coïncident"; A. Einstein, "Demostración de la no existencia de campos gravitacionales sin singularidades de masa total no nula" and "Demonstration of the Non-existence of Gravitational Fields with a Non-vanishing Total Mass Free of Singularities"; Edward Kasner, "Transformation Theory of Isothermal Families and Certain Related Trajectories"; C. E. Dieulefait, "Algunas nuevas deducciones de funciones de probabilidades límites"; Ambrogio Longhi, "La Determinazione degli ombelichi di una superficie algebrica e alcune questioni più generali"; Edward Kasner and John De Cicco, "Conformal Geometry of Third

Order Differential Elements"; John De Cicco, "The Two Conformal Covariants of a Field"; Chenkuo Pa, "On the Quadrics of Moutard"; J. Wüschmidt, "Las Relaciones entre las magnitudes mecánicas y ondulatorias"; Gino Fano, "Sui cerchi ortogonali a due cerchi dati"; Félix Cernuschi, "Sobre la teoría de soluciones no extremadamente diluídas de electrolitos fuertes"; Odon Godart, "Mouvement de particules chargées dans le champ d'un dipole magnétique. Sur une famille d'orbites périodiques"; Guido Ascoli, "Sulla forma asintotica degli integrali dell'equazione differenziale  $y'' + A(x)y = 0$  in un caso notevole di stabilità"; Richard Courant, "The Conformal Mapping of Riemann Surfaces Not of Genus Zero"; Carl Ludwig Siegel, "Some Remarks concerning the Stability of Analytic Mappings"; N. Coburn, "Unitary Curves in Unitary Space"; Manuel Balanzat, "Sobre los espacios  $D_0$ "; Rufus P. Isaacs, "A Finite Difference Function Theory"; Virgil Snyder, "Cremona Involutions Belonging to the Bordiga Surface in  $[4]$ "; Lucian Godeaux, "Sur les surfaces algébriques intersections complètes d'hypersurfaces"; J. Rey Pastor, "La fórmula de Riemann en la transformación de Laplace"; Alejandro Terracini, "Sobre la ecuación diferencial  $y'' = G(x, y, y')y'' + H(x, y, y')y''^2$ "; Max Steck, "Die Geometrie der erweiterten Konfigurationen 1. Eine Erweiterung des Konfigurationsbegriffs"; Apéndice: Gino Loria, "Dans quelles circonstances la découverte scientifique a-t-elle lieu?"

*Atoms, Stars, and Nebulae.* By LEO GOLDBERG and LAWRENCE H. ALLER. ("Harvard Books on Astronomy.") Philadelphia: Blakiston Co., 1943. Pp. 323. Figs. 150. \$2.50.

This volume is the fifth in a series of nine books on astronomy by members of the Harvard College Observatory staff. Earlier volumes were devoted to the problems of the Milky Way, the solar system, and the variable stars. Stellar interiors, the physics of the sun, the galaxies, and astronomical instruments are to be discussed in the remaining volumes. The entire series "is intended primarily for the intelligent layman and beginning student," and the exposition is simple and avoids the use of mathematics. The purpose of the authors is "to take the reader with us on a journey of astronomical exploration so that he himself will sample a little of the thrill of discovery." In keeping with this promise they have devoted more than half of the book to the discussion of current problems in astrophysics, and it is this feature which renders the book particularly unusual and interesting.

After a brief review of the methods used in determining the distances, masses, and radii of the stars, one chapter treats the fundamental characteristics of stellar spectra and their classification, while another chapter contains an elementary exposition of the quantum theory. The real subject matter of the book begins with chapter iv, "The Climate in a Stellar Atmosphere," giving the temperature scale and the meaning of the spectral sequence. Chapter v discusses "Dwarfs, Giants and Supergiants," with special emphasis upon absolute-magnitude criteria. The concluding section of this chapter is entitled "The Widths of Spectral Lines." Chapter vi, "Analyzing the Stars," gives an account of the curves of growth in stellar spectroscopy, the composition of reversing layers, and continuous absorption. The final section of the chapter, "A Cross-section of a Stellar Atmosphere," is devoted to the recent results on  $\zeta$  Aurigae. Chapter vii is on "Pulsating Stars," while chapter viii discusses the novae and supernovae. Chapter ix deals with planetary nebulae, and chapter x with irregular gaseous nebulae and interstellar matter. Chapter xi, "Stars with Extended Atmospheres," discusses the Wolf-Rayet stars, the P Cygni stars, and the Be stars. It closes with descriptions of spectrographic observations of  $\gamma$  Cassiopeiae,  $\beta$  Lyrae, and  $\phi$  Persei. The last chapter gives a review of modern theories of energy generation in stars. Several appendices contain useful constants and formulae.

The book is amply illustrated with reproductions of stellar spectra, photographs of nebulae and clusters, and line drawings. But, in spite of the high grade of paper, the spectra are not as good as they might have been. For some the enlargement was not sufficient, so that the relatively coarse screen used obliterates much of the more delicate detail. The presentation is clear and accurate, though it may be doubted that the lay reader will get much information from the reproductions of stellar and nebular spectra. Incidentally, much confusion could have been avoided if the spectra had all been oriented in the same way.

The chapter on the curves of growth, admirable as it is, misses the point, in my opinion. In a summarizing article, written about ten years ago, Minnaert<sup>1</sup> referred to the measurement of equivalent widths as a "method for the investigation of line profiles." As a matter of fact, the

<sup>1</sup> *Observatory*, 57, 328, 1934.

entire curve of growth is simply a method for securing some information concerning the line profiles. It is a powerful method in some respects, but it is, after all, only a makeshift to substitute for the direct measurement of the profiles of lines distorted by the finite resolving-power of the spectrograph. It would have been appropriate to stress this point, and at the same time to bring out the importance of measuring line profiles directly whenever that is possible. The authors give two actual curves of growth: Allen's fine curve for the sun, and Aller's own recent curve for  $\gamma$  Geminorum. Both show a large amount of scatter, by as much as a factor of 4 or 5 in the intensity. Other published curves (not reproduced in the book) show even larger discordances. Some of these discordances may be caused by blends and by incorrect identifications. But it is probable that important physical information concerning stellar reversing layers is buried in these curves, where it can never be brought to light. It should be remembered that one of the most fruitful spectrographic studies in recent years was one on M-type supergiants, where the absence of a genuine continuous spectrum prevented the author from measuring equivalent widths and from constructing curves of growth and compelled him to get individual line profiles. As a result, he discovered some of the most amazing properties of line profiles on record, such as the abnormal central intensities of Fe I lines excited by fluorescence.<sup>2</sup>

In presenting this criticism I do not mean to deny the importance of getting good curves of growth, especially when the lines are narrow and the resolving power of the instrument is moderate. The method is, of course, not a new one. In an embryonic form it has been used whenever an astronomer wanted to compare the observed intensities in stellar spectra with the theoretical intensities within multiplets. The first reliable observed curve of growth was one made by Minnaert and his collaborators for the sun. The theoretical consequences were worked out by Schütz in 1931 for laboratory measurements; the new method was in the same year applied by Unsöld, Elvey, and the reviewer to the problems of interstellar lines. The application to stellar spectra was made a few years later by Elvey and the reviewer. We had found that the intensity gradients of various multiplets were not always the same. For example, in 17 Leporis the gradient was steeper than in  $\epsilon$  Aurigae, and in  $\epsilon$  Aurigae it was steeper than in  $\alpha$  Persei or in 41 Cygni. We designated this phenomenon as the "gradient effect," and in the early thirties it constituted the most tantalizing spectroscopic puzzle with which we were concerned. It did not, at that time, seem reasonable that the slight bending of the curve observed by Minnaert in the sun should give rise to the remarkable differences in gradient observed in the stars. The puzzle was solved when we introduced the idea of turbulence. Goldberg and Aller briefly mention this point, but they do not show that it was only through the recognition of turbulence that the method of curves of growth has become useful in stellar spectroscopy.

In presenting the various causes of broadening of stellar absorption lines (pp. 91-99) Goldberg and Aller fail to mention mechanical effects, such as rotation and expansion. Rotation is mentioned later (p. 241), in connection with Be stars, but the reader is left under the impression that only emission-line stars rotate. This is unfortunate. Stellar rotation in stars of types O, B, A, and F constitutes the most conspicuous type of broadening observed with average dispersion. As long ago as in 1877, Abney proposed the idea of rotation in order to explain the great widths of certain lines. Vogel severely criticized Abney's arguments in an article in the *Astronomische Nachrichten* of the same year, but in 1898 he reversed his stand in a paper on the spectrum of  $\alpha$  Aquilae.<sup>3</sup> Interest in this problem was revived by Schlesinger's discovery of the rotation effect in eclipsing binaries and by the observations of Adams and Joy on diffuse lines in several short-period spectroscopic binaries. Rotations in single stars can be proved only indirectly—by comparison with spectroscopic binaries—but the evidence is so overwhelming that it may be safely relied upon. Incidentally, on page 240 Goldberg and Aller incorrectly attribute the broad underlying absorption wings of a Be star to rotation. In the hydrogen lines the wings are largely caused by Stark effect, while the helium and magnesium lines, though broadened by rapid rotation, usually do not show emission. The theory of reflection nebulae by Henyey on page 219 does not only apply to large particles. The phase function may be chosen to represent any law of diffuse reflection, and the results are quite general. Attention may also be called to an error in the legend of Figure 127.

Considered as a whole, the book is a great success. It is certain to exert a lasting influence upon astronomical writing by recognizing as a separate topic the results of the physical study of stellar spectra. Not so long ago, in the six original volumes of the *Handbuch der Astrophysik*, there was no chapter on the physics of stellar spectra as a topic separate from the theory of stellar

<sup>2</sup> L. Spitzer, Jr., *Ap. J.*, **90**, 494, 1939.

<sup>3</sup> *Sitz.-Ber. Berlin Akad. Wiss.*, 1898.

atmospheres, and stellar spectroscopy figured only as a means of classifying the stars according to temperature and luminosity. Line profiles, curves of growth, Stark effect, symbiotic spectra, etc., were either unknown or considered so new and untrustworthy that little or no mention was made of them. The authors have, with pleasing modesty, anonymously included the results of some of their own researches. Goldberg's study of the *He* lines in stellar spectra and Aller's work on Wolf-Rayet stars are a few of these contributions. The choice of material presented in this book has been partly a matter of taste. The reviewer regrets that the subject of central intensities and the results on convection in reversing layers were omitted. The reference on page 276 to the cool companion of  $\epsilon$  Aurigae as "a star at the beginning of its life" is misleading without a description of the system. But limitations of space would have made it impossible to include all interesting topics. The reader will find this book exceptionally stimulating, and the authors deserve only praise for having been sufficiently bold to include a large amount of highly interesting new material which cannot be found in other books.

O. STRUVE

Yerkes Observatory

---

*Dictionary of Science and Technology.* By MAXIM NEWMARK. New York: Philosophical Library, 1943. Pp. viii + 386. \$6.00.

This book contains some ten thousand current terms which are most frequently used in the physical sciences and their applied fields. In the first 205 pages the words are arranged in the English language, with their French, German, and Spanish equivalents. There are separate indexes for these three languages. Several conversion tables and lists of technical abbreviations enhance the value of the book. The paper is of poor quality.

---

#### ERRATA

In equation (1), page 181 of Volume 97, the exponent should read " $-C(\nu) \sec z$ ," not " $-C(\nu) \sec 2$ ." In equation (2) on that page,  $\nu$  should be substituted for  $z$ .

On page 454 of the May, 1943, issue (Vol. 97) the name of the author of *Weather: An Introductory Meteorology* is W. G. Kendrew, not W. G. Kendren.

Professor Horace S. Uhler calls attention to an error at the bottom of page 454, Volume 97. His book was not issued by the Yale University Press but was printed by the New Haven Printing Company. Copies of the book can be obtained directly from the author and not from the Yale University Press.

In Plate XXXV of Volume 97, "*Ca II 4226*" should read "*Ca I 4227*."

On the title-page to Volume 97 the collaborating editors should read:

S. A. MITCHELL, Leander McCormick Observatory  
 LYMAN SPITZER, JR., Yale University  
 W. W. MORGAN, Yerkes Observatory  
 CECILIA H. PAYNE-GAPOSCHKIN, Harvard College Observatory  
 H. N. RUSSELL, Princeton University  
 F. H. SEARES, Mount Wilson Observatory  
 S. B. NICHOLSON, Mount Wilson Observatory  
 D. B. McLAUGHLIN, University of Michigan  
 J. A. PEARCE, Dominion Astrophysical Observatory, Victoria